THE ISOTOPE GEOCHEMISTRY OF ABYSSAL PERIDOTITES AND RELATED ROCKS

by
Jonathan Edward Snow

B.A. Indiana University (1983)
B.A. Indiana University (1983)
M. Sc. University of Rochester (1986)

SUBMITTED IN PARTIAL FULFILLMENT OF THE
REQUIREMENTS FOR THE DEGREE OF
DOCTOR OF PHILOSOPHY
at the
MASSACHUSETTS INSTITUTE OF TECHNOLOGY
and the
WOODS HOLE OCEANOGRAPHIC INSTITUTION

June, 1993

Signature of Author _____
Joint Program in Oceanography,
Massachussets Institute of Technology/Woods Hole
Oceanographic Institution

Certified by _____
Henry J. B. Dick
Thesis Supervisor

Accepted by _____
M.K. McNutt
Chair, Joint committee for Marine Geology and Geophysics,
Massachusetts Institute of Technology / Woods Hole
Oceanographic Institution

THE ISOTOPE GEOCHEMISTRY OF ABYSSAL PERIDOTITES AND RELATED ROCKS

by
Jonathan E. Snow

Submitted to the Department of Earth, Atmospheric and Planetary Sciences
Massachusetts Institute of Technology
and
the Department of Geology and Geophysics
Woods Hole Oceanographic Institution
on March 9, 1993
in partial fulfillment of the requirements
for the degree of Doctor of Philosophy.

Abstract

This dissertation studies several aspects of the formation of the Earth's oceanic mantle and crust, using a variety of geologic techniques, principally major elements, radiogenic isotopes and trace elements, but including petrography, mineral chemistry, x-ray diffraction, seafloor geomorphology, and analysis of the tectonics of fracture zones. The first chapter is an introduction to the problems to be addressed in this work. The second chapter examines the composition of basalts erupted near the Atlantis II Fracture Zone on the Southwest Indian Ridge. Trends in major element compositions of those basalts can be related directly to the nearby presence of the fracture zone. The effects of mantle composition and crustal level lateral transport of magma in the rift system can be ruled out by the analysis of isotopes and the geomorphology of the fracture zone floor. This is the best demonstration to date of a transform fault effect on basalt compositions. In trying to quantify putative transform fault effects documented at other fracture zones, no systematic correlation of transform offset age with mantle temperature change can be found, suggesting that mantle composition and lateral transport phenomena play a larger than expected role in the evolution of those areas.

The third chapter relates to oceanic mantle rocks as they are altered at or near the Earth's surface. The major elements which make up abyssal peridotites are extensively redistributed by the alteration they have undergone. Mg is shown to be extracted from the peridotites, and a variety of trace elements added. This elemental redistribution is taken as evidence for extensive Mg transport by circulating waters. Since the solubility of Mg-bearing minerals in hydrothermal solutions is quite limited, much lower temperatures and much higher water/rock ratios are required to explain the major element compositions of the peridotites than had previously been assumed.

The behavior of the Nd, Sr and Os isotopic systems during seafloor alteration was also studied. The isotope systematics of these rocks strongly support the hypothesis of high water/rock ratios in the formation of serpentinized abyssal peridotites. Nonetheless, Nd and Sr reside in a phase which is resistant to alteration (clinopyroxene) and the concentration of Os is high relative to that of seawater, so that it too appears resistant to alteration. Primary mantle isotopic signatures may be obtained from abyssal peridotites by careful analysis, even of extremely weathered rocks.

Radiogenic strontium in excess of what could be introduced by seawater contamination or *in situ* radiogenic growth in a reasonable period of time was also found. These observations confirm earlier work which had been discredited for many years. The only plausible mechanism for the formation of this "orphan" ^{87}Sr is that it is introduced as part of a sedimentary component which infiltrates the rock during metamorphism and/or weathering. The ^{87}Sr may be contained by or sorbed onto extremely fine clay particulates, or colloidal suspensions, as opposed to the dissolved ionic Sr which is normally thought of as characterizing the Sr isotopic composition of seawater. The high water/rock ratios required by the bulk isotopic analysis, as well as the pervasive elemental redistribution arguing for extensive near-surface weathering at high water/rock ratios strongly support this hypothesis. Given pervasive percolation of water throughout the samples, sufficient radiogenic, sediment-derived strontium may be drawn deep into the crust in the course of its weathering to cause such high $^{87}Sr/^{86}Sr$ ratios.

The fourth chapter deals exclusively with primary mantle isotopic information from abyssal peridotites. This is the first study which has attempted to relate the Os isotopic system in the oceanic mantle to other isotopic systems and to trace elements. It is possible, with some extreme assumptions, to model the range of Os isotopes in the oceanic mantle alone in a standard model of formation of the depleted mantle by extraction of the crust. The additional constraints provided by the study of Nd isotopes in depleted mantle rocks from the oceans show that partial melt extraction and the formation of a depleted reservoir alone are not sufficient to account for the range of both Nd and Os isotopes in the Earth's mantle. Possible mechanisms for the decoupling of the Os and Nd isotopic systems include elemental fractionation via the porous flow of basalt through the mantle, mantle metasomatism, recycling of a subducted component in the mantle and core formation. The core extraction model is pursued in some detail. Such core extraction models can account for the distributions and isotopic compositions of compatible and incompatible trace elements in the Earth's mantle, but they are highly non-unique, and thus difficult to test.

Acknowledgments

I would like to thank my wife, Laura M. Feld, for her emotional support and perseverance through the many difficult circumstances required by this thesis.

I would like to thank my advisor, Henry J.B. Dick and the rest of my thesis committee; Stan Hart, Mark Kurz, Nobu Shimizu, Fred Frey, Peter Kelemen and Ralph Stephen (chair) for their many hours of fruitful discussion, both individually and collectively, and for their material support of this research.

I also wish to thank the following people who directly contributed their time and energy to helping me to complete this thesis: Linda Angeloni, Jurek Blustajn, Henry Dick, Erik Hauri, Dave Kammer, Greg Ravizza, Peter Saccocia, and Margaret Sulanowska.

Lastly, I wish to thank my family for their support through the past six years, which have been important times of change for all of us; Joel Snow, Nicholas Snow, Deborah Snow, Roger Snow, Cynthia Snow, Andrew Feld, Maury Feld and Marian Parry.

This thesis was supported by an NSF Graduate Fellowship, and by a grant from the WHOI Ocean Ventures Fund.

Dedicated to Laetitia Mary Harrer Snow (1936-1989)

and

Samuel Adam Snow (b. December 21, 1992)

Biographical Note

Jonathan Edward Snow
WHOI-McLean
Woods Hole, MA 02543

Tel: (508) 457-2000 x2829
Fax: (508) 457-2813
Email: jesnow@athena.mit.edu

Education:

Attended:

1979-1983: Indiana University, Bloomington Indiana, B.A. program.
1981: Summer Work/Study Program, Bayer,AG. Leverkusen, Germany.
1981-1982: I.U. Overseas Program, Hamburg University, Hamburg, Germany.
1983: Indiana University Geologic Field Station, Cardwell, Montana.
1983-1986 University of Rochester, Rochester, NY. M.Sc. program.
1986 - Present Woods Hole Oceanographic/MIT Joint Program in Oceanography.

Awards:

1979 National Merit Semifinalist.
1983 Winner, Grace B. Martin German Essay Contest, Indiana University.
1983 Merit Scholarship to Attend Indiana University Geologic Field Station.
1983 - 1984 Rush Rhees Fellow (University of Rochester)
1984 - 1987 National Science Foundation Graduate Fellow.
1991 WHOI Ocean Ventures Fund Grantee, Title: Osmium Isotopes in the oceanic mantle and the formation of the Earth's core.

Degrees:

B.A. Economics and Germanic Languages, June, 1983. Indiana University
B.A. Geology, August 1983. Indiana University
M.Sc. Geology, University of Rochester, May, 1986. Thesis title: Isotopic Investigations in Two Ancient Basaltic Complexes and their Implications for the Evolution of the Crust and Mantle.

Publications:

Snow, J., Basu, A. and Tatsumoto, M. (1986) "The Sittampundi Complex, S. India–Nd geochronology of Lower Crustal Granulites" EOS vol. 67:p.400 American Geophysical Union.

Snow, J., Bennett, M. Basu, A., Tatsumoto, M. and Yeo, W. (1986) "The Melkvann Complex, N. Norway: Nd and Sr isotopic evidence for the origin of Alaskan-type Ultramafic Complexes." Terra Cognita 6:p.184 European Geophysical Union.

Snow, J., Dick, H.J.B., and Hart, S.R., (1987) "Preliminary results from a transform volcano, Atlantis II Fracture Zone, SW Indian Ridge" EOS Vol. 68 No 10, p. 408. American Geophysical Union.

Henry J.B. Dick, Hans Schouten, Peter S. Meyer, David Gallo, Hugh Bergh, Robert Tyce, Phillippe Patriat, Kevin T.M. Johnson, Jonathan **Snow** and Andrew Fisher. (1991) Tectonic Evolution of the Atlantis II Fracture Zone *in:* Von Herzen, R.P, Robinson, P.T., et al. (1991) *Proceedings of the Ocean Drilling Program, Scientific Results* Vol. 118.

Snow, J., Hart, S.R. and Dick, H.J.B. (1991) "Os Isotopic composition of the Oceanic Upper Mantle" EOS Vol. 72:p.527., America Geophysical Union.

Snow, J, Hart, S.R. and Dick, H.J.B, (1992) "Os isotopes in the depleted Mid-Ocean Ridge Mantle: Implications for the Evolution of the Early Earth" V.M Goldschmidt Conference, Program and Abstracts, The Geochemical Society, p. A-106.

Table of Contents

Chapter 1: Introduction

Chapter 1: Introduction

The processes which form the Earth's mantle and crust have been the object of geologic investigation since the advent of modern geology with the publication of Hutton's *A Theory of the Earth* (Hutton, 1788) and Lyell's *Principles of Geology* (Lyell, 1833). The recognition that the deep Earth has a different composition than rocks found on the Earth's surface came first from the study of the earth's seismicity. The study of the Earth's mantle as a separate entity has since extended to the geology, petrology, and geochemistry of mantle rocks, as well as their physical and acoustic properties. The first indications that the oceanic crust was of a fundamentally different composition than the continental crust came from direct observation of emergent volcanic islands in the ocean basins (Darwin, 1933) and from rocks recovered from the ocean bottom (Wiseman, 1936) by dredging from surface ships, a sampling technique which continues to be employed to this day. The discovery of the igneous nature of the mid-ocean ridge was one of the key insights which led to the theory of plate tectonics (Dietz, 1961). Study of such rock samples has resulted in a wealth of information about the geology of the igneous portion of the ocean floor (Engel, et al., 1965; Kay, et al., 1970; Bryan, et al., 1976; Bryan and Dick, 1982; Dick, et al., 1984; Klein and Langmuir, 1987, 1989). Radiogenic isotopes have played an important role in elucidating the age and timing of important events in Earth history, and of the composition of different reservoirs within the Earth's mantle (Gast, 1968; Schilling, 1971; Hart, 1971; Schilling, 1973a, b; Hart, et al. 1973; Tatsumoto, 1978).

Fracture zones, mantle melting and source composition

The principal tectonic features of the ocean floor: ridges, rises, seamounts and fracture zones, are the major geologic context by which the compositions of basalts recovered from the ocean floor may be interpreted. The central dichotomy in the study of the petrogenesis of abyssal basalts is between mantle composition (Schilling, 1973; Hart et al., 1973; Zindler and Hart, 1979) and the melting process by which that mantle forms basaltic melt (Whitehead, et al., 1984; Langmuir and Bender, 1984; Dick, et al., 1984; Klein and Langmuir, 1987; Johnson, et al., 1990; Johnson and Dick, 1992). Mantle composition is thought of as a long-lived phenomenon transcending individual melting events. Dynamic processes, such as partial melting, also affect many of the same compositional

parameters which are affected by mantle heterogeneity. Frequently, geochemical studies tend to focus on process and ignore source composition, or focus on source composition, forgetting mantle dynamics as a source of variations. Relating the compositions of erupted basalts to their tectonic context requires that both mantle composition and mantle dynamics be taken into account.

It has long been postulated that transform faults have an effect on the composition and structure of the nearby oceanic crust (Fox, et al., 1980; Natland and Melson, 1980; Stroup and Fox, 1981; Langmuir and Bender, 1984). This effect is thought to be due to the conduction of heat across the transform away from the active ridge segment. This would tend to lower the overall degree of melting as well as the total magmatic budget of the ridge segment, and result in thinner crust near the fracture zone than far from it (Fox, et al., 1980). The second chapter of this thesis develops the analytical tools necessary to examine the case for a transform fault effect on the compositions of basalts erupted in the vicinity of the Atlantis II Fracture Zone. This analysis is extended to other fracture zones studied in the literature.

Several fundamental assumptions must be addressed in order to study the effect of fracture zone proximity on the compositions of erupted basalts. First, the tectonic setting must be free of features which are known *a priori* to be associated with mantle compositional anomalies. This requires careful analysis and interpretation of the tectonic features of the fracture zone. Second, the effect of mantle heterogeneity on the compositions of the basalts must be well known. This is only possible through the study of radiogenic isotope ratios, which are not changed by melting. They reflect only the average composition of the underlying mantle (Hofmann and Hart, 1978). Third, the crustal level fractionation history must be consistent with similar evolution paths, as polybaric fractionation and mixing of evolved and primitive liquids can produce effects mimicking those produced by melting in the mantle source. This last assumption is not met in many of the data sets examined in previous studies (Bender, et al., 1983; Langmuir and Bender, 1984).

Once these three assumptions have been shown to be reasonable for a given abyssal basalt suite, a semi-quantitative analysis of differences in temperature between two mantle source regions may be carried out. Using the experimental major element data of Kinzler and Grove (1992a) and the near-fractional, near-adiabatic polybaric melting model of Kinzler and Grove (1992b), offsets

between liquid lines of descent can be extrapolated to differences in the potential temperature of the mantle beneath regions near to and far from a fracture zone. This study shows a measurable transform edge effect for the Atlantis II Fracture Zone. Compared to other fracture zone data sets (Langmuir and Bender, 1984), the transform edge effect at the Atlantis II Fracture Zone is quite small given its large age offset. The lack of a strong correlation between the magnitude of fracture zone age offsets and observed edge effects makes it likely that mantle heterogeneity effects and/or crustal level fractionation effects are responsible for much of the variation in those data sets.

Radiogenic isotopes in the abyssal mantle

From the study of the interplay of mantle composition and mantle dynamics as it is expressed in the compositions of erupted basalts, we turn to the study of the compositions of mantle rocks themselves. The study of the isotopic compositions of erupted basalts from mid-ocean ridges (MORB) has provided important information about the composition of the depleted portion of the mantle, integrated over the age of the Earth (Gast, 1968; Schilling, 1971; Hart, 1971; Schilling, 1973a, b; Hart, et al. 1973; Tatsumoto, 1978). Other occurrences of mantle rocks have been more extensively studied, such as peridotite xenoliths in basalts and kimberlites (Peterman, et al., 1970; Shimizu, 1975; Basu and Murthy, 1977 and many others) or peridotite tectonites in ophiolites (Jacobsen and Wasserburg, 1979; McCulloch, et al., 1980; Edwards and Wasserburg, 1985 and many others). In contrast to these well-documented occurrences of peridotite, the major element, trace element and isotopic compositions of mantle rocks from mid-ocean ridge environment have only recently been studied in detail (Dick, et al., 1984; Michael and Bonatti, 1985; Shibata and Thompson, 1986; Johnson, et al., 1990; Martin, 1990; Snow, et al., 1992; Johnson and Dick, 1992). This is partly due to the relatively low abundances of incompatible elements in abyssal peridotites, the coarse grain size of the primary peridotite and the pervasive hydrous alteration of the samples.

Chapter Three of this thesis examines the alteration of abyssal peridotite and its effect on the systematics of Sr, Nd and Os isotopes in abyssal peridotites. The primary objects of this study are to determine what the major isotopic reservoirs are in abyssal peridotites, how they formed and how they may be separated from each other. Particular attention is given to the assumptions which

must be made in order for isotopic information about the oceanic mantle to be derived from abyssal peridotites. Abyssal peridotites are found to have undergone large scale elemental redistribution during alteration. In almost all of the samples studied here, Mg has been removed from the sample during alteration, and alkali elements added. The degree of major element redistribution in abyssal peridotites correlates strongly with the degree of mixing of abyssal peridotite and seawater Sr and Nd. The model water to rock ratios are orders of magnitude higher than was previously assumed to be the case for the alteration of peridotite. These water to rock ratios in some cases exceed 10^6. The high water-rock ratios support the hypothesis that significant portions of the alteration of abyssal peridotite occur at low temperatures.

Leaching studies on clinopyroxenes separated from abyssal peridotites show that it is possible to measure primary mantle Sr from abyssal peridotites in some cases. In most cases, however, it is impossible to remove all of the seawater Sr contamination. Nd isotopic compositions may be measured with confidence in most cases. Though the range of Nd isotopic compositions is similar for abyssal basalts and abyssal peridotites as a group, abyssal peridotite clinopyroxenes tend to have different Nd isotopic compositions than spatially associated basalts. Os isotopes are sufficiently resistant to alteration to be measured in unleached whole rocks, as there is as yet no evidence that the water/rock ratios needed to disturb the Os isotopic composition of a peridotite.

A reservoir of Sr with very high $^{87}Sr/^{86}Sr$ was found, which can not have been derived by *in situ* decay of Rb in any geologically reasonable period of time. This observation confirms reports of $^{87}Sr/^{86}Sr$ in peridotites higher than seawater from the early literature. The explanation for the "orphan" ^{87}Sr may lie in the high water/rock ratio of peridotite alteration and the low Sr concentration of the olivine and enstatite which are being altered. Minute quantities of detrital material suspended in the invading seawater and deposited in the peridotite are the most likely cause for these high $^{87}Sr/^{86}Sr$ ratios.

Coupling of Os and Nd isotopes: mechanisms for formation of the depleted MORB reservoir.

Mid-ocean ridge basalt is seen as a mixture of basaltic melts derived from an incompatible element depleted source and two or more enriched sources (e.g.

Table 1: Isotope systems referred to in this dissertation. (Faure, 1986).

Isotopic system (P/D)	Half-life (y)	Approximate Bulk Earth P/D ratio (elemental)	Isotopic ratio measured	Approximate Bulk Earth Isotopic composition
$^{238}U \rightarrow ^{206}Pb$	4.468×10^9	8-10	$^{206}Pb/^{204}Pb$	18.0-19.0
$^{235}U \rightarrow ^{207}Pb$	0.7038×10^9	8-10	$^{207}Pb/^{204}Pb$	15.5-15.8
$^{232}Th \rightarrow ^{208}Pb$	14.010×10^9	35	$^{208}Pb/^{204}Pb$	37.5-38.2
$^{85}Rb \rightarrow ^{87}Sr$	48.8×10^9	0.602	$^{87}Rb/^{86}Sr$	0.7045
$^{147}Sm \rightarrow ^{143}Nd$	1.06×10^{11}	0.320	$^{143}Nd/^{144}Nd$	.51264
$^{187}Re \rightarrow ^{187}Os$	4.56×10^{10}	0.085	$^{187}Re/^{186}Os$	1.05-1.10

Hart and Zindler, 1986). While the origin of the enriched sources and their geologic significance has been a primary topic of investigation in geochemistry, the origin of the depleted mantle has not been seriously questioned. It has always been assumed that the depleted mantle was formed by the process of extraction of the Earth's crust through time (Gast, 1968, and many others). In this way, a mantle reservoir is formed which has low Rb/Sr and Re/Os, and high Sm/Nd. Chapter Four of this dissertation uses Os and Nd isotopes measured in abyssal peridotites to test this hypothesis with respect to the Sm/Nd and Re/Os isotopic systems. The rough correlation of Sr and Nd isotopes in MORB can easily be explained by such a crustal extraction mechanism. The same mechanism should produce a tight coupling of Os and Nd isotopes in rocks derived from the mid-ocean ridge mantle. Such a tight coupling is not observed. Chapter Four also examines some possible models for the decoupling of Os and Nd isotopes in the depleted mantle. Re and Os are unique among the radiogenic isotope systems in that Re and Os should be fractionated by core formation. The possibility that core formation played a role in the evolution of Os and Nd in the deleted mantle is explored in greater detail.

A note on isotopic systematics

The reader of this thesis will be exposed to extensive reference to, and use of, the five major radiogenic isotopic systems in use today; U-Pb, Th-Pb, Rb-Sr, Sm-Nd and Re-Os. These isotope systems are all based on the radioactive decay of a parent element to a daughter element. It is a general convention that when these systems are referred to, the parent is mentioned first and the daughter second, as in U-Pb, Th-Pb, Rb-Sr, Sm-Nd and Re-Os. The product of radioactive

decay is always a single isotope of the daughter element (except for uranium, which has two long-lived radioactive isotopes which decay to separate isotopes of lead). Isotopes of an element share all the characteristics of that element, but differ in their weight, thus a reference to ^{204}Pb refers to its weight of 204 atomic mass units, whereas an atom of ^{208}Pb has a weight of 208 atomic mass units.

Typically, the relative abundance of the radiogenic component in a daughter element (such as Pb) to that component which has existed since the formation of the solar system is measured by the ratio of the radiogenic isotope to a non-radiogenic isotope of the daughter element. This ratio (e.g. $^{208}Pb/^{204}Pb$) is often referred to as the isotopic composition of the element in a sample, even though the other isotopes of the element are not included; these can be calculated from their known abundances. The ratio of radiogenic to nonradiogenic isotopes in the sample encapsulates the entire variation in the isotopic composition of that element within the precision of the analysis.

Table 1 lists the important characteristics of each of the isotope systems used in this dissertation. It may serve as a useful guide to the reader unfamiliar with isotope geochemistry. For further information, the reader is referred to the excellent text on the subject by Faure (1986).

References

Anders, E. (1964) Origin, age and composition of meteorites **Space Science Reviews** 3:583-714.

Basu, A and V.R. Murthy (1977) Trace element and Sr-isotopic geochemistry of the constituent minerals in ultramafic xenoliths from San Quentin, California *in:* **Extended Abstracts- The 2nd Annual International Kimberlite Conference 1977** American Geophysical Union, Washington, D.C.

Bender, J.F., Langmuir, C.H. and Hanson, G.N. (1984) Petrogenesis of glasses from the Tamayo region, East Pacific Rise. **Journal of Petrology** 25:213-254.

Bougault, H., Dimitriev, L., Schilling, J.-G., Sobolev, A., Joron, J.L. and Needham, H.D. (1988) Mantle heterogeneity from trace elements: MAR triple junction near 14°N. **Earth and Planetary Science Letters** 88:27-36.

Bryan, W.B., Thompson, G., Frey, F and Dickey, J.S. (1976) Inferred settings and differentiation in basalts from the deep sea drilling project **Journal of Geophysical Research** 81:4285-4204.

Bryan, W.B. and Dick, H.J.B (1982) Contrasted abyssal basalt liquidus trends: evidence for mantle major element heterogeneity **Earth and Planetary Science Letters** 58:15-26

Darwin, C.R. (1933) Diary of the voyage of H.M.S. *Beagle.* N. Barlow, ed. Cambridge University press, Cambridge.

Dick, H.J.B., Fisher, R.L. and W.B. Bryan (1984) Mineralogic variability of the upper mantle along mid-ocean ridges **Earth and Planetary Science Letters** 69:88-106.

Dietz, R.S. (1961) continent and ocean basin evolution by spreading of the sea floor **Nature** 190:854-857.

Edwards, R.L and G.J. Wasserburg (1985) the age and emplacement of obducted oceanic crust in the Urals from Sm-Nd and Rb-Sr systematics **Earth and Planetary Science Letters** 72:389-404.

Engel, A.E., Engel, C.G. and Havens, R.G. (1965) Chemical characteristics of oceanic basalts and the upper mantle. **Geological Society of America Bulletin** 76:719-734.

Faure, G. (1986) **Principles of Isotope Geology** John Wiley and Sons, 589p.

Fox, P.J., R.S. Detrick and G.M. Purdy (1980) Evidence for crustal thinning near fracture zones; implications for ophiolites *in:* Panayioutou, A. (*ed.*) **Ophiolites; Proceedings, International Ophiolite Symposium** p. 161-168.

Gast, P. (1968) Trace element fractionation and the origin of tholeiitic and alkaline magma types **Geochimica et Cosmochimica Acta** 32:1057

Hart, S.R. (1971) K, Rb, Sc, Sr and Ba contents and Sr isotope ratios of ocean floor basalts **Philosophical Transactions of the Royal Society of London** A26:573-587.

Hart, S.R., Schilling, J-G. and Powell, J.L. (1973) Basalts from Iceland and along the Reykjanes Ridge: Sr isotope geochemistry. **Nature and Physical Science** 246:104-107.

Hart, S.R., and A. Zindler (1986) In search of a bulk-Earth composition **Chemical Geology** 57:247-267.

Hofmann, A.W. and S.R. Hart (1978) An assessment of local and regional isotopic equilibrium in the mantle **Earth and Planetary Science Letters** 38:44-62.

Hutton, J. (1788) Theory of the Earth **Transactions of the Royal Society of Edinburgh** 1:209-304.

Jacobsen, S.J. and G.J. Wasserburg (1979) Nd and Sr isotopic study of the Bay of Islands Ophiolite Complex and the evolution of the source of mid-ocean ridge basalts **Journal of Geophysical Research** 84:7429-7445.

Johnson, K.T.M. (1990) Trace Element Geochemistry of Oceanic Peridotites and Silicate Melt Inclusions: Implications for Mantle Melting and Ocean ridge Magmagenesis Ph.D. Thesis. **MIT/WHOI, WHOI**-90-36.

Johnson, K.T.M., Dick, H.J.B. and Shimizu, N. (1990) Melting in the upper oceanic mantle: an ion microprobe study of diopsides in abyssal peridotites. **Journal of Geophysical Research,** 95:2661-2678.

Johnson, K.T.M. and H.J.B. Dick (1992) Open system melting and temporal and spatial variation of peridotite and basalt at the Atlantis II Fracture Zone **Journal of Geophysical Research** 97:9219-9241.

Kay, R., Hubbard, N., and Gast, P.W. (1970) Chemical characteristics and origin of oceanic ridge volcanic rocks **Journal of Geophysical Research** 75:1585-1613.

Kinzler, R. and Grove, T. (1992a) Primary Magmas of Mid-Ocean Ridge Basalts 1. Experiments and Methods **Journal of Geophysical Research** 97 :6885-6906.

Kinzler , R. and Grove, T. (1992b) Primary Magmas of Mid-Ocean Ridge Basalts, 2. Applications **Journal of Geophysical Research** 97:6907-6926.

Klein, E.M., and Langmuir, C.H. (1987) Global correlations of ocean ridge basalt chemistry with axial depth and crustal thickness. **Journal of Geophysical Research** 92:8089-8115.

Klein, E.M and Langmuir, C.H. (1989) Local versus global correlations in ocean ridge basalt composition: a reply. **Journal of Geophysical Research** 94:4241-4252.

Langmuir, C.H., and Bender, J.F. (1984) The Geochemistry of oceanic basalts in the vicinity of transform faults: observations and implications. **Earth and Planetary Science Letters** 69:107-127.

Lyell, C. (1830-1833) *Principles of Geology, being an attempt to explain the former changes of the Earth's surface by references to causes now in operation.* London, John Murray.

Martin, C.E. (1991) Osmium isotopic characteristics of mantle-derived rocks **Geochimica et Cosmochimica Acta** 55:1421-1434.

McCulloch, M.T, R. Gregory, G.J. Wasserburg, and Hugh P. Taylor, Jr. (1980) A neodymium, strontium and oxygen isotopic study of the Cretaceous Samail ophiolite and implications for the petrogenesis and seawater-hydrothermal alteration of the oceanic crust. **Earth and Planetary Science Letters** 46:201-211.

Michael, P.J. and Bonatti, E. (1985) Peridotite composition from the North Atlantic: Regional and tectonic variations and implications for partial melting **Earth and Planetary Science Letters** 73:91-104.

Morgan, W.J. (1968) Rises, trenches, great faults and crustal blocks. **Journal of Geophysical Research** 73:1959-1982.

Natland, J.H. and W.G. Melson (1980) Compositions of basaltic glasses from the East Pacific Rise and Siqueiros Fracture Zone, near 9N, *in:* **Initial reports of the Deep Sea Drilling Project** 54:705-723. U.S. Government Printing Office.

Peterman, Z, I. Carmichael and A.L. Smith (1970) Strontium isotopes in Quaternary basalts of southeastern California. **Earth and Planetary Science Letters** 7:381-384.

Schilling, J.-G. (1971) Sea floor spreading: rare-earth evidence **Philosophical transactions of the Royal Society of London** A268:663-706.

Schilling, J.-G. (1973) Iceland mantle plume: geochemical evidence along Reykjanes Ridge **Nature** 242:565-571.

Shibata, T. and G. Thompson (1986) Peridotites from the Mid-Atlantic Ridge at 43N and their petrogenetic relation to abyssal tholeiites **Contributions to Mineralogy and Petrology** 93:144-159.

Shimizu, N. (1975) Geochemistry of ultramafic inclusions from Salt Lake Crater, Hawaii and from South African Kimberlites. **Physics and Chemistry of the Earth** 9:655-669.

Stroup, J.B. and Fox, P.J. (1981) Geologic investigations in the Cayman Trough: evidence for thin crust along the mid-Cayman Rise **Journal of Geology** 89:395-420.

Tatsumoto, M (1978) Isotopic composition of lead in oceanic basalt and its implication to mantle evolution. **Earth and Planetary Science Letters** 38:63-87.

Whitehead, J. A. H.J.B. Dick and H. Schouten (1984) A mechanism for magmatic accretion under spreading centres **Nature** 312:146-148.

Wiseman, J.D.H. (1936) The petrography and significance of a rock dredged from a depth of 744 fathoms near to Providence reef, Indian Ocean **Linnean Society of London Transactions, 2nd. Ser.** 19:437-443.

Zindler, A. and S.R. Hart (1986) Chemical Geodynamics **Annual Review of Earth and Planetary Sciences** 14:493-571.

Chapter 2: Petrogenesis of basalts from the Atlantis II Fracture Zone, SW Indian Ridge: A Re-examination of the Transform Fault Effect.

Chapter 2: Petrogenesis of basalts from the Atlantis II Fracture Zone, SW Indian Ridge: A Re-examination of the Transform Fault Effect.

Abstract

The transform edge effect is an important paradigm for interpretation of crustal evolution at fracture zones. The great age offset across the Atlantis II Fracture Zone makes it a suitable area for the study of the transform edge effect. This chapter reports the results of combined morphologic, major element, trace element and isotopic study of the Atlantis II Fracture Zone.

A small volcano in the transform valley near the ridge-transform intersection is unambiguously the result of transform domain volcanism. Basalts from the northern ridge and the transform domain volcano have very similar isotopic compositions suggesting that they were derived from similar mantle sources. There are marked differences in the liquid lines of descent of these two basalt suites. These can be traced to lower degrees of partial melting proximal to the transform. This is evidence for a transform edge effect.

It is possible to model the compositional effect of a given temperature shift in the mantle on the liquid lines of descent of basalts. This study uses a polybaric, near-adiabatic, near-fractional melting model to estimate temperature differences in the mantle from the compositions of basalts. Using this model, differences in mantle temperature between fracture zone and rift valley basalt suites can be estimated. Comparing the temperature and age offsets from various fracture zones, it is expected that temperature offsets will increase with the age offsets across fracture zones. From a review of data in the literature, no such strong thermal signal emerges. It is likely that transform edge effects generally are overprinted by the much more pronounced effects of polybaric fractionation and mantle source heterogeneity.

Introduction

Ever since the significance of transform faults offsetting mid-ocean ridges was recognized (Morgan, 1967), the effect of these major structures on the igneous provinces they separate has been an object of speculation and study. Hekinian and Thompson (1976) noted the greater degree of fractionation in ba-

salts erupted in the rift system of the mid-Atlantic ridge near to fracture zones. Fox, et al. (1980) note the thinning of oceanic crust near transforms. This thinning requires a reduced rate of crustal production and a lower degree of overall partial melting near to fracture zones. They called upon the thermal effect of the transform edge to explain these observations.

Natland and Melson (1980) proposed that the presence of relatively old lithosphere on the plate opposite the ridge-transform intersection of a fracture zone could result in cooling of the upwelling asthenosphere near the end of a rift. This cooling would cause melting in the mantle to become both shallower in depth and lower in total extent near the transform. They called on this effect to explain chemical trends in Siqueiros Fracture Zone glasses on the East Pacific Rise. They inferred lower degrees of partial melting in the mantle due to the temperature effect of the transform, though they did not attempt to separate this effect from that of small source composition differences. Langmuir and Bender (1984) and Bender, et al. (1984) called on this "transform fault effect" or "transform edge effect" to explain the systematics of trace element variations at the Tamayo fracture zone and at fracture zones in general. When this term is used here, it refers only to mantle melting effects and not ones of petrologic diversity *per se* or of crustal level magmatic evolution.

Michael and Bonatti (1985) also note that peridotites from rift mountains are more depleted than those adjacent to fracture zones. This is consistent with a transform edge effect, since the extent of melting recorded in residual peridotites would be expected to be greater far from a transform than near to one. Such an effect on residual peridotites is interesting and significant, since the majority of abyssal peridotites are sampled near fracture zones (Aumento and Loubat, 1970; Engel and Fisher, 1975; Dick, et al., 1984; Michael and Bonatti, 1985; Johnson, et

al., 1990; Johnson and Dick, 1992). A transform edge effect in abyssal peridotites would seriously affect the results of the latter studies. Consequently, most abyssal peridotite studies would be of compositions which are less depleted than the norm for the oceanic mantle. Much of our understanding of melting processes in the upper mantle is derived from studies of fracture zone peridotites. Further examination of possible transform edge effects on peridotite compositions would thus be quite useful.

There are several ambiguities associated with the identification of transform fault effects on basalt compositions. First is the effect of differences in source composition (Natland and Melson, 1980). Different source compositions can mimic the effects of differing mantle temperatures with respect to basalt compositions. Second is the ambiguous provenance of basalts erupted in the fissure systems characteristic of mid-ocean ridges. Significant lateral transport of magma (i.e., several km.) in such rift systems (Wright, et al., 1968; Sigurdsson and Sparks, 1978) can obscure a transform fault effect. Last is the problem of crustal level fractionation of primary magmas. This fractionation can also mimic or obscure any compositional effects of a nearby transform fault.

Basalts from the Atlantis II Fracture Zone have a geologic context which makes them an important test case for the transform fault effect. This study directly addresses issues of sample provenance, crustal fractionation and source heterogeneity which have not been addressed in such studies before. Combined with the large age offset across the fracture zone, the basalts studied here should provide an evidence of such a transform edge effect, if it exists. I present here the results of an investigation of the geologic, major element, trace element and isotopic evidence for the existence of a transform edge effect at the Atlantis II

Fracture Zone. This investigation was carried out as part of the study of the geology and geochemistry of the fracture zone as a whole.

Geology of the Atlantis II Fracture Zone.

The Southwest Indian Ridge extends from the Bouvet triple junction in the west to the Indian Ocean Triple Junction (also known as the Rodriguez Triple Junction) in the east and forms the boundary between the African and Antarctic plates. The regional half spreading rate is about 7-8 mm./year. (DeMets, et al., 1990; Sclater, et al., 1978; Tapscott, et al., 1980; Sclater, et al., 1981). The Southwest Indian Ridge is thus one of the most slowly spreading mid-ocean ridges. The major regions of plume related magma genesis along the Southwest Indian Ridge are the Bouvet hot spot (Le Roex, et al., 1983; 1985), the Marion-Prince Edward hot spot and the 11°E disturbed zone (Le Roex et al., 1992)

The Atlantis II Fracture Zone (Engel and Fisher, 1975) is one of the best studied fracture zones on the Southwest Indian Ridge. It has been the object of several cruises, including a combined geophysics and petrology cruise (R/V Robert Conrad 27-09: Dick, et al., 1991) and an ocean drilling leg (ODP Leg 118, von Herzen, Robinson, et al., 1991). The cruise RC-27-09 collected single channel seismic profiles, gravity, magnetics, and SEABEAM bathymetry covering 80% of a 170 by 30 nautical mile strip of seafloor centered on the transform (Figure 1). That cruise also extensively dredged the transform and adjacent ridge axes. ODP leg 118 conducted preliminary drilling, seismic profiling and television surveys of several sites in the transform. It then drilled a 500 m. deep core into the gabbros of the transverse ridge on the eastern margin of the fracture zone. The drilling site is marked 735b in Figure 1.

The Atlantis II Fracture Zone is located at a longitude of approximately 57° E on the Southwest Indian Ridge (Figure 1). The actively slipping portion of the Atlantis II Fracture Zone extends north-south from 31° 51' S to 33°40' S, an offset of 220 km. The combination of the great length and very-slow slip rate of the fracture zone (about 16 mm./year) produces a maximum age offset of 22 million years, one of the largest anywhere. The Atlantis II Fracture Zone is located far from any hot spot, the nearest being the Marion-Prince Edward island chain some 2000 km distant (le Roex, et al., 1989).

The fracture zone itself is an impressive physiographic feature, marked by over 5 km. of relief. The actively slipping portion of the transform (marked with a single shaded line in the map of the fracture zone in Figure 1) is characterized by a N-S valley approximately 40 km wide extending to a depth of 5-6 km. Recent active faulting in the transform valley occurs along a single principal tectonic deformation zone (PTDZ) (Fox and Gallo, 1984; Dick, et al., 1991). This subtle, nearly linear feature can be identified on detailed bathymetric maps. It is marked by a series of small offsets in topographic features, saddles in small ridges, and disruptions in talus fans in the transform domain (Fox and Gallo, 1984). The PTDZ is thought to be the principal locus of faulting in the transform domain. As faults strain harden and lock, the PTDZ is thought to migrate back and forth across the valley floor, creating a zone of extreme tectonic disruption due to strike slip tectonism. Additionally, the Atlantis II Fracture Zone shows evidence of a tectonic realignment in spreading direction which enlarged the transform valley in the north. This resulted in the capture of the median tectonic ridge and paleotransform to the west of it by the western plate (Dick, et al., 1991). Thus the floor of the Atlantis II Fracture Zone, like those of most other fracture zones, is the site of intense, ongoing strike-slip tectonism.

Figure 1: Location map for the Atlantis II Fracture Zone. Contour interval for the main index map is 500m. Symbols show locations of dredge hauls discussed in the text. D1 and D2 denote the positions of MD34 dredges 1 and 2 (Hamelin and Allègre, 1985). These dredge hauls are located on the ridge segments that intersect the transform in the north and south respectively. Their positions, just outside of the bounds of the SEABEAM survey, are shown relative to the main index map and are also shown on the Indian Ocean index map in the upper right. The inset at the lower right shows details of the transform domain volcano, which was sampled in Dredge 12. The track of Dredge 12 is shown as a shaded bar. The contour interval of the inset is 25m. The 5100-5200m contour intervals have been shaded to show detail.

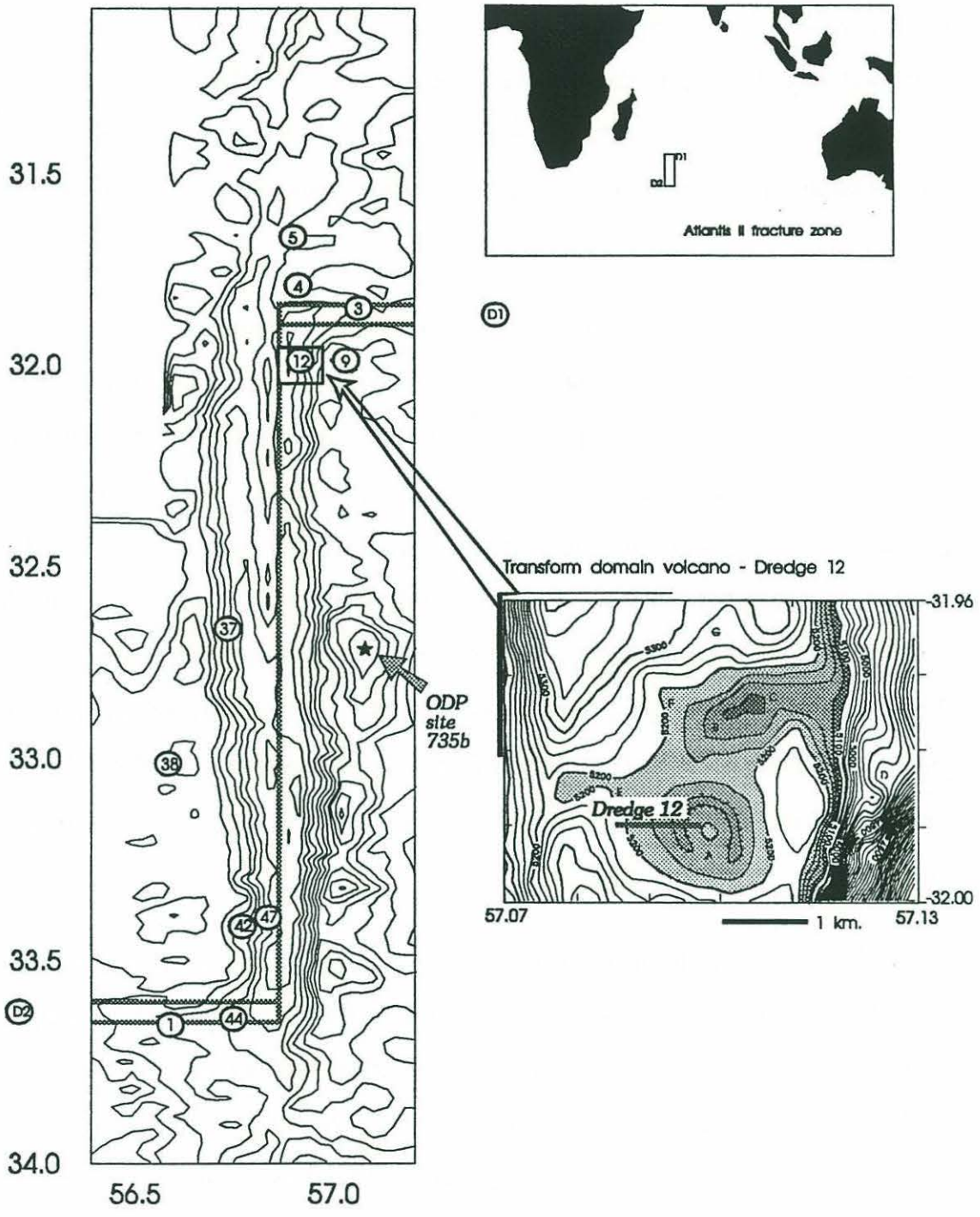
31.5
32.0
32.5
33.0
33.5
34.0
56.5
57.0
D1
D2
5
4
3
12
9
37
38
42
47
1
44
ODP
site
735b
Atlantis II fracture zone
Transform domain volcano - Dredge 12
Dredge 12
-31.96
-32.00
57.07
57.13
1 km.

The rift valleys which are the locus of spreading on the Southwest Indian Ridge enter the transform valley from the east and west (they are marked with double shaded lines in Figure 1). They intersect the northern and southern ends of the actively slipping portion of the transform at the northern and southern ridge-transform intersections, and will be referred to as the northern and southern rift valleys in the remainder of this work (as opposed to eastern and western).

The physiography of the rift valleys includes numerous small, isolated seamounts, linear seamount chains, elongate ridges and closed-contour depressions, all lying along and parallel to the rift valley axis. All of these features are interpreted as being due to successive fissure eruptions along the valley floor. The area of most recent volcanic activity (or neovolcanic zone) can be identified from magnetic anomalies and from the eruptive morphology of the sea floor in the rift valley (Dick, et al., 1991). At the northern ridge-transform intersection, these linear rift-axis morphologies appear to extend uninterrupted down the rift valley and across the transform valley floor. This is evidence that the volcanic activity that characterizes the rift valley of the mid-ocean ridge in this area continues well into the transform domain.

The deepest point in the fracture zone at 6500 m. depth is the southern nodal basin. It lies just to the east of the transform near its intersection with the northern ridge segment. The axis of the northern rift valley deepens and merges into this closed-contour basin as it approaches the fracture zone. The northern and southern nodal basins are the site of normal faulting of enormous vertical displacement. Crust originating from the northern ridge-transform intersection is uplifted from the rift valley floor to a depth of less than two kilometers adjacent to the nodal deep at the inside-corner high. The southern nodal deep and

western transverse ridge are less well developed. Nodal deeps, and their attendant tectonic uplift at the adjacent inside-corner high, are characteristic of slowly slipping transforms (Karson and Dick, 1983; Severinghaus and MacDonald, 1988).

The spatial distribution of dredged lithologies has important implications for the style of tectonism in the transform floor and walls. Dredge sampling was carried out by the Robert Conrad cruise RC2709, the R/V Atlantis II cruise AII93 (Engel and Fisher, 1975), by the R/V Marion Dufresne cruise MD34, and drilling by ODP leg 118 (von Herzen, Robinson, et al. 1991). Sampling of the rift valley floor and from areas that spread northward from the northern neovolcanic zone (the area of most recent volcanic activity) produced only glassy basalt. Slightly farther to the south, however, in the areas south of the northern margin of the northern nodal deep, dredging in the fracture zone valley and the walls of the transform produced principally gabbro, serpentinized peridotite, diabase and greenstone. Numerous plutonic rocks were dredged from the fracture zone wall. The wall is interpreted as consisting of a major set of steep normal faults which originated during uplift of the transverse ridge at the inside-corner high (cf. Dick, et al., 1991). The one exception to these observations is an occurrence of fresh, glassy pillow basalt in the transform valley. These basalts apparently erupted over altered mantle and lower crustal lithologies at a small transform domain volcano described below.

Transform Volcano

An unusual eruptive structure was observed approximately 12 km south of the northern ridge-transform intersection. The crust at this location is 1.5 million years old. The transform volcano is located on the southern extremity of the

northern nodal deep. The morphology of this plainly circular structure is shown in detail in the lower inset in Figure 1. It is a half-ring structure formed by a series of satellite cones (Labeled A, B, C, and D in Figure 1), the largest of which itself has a clearly defined caldera and central cone (A in Figure 1). The satellite cones all have lobate structures (labeled E, F, and G) on their flanks that may be interpreted as individual flow units. Figure 1 also shows the location of the transform volcano with respect to the Atlantis II Fracture Zone. Dredge haul 12 of the R/V Robert Conrad RC2709 sampled the largest of these cone structures and the talus slop at its base. The dredge track is shown as a shaded line in the inset to Figure 1.

The half ring structure is about 3 km across and about 300 m high and extends onto the side of the fracture zone wall, a recent tectonic feature. The circular morphology of this constructional volcanic structure indicates that it formed after the uplift of the transverse ridge. Tectonic activity associated with the uplift of the inside-corner high would certainly erase this relatively small feature. The ring morphology is unusual near the ridge axis in a slow-spreading mid-ocean ridge environment. Young seamounts, such as observed near the East Pacific Rise (e.g., Batiza and Vanko, 1984), are rarely observed along the slowly spreading ridges. No other known examples of off-axis volcanism are present in the Atlantis II Fracture Zone study area.

The crust underlying the transform volcano originated at the neovolcanic zone and passed through the nodal basin area, which is the site of intense tectonic activity (Fox and Gallo, 1984; Karson and Dick, 1983). Wherever nodal basins have been studied in detail (Karson and Dick, 1983; MacDonald, et al., 1986; Severinghaus and MacDonald, 1988), the tectonic construction of the nodal basin is believed to be responsible for the dismemberment of the crust and for the un-

roofing of the plutonic rocks exposed along the walls and floor of the transform valley (Dick, et al., 1991). It is unlikely that the delicate features of the transform volcano could have been preserved had it been produced at the ridge axis and passed through the nodal basin.

The freshness of the basalts recovered from the transform volcano offers additional support for the youth of the transform volcano. The transform volcano samples are nearly all fresh, aphyric to sparsely plagioclase phyric basalt glass. They have almost no trace of manganese coating or devitrification. Though the qualitative appearance of mid-ocean ridge basalts can be deceiving, it is unlikely that basalts erupted 1.5 million years ago in a tectonically active rift system would be this fresh in appearance. Rocks from crust of the same age dredged from the inside-corner high (Dredge 9) are much more weathered-looking than the transform volcano basalts. Most of the basalts dredged from the neovolcanic zone of the rift axis (Dredges 3, 4, and 5) are also more weathered-looking than the Dredge 12 basalts.

One of the many difficulties in interpreting geochemical analyses of dredged rocks is the ambiguous significance of their sample locations. Dredging is most successful at the base of steep slopes, where talus piles of mass-wasted material accumulate. Dredged samples and submersible samples are almost never samples of outcrop, and thus cannot be associated with any particular eruptive center. Even in a case where the location of the eruptive center of a particular flow can be identified, the magma may well have been transported large distances laterally down the rift valley along a crustal fissure system prior to its eruption (Wright, et al., 1968; Sigurdsson and Sparks, 1978; Dick, et al. 1991).

The transform volcano has an atypical morphology for rift-related fissure eruptions. It also erupted on crust which was tectonically disrupted after its formation at the rift axis. These observations make it clear that a rift valley origin for the basalts from the transform volcano is unlikely. The basalts erupted from the transform volcano are interpreted instead as the product of off-axis volcanism in the transform domain. They are thus unlikely to be the result of along-rift migration of basalt from an upwelling center nearer to the center of the rift system. While the overall density of sampling of this study is low, the unambiguous tectonic setting of the transform volcano provides a unique opportunity to compare basalts from both inside and outside the transform domain.

Table 1: Locations and tectonic settings.

Sample	Latitude	Longitude	Tectonic Setting	Lithologies
			Southern Ridge	
44-9	33.628 S	56.931 E	Inside-corner high, S RTI.	Aphyric basalt pillow fragments; moderately weathered.
47-3	33.383 S	57.017 E	Southern RTI, W. wall.	Aphyric basalt, lightly weathered
47-2	33.383 S	57.017 E	Southern RTI, W. wall.	Aphyric basalt, lightly weathered
MD34 D2	33.755 S	56.273 E	Center, S. Ridge segment	Basalt
			Northern Ridge	
4-20	31.760 S	57.073 E	Northern hooked ridge	Aphyric basalt, moderately weathered
4-10	31.760 S	57.073 E	Northern hooked ridge	Aphyric basalt, lightly-moderately weathered.
9-9	31.981 S	57.210 E	N. RTI.; Rift Mt. seamount.	Pl phyric basalt, moderately weathered
MD34 D1	31.693 S	57.842 E	Center, N. ridge segment	Basalt
735b			Shallow ridge W. of F.Z.	Gabbro, Fe-gabbro, lightly-moderately weathered.
			Transform Domain volcano	
12-19	32.003 S	57.090 E	Transform volcano, N. RTI	Aphyric pillow basalt; lightly weathered
12-39	32.003 S	57.090 E	Transform volcano, N. RTI	Aphyric pillow basalt; lightly weathered
12-28	32.003 S	57.090 E	Transform volcano, N. RTI	Aphyric pillow basalt; lightly weathered
12-27	32.003 S	57.090 E	Transform volcano, N. RTI	Sparsely Pl phyric; mod w.

Data are for samples analyzed for trace elements and isotopes, and for other samples referred to in this study. Major element data including locations and tectonic settings are in Johnson and Dick (1992). Samples without a cruise identifier are from R/V Robert D. Conrad Cruise 27 Leg 9. Samples MD34 D1 and D2 are from Hamelin and Allègre (1985). 735b denotes ODP Site 735b (von Herzen, Robinson, et al., 1991).

Data:

Sample Locations:

Table 1 shows the locations and tectonic settings of all the samples selected for isotopic analysis. The locations are plotted in Figure 1. Locations of additional samples referred to in this study are also shown in Figure 1. Of the samples recovered in Cruise 34 of the R/V Marion Dufresne (MD34) (Hamelin and Allègre, 1985), samples D1 and D2 were recovered from the northern and southern ridge segment abutting the Atlantis II Fracture Zone respectively. Their distances along the rift system from the Atlantis II Fracture Zone are 74.6

km. for D1 in the north and 72.0 km for D2 in the south. In the northern region, the age range of the crust from which samples were collected spans some 1.2-1.5 million years, except for site 735b which is located on 11.3 million year old crust. The southern samples span 6 million years.

Major elements:

There are three major element data sets detailing the compositions of basalt glasses from the Atlantis II Fracture Zone (Natland, personal communication, 1991; Johnson and Dick, 1992; Dick, et al., 1991). All three data sets analyze the same set of samples from the cruise RC 2709, and are in good agreement. Only Johnson and Dick (1992) include extensive analysis of Dredge 12, the transform volcano. That major element data set will be used throughout this study, although the same conclusions can be drawn independently from any of the three data sets.

The major element data from the ridge-transform intersections show trends consistent with variable degrees of partial melting followed by low pressure fractional crystallization (Dick et al., 1991; Johnson and Dick, 1992). Samples from opposite sides of the fracture zone define two distinct liquid lines of descent, reflecting similar low pressure fractionation of different primary magmas. The basalts from each ridge-transform intersection are not derived from a single common primary magma. Rather, each group represents the end result of fractionation and mixing of a few primary magmas; those from the northern ridge are the result of a lower degree of partial melting *on average* than those from the southern ridge (Johnson and Dick, 1992).

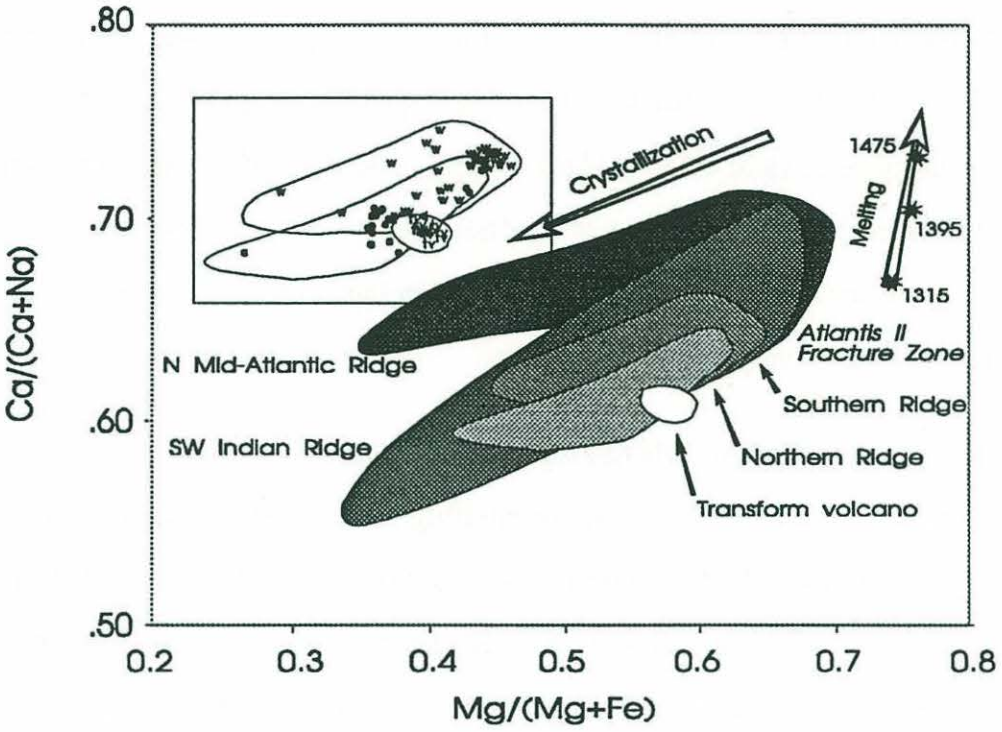

Figure 2: Ca# vs. Mg# for SW Indian Ridge basalts. Compositions of aggregate liquids are given along a vector of increasing mantle potential temperature based on model 3 of Kinzler and Grove (1992). Next to the points are listed the corresponding mantle potential temperatures. In this figure, as in all of the remaining figures, e denotes samples from the northern ridge segment, w denotes samples from the southern ridge segment, and tv denotes samples from the transform volcano.

The basalts from both sides of the fracture zone are mildly alkali enriched, and have from 2 to 12 percent hypersthene in their norms. In this they are broadly similar to transitional MORBs dredged from other fracture zones (Bryan et al., 1981; Walker, et al., 1979), although they are on average slightly higher in TiO_2 (1.6-2.4 Wt, %) and in $Na_2O + K_2O$ (3-4 Wt. %).

On a plot of Ca/(Ca+Na) vs. Mg/(Mg+Fe) (Figure 2), low and moderate pressure fractional crystallization trajectories are defined by gently sloping liquid lines of descent (Schouten, et al., 1987; Dick, et al., 1991). Plotting compositional data from cogenetic suites of natural basalts on this diagram

produces nearly linear fractional crystallization trends. These extend from the upper right of the diagram to the lower left, as Mg/(Mg+Fe) of the liquid changes strongly relative to Ca/(Ca+Na). Such liquid lines of descent represent in most cases cotectic crystallization of olivine and plagioclase. This is illustrated by the arrow labeled "crystallization" in Figure 2, and will be explored more quantitatively in a later section.

Displacement of an individual liquid line of descent in a vertical sense is largely controlled by the degree of partial melting which produced the primary magma. This is because the Na content of aggregate melts is a strong function of the degree of partial melting, whereas the Mg number is not (Dick, et al., 1984; Klein and Langmuir, 1987,1989). Model aggregate melts from Kinzler and Grove (1992b) (sequential, near-fractional polybaric batch melting model; model 3 of Kinzler and Grove, 1992b) are shown on the right of the diagram to illustrate the effects of melting. These model compositions are aggregate compositions which are controlled by the temperature and pressure of melting of the instantaneous liquids, which are then aggregated. Both the temperature and pressure of the individual batches of melt are in turn controlled by the mantle potential temperature. Both fractionation and melting effects will be discussed at greater length in the section on "Assessing a mantle temperature change."

Observed in detail (Figure 2, inset), the Atlantis II Fracture Zone basalts from the northern and southern ridges and from the transform volcano define three overlapping groups. Each of these groups was derived from a few distinct primary magmas which fractionated to produce the elongate fields shown. The transform volcano basalts cluster tightly, indicating that the range of evolution of these lavas is not large. The southern ridge basalts have the highest average Ca/(Ca+Na) for a given Mg/(Mg+Fe), followed by the basalts from the northern

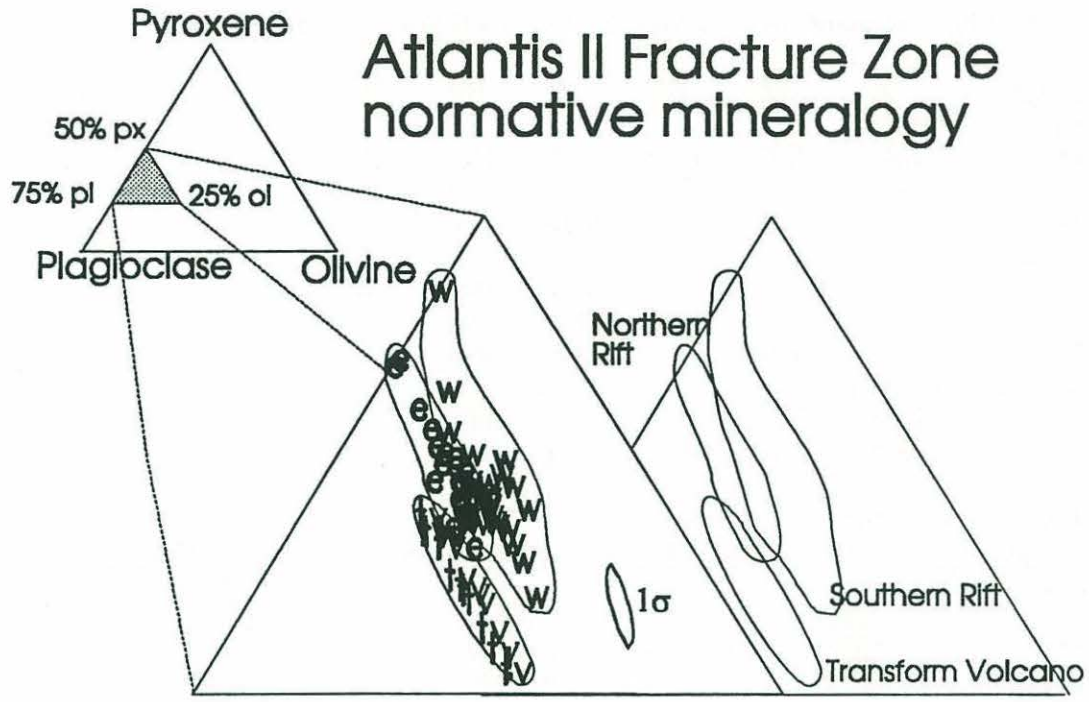

Figure 3: Normative mineralogy of Atlantis II Fracture Zone Basalts. A 1-σ error ellipse from propagation of normal uncorrelated electron microprobe errors is shown (see Appendix IV). Symbols as in Figure 2.

ridge at a lower average Ca/(Ca+Na). The transform volcano rocks cluster at the lowest Ca/(Ca+Na). Their position on this diagram suggests a relatively low degree of partial melting relative to the northern ridge suite.

The normative plagioclase-pyroxene-olivine ternary shown in Figure 3 (Cross, et al., 1903; Miyashiro, et al., 1970; Bryan and Dick, 1982) is a useful projection for examining the aggregate chemistry of mid-ocean ridge basalts. It incorporates all 10 elements in the basalt major element analysis into a few components whose significance is known by most geologists. On this diagram, the three geographic groupings defined above adhere even more distinctly to individual liquid lines of descent than they do on binary oxide or oxide ratio plots. The basalts from the transform volcano are offset to the plagioclase rich corner of

Table 2: Trace element analyses from the Atlantis II Fracture Zone

Sample	K	Rb	Ba	Sr	Nd	Sm
Southern Ridge						
44-9	1082	0.87	12.4	137.2	15.8	5.47
47-3	1117	1.10	12.5	132.2	16.8	-
47-2	796	0.53	-	127.0	12.6	-
Northern Ridge						
4-20	1867	1.09	-	179.5	16.4	5.25
4-10	2255	1.87	20.2	188.6	17.4	-
9-9	1465	1.32	-	198.0	14.8	-
Transform Volcano						
12-39	2076	1.19	15.1	172.0	18.5	5.82
12-28	2075	1.17	14.1	172.1	11.4	-

Trace element ratios.

Sample	K/Rb	K/Ba	K/Sr	Rb/Sr	Sm/Nd	Mg/(Mg+Fe)
Southern Ridge						
44-9	1244	87.3	7.9	0.00634	0.346	0.54
47-3	1015	89.5	8.5	0.00832	-	0.54
47-2	1505	-	6.3	0.00417	-	0.57
Northern Ridge						
4-20	1713	-	10.4	0.00607	0.321	0.51
4-10	1206	111.7	12.0	0.00992	-	0.53
9-9	1110	-	7.4	0.00667	-	0.58
Transform Volcano						
12-39	1745	137.2	12.1	0.00692	0.316	0.56
12-28	1774	147.3	12.1	0.00680	-	0.55

All analyses by isotope dilution except Mg/(Mg+Fe) from the major element data set of Johnson and Dick (1992). For major element data, see Johnson and Dick (1992).

the ternary from the northern ridge data. This also suggests a lower degree of partial melting or a different mantle source composition (Bryan and Dick, 1982; Dick, et al., 1984; Dick, et al., 1991). The similar offset of the northern RTI basalts from the southern RTI basalts, coupled with systematic differences in modal and trace element chemistry of spatially associated abyssal peridotites, led Johnson and Dick (1992) to conclude that basalts and peridotites which originated at the northern rift were the products of a generally lower degree of melting than those from the southern rift.

Trace elements:

Isotope dilution measurements of alkali metal and alkaline earth elements are shown in Table 2. Analytical methods are given in Brooks and Hart (1977). All of the analyses of K, Rb, and Ba were made on the 12" Mass spectrometer (TIMER) at MIT. Some of the measurements of Sr, Nd and Sm concentration were also made at Woods Hole Oceanographic Institution. These are not differentiated in Table 2, as agreement of isotope dilution measurements between the two facilities is nearly perfect. In all cases the same isotopic spike was used. The nominal uncertainty in these measurements is $\pm$ 1%.

The consistent trends seen in the major element data are not well repeated in the trace element abundances and ratios. Given that trace element ratios are insensitive to fractional crystallization, the more incompatible elements should be enriched in basalts formed from lower degree partial melts. Interestingly, K/Rb and K/Ba have systematic differences exactly the opposite of those expected for lower degrees of melting for the transform basalts; they are higher on average in the transform domain basalts than in the other two groups. The ratios Rb/Sr and Ba/Sr are inconclusive, while K/Sr and Sm/Nd agree with the hypothesis of lower degrees of melting for the transform volcano.

The trace elements should be sensitive indicators of the degree of partial melting. Instead, the information they seem to contain is contradictory. Sr concentration data are strongly affected by fractional crystallization, since Sr is compatible in plagioclase. It is not clear what metasomatic or alteration processes could have affected the alkalis and Ba without also affecting the K/Sr ratio. The K/Sr ratios could be taken as evidence for the lower melting hypothesis for the transform volcano, if all the other alkali and alkaline earth data were not opposed to that hypothesis or inconclusive. In any event, the trace element data do not strongly constrain the overall interpretation of the basalt data, as they repre-

sent a small subset of an already small data set. Dredge 4 is on crust which is approximately the same distance from the paleotransform as Dredge 12. Dredges 3 (not represented in the isotope dilution data) and 9 (which is a whole rock, not a glass analysis, and thus subject to alteration) thus form the primary comparison between the rift valley basalts and the transform basalts from Dredge 12.

Pb, Nd and Sr Isotopes:

Basalt isotopic compositions are of fundamental interest when studying mid-ocean ridge petrogenesis. The isotopic composition of a basalt records the ratio of the parent element to the daughter element (in this case, (U and Th)/Pb, Rb/Sr and Sm/Nd) in the mantle integrated over time. Thus basalts with a high $^{206}Pb/^{204}Pb$ can be said to have been derived from a high U/Pb source. Similarly, basalts with high $^{143}Nd/^{144}Nd$ can be said to be derived from mantle which has a high Sm/Nd ratio, implying light rare earth element depletion. Similarity of basalt isotopic compositions implies that the basalts were derived from mantle sources which had similar ratios of the parent and daughter elements. While isotopic ratios are generally believed to be unaffected by melting and fractionation processes, basalts from source regions with distinct isotopic compositions can be mixed during aggregation of melts and fractionation at crustal levels.

Isotopic analyses were carried out on samples selected to represent all the tectonic features from which glass was recovered. Measurement of Pb isotopic compositions were done on approximately 500 mg. samples which contained occasional spherulites and steel blue surface coatings, but no palagonite. Samples used for the analysis of Sr and Nd were approximately 30 mg. of perfectly fresh

Table 3: Isotopic data from the Atlantis II Fracture Zone.

	Pb System			Sr System		Nd System.	
Sample	206/204	207/204	208/204	87/86	err	143/144	err
			Northern ridge				
4-20	17.474	15.394	37.136	0.702724	32	0.513126	2E-05
4-10	17.462	15.386	37.127	0.702893	23	0.513077	2E-05
9-9	17.494	15.393	37.157	0.702834	28	0.512921	2E-05
D1	17.554	15.433	37.289	0.702750	20	0.513081	2E-05
D1	17.497	15.399	37.181	0.702760	20		
735b avg.	17.499	15.424	37.205	0.702849		0.513149	
			Transform volcano				
12-19	17.471	15.382	37.089	0.702805	24	0.513113	3E-05
12-39	17.48	15.393	37.153	0.702695	27	0.512966	3E-05
12-28	17.499	15.398	37.175	0.702736	25	0.513097	1E-05
12-27	17.501	15.406	37.196	0.702828	24	0.513111	1E-05
			Southern Ridge				
44-9	17.983	15.462	37.636	0.702764	27	0.512937	3E-05
47-3				0.702858	23	0.513057	3E-05
47-2	17.796	15.448	37.499	0.702838	24	0.513061	1E-05
D2	18.114	15.505	37.839	0.702690	10	0.512981	2E-05
D2				0.702690	20	0.513001	3E-05

Pb isotopic data are reported normalized to NBS 981 Pb standard values of 16.938, 15.494, and 36.711. Uncertainties in the Pb data are dominated by the standard correction and are approximately .010, .012 and .040 for 6/4, 7/4 and 8/4 respectively. Sr isotopic compositions are reported normalized to 86/88 =.1194 and Eimer & Amend standard value of .70800 and NBS SRM 987 of .710240. Nd isotopic compositions are reported normalized to 146/144=.7219 and a mean LaJolla standard value of .51184. Errors are reported as 2σ of the mean.

Samples D1 and D2 are from Hamelin and Allègre (1982). The average of 735b analyses from Kempton, et al. (1991) includes only unaltered samples (discussed in text).

glass, with fresh conchoidal surfaces on all sides and no spherulites. One sample, 9-9, was run for Pb, Nd and Sr on whole rock from the interior of a phenocryst free pillow fragment. The samples were leached in warm 6.2N HCl for 20 minutes. All showed some signs of etching (such as discoloration or yellowing of the solution). Weight loss was not detected.

Analytical methods for Pb and Sr are given in Manhes, et al. (1978) and Brooks and Hart (1977), respectively. Nd analytical methods are given in Zindler, et al. (1979). Nd and Sr analyses were made on the same hand-picked

glasses used for isotope dilution concentration measurements. Pb isotopic compositions were determined on the MIT 12" mass spectrometer. Nd and Sr isotopic measurements were carried out on the WHOI VG-354 multicollector mass spectrometer in multi-dynamic mode (see Appendix II). Some of the measurements were made on the MIT 9" single collector machine, though these are not noted in Table 3. Pb, Nd and Sr isotopic compositions are given in Table 3 and are plotted against one another in Figures 4a-c.

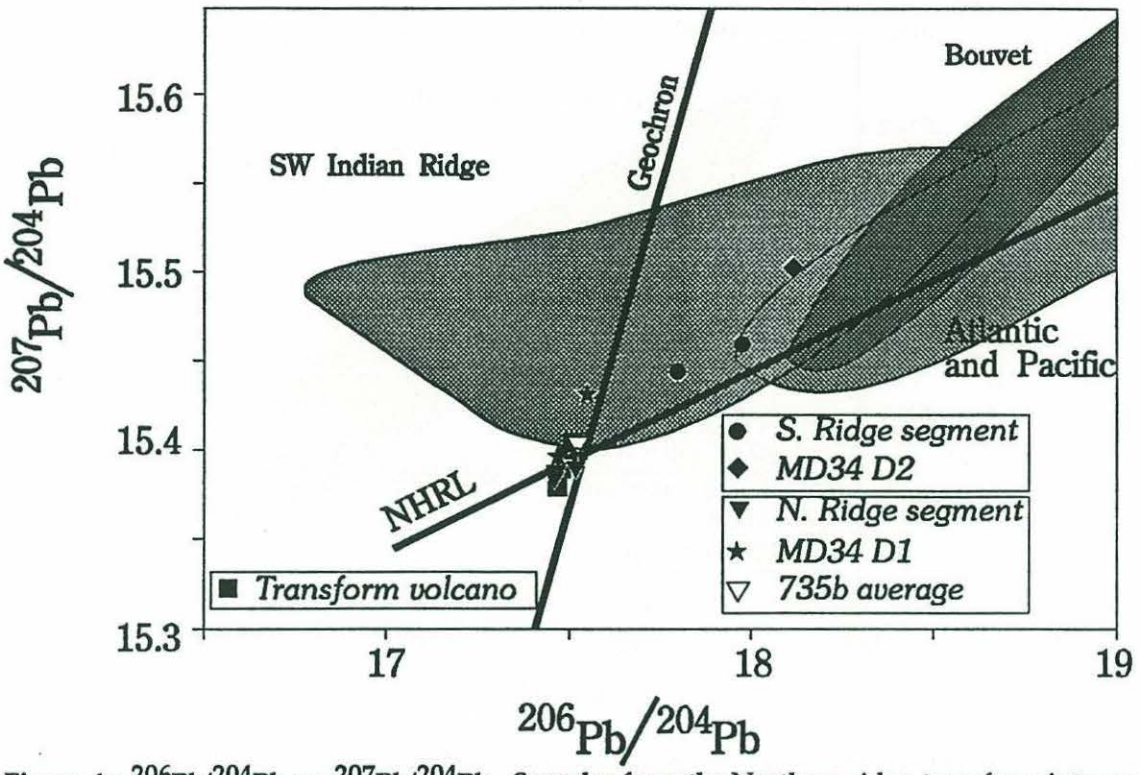

Figure 4a: $^{206}Pb/^{204}Pb$ vs. $^{207}Pb/^{204}Pb$. Samples from the Northern ridge-transform intersection (northern limb of the fracture zone) cluster strongly, except for one of the two published analyses of D1 (denoted with a star) (Hamelin and Allègre, 1983). NHRL denotes the Northern Hemisphere Reference Line (Hart, 1984). Data fields shown are data from Hamelin and Allègre (1985), Dupré and Allègre (1983), Michard, et al. (1986), Price, et al. (1986), Mahoney, et al. (1989) and Kurz, et al. (in press).

Northern Ridge

Figures 4a-c show the new analyses in this study for the northern ridge segment (filled triangles). The Sr and Nd isotopic compositions of these basalts are similar (Figure 4b). The Pb isotopic analyses (Figure 4a) are also nearly identical. The analyses differ from each other along a line whose slope suggests that the primary source of the difference is uncertainty in the measurement of ^{204}Pb. The position of the cluster of analyses in Pb isotopic space is also somewhat unique. Mid-ocean ridge basalt samples with $^{206}Pb/^{204}Pb$ falling to the left

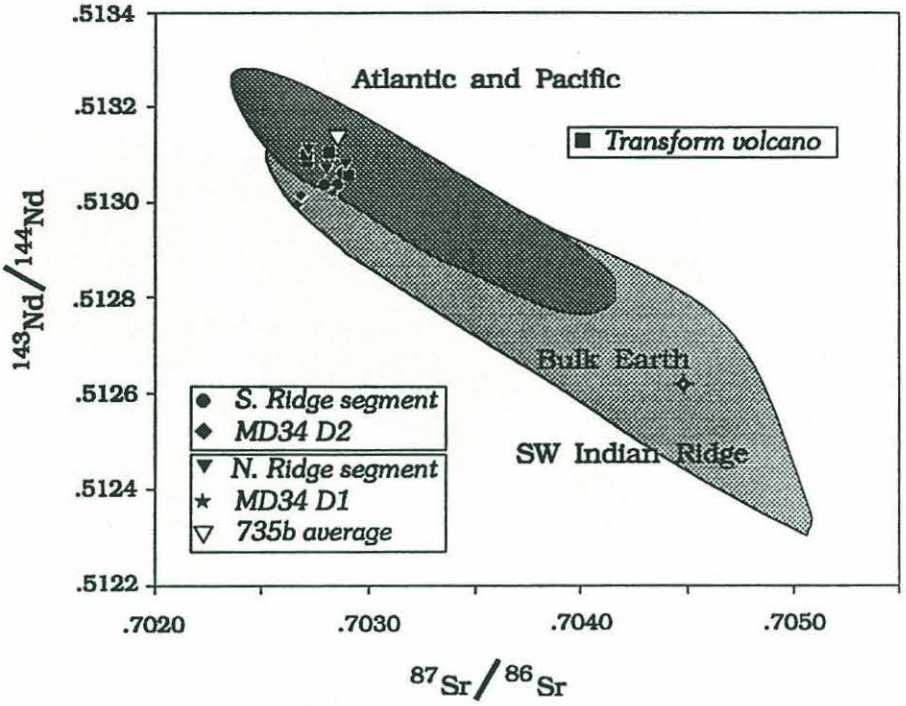

Figure 4b: $^{143}Nd/^{144}Nd$ vs. $^{87}Sr/^{86}Sr$. Symbols as in Figure 4a.

of the geochron in Pb-Pb space are quite rare. The Atlantis II Fracture zone basalts thus represent an extreme of Pb isotopic composition. They are similar to, but lower in $^{206}Pb/^{204}Pb$ and $^{207}Pb/^{204}Pb$ than the DMM (depleted MORB mantle) endmember of Hart and Zindler (1986). The complete spectrum of isotopic compositions seen in the Indian Ocean can be reproduced by mixing of endmember basalts of this composition with basalts derived from the various enriched endmembers (Zindler and Hart, 1986).

All the analyses from the northern ridge-transform intersection cluster tightly in their Pb, Nd and Sr isotopic compositions. It can readily be seen that the differences between samples are especially small compared to the total variation of SW Indian Ridge MORB (Figure 4a). Included in this grouping are the three new analyses from this study, two analyses from the center of the

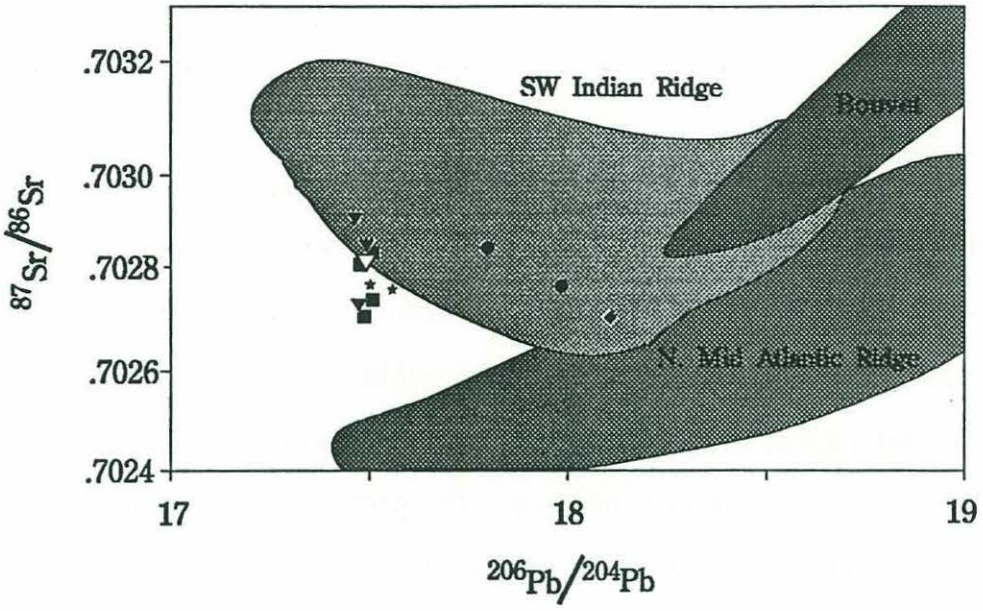

Figure 4c: $^{87}Sr/^{86}Sr$ vs. $^{206}Pb/^{204}Pb$. Symbols as in Figures 4a and b.

northern ridge segment (Hamelin and Allègre, 1985), and the average of 85 sample measurements on the gabbros in ODP hole 735b (Kempton, et al., 1991).

MD34-D1:

The MD34 sample (D1 in the notation of Hamelin and Allègre, 1985) is from the approximate center of the ridge segment abutting the Atlantis II Fracture Zone in the north. One of the two analyses of sample D1 they report falls within the cluster of analyses from this study. The other analysis of sample D1 differs from the first along a line with a slope of approximately 1 in $^{206}Pb/^{204}Pb$ vs. $^{207}Pb/^{204}Pb$ space. This slope suggests that the difference between the two analyses of the same sample is probably controlled by measurement error in ^{204}Pb. The two Pb isotopic analyses of this sample can thus be interpreted as having nearly the same isotopic composition, one which is nearly identical to the other samples from the northern ridge of the Atlantis II Fracture Zone.

Hole 735b

The gabbros of ODP leg 118, Hole 735b (von Herzen, Robinson, et al., 1991) provide, among other things, a unique view of the isotopic variability in a 500m. thick, *in-situ* section of oceanic Layer 3. The lithologic makeup of the 735b rocks ranged from fairly primitive olivine gabbros to evolved, oxide-bearing, Ti enriched ferrogabbros. The isotopic compositions of these gabbros (Kempton, et al., 1991) do not vary greatly, however. The primary magmas which mixed to form the 735b magma chamber(s) were probably isotopically uniform. This uniformity is consistent with the general isotopic uniformity seen in the basalts from the northern ridge segment of the Atlantis II Fracture Zone (Snow, et al., 1987; Kempton, et al., 1991 and this study). The $^{143}Nd/^{144}Nd$ ratios of the gabbros differ somewhat from those of the other studies (see Figure 4b), but this may be due to differences in inter-laboratory standard calibration, as different Nd isotopic composition standards were used for the Kempton, et al., study than for any of the other studies (Hamelin and Allègre, 1985; Snow, et al., 1987; this study). The difference between the data sets is quite small, smaller than the stated reproducibility of the Nd isotopic standard in Kempton, et al. (1991).

Observed in detail, it is difficult to make a case for any primary isotopic variability in the data set in Kempton, et al. (1991). In the 500m of cored gabbro, alteration effects control the Sr isotopic compositions of many of the samples. These are easily detected, having elevated $^{87}Sr/^{86}Sr$ but not a correspondingly low $^{143}Nd/^{144}Nd$. For the current purpose, these samples can be ignored. Ignoring the samples obviously affected by seawater, there are only two core sections which could possibly have been influenced by enriched magmas.

The first of these is the interval from 57-118 m. depth in lithologic unit II (the reader is referred to Robinson, von Herzen, et al., 1991 and the papers therein for the significance of these lithologic units). These samples are all hornblendes, except for one amphibole-bearing whole rock. All of them have elevated $^{206}Pb/^{204}Pb$ and $^{207}Pb/^{204}Pb$. The samples also have $\delta^{18}O$ values suggestive of seawater interaction, but they have $^{87}Sr/^{86}Sr$ which are near to the average for the rest of the section. In any case they do not exceed 0.7029. The Sr isotopic compositions of these samples seem to make it difficult to argue that seawater alteration accounts for the relatively high $^{206}Pb/^{204}Pb$ ratios (17.8-17.9) distinguishing these samples from the remainder of the samples from the northern ridge segment. Coexisting plagioclase from one of the samples (15R-1, 56-62; 57m. depth) has Pb, Nd and Sr isotopic compositions which are near to the 735b average listed in Table 3 of this Chapter. If a two-point Pb-Pb isochron is calculated from the whole rock and plagioclase of this sample, the resulting age is 2.2 billion years; a relatively meaningless result. This spurious age reflects the fact that the plagioclase in the sample cannot have been in isotopic equilibrium with the whole rock.

Taken together, the Pb isotopic compositions of the 57-118m samples, the mineral disequilibrium in sample 15R-1, 56-62 and the generally low $\delta^{18}O$ of the samples relative to the remainder of the core suggest that seawater exchange is responsible for the variations in their isotopic compositions. This interpretation is unexpected, in that the low $^{87}Sr/^{86}Sr$ of these samples does not seem consistent with seawater exchange. The seawater exchange could be explained on somewhat of an *ad hoc* basis if the concentrations of Pb in the hornblende and hornblende-bearing samples were very low and the concentrations of Sr very high. Exchange of Pb and Sr isotopes with seawater would then change Pb isotopic

compositions more readily than Sr isotopic compositions. In that case, the result would be a Pb isotopic composition which shows mixing with seawater and a Sr isotopic composition which does not. In the absence of concentration data for Pb and Sr in these samples, however, this is pure speculation.

The second core section which is indicative of possible primary variability is lithologic unit VI. The average Pb isotopic composition for this unit is essentially identical to the other units, but the average $^{87}Sr/^{86}Sr$ is higher and the average $^{143}Nd/^{144}Nd$ lower than the rest of the core. While the elevated $^{87}Sr/^{86}Sr$ could easily be ascribed to seawater exchange, the $^{143}Nd/^{144}Nd$ cannot. Nd is typically more concentrated in basaltic rocks and minerals relative to seawater than is Sr, so $^{143}Nd/^{144}Nd$ is much more resistant to alteration than is $^{87}Sr/^{86}Sr$. An equal volume of exchange will generally change Nd isotopic compositions less than Sr isotopic compositions. The lower Nd and higher Sr isotopic compositions of these samples must therefore be treated as real, and not due to some alteration process. One sample in particular (sample 85-6, 36-40) has a lower $^{143}Nd/^{144}Nd$ than the average for unit VI. The entire unit has an average $^{143}Nd/^{144}Nd$ (disregarding that sample) of 0.513122 which is lower than the mean of the whole core (0.513149). This difference is not greater than the stated between-run reproducibility quoted for that study of 0.000030. If there is a real difference in isotopic composition between this unit and the rest of the core, it is quite small, and is not outside the range for the other samples from the northern ridge segment (Snow, et al., 1987; Hamelin and Allègre, 1985 and this study). The 735b data (Kempton, et al., 1991) may be interpreted as having Pb, Sr and Nd isotopic compositions essentially identical to those of this study and those of Hamelin and Allègre (1985).

Transform Volcano

The basalts from the transform volcano define a vector in $^{206}Pb/^{204}Pb$ space which suggests that uncertainty in the determination of ^{204}Pb underlies the differences between the measured isotopic compositions. They otherwise have Pb, Nd and Sr isotopic compositions which are similar to each other (Figures 4a-c). The mean isotopic composition of the transform volcano basalts is also similar to those from the remainder of the northern ridge segment (Hamelin and Allègre, 1985, Snow et al., 1987, Kempton, et al., 1991 and this study), suggesting that they were derived from a mantle whose time-integrated U/Pb, Th/Pb, Rb/Sr and Sm/Nd ratios were similar to each other. The relative isotopic homogeneity of the basalts from this region is somewhat of an anomaly, because in most other parts of the Southwest Indian Ridge isotopic variability is common (le Roex, et al., 1983; 1985; 1989; 1992) and is often extreme, even in a single dredge haul.

Southern Ridge

The southern ridge is not nearly as well sampled as the northern ridge. The three samples from the southern ridge-transform intersection show a much more radiogenic and much more variable Pb isotopic signature than those from the northern ridge segment. The two new analyses are significantly different from each other in their Pb isotopic compositions and are both clearly different from the one sample (MD34:D2) from the southern ridge segment analyzed by Hamelin and Allègre (1985). None of the southern samples fall outside the field defined for SW Indian Ridge MORB in that study. Nd and Sr isotopic compositions for the southern ridge segment are nonetheless quite similar to one another.

There is a marked contrast across the fracture zone, not only in the Pb isotopic compositions, but also in the degree of Pb isotopic variability seen in the basalts. The Pb isotopic composition of the southern ridge segment is not only more radiogenic than that of the northern ridge segment, it is also more variable. The southern ridge segment shows almost half the total isotopic variation seen on the South West Indian Ridge just in three extant analyses. This variability is in keeping with the generally quite variable isotopic data for individual ridge segments from the whole of the ridge (Dupré and Allègre, 1983; le Roex, et al., 1983; Hamelin and Allègre, 1985; le Roex, et al., 1985; Price, et al., 1986; Michard, et al., 1986; le Roex, et al., 1989; Mahoney, et al., 1989; le Roex, et al., 1992), but is quite a contrast to the Pb isotopic uniformity of the northern ridge segment.

The Nd and Sr isotopic data, by contrast, show little variation across the fracture zone, as can be seen in Figure 4b. This is true along the entire length of the SW Indian Ridge. Away from such obvious geochemical anomalies as Marion-Prince Edward, Bouvet and the 11° East area (le Roex, et al., 1983; le Roex, et al., 1985; le Roex, et al., 1992; Kurz, et al., in press), Nd and Sr isotopic compositions on the Southwest Indian Ridge cluster around $^{87}Sr/^{86}Sr = .7028$ and $^{143}Nd/^{144}Nd = .5130$.

Discussion

The Transform Fault Effect: possible false signals.

Langmuir and Bender (1984) examined the evidence for transform fault effects at several fracture zones for which major element and/or trace element data were available. All of the fracture zones studied showed shifted liquid lines of descent near the transform which were consistent with a transform edge effect. They also mentioned three important assumptions which must be made when comparing liquid lines of descent in basalts from oceanic rift systems: tectonic setting, source heterogeneity and fractionation history. The following sections will discuss these assumptions and their relevance to the Atlantis II Fracture Zone data set.

Tectonic setting

In an investigation of transform fault effects, the tectonic setting of the basalts is an important factor in their melting history. Basalts erupted from ridge segments near to off-axis or on-axis seamounts often show differences in degree of melting and in the composition of their mantle source (Batiza and Vanko, 1984; Hanan et al., 1986; Kurz et al., in press). For this reason, the tectonic setting of basalts used to study transform fault effects must be well characterized with regard to their position relative to major tectonic features. These include hot spots, propagating rifts, DEVALs (deviations from axial linearity), and other tectonic anomalies. Such features could interfere with the thermal or compositional makeup of the mantle at the fracture zone.

An example of the interference of tectonic and geochemical signals can be found at the Tamayo Fracture Zone (Bender, et al. 1984). A seamount in the area of the ridge far from the fracture zone (approximately 50 km.) shows a distinct chemistry from that of the basalts from the swell, rift or transitional regions. The major element data further suggest that mixing between the isotopically distinct source composition of the seamount samples and that of the swell samples played a role in the formation of swell region. Isotopic studies which would establish or rule out the presence of an influence of plume-related magmas in the genesis of the rift or swell magmas have not been published.

There are many other factors involved in transporting a magma from the mantle to the point of sampling on the ocean floor. These physical transport processes could cause misinterpretation of geochemical evidence for or against the presence of a transform fault effect. These include lateral transport of magma in the crust down a rift system, and faulting and mass wasting in the rift valley all of which can juxtapose basalts of different age and mantle provenance.

The impossibility of precisely knowing the geologic context of a sample plagues many studies of ocean floor volcanic rocks. There are particular problems when identifying possible transform fault effects. The interpretation of the data is critically dependent upon the proximity of the melting region of the basalt to the fracture zone. Such an effect could obscure a transform fault effect if basalt flows originating from near the fracture zone were intercalated with flows of basalt transported down the rift system from a more distant portion of the ridge. This hypothetical example points out that good geologic and tectonic control of the samples is important for the identification and evaluation of a transform fault effect. The geologic setting of the transform valley samples dis-

cussed in the introduction precludes their having originated from a laterally extensive fissure eruption in the rift valley.

Source mixing

Variations in the mixing of depleted mantle endmembers with enriched ones can produce a false transform edge effect as great in magnitude as any true effect yet proposed. An excellent example of this is the fracture zone at 43°N on the Mid-Atlantic Ridge which was an example of this problem in Langmuir, et al. (1984). The light rare-earth element enriched basalts there have been found to be the result of mixing of an enriched mantle endmember with a depleted one. The degree of enrichment increases as the fracture zone is approached, and would indicate a huge transform fault effect in the absence of isotopic data (White and Schilling, 1978). Source mixing considerations as detected by isotopic analysis would render many fracture zones inappropriate for the study of transform edge effects. These include 43°N, just mentioned, the Oceanographer Fracture Zone (Shirey, et al., 1987) and the 15°20'N Fracture Zone on the mid-Atlantic Ridge (Dosso, et al., 1991).

In order to detect source heterogeneity, studies purporting to show a transform edge effect must include isotopic information to detect the influence of regions of mantle which have been enriched in incompatible trace elements for a long period of time. In order for isotopic information to be permissive of a relatively uniform mantle composition, the basalts near to the transform and those far from the transform must have at least similar isotopic signatures. This stipulation invalidates all but one of the cases studied by Langmuir and Bender (1984). That example cites isotopic data for samples from the Tamayo fracture zone (Bender, et al., 1984) which do not appear in the cited paper. There are no

published isotope data accompanying any of other the fracture zones studied in Langmuir and Bender (1984) except for the Kane fracture zone (Machado, et al., 1982). In that case, the sampling was not sufficiently complete to evaluate differences in mantle source both close to the transform and far from it.

Fractionation history

The apparent degree of melting of a MORB sample can be influenced by its fractionation history, even at low pressure. Two crustal level effects are capable, in theory, of disturbing the liquid line of descent of a magma series. First, the mixing of evolved lavas with more primitive lavas will mimic a crystal fractionation trend with a different slope. The new trend will be offset from the original liquid line by a degree determined by the curvature of the liquid line of descent in the particular space being examined. In Ca/(Ca+Na) vs. Mg/(Mg+Fe) space, the liquid line of descent of a basaltic liquid crystallizing only olivine at low to moderate pressure takes a downward turn when the olivine-plagioclase cotectic is reached. Given two liquids derived from identical sources, one of which has crystallized significant plagioclase and the other of which has not, the mixture of these two liquids will appear to have been derived from a source richer in Na_2O (lower Ca/(Ca+Na)) than either of the two original liquids.

Polybaric crystallization is a second possible crustal-level effect which can complicate the comparison of liquid lines of descent. The pressure of crystallization has a strong effect both on the phase appearances and on the solid solution compositions in a fractionating lava, and thus on the shape of the resulting liquid line of descent. Two identical primary magmas fractionating at different pressures will result in liquid lines of descent which may not be parallel in com-

position space. Relating two such magma series to parental liquids is exceedingly difficult. For this reason, liquid lines of descent calculated for different magma series should only be compared if their fractionation histories are believed to be similar. Given that the point of this investigation itself postulates a different thermal regime for the near-transform region than for the region far from the transform, this condition may be impossible to satisfy. At the very least, it is reasonable to require that observed liquid lines of descent be parallel, except for an offset which could be reasonably ascribed to the degree of melting. This would imply similar liquidus phase assemblages for the two groups of basalts.

In many of the regions investigated by Langmuir and Bender (1984), as in this study, liquid lines of descent defined for the regions near and far from the fracture zone are parallel (as at Kane North and Tamayo). This suggests that the phase proportions fractionating are similar and thus that the conditions of fractionation are similar. Data sets from Langmuir and Bender (1984) that fail that test are Kane South (Langmuir and Bender, 1984, Fig. 3B) and Charlie Gibbs south (Langmuir and Bender, 1984: Figure 4A). In the latter two cases, the trends of TiO_2 vs. MgO intersect within the field of the data. This implies that the proportions of phases segregating from the melt which define the liquid lines of descent for those rock suites are quite different.

The transform edge effect has become part of the litany of possible effects which are commonly cited to account for variations in crustal thickness (Fox, et al., 1980) and in basalt composition seen near to fracture zones (Natland and Melson, 1980; Perfit, et al., 1983; Bender, et al., 1983; Langmuir and Bender, 1984). A case can be made that there has not yet been a definitive demonstration of a transform edge effect. No study so far has addressed the isotopic, geologic

and petrologic issues necessary to rule out the effects of mantle source variability and lateral magma transport in the crust.

The case for the Atlantis II fracture Zone

The Atlantis II Fracture Zone represents a limiting case for the detection of a transform fault effect for the following reasons. First, the age offset is very large. At 22 million years, the age offset across the Atlantis II Fracture Zone is twice that at the Kane Fracture Zone and more than fifteen times that at Tamayo. The great age offset implies that the cold lithosphere on the opposite side of the transform from the rift valley is older and colder at the Atlantis II Fracture Zone than at any other well-studied fracture zone. Basalts from near the Atlantis II Fracture Zone should exhibit a particularly large compositional effect relative to other fracture zones. Second, the Atlantis II Fracture Zone is far from any mantle plume or hot spot, so the mantle near the fracture zone should have a fairly uniformly depleted mantle source composition. Third, the geology of the fracture zone strongly constrains the point of upwelling of the transform volcano samples. The ability to sample basalts from the transform volcano, which unambiguously erupted in the transform domain, seems to preclude their having been diluted by lavas from the main rift system.

Lastly, the isotopic compositions of the transform volcano and the northern ridge-transform intersection basalts are similar. This implies that variations in source composition are not responsible for the observed variations in the composition of those two basalt suites. All of the factors just mentioned should serve to maximize the signal of the transform fault effect seen in the basalts and to minimize the noise. The shift in observed basalt compositions due to a transform edge effect at the Atlantis II Fracture Zone should thus be the largest

yet studied. This limiting case should shed light on the magnitude of the transform edge effect relative to other mid-ocean ridge petrogenetic processes.

A strong qualitative case can be made for the existence of a transform edge effect at the Atlantis II Fracture Zone. The offset of trends in both Ca-number vs. Mg-number space and in the CIPW normative ternary both indicate lower degrees of overall melting, as shown in Figures 2 and 3. As will be seen in the next section, several other well-formulated measures of overall degree of melting agree in this respect. The isotope dilution trace element data in Table 2 do not provide strong evidence either way. Since the issues of mantle heterogeneity and geologic provenance have been adequately addressed, the major element data provide *prima facie* evidence for the existence of a transform fault effect.

Assessing a mantle temperature change

Using the data in Kinzler and Grove (1992, a, b), a method can be devised for *semi-quantitatively* estimating the temperature offset represented by a shifted liquid line of descent. This involves a linearization of the fractionation relationships of the 10 major elements, and an estimation of the compositional shift caused by a given mantle temperature shift. Such an inverse technique can be expanded substantially in sophistication if the fundamental approach proves useful.

If differences in melting are to be inferred from two basalt suites, the effects of fractional crystallization must be corrected to some degree. The correction applied here requires the assumption that liquid lines of descent conform to a first approximation to the fractionation model developed by Grove, et al.

(1990) and calculated in Kinzler and Grove (1992). A second assumption is that mantle source compositions do not differ between the basalt suites. It is then possible to estimate the temperature difference required to produce a given shift in the corrected compositions of the basalts. This is done using a melting model which aggregates the compositions of liquids produced at varying pressures in a column of ascending mantle. The model also incorporates a finite efficiency of melt extraction (Kinzler and Grove, 1992a, model 3).

The reader is referred to Kinzler and Grove (1992a) for the details of their melting model. The model is summarized here briefly, since it is the basis for most of the semi-quantitative analysis of temperature differences between basalt suites. Their model proposes a mantle column geometry, with melt generated and extracted at all levels in the column. As the column of model mantle rises adiabatically, it melts at a rate of 1% per kbar. Following melting of each increment, 90% of the melt is extracted and aggregated. 10% of the melt (or 0.1% by weight of the residue in each increment) is retained in the matrix. The potential temperature of the mantle (temperature extrapolated adiabatically to the surface) and the starting composition of the mantle are given. In the present study, a fixed starting composition was used (Hart and Zindler (1986) depleted 1, discussed in Kinzler and Grove (1992b)). The melting model predicts the pressure range of melting, and the compositions of instantaneous and aggregate melts, in a manner analogous to that of McKenzie (1984) and McKenzie and Bickle (1988), but with different results.

The differences between Kinzler and Grove, 1992 and McKenzie and Bickle (1988) are due partly to differences in the melting models used. McKenzie and Bickle (1988) is a purely equilibrium polybaric batch melting model, while Kinzler and Grove (1992) is an incremental batch model. Their model is much

closer to the near-perfect polybaric fractional melting required by trace element studies of the residues of mantle melting (Johnson, et al., 1990; Johnson and Dick, 1992). The remainder of the differences are in the much more extensive and more critically selected data set used in Kinzler and Grove (1992) to provide the major element inversion which forms the basis of their forward model.

The experimental data of Kinzler and Grove (1992a) are encapsulated by the forward melting models of Kinzler and Grove (1992b). The near-adiabatic, near-fractional polybaric melting model used there provides a model for the relationship between the mantle potential temperature and the compositions of primary liquids. This relationship may not reflect reality, but it does reflect melting relationships observed in experiments under the conditions of pressure, temperature and composition at which melting is thought to occur in the mantle. For that reason, they are a good starting point for discussion of temperature effects on aggregate melts from a given starting composition.

In order to address the differences in composition of primary melts for a given magma series, it is necessary to remove the effect of crystal fractionation as much as possible. Typically, a compositional parameter is selected which is little affected by melting, but greatly affected by fractional crystallization. A second compositional parameter is chosen which is affected as little as possible by fractional crystallization, and as much as possible by melting. The first parameter is then used to extrapolate the second parameter back to some reference value of the first along a liquid line of descent. This procedure is implicit, for example, in the comparison of shifts in the normative Pl-Px-Ol liquidus trends at 10% normative olivine by Dick, et al. (1984). It is also implicit in the $Na_{8.0}$ and $Fe_{8.0}$ calculations of Klein and Langmuir (1987; 1989). In that study, Na and Fe are corrected for fractional crystallization to an MgO content of 8.0 weight percent by

means of an empirical liquid line of descent which fit many of the observed basalt suites.

This approach can be extended to any element or parameter pair in which one is more sensitive to melting than the other, even if both are affected by fractional crystallization. First the melting-sensitive element for a given sample is extrapolated along a liquid line of descent (real or assumed) to a reference value of the melting-insensitive element. The corrected value of the melting-sensitive element is then calculated. The difference in the means for two basalt suites under comparison then reflects the difference between their primary liquids. It is then possible to estimate the difference in mantle potential temperature required in the Kinzler and Grove (1992b) model to produce that shift in the melting-sensitive parameter. Several pairs of compositional data will now be examined and used to calculated estimated temperature shifts for the Atlantis II Fracture Zone data set in order to illustrate the approach.

$\underline{K_2O/TiO_2 \text{ vs. } Mg/(Fe + Mg)}$

Using the approach outlined above, it is possible to make a semiquatitative correction for crystal fractionation and an estimate of the magnitude of the mantle potential temperature shift across the transform. Potassium is highly incompatible, while titanium is only moderately incompatible. The ratio of these two elements is strongly affected by partial melting in the mantle, but it is relatively insensitive to fractional crystallization of mid-ocean ridge basalt liquidus phases at low and moderate pressures. Mg/(Mg+Fe) shows the opposite relationship; it is only slightly affected by partial melting and is strongly affected by crystallization. The result is that melting and crystallization vectors are nearly orthogonal in K_2O/TiO_2 vs. Mg/(Fe + Mg) space.

Figure 5 shows the melting and fractional crystallization relationships for the K_2O/TiO_2 vs. Mg/(Fe + Mg) parameter space. Figure 5 also shows the major element data from the Atlantis II Fracture Zone. Extrapolating a given basalt composition back to a primary melting vector is quite easy. As Figure 5 shows, the slope of fractionation vectors in this diagram is nearly zero, so that little correction is necessary. Other element pairs are not so well behaved, however, so a correction algorithm is necessary, using the following procedure.

In general, we wish to extrapolate individual analyses back along their fractionation paths to the intersection point with a reference vector which is parallel to a melting vector. This allows differences in the primary concentration to be evaluated. If the reference melting vector is steep (as with Na_2O vs. MgO or K_2O/TiO_2 vs. Mg/(Fe + Mg)) a vertical vector may be used. This is the approach taken by Klein and Langmuir (1987; 1989). The following general calculation will be carried through for each element pair examined here. Given a melting vector:

$$Y = C_m + M_m X \qquad (1)$$

where Y is the element on the Y axis, X is the element on the X axis, C_m is the constant and M_m is the slope of the line. We wish to know the intersection of that vector with a fractionation line passing through our $(\tilde{x}, \tilde{y})$ analysis. Using the point-slope equation gives:

$$Y - \tilde{y} = M_f(X - \tilde{x}) \qquad (2).$$

Combining these equations results in

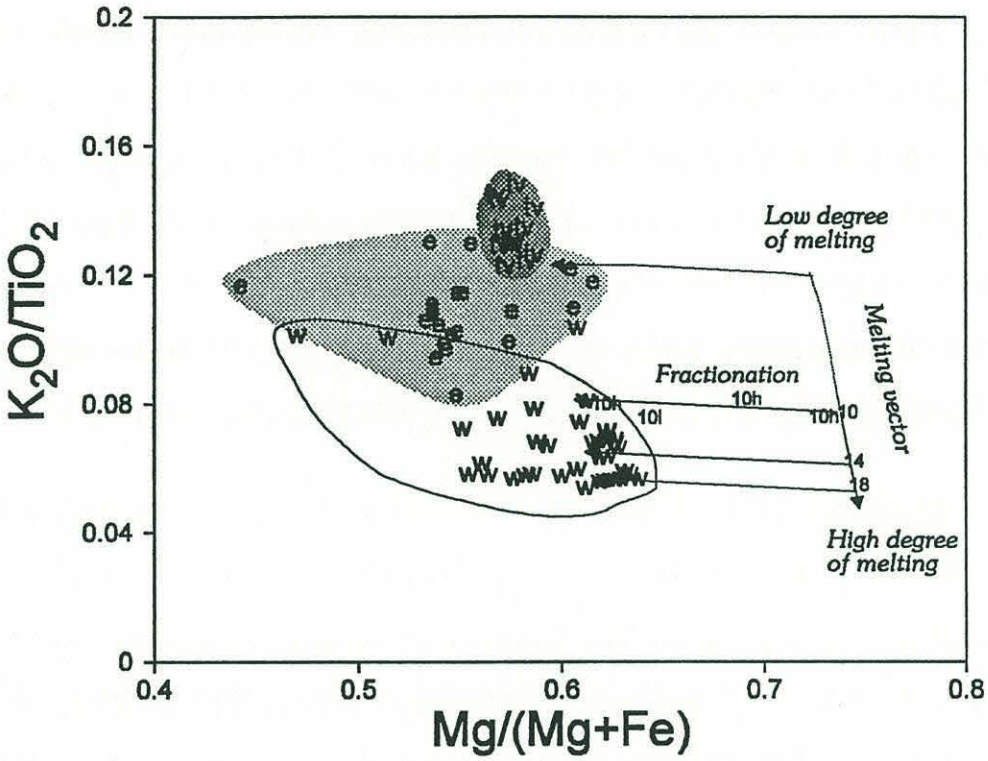

Figure 5: K_2O/TiO_2 vs. Mg/(Mg+Fe) for Atlantis II Fracture Zone basalts and Model liquids. Model data are from Kinzler and Grove (1992b). The numbers 10, 14 and 18 denote the percentage of melt in their Model 3. 10l and 10h show the trajectory of liquids undergoing low and high pressure fractional crystallization, respectively.

$$X = \left(\frac{\tilde{y} - C_m - M_f \tilde{x}}{(M_m - M_f)} \right) \qquad (3)$$

and Y is found by back-substitution in (1) above. The value of C_m is arbitrary, as any value will give the same relative result as long as fractionation trends are parallel. For K_2O/TiO_2 vs. Mg/(Mg+Fe), the following constants can be calculated from the Kinzler and Grove (1992b) fractionation and melting model data: $M_f = -0.2138$; $M_m = -4.27813$; $C_m = 3.2464$. These constants simply express the

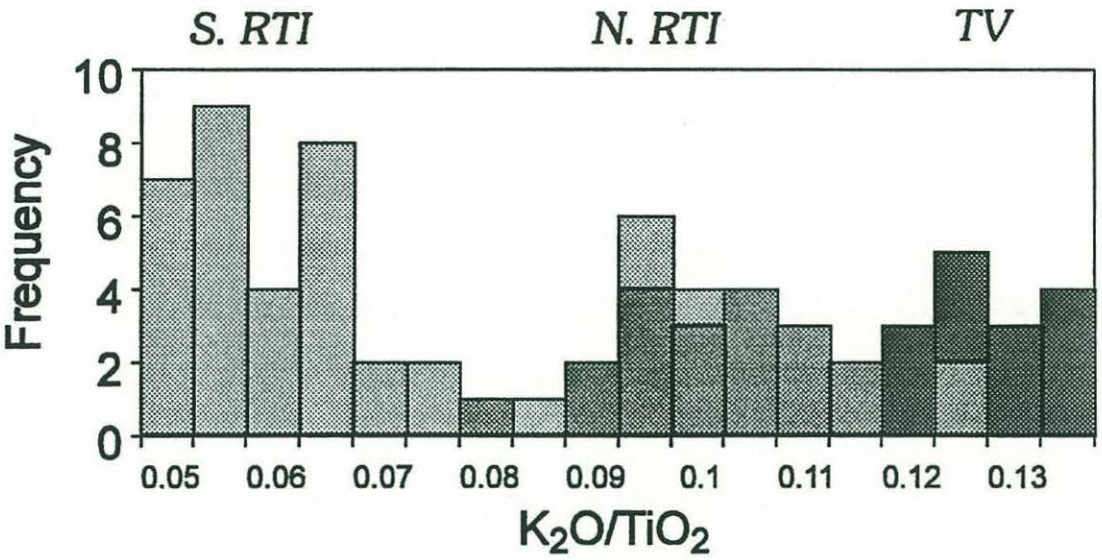

Figure 6: Fractionation-corrected K_2O/TiO_2 histogram for Atlantis II Fracture Zone basalts. The basalts from the three geologic areas plot in distinct groupings which can be related by differences in partial melting. The southern ridge-transform intersection, northern ridge-transform intersection and transform volcano analyses are denoted by light, medium and heavy shading, respectively.

slope and intercept of the melting vector shown in Figure 5 and the slope of the fractionation vectors.

Using Equations (2) and (3), a corrected K_2O/TiO_2 can be calculated for each Atlantis II Fracture Zone basalt. The results are shown in a histogram in Figure 6. Means can be calculated for the corrected K_2O/TiO_2 values for the northern ridge basalts and the transform volcano basalts. Their difference is -.0256 $\pm$ .00473 (18%). The uncertainty (standard error of the mean) is meant to express the significance of the difference between the two liquid lines of descent. It is not intended to express the uncertainty in the temperature shift calculated from that difference, which is subject to yet another layer of model-dependent uncertainty.

Once the fractionation correction is made, the Kinzler and Grove (1992a) data can then be used to draw inferences about the melting history of the two groups of basalts. In their Model 3, the K_2O/TiO_2 of primary liquids goes down by 0.01 for each 70.2 °C increase in the potential temperature of the mantle. In the remainder of this work similar relationships will be denoted as follows: $\partial T/\partial(K_2O/TiO_2) = -7023°C$. Since K_2O/TiO_2 is a ratio it has no units. The partial derivative of temperature with respect to K_2O/TiO_2 thus has units of °C. Using this relationship, the shift in mantle potential temperature required to produce the observed mean shift in the K_2O/TiO_2 can be estimated at 179 degrees. As we will see, this is higher than most of the other estimates of temperature drawn from other element pairs.

With K_2O/TiO_2, the correction for fractionation is quite simple, since the fractionation and melting vectors are nearly orthogonal in this plane. Most other ways of looking at basalt data do not share this characteristic. The procedure outlined above for K_2O/TiO_2 will now be carried out for a variety of basalt compositional parameters. As will be shown, some of these have more predictive power than others.

TiO_2 vs. MgO

Langmuir and Bender (1984) use this element pair to assess the evidence for transform edge effects at various fracture zones. The application of the procedure above is quite straightforward. Figure 7 shows the melting and fractionation relationships from Kinzler and Grove (1992b). The following constants can be derived from Kinzler and Grove (1992b): $M_f = -0.1565$; $M_m = -0.88$; $C_m = 1.92$. Performing the correction calculation on each of the Atlantis II Fracture Zone basalts and calculating means for the northern ridge and

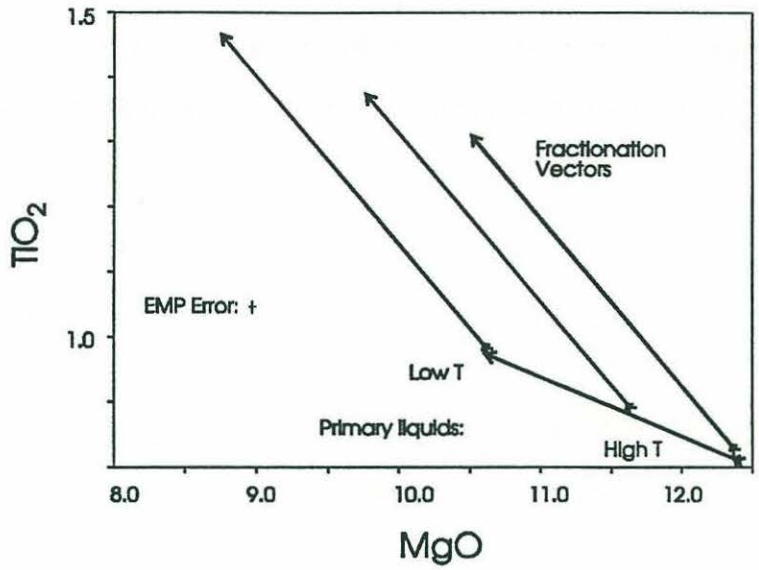

Figure 7 : TiO_2 vs. MgO model liquid calculation. Linearized model data are from Kinzler and Grove (1992).

the transform volcano results in a mean difference of -0.253 Wt. % TiO_2 between the northern RTI basalts and the transform volcano basalts, with a standard deviation of the mean of 0.1034 (40%).

Using the melting data from Kinzler and Grove (1992) the slope of the relationship $\partial T/\partial TiO_2$ can be calculated at -994 °C/Wt. %TiO_2. Multiplying the Δ TiO_2 just calculated by this value yields a temperature difference of 251 degrees between the transform volcano and the northern RTI. The large uncertainty quoted above for this calculation can be attributed to the small amount of leverage that mantle potential temperature has on TiO_2. There is also a significant overlap in the two sample populations in this projection of composition space. This uncertainty is a minimum estimate of the uncertainty in the temperature calculation. It suggests that this calculation should not be interpreted as having strong predictive value as to the presence or absence of a transform edge effect. This particular combination of elements cannot provide strong evidence for a

transform edge effect or against one in this case, though the result is suggestive of one. The procedure can be applied, however, to any element pair.

Ca/(Ca+Na) vs. Mg/(Mg+Fe)

The Ca/(Ca+Na) vs. Mg/(Mg+Fe) diagram (Figure 2) is particularly useful in estimating the mantle potential temperature differences between two related liquid lines of descent. The calculation is simplified somewhat due to the near vertical slope of the melting line in this diagram (the actual value of the slope is 11.08; see Figure 2). The near orthogonality of the fractionation and melting vectors reduces the error magnification inherent in the extrapolation. It also reduces the sensitivity of the correction to model dependent errors (such as mis-estimates of melting slopes). Melting also has more leverage on Na than on Ti relative to their respective uncertainties.

The relevant constants from Equations 1-3 are as follows: Cm = -7.39; Mm = 11.08 and Mf = 0.18. Carrying out the projection to the melting vector, we calculate a corrected Ca/(Ca+Na) for each sample and average them by geographic group. The difference in Ca/(Ca+Na) between the means of the fractionation corrected analyses of the transform volcano basalts and the northern RTI basalts is $-.0147 \pm .0044$. We can derive a value for $\partial T / \partial(Ca/(Ca+Na))$ from Kinzler and Grove (1992) of 2655 °C. Since the calcium number is a ratio, it has no units, and thus the partial derivative of temperature with respect to Ca number has units of degrees centigrade. An increase in Ca/(Ca+Na) of 0.01 would be the result of a mantle potential temperature increase of 26.5°C. Correcting the basalt compositions for fractionation and averaging the northern ridge segment and

transform volcano basalt data for the Atlantis II Fracture Zone results in a mean temperature difference of 39 °C. This is a much lower estimate than was provided by the TiO_2 - MgO estimation and the K_2O/TiO_2 vs. Mg/(Mg+Fe) estimation. The formal uncertainty is much better, though not as small as the K_2O/TiO_2 vs. Mg/(Mg+Fe) uncertainty. Given the substantial uncertainty in the TiO_2 - MgO calculation, the numbers are not far out of agreement with each other.

CIPW normative Pl-Px-Ol ternary.

The CIPW Pl-Px-Ol ternary (Cross, et al., 1903) has distinct advantages over many of the other ways of viewing multi-element data for basalts. It maps all 10 elements in a basalt analysis into three components whose meanings are well known to most geologists. Bryan and Dick (1982) and Dick, et al. (1984) used this same projection to distinguish liquid lines of descent from different localities. Consanguinous basalts tend to plot on a single line on this diagram, nearly parallel to the slope of the olivine-plagioclase cotectic. Moreover, Dick, et al. (1984) showed that the composition of spatially associated residual mantle peridotites have a complementary shift to that of the basalts in this projection.

Bryan and Dick (1982) decline to make a definitive statement regarding the relationship between melting, fractionation and the position of individual basalt analyses along cotectic lines. They note that since the CIPW normative ternary is a projection of many elements into two dimensions, points on the diagram are nonunique. Basalts with quite different histories can plot at the same point on this diagram due to compositional differences. These compositional differences, particularly those relating to source composition, are not well differentiated on this diagram. In that study, basalt suites were compared from the

entire length of the mid-ocean ridge. Significant source heterogeneity between suites was both expected and found.

The current study is a case of spatially related basalt suites, where the compositional differences between the sources of the suites is assumed to be small. Some generalization about melting and fractionation trends in the CIPW normative Pl-Px-Ol ternary is thus appropriate. In cogenetic suites, more primitive compositions typically plot on the end of the cotectic closer to the Ol-Pl edge and evolve toward the Pl-Px edge (Bryan and Dick, 1982). The plagioclase content often decreases somewhat with progressing fractionation. This is consistent with olivine fractionation followed by simultaneous olivine + plagioclase fractionation. The slight curvature of the various liquid lines of descent away from the plagioclase apex (Bryan and Dick, 1982) is also consistent with these phase appearances.

One useful feature (for my purpose) of the CIPW normative Pl-Px-Ol ternary is that the major axis of the error ellipse for electron microprobe analyses of basalt glasses is colinear with the trend produced by fractional crystallization (see the more thorough discussion of this topic in Appendix IV). The melting vector has a strong component in the direction normal to the fractionation vectors, as is apparent in Figure 8. This simplifies the task of computing a temperature offset enormously. The temperature offset in this diagram can be calculated as a direct function of the plagioclase content of the melt. When norms are calculated for the melting model data of Kinzler and Grove (1992b), the slope of normative plagioclase content with respect to mantle potential temperature can be estimated at $\partial Pl/\partial T = -0.0189$ Wt. % /°C.

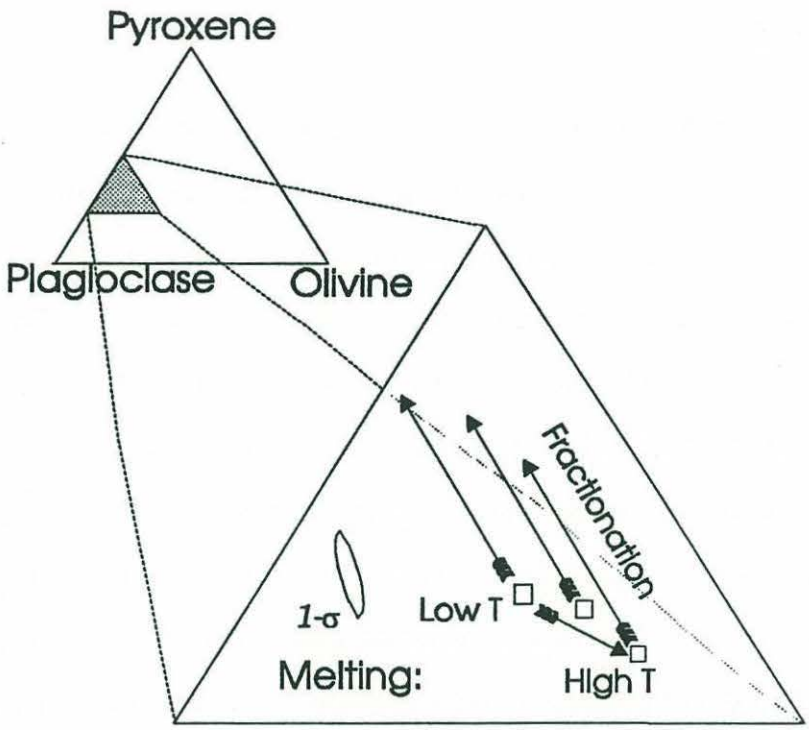

Figure 8: Fractionation and melting vectors in the CIPW normative Pl-Px-Ol ternary. Data are from Kinzler and Grove (1992), averaging low and high pressure fractionation paths to show the general trend.

In the case of the Atlantis II Fracture Zone, the difference in normative plagioclase between the transform volcano ($\bar{x}$ = 60.84, σ_{mean}= .078) and the northern ridge-transform intersection basalts ($\bar{x}$ = 58.7, σ_{mean}= .18) is 2.1±.3. The uncertainty in the difference is quoted not in order to claim a precision for the final result, but to emphasize that the shift in normative plagioclase is clearly significant for this set of samples. Dividing through by $\partial Pl/\partial T$, the result is a temperature difference of 111 °C. This result is higher than the result from the Ca# vs. Mg# diagram, but it is much more reliable than the TiO_2 - MgO estimate. This estimate compares in reliability to the one derived from the Ca# vs. Mg# plot in that it has some meaning, as compared to the estimate from TiO_2 - MgO, which has little.

$\underline{Na_{8.0}}$ vs. $\underline{Fe_{8.0}}$

Na_2O and FeO contents of rocks with different degrees of fractionation can be corrected to a constant degree of fractionation for the purpose of comparing their degree of melting (i.e. mantle potential temperature). This is done in the same way as demonstrated in the preceding three sections. The $Na_{8.0}$ and $Fe_{8.0}$ calculations introduced by Klein and Langmuir (1987) are intended to accomplish this same objective. In this they are similar to those used by Bryan and Dick (1982), Dick et al. (1984) and Langmuir and Bender (1984). Figure 9 illustrates the melting and fractionation relationships in the $Na_{8.0}$ vs. $Fe_{8.0}$ diagram, as well as the Atlantis II Fracture Zone basalt glass data. If $Na_{8.0}$ and $Fe_{8.0}$ were truly independent of fractional crystallization, the fractionation vectors in this diagram would be short or non-existent. The data from the transform volcano, the northern ridge segment and the southern ridge segment fall in elongate fields parallel to fractionation trends predicted by Kinzler and Grove (1992). This implies that the $Na_{8.0}$ vs. $Fe_{8.0}$ diagram is not fractionation-independent for natural or experimental systems (Klein and Langmuir, 1987; 1989 notwithstanding). Figure 9 seems to indicate that the "local trends" of Klein and Langmuir (1989) are in fact fractional crystallization trends.

The lack of fractionation-independence in the $Na_{8.0}$ vs. $Fe_{8.0}$ diagram makes it amenable to the same treatment as in the preceding sections. The slopes of melting vectors in this diagram result in the following constants: Cm = 4.202; Mm = -0.06554; Mf = .3258. The calculation in Equation (3) is then carried through on the Atlantis II Fracture Zone basalts, resulting in a difference in corrected $Fe_{8.0}$ of 0.569 ± 0.166 Wt. percent. Returning once again to Kinzler and Grove (1992), the relationship $\partial Fe_{8.0}/\partial T$ is 0.0250 /°C. Dividing through results in a temperature estimate of 23 °C for the transform edge temperature shift. This

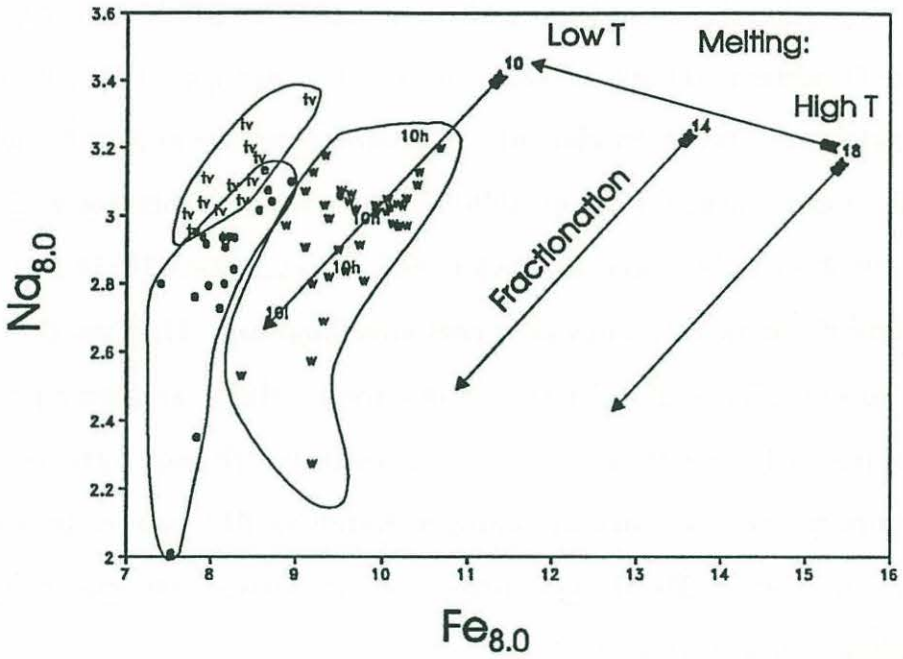

Figure 9: $Na_{8.0}$ vs. $Fe_{8.0}$. Shown in this diagram are the basalt analyses from the Atlantis II Fracture Zone and the melting model and fractionation models of Kinzler and Grove (1992b). The numbers 10, 14 and 18 at the bases of the fractionation arrows refer to the total extent of melting in the model mantle column which produced the model basalts. The numbers 10h and 10l are varying extents of high- and low pressure fractionation respectively.

is the lowest of the temperature estimates. The parameter difference used to calculate the temperature has about the same formal error (±30%) as the Ca# - Mg# estimate.

Rare Earth Elements

Rare earth elements are potentially sensitive indicators of partial melting processes in the mantle. Their ratios can be changed during mantle partial melting and aggregation processes (Johnson, et al., 1990), but are little affected by fractional crystallization beneath mid-ocean ridges, or by alteration effects on the sea floor. Figure 10 shows the Ce/Sm ratio in Atlantis II Fracture Zone basalts (Johnson and Dick, 1990), normalized to the chondritic ratio and plotted

against $Fe_{8.0}$. Also shown on Figure 10 are incremental batch melts calculated using the D values and melt modes adopted by Johnson, et al. (1990). An incremental batch equilibrium model with 1% melt increments and 0.1% melt retention in the solid is used for compatibility of data between this study, Grove and Kinzler (1992b) and Johnson and Dick (1992). The numbers 10, 14 and 18 in Figure 10 have the same meanings as in previous diagrams. They are the compositions of liquids calculated at 10, 14 and 18% total melting, at mantle potential temperatures of 1315, 1395 and 1475 °C respectively. The solid arrow represents those compositions calculated assuming a chondritic REE pattern for the mantle starting composition. The dashed arrow, for comparison, assumes a depleted composition with a (Ce/Sm)n of 0.6.

The rare earth element data generally support the statement in Johnson and Dick (1992) that the lavas from the two sides of the transform can be derived by different degrees of melting of a generally similar mantle. If the transform volcano is indeed the product of a lower degree of melting, the basalts from the transform volcano would have a higher (Ce/Sm)n ratio than the basalts from the northern ridge-transform intersection. The rare earth data in Figure 10 do not indicate a higher (Ce/Sm)n ratio for the transform volcano than for the northern ridge segment.

Johnson and Dick (1992) quote analytical uncertainties of 30% for the Ce and Sm concentrations of individual basalt glass analyses made on the (then) MIT ion microprobe. The large part of this uncertainty is due to the reproducibility of the Si/REE intensity determination. Errors between the rare earth elements relative to one another are somewhat better. Uncertainties in the (Ce/Sm)n ratio are quoted as being on the order of 10% (a 10% 1-σ error bar is shown in Figure 10). It is clear from the diagram that the entire variation to be

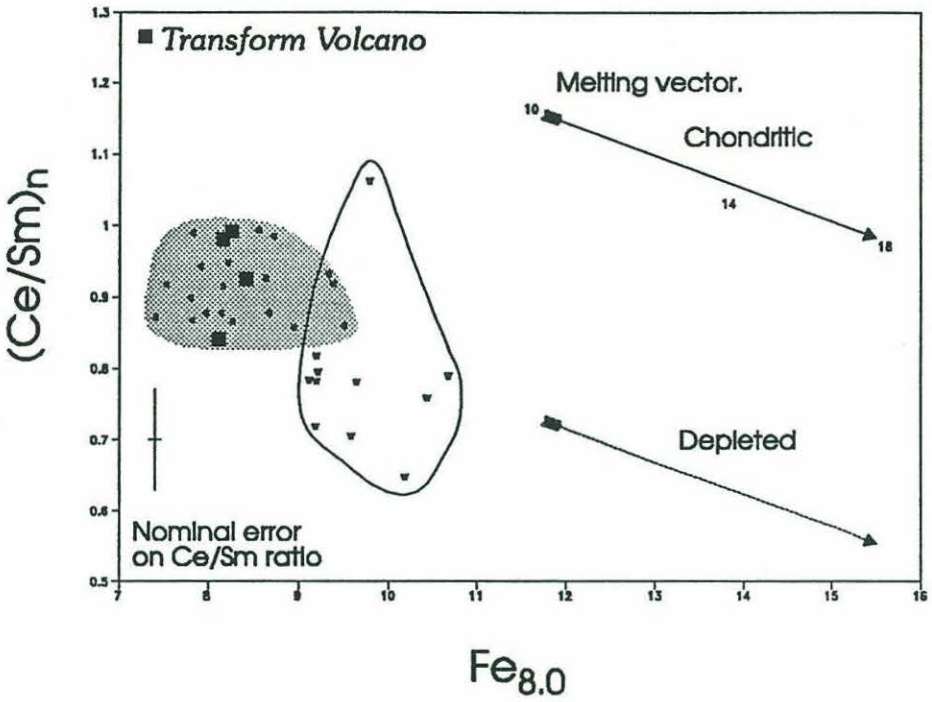

Figure 10: Chondrite normalized Ce/Sm vs. $Fe_{8.0}$. Atlantis II Fracture Zone basalts are shown as are calculated melting vectors (discussed in the text). Nominal 1-σ error cross shown for $Fe_{8.0}$ is the analytical precision of FeO for the MIT electron probe. (Ce/Sm)n error bar is from the quoted errors in Johnson and Dick (1992) for the (Ce/Sm)n ratio. Northern ridge data are enclosed by a shaded region, southern ridge data are enclosed by an unshaded region. Transform volcano basalts are represented by filled squares.

expected in (Ce/Sm)n in basalts due to a 160 degree span in temperature of melting is only about 20%. A hypothetical 100 degree offset in temperature due to a transform edge effect is within the nominal 1-σ error of these analyses. Quantifying a temperature shift on the basis of these rare earth element data is unfortunately not possible using these data. The rare earth element ratios are not sufficiently well determined by this method, compared to the total range expected for the melting of mid-ocean ridge basalt.

Other fracture zones

Langmuir and Bender (1984) use the TiO_2 vs. MgO diagram for the purpose of demonstrating the transform fault effect. That choice of elements is somewhat unfortunate for the purpose of calculating the offset in liquid lines of descent, as noted earlier, because melting vectors in that diagram are nearly parallel to fractional crystallization vectors. Small uncertainties in the determination of the slope of the liquid line of descent are greatly magnified in the calculated ΔTiO_2. For the Tamayo fracture zone, major element data are given in Bender, et al. (1984) which allow ΔT to be calculated using the semi-quantitative temperature shift estimation developed above. The results are listed in Table 4.

The assumptions regarding tectonic setting, fractionation history and mantle source composition described in the introduction to this section are not met rigorously by any of the fracture zones described in Langmuir and Bender (1984). Nonetheless temperatures were calculated using each of those data sets for which parallel liquid lines of descent could be fitted and ΔTiO_2 determined. These results are also listed in Table 4. In each case, the temperature shift is calculated by comparing the mean corrected compositions of basalts near the transform to those far away.

Thermal model

The thermal structure beneath a complicated spreading geometry such as a ridge-transform intersection has a variety of independent variables. These include the spreading rate, the age offset across the fracture zone, and the mean distance of the melting volume from both the fracture zone and the ridge axis (Phipps-Morgan and Parmentier, 1984; Phipps-Morgan and Forsyth, 1986;

Table 4: Temperature shifts calculated for fracture zones.

Fracture zone	Limb	Age offset (Ma)	Parameter	ΔX	ΔT°C
Charlie-Gibbs	S	29	TiO_2 -MgO	.2	198
Atlantis II	N	22	TiO_2 -MgO	.253	251
Atlantis II	N	22	Ca/(Ca+Na)	.0165	44
Atlantis II	N	22	CIPW Pl	2.1	111
Atlantis II	N	22	K_2O/TiO_2	-.0256	179
Atlantis II	N	22	$Fe_{8.0}$ - $Na_{8.0}$	.57	23
Kane	N	13	TiO_2 -MgO	.06	60
Blanco	E	3	TiO_2 -MgO	.11	109
Tamayo	SW	1.3	Ca/(Ca+Na)	.0075	20
Tamayo	SW	1.3	TiO_2 -MgO	.0535	53

Cordery MIT Ph.D. Thesis, 1990). I will calculate a crude means of comparing the temperature differences to be expected across fracture zones of differing age offsets. It is expected that the temperature difference across the fracture zone, and hence the transform edge effect, will increase with the age offset across the fracture zone.

Cooling of an infinite half-space is a reasonable approximation of the thermal state of the lithosphere away from fracture zones (cf. Turcotte and Schubert, 1982). Such a model reasonably approximates bathymetric and gravity observations on the oceanic crust. The temperature difference between the ridge axis mantle and the older transform mantle given by:

$$\Delta T = T_m - T_m erf\left(\frac{z}{2\sqrt{\kappa t}}\right) \qquad (4).$$

It should be kept in mind that in the half-space model, the temperature of the lithosphere at the ridge axis is the same as that of the ambient mantle at all depths. In Equation 4, Tm is the temperature of the ambient mantle, z is depth, t is the age offset across the fracture zone, and κ is the thermal diffusivity of the mantle. The crude calculation embodied in Equation 4 ignores many important

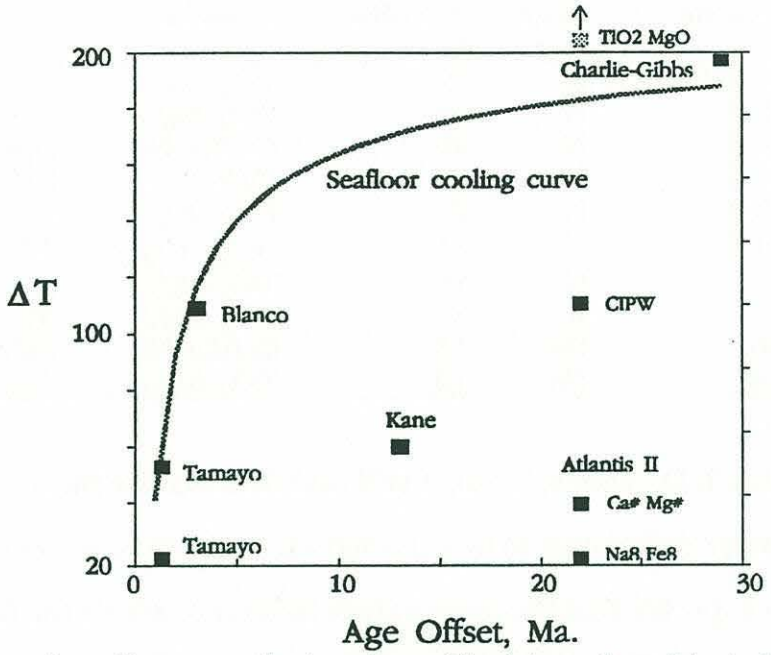

Figure 11: ΔT vs. Age offset across the transform. The data are from this study, Bender, et al., 1983 and Langmuir and Bender, 1984. The seafloor cooling curve is proportional to the model expressed in Equation 4 at an arbitrary depth.

aspects of the thermal state of the crust and lithosphere at ridge-transform intersections and of melt generation. It also ignores heat diffusion across the fracture zone and the shape of the melting region with relation to the plane of the transform fault. Nonetheless, the temperature offset across a fracture zone should be dominated by the temperature contrast in Equation 4. Basalt suites which show a transform edge effect should demonstrate this thermal effect.

It is not possible here to completely model the thermal evolution of fracture zones. Such a model, coupled with reasonable assumptions regarding mantle rheology, porosity and advection of heat by basaltic melts (e.g. M. Cordery, WHOI/MIT Ph.D. Thesis, 1990) would be a better representation of the thermal state of the lithosphere and asthenosphere at the ridge-transform intersection than Equation 4. The actual temperature shift from Equation 4 thus cannot be compared directly with basalt thermal estimates. I propose that tem-

perature shifts across fracture zones should be proportional to the temperature shift in Equation 4. For the purpose of comparing the temperature shift data derived from several fracture zones in the previous sections, a curve is included in Figure 11 which is proportional to the ΔT in Equation 4.

The age offset of the Atlantis II Fracture Zone is 20 times that of the Tamayo fracture zone. A much stronger thermal effect on melting is thus expected there. Instead, the calculated thermal effect at the Atlantis II Fracture Zone is about the same order of magnitude as that of the Tamayo. The same is true for the Kane fracture zone. Taken together, the data from fracture zones studied by Langmuir and Bender (1984) and the Atlantis II Fracture Zone do not demonstrate a convincing thermal signal, as two of the best-studied fracture zones fail to fall along the expected positive relationship with age offset.

The data shown in Figure 11 do not show a strong increase in estimated temperature offset with transform age offset. The lack of a strong transform fault thermal signal is probably due to violations of the basic assumptions of the comparison between rift valley and fracture zone basalts. The necessary data to evaluate these sources of error are, in most cases, still lacking; Charlie-Gibbs south and Kane south (Langmuir and Bender, 1984) failed to show parallel liquid lines of descent and so are not amenable to calculation of ΔT. Kane north, Tamayo, Charlie Gibbs south and Blanco are insufficiently documented with isotopes to preclude mixing of distinct mantle sources as the cause of the variations in the liquid lines of descent for those areas. At Tamayo, an isotopically distinct seamount in the ridge segment abutting the fracture zone has a clear mixing relationship with the basalts of the study area (Bender, et al., 1983). It is likely that mixing of magmas derived from distinct mantle sources played a strong role in the genesis of the Tamayo magmas.

Conclusion

The Transform Fault Effect (Fox, et al., 1980; Natland and Melson, 1980; Bender, et al., 1984; Langmuir and Bender, 1984) is a paradigm for understanding the genesis of magmas erupted close to transform faults on the mid-ocean ridge system. Juxtaposition of relatively old lithosphere with the active rift system has a cooling effect on the melting regime beneath the rift near to the transform (Natland and Melson, 1980; Fox and Gallo, 1983). The purpose of this paper has been to examine critically the evidence for a transform fault effect at the Atlantis II Fracture Zone and at other documented fracture zones.

Three major issues must be addressed with regard to any basalt data set from a fracture zone before the question of a transform fault effect can be evaluated. First, the geologic setting of the samples must be carefully documented in the context of an overall understanding of the geology of the area. Second, calculated liquid lines of descent for the rift near and far from the transform must be permissive of a generally similar crustal-level fractionation history. Steps must be taken in the interpretation of the data to shut out the effects of low and moderate pressure crustal evolution from affecting the interpretation. Third, isotopic study of the basalts in question must be permissive of their derivation from similar mantle sources.

No previous study purporting to demonstrate a transform fault effect (Natland and Melson, 1980; Bender, et al., 1983; Perfit, et al., 1983; Langmuir and Bender, 1984) has adequately addressed more than one or two of the above criteria. These criteria are necessary, but not in themselves sufficient to rule out effects on the liquid line of descent unrelated to the temperature of the mantle.

The Atlantis II Fracture Zone provides a limiting case for the study of mantle thermal effects, since its age offset is great and its geology has been studied in detail (Dick, et al., 1991). These circumstances provide the best yet understanding of the critical issues identified here. For these reasons, the transform fault effect observed at the Atlantis II Fracture Zone should a maximum.

It is important to consider the limitations in the current study. These fall under two categories, model-dependent and data-dependent. The first of these has to do with inadequacies in the modeling carried out here. First, the models involved a great simplification of quite complex experimental melting data from Kinzler and Grove (1992b). Having shown that this approach is useful, a more refined method of calculating offsets in liquid lines of descent could be devised. Second, the calculation of mantle temperatures requires a knowledge of the starting composition of the mantle for each basalt suite. Mantle source composition is impossible to measure for basalts divorced from their source region. It is also probably a flawed concept in any event. Mid-ocean ridge basalts are an aggregation of melt batches derived from many different points in the mantle, which may have different compositions. This is not a problem if the two basalt suites have similar sources and our understanding of basalt systematics is correct.

The third model-dependent problem is our inability to account for processes, such as the mixing of primitive magmas with evolved magmas or high-temperature magmas with low-temperature magmas, wall rock assimilation (Kelemen, Dick and Quick, 1992) or elemental fractionation by melt-matrix reaction during porous flow in the mantle (Navon and Stolper, 1987). These processes are all thought to occur in the mantle but the evidence for them in basalts may have been obscured by the process of mixing.

The second category of limitation to this study is data-dependent, that is, the data included here may not be a perfect example of the transform edge effect. The samples in this study are all close to the transform in absolute terms. Absent further dredging this cannot be altered. The closeness of all the northern RTI basalts to the transform could help explain why the temperature shift is so small compared to other transforms studied by Langmuir and Bender (1984). Without knowing precisely how the temperature shift should vary with distance from the transform, the effect of differing distances from the transform is difficult to evaluate. The unambiguous nature of the geologic setting of the transform volcano and the isotopic homogeneity of the northern ridge segment basalts offsets this difficulty somewhat, as two of the major ambiguities plaguing earlier studies of transform basalts are controlled for.

Another weakness of this study is the lack of sophistication of the thermal model for the ridge-transform intersection melting region. Basalts from "near" the transform are compared with basalts "distant" from the transform without any attempt to account for the relative distance of each group of basalts from the other. These effects could be incorporated into a mantle flow model based on plate driven flow, temperature dependent viscosity, and advection of heat by rising basalt magma for each transform studied (cf. M. Cordery, WHOI/MIT Ph.D. thesis 1991). Such modeling is beyond the scope of the current study.

I have been at pains to state the assumptions attendant on an examination of petrologic and geologic data relating to a transform fault effect and examine those assumptions as they pertain to the current data set. I have also attempted to measure the temperature shift from fracture zone domain to rift valley basalts in a semi-quantitative fashion. The isotopic and morphologic data permit the interpretation of the transform basalts as the products of melting of similar man-

tle compositions. The geology of the transform volcano also precludes the contamination of the basalts there with rift-related magmas. The data set may thus be interpreted in terms of a mantle temperature difference between the two basalt suites. Several independent measures of the relative degree of melting indicate that the transform volcano is the product of a lower degree of partial melting than are the basalts from the northern rift valley. This lower degree of partial melting is caused by a transform fault effect. The calculated magnitude of that thermal effect is small relative to that calculated for other fracture zones. Given the great age offset (and hence thermal offset) of the Atlantis II Fracture Zone, a much larger temperature shift would be expected.

When temperature offsets at fracture zones are compared to the thermal effect predicted by a simple ridge-transform intersection model, no clear trend of increasing temperature with increasing age offset emerges. At the very least, the thermal offset should increase steadily with age offset, which it does not. It may be concluded that transform fault thermal effects are not strongly expressed compared to variations produced by random fluctuations in mantle sources, mantle upwelling (e.g., Johnson and Dick, 1992), and polybaric fractionation. Before transform fault-related thermal effects on the genesis of magmas can be studied with rigor, great care in sampling, study of the geologic setting, documentation of polybaric fractionation effects and mantle source heterogeneity in each area are necessary. Improved thermal modeling of the rising asthenosphere will allow the results to be interpreted more easily.

Acknowledgments:

This work was supported by an NSF Graduate Fellowship.

References:

Aumento, F., and H. Loubat (1970) The mid-Atlantic ridge near 45°N XVI Serpentinized ultramafic intrusions. **Canadian Journal of Earth Sciences** 8:631-663.

Batiza, R., and D. Vanko (1984) Petrology of Young Pacific Seamounts. **Journal of Geophysical Research** 89:11235-11260.

Bender, J.F., C.H. Langmuir and G.N. Hanson (1984) Petrogenesis of glasses from the Tamayo region, East Pacific Rise. **Journal of Petrology** 25:213-254.

Brooks C., and S.R. Hart (1977) The geochemistry and evolution of early Precambrian mantle. **Contributions to Mineralogy and Petrology** 61:109-128.

Bryan, W.B., G. Thompson and J.N. Ludden (1981) Compositional variation in Normal MORB from 22°-25°N: Mid-Atlantic ridge and Kane Fracture Zone. **Journal of Geophysical Research** 86:11815-11836.

Bryan, W.B., and H.J.B. Dick (1982) Contrasted abyssal basalt liquidus trends: evidence for mantle major element heterogeneity. **Earth and Planetary Science Letters** 58:15-26.

Cordery, M. (1990) MIT/WHOI Ph.D. Thesis.

Cross, W., J.P. Iddings, L.V. Pirsson and H.S. Washington (1903) *Quantitative Classification of Igneous Rocks* University of Chicago Press.

DeMets, C., R.G. Gordon, D.F. Argus and S. Stein (1990) Current plate motions. **Geophysical Journal International** 101:425-478.

Dick, H.J.B., R.L. Fisher, and W.B. Bryan (1984) Mineralogic variability of the upper mantle along mid-ocean ridges **Earth and Planetary Science Letters** 69:88-106.

Dick, H.J.B. (1989) Abyssal Peridotites, Very-Slow Spreading Ridges and Ocean Ridge Magmatism. in: **Magmatism in the Ocean Basins** edited by A.D. Sanders and M.J. Norry, Journal of the Geological Society of London Special Publication No. 42: pp. 75-109.

Dick, H.J.B., H. Schouten, P. Meyer, D. Gallo, H. Bergh, R. Tyce, P. Patriat, K.T.M. Johnson, J. Snow, and A. Fisher (1991) Tectonic evolution of the Atlantis II Fracture Zone, **Proc. Ocean Drilling Program** v. 118 part B.

Dosso, L., B. Hanan, H. Bougault and J.-G. Schilling (1991) Sr-Nd-Pb geochemical morphology between 10 degrees and 17 degrees N on the Mid-Atlantic Ridge; a new MORB isotope signature. **Earth and Planetary Science Letters** 106:29-43.

Dupré, B. and C.J. Allègre (1983) Pb-Sr isotope variation in Indian Ocean basalts and mixing phenomena. **Nature** 303:142-146

Engel, C.E. and R.L. Fisher (1975) Granitic to ultramafic rock complexes of the Indian Ocean ridge system, western Indian Ocean. **Geological Society of America Bulletin** 80:1353-1578.

Fox, P.J., R.S. Detrick and G.M. Purdy (1980) Evidence for crustal thinning near fracture zones; implications for ophiolites *in:* Panayioutou, A. (*ed.*) **Ophiolites; Proceedings, International Ophiolite Symposium** p. 161-168.

Fox, P.J., and D.G. Gallo (1984) A tectonic model for Ridge-Transform-Ridge plate boundaries: implications for the structure of oceanic lithosphere. **Tectonophysics** 104:205-242.

Gallo, D.G., H.J.B. Dick, H. Schouten, H. Bergh, and P. Patriat (1987) The Atlantis II Fracture Zone **EOS** 68:408.

Grove, T., R. Kinzler and W. Bryan (1990) Fractionation of Mid-Ocean Ridge Basalt *in:* **Proceedings of the RIDGE short course on magmatic processes.**

Hamelin, B. and C.J. Allègre (1985) Large-scale regional units in the depleted upper mantle revealed by an isotope study of the Southwest Indian Ridge. **Nature** 315:196-199.

Hanan, B.B., R.H. Kingsley and J.-G. Schilling (1986) Pb isotopic evidence in the South Atlantic for migrating ridge-hotspot interactions **Nature** 322:137-144.

Hart, S.R. (1984) A large scale isotope anomaly in the Southern Hemisphere mantle. **Nature** 309:753-757.

Hekinian, R., and G. Thompson (1976) Comparative geochemistry of volcanoes from rift valleys, transforms and aseismic ridges. **Contributions to Mineralogy and Petrology** 57:145-162.

Johnson, K.T.M. (1990) Trace Element Geochemistry of Oceanic Peridotites and Silicate Melt Inclusions: Implications for Mantle Melting and Ocean ridge Magmagenesis Ph.D. Thesis. **MIT/WHOI, WHOI**-90-36.

Johnson, K.T.M., H. Dick, and N. Shimizu (1990) Melting in the Oceanic Mantle: an ion Microprobe study of diopsides in abyssal peridotites. **Journal of Geophysical Research** 95:2661-2678.

Johnson, K.T.M. and H.J.B. Dick (1992) Open system melting and temporal and spatial variation of peridotite and basalt at the Atlantis II Fracture Zone **Journal of Geophysical Research** 97:9219-9241.

Karson, J.A. and D. Elthon (1987) Evidence for variations in magma production along oceanic spreading centers: A critical appraisal. **Geology** 15:127-131.

Karson, J.A and H.J.B. Dick (1983) Tectonics of ridge-transform intersections at the Kane Fracture Zone **Marine Geophysical Researches** 6:51-98.

Kelemen, P., Henry J.B. Dick and J.E. Quick (1992) Formation of harzburgite by pervasive melt/rock reaction in the upper mantle. **Nature** 358:635-641.

Kempton, P.D. C.J. Hawkesworth and M. Fowler (1991) Geochemistry and isotopic composition of gabbros from layer 3 of the Indian Ocean crust, Hole 735b *in:* von Herzen, R.P., P.T. Robinson, et al. (1991) **Proceedings of the Ocean Drilling Program, Scientific Results** 118:127-142.

Kinzler, R. and T. Grove (1992) Primary Magmas of Mid-Ocean Ridge Basalts 1. Experiments and Methods **Journal of Geophysical Research** 97 :6885-6906.

Kinzler , R. and T. Grove (1992) Primary Magmas of Mid-Ocean Ridge Basalts, 2. Applications **Journal of Geophysical Research** 97:6907-6926.

Klein, E.M., and C.H. Langmuir (1987) Global correlations of ocean ridge basalt chemistry with axial depth and crustal thickness. **Journal of Geophysical Research** 92:8089-8115.

Klein, E.M and C.H. Langmuir (1989) Local versus global correlations in ocean ridge basalt composition: a reply. **Journal of Geophysical Research** 94:4241-4252.

Klitgord, K., and H. Schouten (1986) Plate Kinematics of the central Atlantic. in: **The Geology of North America** vol. M., The Western North Atlantic. Geological Society of America pp. 351-378.

Karson, J.A. and H.J.B. Dick (1983) Tectonics of Ridge-Transform intersections at the Kane Fracture Zone. **Marine Geophysical Researches** 6:51-98.

Kurz. M., A. le Roex and H. Dick (in press) Geochemistry of the Bouvet Mantle Plume **Geochimica et Cosmochimica Acta.**

Langmuir, C.H., and J.F. Bender (1984) The Geochemistry of oceanic basalts in the vicinity of transform faults: observations and implications. **Earth and Planetary Science Letters** 69:107-127.

le Roex, A., H.J.B Dick, A. Erlank, A. Reid, F. Frey, and S.R. Hart (1983) Geochemistry, Mineralogy, and Petrogenesis of Lavas Erupted along the southwest Indian Ridge Between the Bouvet Triple Junction and 11 Degrees East. **Journal of Petrology** 24:267-318.

le Roex, A., H.J.B Dick, A. Erlank, A. Reid, and F. Frey (1985) Petrology and Geochemistry of basalts from the American-Antarctic Ridge, southern ocean.: implications for the westward influence of the Bouvet mantle plume. **Contributions to Mineralogy and Petrology** 90:367-380.

le Roex, A., H.J.B. Dick, and R.L. Fisher (1989) Petrology and Geochemistry of MORB from 25°N to 46°N along the Southwest Indian Ridge: Evidence for contrasting styles of mantle enrichment. **Journal of Petrology** 30:947-986.

le Roex, A., Dick, H.J.B. and Watkins, R. (1992) Petrogenesis of anomalous K-enriched MORB from the Southwest Indian Ridge 11°53'E to 14°38'E. **Contributions to Mineralogy and Petrology** 110:253-268.

Machado, N., J.N. Ludden, C. Brooks and G. Thompson (1982) Fine scale isotopic heterogeneity in the sub-Atlantic mantle. **Nature** 295:226-229.

MacDonald, K.C., D.A. Castillo, S.P. Miller, P.J. Fox, K.A. Kastens and E. Bonatti (1986) Deep-tow studies of the Vema Fracture Zone; 1, Tectonics of a major slow slipping transform fault and its intersection with the Mid-Atlantic Ridge **Journal of Geophysical Research** 91:3334-3354.

Macdougall, J.D. and G.W. Lugmair (1986) Sr and Nd isotopes in basalts from the East Pacific Rise: significance for mantle heterogeneity. **Earth and Planetary Science Letters** 77:273-284.

Mahoney, J. J.N. Ludden, W.M. White, R. Poreda, S. Bloomer, R.L. Fisher, and A.N. Baxter (1989) Isotopic and geochemical provinces of the western Indian Ocean spreading centers. **Journal of Geophysical Research** 94:4033-4052.

Manhes, G., J.F. Minster and C.J. Allègre (1978) Comparative uranium-thorium-lead and rubidium-strontium of St. Severin amphoterite: consequences for early solar system chronology **Earth and Planetary Science Letters** 39:269-278.

Michael, P.J. and Bonatti, E. (1985) Peridotite composition from the North Atlantic: Regional and tectonic variations and implications for partial melting **Earth and Planetary Science Letters** 73:91-104.

Michard, A., R. Montigny and R. Schlich (1986) Geochemistry of the Rodriguez triple junction and the South-East Indian Ridge. **Earth and Planetary Science Letters** 78:104-114.

McKenzie, D. (1984) The generation and compaction of partially molten rock. **Journal of Petrology** 25:713-765.

McKenzie, D., and M. Bickle (1988) The volume and composition of melt generated by extension of the lithosphere. **Journal of Petrolgy** 29:625-629.

Miyashiro, A., F. Shido and M. Ewing (1970) Crystallization and differentiation of abyssal tholeiite and gabbros from mid-ocean ridges **Earth and Planetary Science Letters** 7:361.

Morgan, W.J. (1967) Rises, trenches, great faults and crustal blocks **Journal of Geophysical Research** 73:1959-1982.

Natland, J.H. and W.G. Melson (1980) Compositions of basaltic glasses from the East Pacific Rise and Siqueiros Fracture Zone, near 9N, *in:* **Initial reports of the Deep Sea Drilling Project** 54:705-723. U.S. Government Printing Office.

Navon, O. and E. Stolper (1987) Geochemical consequences of melt percolation: the upper mantle as a chromatographic column. **Journal of Geology** 95:285-307.

Perfit, M.R., D.J. Fornari, A. Malahoff and R.W. Embley (1983) Geochemical Studies of Abyssal Lavas Recovered by DSRV Alvin from Eastern Galapagos Rift, Inca Transform, and Ecuador Rift 3. Trace element Abundances and Petrogenesis. **Journal of Geophysical Research** 88, B12:10551-10572.

Price, R.C., A.K. Kennedy, M. Riggs-Sneeringer and F. Frey (1986) Geochemistry of basalts from the Indian Ocean triple junction: implications for the generation and evolution of Indian Ocean ridge basalts. **Earth and Planetary Science Letters** 78:379-396.

Reid, I and H.R. Jackson (1981) Oceanic spreading rate and crustal thickness **Marine Geophysical Researches** 5:165-172.

Schilling, J.-G. and H. Sigurdsson (1979) Thermal minima along the mid-Atlantic Ridge **Nature** 282:370-375.

Schouten, H. H. Dick and K. Klitgord (1987) Migration of mid-ocean ridge volcanic segments **Nature** 317:225-229.

Sclater, J., H. Dick, I. Norton and D. Woodruffe (1978) Tectonic structure and petrology of the Antarctic plate boundary near the Bouvet triple junction. **Earth and Planetary Science Letters** 37:393-400.

Sclater, J.G., R.L. Fisher, P. Patriat, C. Tapscott and B. Parsons (1981) Eocene to recent development of the Southwest Indian Ridge, a consequence of the evolution of the Indian Ocean Triple Junction. **Geophysical Journal of the Royal Astronomical Society** 64:587-604.

Severinghaus, J.P and K.C. MacDonald (1988) High inside-corners at ridge-transform intersections. **Marine Geophysical Researches** 9:353-367.

Shirey, S.B., J. Bender and C. Langmuir (1987) Three-component isotopic heterogeneity near the Oceanographer Transform, Mid-Atlantic Ridge. **Nature** 325:217-223.

Sigurdsson, H., and S.R.J. Sparks (1978) Lateral magma flow within rifted Icelandic crust **Nature** 274:126-130.

Stroup, J.B. and Fox, P.J. (1981) Geologic investigations in the Cayman Trough: evidence for thin crust along the mid-Cayman Rise **Journal of Geology** 89:395-420.

Snow, J., H.J.B Dick and S.R. Hart (1987) Preliminary results from a transform volcano, Atlantis II Fracture Zone, SW Indian Ridge. **EOS** 68:408.

Tapscott, C., P. Patriat, R.L. Fisher, J. Sclater, H. Hoskins and B. Parsons (1980) The Indian Ocean Triple Junction. **Journal of Geophysical Research** 85:4723-4739.

Tormey, D., T. Grove and W.B. Bryan (1987) [Melting Experiments on KFZ Basalts] **Contributions to Mineralogy and Petrology** 96:121-139.

Turcotte, D. and G. Schubert (1982) **Geodynamics** John Wiley and Sons, 450 pp.

von Herzen, R.P., P.T. Robinson, et al. (1991) **Proceedings of the Ocean Drilling Program, Scientific Results** 118

Walker, D., T. Shibata, and S.E. DeLong (1979) Abyssal tholeiites from the Oceanographer Fracture Zone II: phase equilibria and mixing. **Contributions to Mineralogy and Petrology** 70:111-125.

White, W.M., A.W. Hofmann and H. Puchelt (1987) Isotope geochemistry of Pacific mid-ocean ridge basalt **Journal of Geophysical Research** 92:4881-4893.

Whitehead, J.A., H.J.B Dick, and H. Schouten (1984) A mechanism for accretion under spreading centers. **Nature** 312:146-148.

Wright, T.L., W.T. Kinosha and D.L. Peck (1968) March 1965 eruption of Kilauea Volcano and the formation of Makaopuhi Lava Lake. **Journal of Geophysical Research** 73:3181.

Zindler, A., S.R. Hart, F.A. Frey, and S.P. Jacobsen (1979) Nd and Sr isotope ratios and rare-earth element abundances in Reykjanes Peninsula basalts: evidence for mantle heterogeneity beneath Iceland **Earth and Planetary Science Letters** 45:249-262.

Zindler, A. and S.R. Hart (1986) Chemical Geodynamics **Annual Review of Earth and Planetary Sciences** 14:493-571

Chapter 3: Seafloor alteration of abyssal peridotite and its effect on the Sr, Nd and Os isotopic systems.

Chapter 3: Seafloor alteration of abyssal peridotite and its effect on the Sr, Nd and Os isotopic systems.

Abstract

This study reports the results of an investigation of peridotite alteration relative to the isotopic systematics of Sr, Nd and Os in abyssal peridotite. Sr isotopic compositions in abyssal peridotites are highly susceptible to alteration at the water/rock ratios which prevail during serpentinization and seafloor weathering. No amount of mineral separation or leaching reliably removes the seawater overprint on the Sr isotopic composition in every case. The Sm-Nd isotopic system is far more robust than the Sr isotopic system during hydrothermal alteration. Almost every leached mineral separate in this study, as well as some of the whole rocks, yielded pristine mantle Nd isotopic compositions. Os is more robust during hydrothermal alteration than Nd. No evidence was found for the disturbance of Os isotopic compositions even in the most altered abyssal peridotite.

The alteration of abyssal peridotite involves the isochemical reaction of primary mantle minerals with water to form serpentines + magnetite and other minerals. The reactions by which serpentinite forms from peridotite occur at every temperature from amphibolite grade down to the temperature of ambient seawater. Additionally, the alteration redistributes the major elements within the rock, removing some and adding others. The abyssal peridotites studied here lie on a compositional trend that implies the removal of Mg from the rock, probably during the later stages of the alteration process. These reactions occur at a high ratio of water to rock, and are characterized by incomplete reaction progress and disequilibrium.

Many abyssal peridotites, including some from this study, contain sea water-derived aragonite. Mg^{2+} in solution catalyzes the precipitation of aragonite from sea water (Bischoff and Fyfe, 1968), which would otherwise precipitate calcite, implying a high activity of Mg in solution during the formation of the aragonite. These two independent lines of evidence for the existence of Mg-bearing water circulating in abyssal peridotite are surprising, considering the reactivity of Mg and the low solubility of Mg-minerals in hydrothermal solutions.

A component of Sr has been identified in olivine alteration phases (serpentine + magnetite) which has an extremely high $^{87}Sr/^{86}Sr$, in excess of that of seawater. This component may explain anomalously high $^{87}Sr/^{86}Sr$ whole rock values reported in the early literature (Roe, 1965; Bonatti, 1970). This orphan ^{87}Sr is probably due to the infiltration of the weathered rock by a sedimentary component suspended in seawater.

Introduction

Perhaps the most obvious characteristic of abyssal peridotite is its spectacular degree of alteration. This alteration occurs during the transport of the abyssal peridotite from the mantle to the point of sampling on the ocean floor. Previous studies of the metamorphic alteration of abyssal peridotite (Kimball, et al., 1985; Kimball and Gerlach, 1986) have concentrated on those samples that best displayed high pressure and temperature metamorphic grade (up to amphibolite facies) as well as the lower grade of alteration found more commonly in the remaining abyssal peridotite samples.

This study examines a few well-preserved abyssal peridotites with particular reference to the behavior of the Rb-Sr, Sm-Nd and Re-Os isotopic systems under conditions of metamorphism experienced by the peridotite on its way from the mantle. There are three major questions to be addressed by this study. First, how has the serpentinization and weathering of abyssal peridotite affected its composition? Second, what are the major reservoirs that make up the budget of Sr, Nd and Os in abyssal peridotite, and what processes led to the formation of these reservoirs? Last, to what extent can isotopic and trace element information about the mantle be extracted from typical abyssal peridotites?

This study addresses the compositional changes attendant upon serpentinization and weathering of peridotite on the sea floor. The link between sea floor alteration and isotopic exchange with seawater is studied, and the reservoirs of Sr, Nd and Os isotopes in altered mantle rocks are examined. This characterization of the alteration of abyssal peridotite allows the extraction of primary information about the mantle beneath mid-ocean ridges.

The primary mineralogy of abyssal peridotites is a close analog of that observed in peridotite xenoliths and alpine peridotites. Their primary mineralogy is typically interpreted as having been four phase assemblages of olivine, orthopyroxene, clinopyroxene and spinel (Miyashiro, et al., 1969; Aumento and Loubat, 1970; Bonatti and Hamlyn, 1981; Dick, et al., 1984; Michael and Bonatti, 1985a, b; Shibata and Thompson, 1986). Plagioclase is present in about one third of all abyssal peridotites, however its significance in abyssal peridotites is controversial. The most important determinant of the primary mineral assemblage is the extent of melting experienced by the peridotite (Dick, Fisher and Bryan,

1984; Michael and Bonatti, 1985; Dick 1989). In addition, there are other processes which can affect the modal mineralogy of abyssal peridotites. These include various melt/wallrock interactions. Trapping melt in the peridotite matrix (Dick, et al., 1984; Elthon, 1992) will have a substantial effect on the modal mineralogy (essentially the reverse of melting). Reactive exchange between the peridotite and melt traversing the mantle by porous flow (Kelemen et al., 1992) enriches the peridotite in orthopyroxene at the expense of olivine and clinopyroxene. This process can produce peridotite modal compositions which are too orthopyroxene-rich to be the residue of partial melting in the mantle. The evidence shows, however, that this effect is not commonly observed in abyssal peridotite (Kelemen, et al., 1992).

The isotopic composition of bulk abyssal peridotite has received little attention in recent years, though many measurements were made in the early literature (Roe, 1965; Bonatti, et al., 1970 and others). Part of the problem lies in the pervasive alteration of the peridotite. The isotopic composition of Sr and to some extent Nd have been changed in the bulk peridotite due to the interaction if the peridotite with seawater. The early studies also uncovered the problem of "orphan" ^{87}Sr, which could not be explained by *in situ* radioactive decay or by addition of Sr from seawater. This study will examine the issues of seawater interaction on the Sr, Nd and Os isotopic systems, including the "orphan" Sr problem.

Since the pervasive contamination of bulk abyssal peridotite became apparent, analysis of abyssal peridotite clinopyroxenes has been slowed by the rarity of fresh abyssal peridotite clinopyroxene. The residual nature of abyssal peridotite adds the additional difficulty of low concentration. Abyssal peridotite clinopyroxenes are typically lower in Sr and Nd than are clinopyroxenes from other types of peridotites. Hart (1972) was the first study to attempt the Sr isotopic analysis of leached abyssal peridotite clinopyroxene. This study is the second. The goal of this analysis is to relate the abyssal mantle isotopic data generally to those inferred from the isotopic compositions of abyssal basalts. It is probably not appropriate to try to directly relate abyssal peridotite clinopyroxene data to those from nearby basalts. The comparison is nonetheless an interesting one.

Data

Sample description

Bulk samples

12 samples were studied from the SW Indian and American-Antarctic ridges. The locations, tectonic settings, and crustal ages of the samples are listed in Table 1. The localities of the samples are shown relative to the major tectonic features of the Southwest Indian Ridge and American Antarctic Ridge in Figure 1. The sample suite was chosen such that it included samples close to the Bouvet hot spot, as well as samples at varying distances from any mantle hotspot. The samples are all spinel bearing harzburgites and lherzolites, having between 3 and 12 percent modal clinopyroxene by volume. All are variably serpentinized, but do not contain abundant high temperature alteration phases or plagioclase. Two samples of peridotite mylonite (AII107:61-78 and 61-83) from the Shaka Fracture Zone were included for some of the experiments because of their good state of preservation, being less than 5% serpentinized in their unweathered

Table 1: Sample locations and tectonic settings.

		Latitude:			Longitude:				
Cruise	Sample	Deg.	Min.		Deg.	Min.		Age[1]	Tectonic Setting.
PS86	6-37	52	21.0	S	13	8.0	E	0-5	Dingaan F.Z, NW wall.
AII107	61-78	53	22.5	S	9	20.3	E	12.6	Shaka F.Z., SE wall.
AII107	61-83	53	22.5	S	9	20.3	E	12.6	Shaka F.Z., SE wall.
AII107	40-27	54	25.4	S	1	34.2	E	17.0	Bouvet F.Z., NW wall.
AII107	40-35	54	25.4	S	1	34.2	E	17.0	Bouvet F.Z., NW wall.
Vulc5	41-29	59	5.2	S	16	48.5	W	2.3	59 deg. S F.Z., N wall.
Vulc5	41-15	59	5.2	S	16	48.5	W	2.3	59 deg. S F.Z., N wall.
RC2709	6-2	31	54.9	S	57	10.7	E	0.6	Atlantis II F.Z., N RTI corner.
RC2709	25-139	32	32.2	S	57	3.8	E	9.7	Atlantis II F.Z., median ridge.
IO11/76	59-26	54	3.4	S	6	30.0	E	6.0	Islas Orcadas F.Z., SE wall.
IO11/76	56-58	54	5.5	S	6	17.1	E	9.7	Abyssal hills SE Islas Orcadas F.Z.
IO11/76	60-61	54	27.5	S	6	29.2	E	7.6	Abyssal hills SE Islas Orcadas F.Z.

Abbreviations: AII: Atlantis II; PS: Polar Stern; VULC: Vulcan; RC: Robert Conrad; IO: Islas Orcadas. RTI: Ridge Transform Intersection.

[1] Crustal ages (in millions of years) from location, plate geometry and spreading velocities. In the case of sample PS86:6-37, a range is given because of the ambiguity of the tectonic setting of the 11°E disturbed zone (le Roex, et al., 1992)

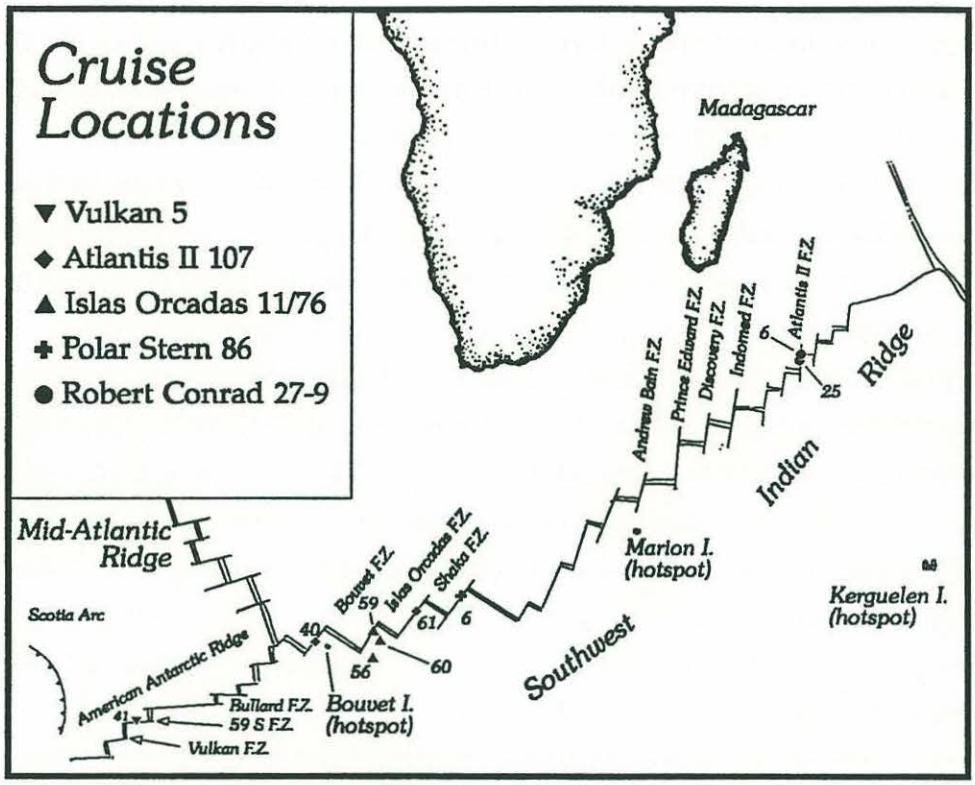

Figure 1: Location map for peridotite samples. Dredge haul numbers are listed next to the corresponding symbols.

cores. These samples were expected to show a strong mantle signal, and the comparison of their cores and weathering rinds was expected to show the contribution of only the lowest-temperature seawater. Complete sample numbers are composed of a cruise designator (e.g. PS86), dredge number and sample number (e.g. 6-37). The reader will note that, while cruise designators (e.g. RC2709) are non-unique, the dredge sample numbers (e.g. 6-2 or 25-139) are unique. For that reason, where circumstances of space demand (as on some diagrams), sample numbers in this study may be truncated to only the dredge and sample, as in 6-2, meaning RC2709:6-2.

Mylonite weathering study

The interpretation of major element, trace element and isotopic results in abyssal peridotites is complicated greatly by their alteration. The cores of abys-

sal peridotite mylonites are often largely unaltered and allow a test of the extent to which submarine weathering affects the major element, trace element and isotopic compositions of abyssal peridotites. Two samples, AII107:61-78 and AII107:61-83, were selected as having the least evidence of alteration in their cores, both in hand samples and in thin section. The presence of abundant, fine-grained (1 mm to less than 10 microns), recrystallized olivine in these mylonites and their high density (see Appendix I) attest to the likelihood that the metamorphic history of the mylonite cores was largely anhydrous. The textures and compositions of augen minerals (orthopyroxene, clinopyroxene and spinel) in the mylonitized peridotites suggest that the protolith was an anhydrous four-phase peridotite (H. Dick and G. Jaroslaw, personal communication). The deformational textures of these peridotites include extreme grain size reduction by kinking, subgrain formation and recrystallization, as well as elongation and rotation of porphyroblasts of primary minerals. These all suggest a relatively low temperature and pressure of deformation, as deformation at mantle temperatures and pressures would likely result in a much coarser and more equant recrystallization texture (cf. Mercier and Nicolas, 1974; Spry, 1983). There is some evidence, therefore, that the abyssal peridotite mylonites may to some extent be considered abyssal peridotites that have not been subject to significant hydrous alteration in their interiors.

The mylonite samples had bright yellow-brown weathered rims from 5-20 mm. thick, and largely unweathered cores. The transition from the weathered zone to the unweathered core is quite sharp in these samples. Rim and core were analyzed separately in order to assess the changes in the samples due to weathering at low temperature seafloor conditions. The weathering rinds were extremely fine-grained and it was difficult to identify any minerals optically beyond serpentine. The weathering rinds were cut off of the samples and both unweathered core and weathered rim samples were crushed separately for analysis, first in a small steel jaw crusher, then in an agate shatterbox.

Table 2: Modal data

		Dredge haul averages[1]:					Primary modes:				primary	
Cruise	Sample	Ol.	Opx.	Cpx.	Sp	Pl.	Ol.	Opx.	Cpx.	Sp	Phases	Rock type
RC 2709	6-2	68.8	25.2	4.8	0.73	0.41	48.1	44.3	6.1	1.1	64.4	Lherzolite
VULK5	41-29	71.1	20.6	7.3	0.96	0.02	67.2	22.0	9.0	0.8	21.2	Lherzolite
VULK5	41-15	71.1	20.6	7.3	0.96	0.02	42.5	44.8	10.6	1.1	18.8	Lherzolite
AII 107	40-35	79.5	17.3	2.6	0.50	0.00	70.6	25.2	3.2	0.5	14.0	Harzburgite
PS 86	6-37	64.2	25.7	9.0	1.08	0.00	65.2	25.3	6.9	1.4	37.9	Lherzolite
IO 11/76	60-61	75.9	19.8	3.6	0.60	0.06	79.0	13.1	7.3	0.3	17.6	Lherzolite
IO 11/76	59-26	73.5	21.5	4.2	0.69	0.01	58.0	36.1	2.1	1.1	15.3	Harzburgite
IO 11/76	56-58	71.6	22.0	5.4	0.91	0.07	76.0	16.7	6.0	1.0	22.8	Lherzolite
AII 107	40-27	79.5	17.3	2.6	0.50	0.00	-	-	-	-	-	Harzburgite
AII 107	61-78[2]	-	-	-	-	-	64.7	26.9	6.7	1.2	99[3]	Lherzolite
AII 107	61-83[2]	-	-	-	-	-	72.4	19.8	5.8	1.4	99[3]	Lherzolite

All modes in percent. Modes were counted on 2"x3" large format thin sections at a point spacing of 0.5 mm. 2500-3000 points per thin section were counted. [1]Dredge haul averages are from H. Dick, personal communication. [2]Mode calculated from bulk composition and phase compositions using linear least squares (Appendix II). [3]Estimated.

Mineralogy

Mineralogy and petrography

In the samples studied here, primary mineral assemblages and textures are cut by low temperature mineral assemblages and textures. Moderate and high temperature metamorphic minerals (amphibole, hydrogrossular garnet, talc, phlogopite, etc.) are generally lacking or poorly represented. This is largely due to a sampling effect, since the samples were chosen with the intention of carrying out isotopic investigations. Greenschist and amphibolite parageneses in abyssal peridotites are generally associated with amphibolitization of clinopyroxene and the formation of secondary clinopyroxene (Kimball, et al., 1985), thus rendering rocks which contained abundant chlorite or amphibole (for example) unsuitable for obtaining primary clinopyroxene separates. Such samples are rare in any event.

Primary mineralogy and textures.

The samples analyzed for this study were all either spinel harzburgites or spinel lherzolites in Streckeisen's (1976) classification of coarse grained igneous

rocks. None of the lherzolites even approaches 60% modal pyroxene, and thus they cannot be considered websterites (Streckeisen, 1976). The primary compositions of the rocks are generally >50% olivine, possessing 1-10% modal clinopyroxene, 1-2% spinel and the rest orthopyroxene. Table 2 presents the results of point counting of primary and secondary minerals. 2500-3000 points were counted per large format (2"x3") thin section, with a point spacing of 0.5 mm. Detailed descriptions of each thin section are presented in Appendix I.

Textures associated with deformation at high temperatures and pressures are apparent in every sample studied. Mercier and Nicolas (1974) provide a system for the classification of such textures in relatively unserpentinized peridotite which can be applied to the present samples. Of the three major categories of mantle tectonite textures they present, two are abundant in the samples from this study and in abyssal peridotites generally. Most of the samples in this study exhibit some mixture of the features characteristic of protogranular and porphyroclastic textures as described by Mercier and Nicolas (1974). Protogranular textures seem to be more prevalent, with their attendant coarse grain size (e.g., 0.5 - 5 cm olivine grains) and curvilinear grain boundaries (where these are recognizable) and only minor polygonalization and formation of neoblastic enstatite and olivine grains with straight grain boundaries and 120° triple junctions (see Mercier and Nicolas, 1974 for a complete discussion of these textural types). The state of alteration of the samples plays a part in the interpretation of the peridotite textures, in that the relatively fine grained neoblasts of olivine and enstatite characteristic of porphyroclastic textures could be overlooked in some cases where they are obscured by a secondary metamorphic overprint. The third major textural grouping of Mercier and Nicolas (1974), the equigranular group, is not represented in this sample set, nor is it generally observed in abyssal peridotites.

The mylonite samples (AII107:61-78 and AII107:61-83) represent a further textural type not discussed by Mercier and Nicolas (1974). These samples are similar in some respects to the equigranular texture described by Mercier and Nicolas (1974) in that they are largely composed of recrystallized olivine and enstatite, but they are much finer grained. Olivine neoblasts in these samples renge from 1 mm down to less than 10 microns. In addition, the mylonites are also strongly layered rocks, with layers defined largely by the grain size of recrystallized olivine. The largest recrystallized olivine grains mantle strained

enstatite augen, similar to the tabular equigranular type of Mercier and Nicolas (1974). There are however two important differences between these mylonites and the equigranular xenoliths described by Mercier and Nicolas (1974). First, these mylonites exhibit extreme variation in the grain size of the recrystallized phases (from 0.1 mm. down to sub-microscopic). Second, both the upper and lower limits of the sizes of recrystallized grains is smaller than the relatively uniform ~0.7 mm. grain size of the equigranular xenoliths.

In highly deformed tectonites, the grain size of neoblastic phases is dependent upon two competing processes: strain and recrystallization (cf. Spry, 1983). Strain tends to reduce grain size at all pressure and temperature conditions, though by different mechanisms in different pressure and temperature regimes. Recrystallization tends to increase grain size, as newly formed grains with low internal stress due to dislocations grow at the expense of highly stressed primary grains (or older neoblasts). The very different grain sizes of the abyssal mylonites studied here suggests strongly that the conditions of strain rate and rate of recrystallization under which they formed were quite different than the tabular equigranular xenoliths of Mercier and Nicolas (1974), which they resemble the most texturally. For this reason, the abyssal mylonites should be considered a separate textural category, and would be a fruitful object for further petrologic and petrophysical study. Detailed petrographic descriptions of the mylonite samples are given in Appendix I.

Olivine

In the non-mylonitic samples, olivines are generally preserved as relicts within a mesh-textured mass of alteration products, mostly consisting of serpentine and magnetite. Where relicts are sufficiently abundant and large, the positions of primary grain boundaries may be inferred from the common extinction of relicts comprising former individual olivine crystals. The grain size determined this way is commonly around 0.5 cm., but ranges as high as 5 cm. This is somewhat larger than is typical for the alpine peridotites and xenoliths studied by Mercier and Nicolas (1974), but is not unusual for abyssal peridotites (Dick, et al., 1984; Michael and Bonatti, 1985). Major element analyses of selected olivines (H. Dick, personal communication) are presented in Table 3. The compositions range from $Fo_{90.0}$ to $Fo_{90.8}$. These are typical for abyssal peridotites (Bonatti and Hamlyn, 1981; Dick, et al., 1984; Michael and Bonatti, 1985a; Cannat, et al., 1992).

Table 3: Olivine analyses

Cruise	AII-107	IO 11/76	VULC 5	VULC 5
Sample	61-78	60-61	41-29	41-15
SiO_2	40.81	40.60	40.42	40.70
FeO	9.41	8.96	9.40	9.78
MnO	0.16	0.07	0.16	0.17
MgO	49.77	49.65	49.13	49.23
CaO	0.00	0.02	0.05	0.04
NiO	0.28	0.25	0.28	0.31
Sum	100.43	99.55	99.44	100.23
Cations on the basis of 4 formula oxygens				
Si	0.995	0.990	0.986	0.993
Fe	0.192	0.183	0.192	0.199
Mn	0.003	0.001	0.003	0.004
Mg	1.809	1.804	1.786	1.789
Ca	0.000	0.001	0.001	0.001
Ni	0.005	0.005	0.005	0.006
Mg#	0.904	0.908	0.903	0.900

Olivine textures divide themselves into two groups, strained and recrystallized. The strained population of olivines are typically relatively coarse grained and undulose, or even divided into subgrains, while the neoblastic, recrystallized olivines are typically not undulose, and have straight grain boundaries culminating in 120° triple junctions. It is interesting to note that neoblastic olivine appears to be less affected by alteration than primary olivine, which is the more strained.

Orthopyroxene

Orthopyroxenes show considerable textural variation in the abyssal peridotites studied here. This is presumably due to the greater complexity of the subsolidus behavior of the pyroxenes. Many samples (e.g. RC 2709:6-2) have large enstatites with no exsolution and little alteration, while in others, sub-solidus exsolution of clinopyroxene, kink banding, and alteration of the enstatite seem to have progressed together.

Where the orthopyroxenes are not pervasively altered to bastite, they are commonly bastitized in the immediate vicinity of through-going cracks. In some cases, these cracks become veins filled with secondary minerals that pinch out at the edge of the orthopyroxene crystal. In some less altered samples, undulose

Table 4: Orthopyroxene analyses

Orthopyroxene analyses in peridotite:				
Cruise	AII-107	AII-107	IO 11/76	VULC 5
Sample	61-78	61-83	60-61	41-29
SiO2	54.44	53.32	54.60	53.88
TiO2	0.04	0.03	0.13	0.00
Al2O3	4.98	3.52	3.93	5.10
FeO	5.96	6.26	5.50	5.49
MnO	0.14	0.14	0.14	0.16
MgO	32.87	34.89	31.80	31.84
CaO	1.67	1.45	1.82	2.40
Na2O	0.05	0.07	0.11	0.04
K2O	0.00	0.02	0.05	0.00
Cr2O3	0.43	0.43	0.97	0.77
Sum	100.58	100.13	99.05	99.68
Mg#	0.908	0.909	0.912	0.912
EN	0.879	0.885	0.879	0.869
WO	0.032	0.026	0.036	0.047

Formula anions based on 6 oxygens:				
	AII-107	AII-107	IO 11/76	VULC 5
	61-78	61-83	60-61	41-29
Si	1.875	1.837	1.881	1.856
Al^{IV}	0.125	0.143	0.119	0.144
Al^{VI}	0.077	0.000	0.040	0.063
Ti	0.001	0.001	0.003	0.000
Fe	0.172	0.180	0.158	0.158
Mn	0.004	0.004	0.004	0.005
Mg	1.687	1.791	1.632	1.635
Cr	0.012	0.012	0.026	0.021
Ca	0.062	0.054	0.067	0.089
Na	0.003	0.005	0.007	0.003
K	0.000	0.001	0.002	0.000
Sum Z	2.00	1.98	2.00	2.00
Sum M	2.02	2.05	1.94	1.97

extinction is observable as well as polygonalization and grain boundary recrystallization. The most altered enstatites are converted completely to bastite. Microprobe analyses of representative orthopyroxenes from this study (H. Dick, personal communication) are shown in Table 4. On a plot of Al_2O_3 vs. Mg/(Mg+Fe*), the orthopyroxenes from this study are typical of those displayed by abyssal peridotites as a group (cf. Dick, 1989). Aluminum content of enstatite decreases with Mg/(Mg+Fe*) and modal olivine, as it does for the global data set, which is attributed to variations in space and time of mantle melting along the ridge (Dick, et al., 1984; Michael and Bonatti, 1985a).

Clinopyroxene

Chrome diopsides in this study are uniformly strongly exsolved into lamellae of orthopyroxene and clinopyroxene. This is strong evidence for their reequilibration at moderate temperatures in the mantle or high levels in the crust. Although these samples were chosen for their freshness, clinopyroxene is generally the best-preserved primary silicate phase in abyssal peridotites, except in those cases where amphibolite facies metamorphism has occurred. Clinopyroxene grains are typically finer than enstatite, 0.5-3 mm., and the grain size of clinopyroxene seems to correlate with the modal abundance of clinopyroxene in

the sample. In samples with very little clinopyroxene, it is generally intergranular and fine-grained, while in samples with more clinopyroxene it is coarser, and may approach orthopyroxene in size. Only in rocks with abundant clinopyroxene does it typically occur as isolated grains, as it otherwise tends to occur in clusters with orthopyroxene and spinel (cf. Mercier and Nicolas, 1974). Table 5 shows electron microprobe analyses of clinopyroxenes in the peridotite samples of this study. Because of the variety of methods used to obtain the clinopyroxene data (some of the data are fused clinopyroxene and others are clinopyroxene lamellae in orthopyroxene), the comparison of these data with other abyssal peridotite clinopyroxenes is not straightforward. As is to be expected, the fused samples show lower CaO than the clinopyroxene lamellae.

Trace elements in clinopyroxene

Trace elements are most usefully measured in clinopyroxene in abyssal peridotite for two reasons: First, it has the highest concentrations of incompatible trace elements and second because this phase is generally better preserved in abyssal peridotites than are olivine or orthopyroxene. Johnson, et al. (1990) use trace element measurements in abyssal peridotites to show that fractional or near-fractional melting is required to produce the trace element characteristics observed in abyssal peridotite clinopyroxenes. Elthon (1992), reinterprets the same trace element data set on the basis of a linear basalt addition model. Mantle depleted completely by fractional partial melting is "refertilized" at a higher level in the mantle by melts ascending from below.

Three of the samples in this study were also studied by Johnson, et al. (1990). In addition to these data, ion probe measurements of three of the remaining clinopyroxenes were carried out for trace elements and rare earth elements. Table 6 gives the Johnson et al. (1990) data and additional analyses for representative samples in this study. As shown in Figure 2, the rare earth patterns range from the steep, light-rare earth depleted pattern of AII107:40-35 to the relatively flat pattern of sample RC2709:6-2. Abundances of incompatible elements in abyssal clinopyroxenes are consistent with a fractional melting process of melt generation in the mantle (Johnson, et al., 1990; Johnson and Dick, 1992). The samples for this study span nearly the entire range of clinopyroxene trace element compositions reported in Johnson, et al. (1990) and Johnson and

Table 5: Diopside analyses from spinel peridotites

Cruise	PS86	AII 107	IO11/76	IO11/76	IO11/76	VULC 5	VULC 5	RC 2709	AII 107
Sample	6-37[1]	61-83[2]	60-61[2]	56-58[1]	59-26[1]	41-29[2]	41-15[1]	6-2[1]	40-35[1]
SiO2	51.33	51.33	51.19	51.88	51.78	50.40	51.74	52.33	52.37
TiO2	0.46	0.14	0.20	0.21	0.13	0.25	0.38	0.13	0.06
Al2O3	7.33	5.21	5.09	6.37	5.3	5.95	7.54	4.94	4.09
FeO	2.91	2.89	2.70	3.05	2.07	3.26	3.04	2.58	2.17
MnO	0.09	0.08	0.09	0.101	0.01	0.09	0.09	0.08	0.075
MgO	15.16	17.89	16.74	16.84	15.94	18.76	15.54	15.85	16.85
CaO	21.58	20.27	20.14	20.81	23.12	19.46	20.97	22.81	24.06
Na2O	1.07	0.70	0.84	0.69	0.54	0.50	1.12	0.78	0.083
K2O	nd	0.02	0.05	nd	nd	0.00	nd	nd	nd
Cr2O3	0.97	0.82	1.70	1.01	1.23	1.27	0.90	1.63	1.202
Sum	100.90	99.35	98.74	100.99	100.12	99.94	101.32	101.13	100.98
Mg#	0.903	0.917	0.917	0.908	0.932	0.911	0.901	0.916	0.933
EN	0.903	0.917	0.917	0.908	0.932	0.911	0.901	0.916	0.933
WO	0.480	0.428	0.442	0.446	0.493	0.405	0.466	0.487	0.489
Formula anions based on 6 oxygens									
Si	1.847	1.847	1.842	1.867	1.863	1.814	1.862	1.883	1.885
Al tet	0.153	0.153	0.158	0.133	0.137	0.186	0.138	0.117	0.115
Al oct	0.158	0.068	0.058	0.138	0.088	0.066	0.182	0.093	0.059
Ti	0.012	0.004	0.005	0.006	0.004	0.007	0.010	0.004	0.002
Fe	0.088	0.087	0.081	0.092	0.062	0.098	0.091	0.078	0.065
Mn	0.003	0.002	0.003	0.003	0.000	0.003	0.003	0.002	0.002
Mg	0.813	0.959	0.898	0.904	0.855	1.006	0.833	0.850	0.904
Cr	0.028	0.023	0.048	0.029	0.035	0.036	0.026	0.046	0.034
Ca	0.832	0.782	0.777	0.802	0.892	0.750	0.809	0.880	0.928
Na	0.075	0.049	0.059	0.049	0.038	0.035	0.078	0.054	0.006
K	0.000	0.001	0.002	0.000	0.000	0.000	0.000	0.000	0.000
Sum Z	2.00	2.00	2.00	2.00	2.00	2.00	2.00	2.00	2.00
Sum M	2.01	1.98	1.93	2.02	1.97	2.00	2.03	2.01	2.00

[1]CPX exsolved Ca-rich lamellae average.

[2]Fused clinopyroxene. H. Dick, personal communication.

Dick (1992). Thus, the known range of conditions of melting in the oceanic mantle is included in this data set.

The clinopyroxenes from this study fall into three clear groups based on their rare earth element patterns. The first of these are the highly depleted samples AII107:40-35 and AII107:40-27. Neither of these samples were successfully analyzed for Nd isotopes. Their rare earth element compositions are within the range of compositions reported for the Bouvet fracture zone in Johnson, et al. (1990). The second group is comprised of the samples PS86:6-37, Vulc5:41-29 and Vulc5:41-15. These samples have light rare earth depleted patterns compatible either with equilibrium with primitive mid-ocean ridge basalt

Cruise	Sample		Sc	Ti	V	Cr	Sr	Zr	Ce	Nd	Sm	Eu	Dy	Er	Yb
Vulc5	41-15	JDS	51.3	2511	295	6727	3.94	8.63	0.31	1.27	0.95	0.43	2.18	1.37	1.36
Vulc5	41-29		55.0	1783	287	8120	1.29	4.72	0.29	0.83	0.82	0.37	2.18	1.31	1.32
AII107	40-35		na	360	239	8182	0.87	1.19	0.01	0.06	0.08	0.02	0.55	0.51	0.57
RC2709	6-2		38.7	1369	295	8870	30.35	6.32	1.60	1.77	0.95	0.35	1.49	0.92	0.97
PS86	6-37	JDS	52.7	2674	293	6829	5.40	11.33	0.75	2.37	1.46	0.64	2.82	1.72	1.69
AII107	40-27	JDS	73.6	326	274	6518	0.79	0.23	0.02	0.05	0.07	0.03	0.52	0.53	0.53

Table 6: Trace elements in abyssal peridotite clinopyroxenes. JDS denotes analyses taken from Johnson, et al., 1989. Other analyses use the same analytical procedure as those of Johnson, et al., 1989.

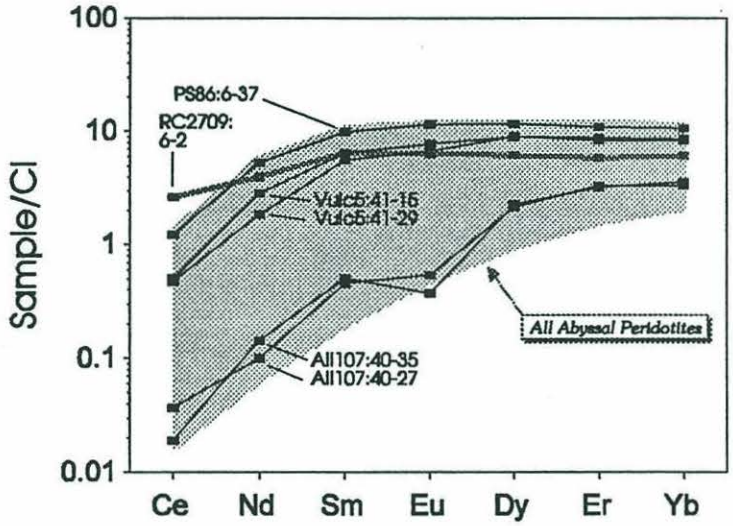

Figure 2: Rare earth concentrations in selected clinopyroxenes from this study. The shaded line indicates sample RC2709:6-2, which is a veined sample. The shaded field shows the compositions of abyssal peridotite clinopyroxenes from Johnson, et al., 1989.

(Johnson, et al., 1990) or with refertilization of highly deleted peridotite by basalt melt (Elthon, 1992). They fall within the compositional range of other peridotite clinopyroxenes from the dredge haul Vulc5:41 (Johnson, et al., 1990).

The sample RC2709:6-2, shown as a shaded line on Figure 2, is somewhat of a special case; its rare earth pattern is much flatter than is normally the case for abyssal peridotite clinopyroxenes in general and for those from the Atlantis II Fracture Zone (Johnson, et al., 1990; Johnson and Dick, 1992). The flatter rare earth pattern in this sample relative to other abyssal peridotites amounts to a light rare earth element enrichment. This sample has a vein of clinopyroxenite running through it in a thin seam of dunite. Sample RC2709-6-3 (not a part of this study) from the same dredge haul has no vein and a more typical depleted

Table 7: Abyssal peridotite spinel analyses.

Cruise	PS86	AII-107	AII-107	IO 11/76	IO 11/76	IO 11/76	VULC 5	VULC 5	RC 2709	AII 107
Sample	6-37[1]	61-78[2]	61-83[2]	60-61[2]	56-58[1]	59-26[1]	41-29[2]	41-15[2]	6-2[1]	40-35[1]
SiO2	0.03				0.020	0.04			0.08	0.065
TiO2	0.10	0.06	0.01	0.09	0.061	0.08	0.12	0.06	0.08	0.088
Al2O3	52.64	50.42	51.19	41.95	53.69	46.5	47.98	54.27	38.03	37.95
FeO	7.89	8.66	9.64	10.85	8.35	8.79	9.60	7.82	11.56	11.12
Fe2O3	3.79	4.74	4.22	3.03	2.8	2.33	3.76	4.44	4.46	3.35
MnO	0.12	0.09	0.08	0.17	0.097	0.12	0.19	0.15	0.15	0.14
MgO	20.58	19.94	19.69	17.88	20.72	19.37	19.29	20.69	17.02	17.46
Cr2O3	12.78	14.70	15.34	25.43	13.76	20.44	18.84	10.40	27.79	29.8
NiO	0.37	0.41	0.41	0.31	0.32	0.27	0.42	0.42	0.19	0.19
Sum	98.30	99.02	100.58	99.71	99.81	97.94	100.20	98.25	99.36	100.18
Number of ions in formula based on 32 oxygens.										
Si	0.006	0.000	0.000	0.000	0.004	0.009	0.000	0.000	0.017	0.014
Ti	0.016	0.010	0.002	0.014	0.010	0.013	0.019	0.010	0.013	0.014
Al	13.204	12.647	12.840	10.523	13.468	11.664	12.035	13.613	9.539	9.520
Fe3+	0.607	0.759	0.676	0.485	0.448	0.373	0.602	0.711	0.714	0.536
Cr	2.150	2.473	2.580	4.277	2.315	3.438	3.169	1.749	4.674	5.012
Fe2+	1.404	1.541	1.715	1.931	1.485	1.564	1.708	1.391	2.057	1.979
Mn	0.022	0.016	0.014	0.031	0.017	0.022	0.034	0.027	0.027	0.026
Mg	6.526	6.323	6.243	5.670	6.570	6.142	6.117	6.561	5.397	5.538
Ni	0.063	0.070	0.070	0.053	0.054	0.046	0.072	0.072	0.033	0.032
Sum A	8.01	7.95	8.04	7.68	8.13	7.77	7.93	8.05	7.51	7.58
Sum B	15.98	15.89	16.10	15.30	16.24	15.50	15.83	16.08	14.96	15.10
Mg#	0.823	0.804	0.784	0.746	0.816	0.797	0.782	0.825	0.724	0.737
Cr#	0.140	0.164	0.167	0.289	0.147	0.228	0.208	0.114	0.329	0.345
Fe3+#	0.038	0.048	0.042	0.032	0.028	0.024	0.038	0.044	0.048	0.036

[1] Data collected by Linda Angeloni at MIT.
[2] Dick and Bullen, 1984.

rare earth element pattern (Johnson, et al., 1990). The significance of this sample will be discussed in greater detail in a later section.

Spinel

Spinel in all of the samples is a dark brown to black chromian spinel. The opacity of the spinel seems to be a function of the degree of alteration of the rock. The spinels exhibit a wormy texture which is characteristic of spinels from abyssal peridotites, xenoliths, alpine lherzolites and ophiolites (Mercier and Nicolas, 1974; Dick and Fisher, 1984; Michael and Bonatti, 1985a, b; Shibata and Thomp-

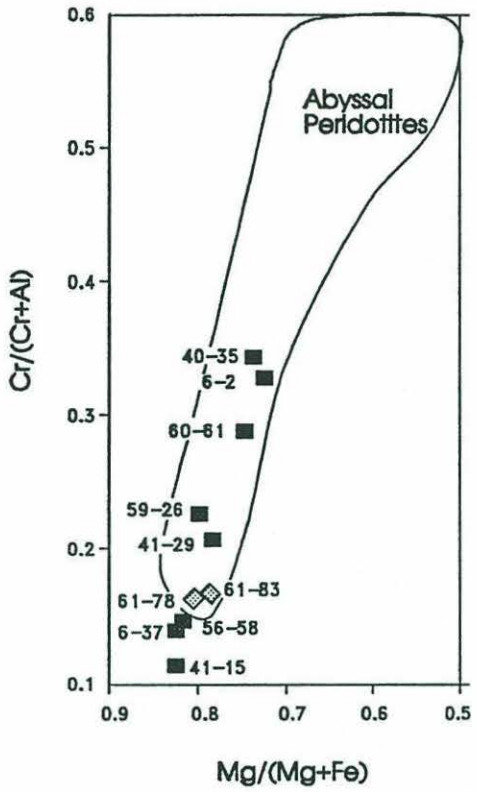

Figure 3: Cr/(Cr+Al) vs. Mg/(Mg+Fe) in spinel. Spinels from this study are shown in relation to the range of abyssal peridotite spinel compositions (Dick and Bullen, 1984). Filled diamonds are spinels from mylonite samples.

son, 1986 and others). There are typically thin cracks running through the spinels filled with a secondary mineral.

Electron microprobe analysis of the spinels showed them to be quite homogeneous in these samples, with no significant variations from core to rim. Table 7 gives the measured spinel compositions. On a diagram of Cr/(Cr+Al) vs. Mg/(Mg+Fe) (Figure 3), the range for spinel compositions is nearly half as great as the entire range of abyssal peridotite data (Dick and Bullen, 1984; Dick, 1989).

Plagioclase

Plagioclase, another common mineral in abyssal peridotite, is not represented in this sample set. If plagioclase peridotites represent mixtures of residual peridotite and trapped melt (Dick and Fisher, 1984; Quick, 1981; Dick, 1989), then the isotopic compositions of lithophile elements in plagioclase peridotites

are dominated by the presence of the trapped basaltic liquid, effectively resetting them. Plagioclase is easily recognizable, even as highly altered masses of sericite or prehnite, and samples containing plagioclase were excluded from consideration for this study.

Secondary mineralogy

The secondary mineralogy of these rocks is unremarkable when compared to the peridotites studied by Kimball, et al. (1985), Kimball and Gerlach (1986), Cannat, et al. (1992), Shibata and Thompson (1986) or Hart (1972). Serpentine (lizardite) comprises 40-90 percent of the rock, pseudomorphous after olivine with magnetite and after orthopyroxene (bastite). These replacement textures are by far the dominant mode of alteration in these particular rocks, and the volume of veins is quite low, commonly less than 1%. In most samples, the fine grained mesh structure which is pseudomorphous after olivine also includes reddish-brown, progressively more oxidized and hydrated iron minerals. These probably include hematite, goethite and limonite, which are not readily distinguished optically. These iron rich phases subsequently replace the magnetite in some of the more altered samples (e.g., IO 11/76 60-61 and 56-58).

Table 8 shows analyses of serpentines from three samples in this study, measured by Linda Angeloni on the MIT JEOL 733 super probe. These data are collected without measuring H_2O, and the totals of the analysis are correspondingly low. They agree largely with published major element analyses of serpentine (Deer, et al., 1966), if the water in those analyses is subtracted. The lack of water data and resulting "low" totals of these analyses complicate the evaluation of the mineral data somewhat. Rather than try to estimate the amount of water in the formula from the total of the analysis, the number of oxygens was adjusted to reflect the missing OH groups in the unit cell. The data can thus be compared usefully to analyses in which H_2O has been measured and the total is the usual 9 oxygens.

There are a number of interesting aspects to the serpentine data. First is the relatively high concentrations of Al_2O_3 and FeO compared to commonly observed serpentines (Deer, et al., 1966). This is typical of abyssal peridotite serpentines (Kimball, et al., 1985; B. Bazylev, personal communication). Hébert, et al. (1990) note that there is a strong correspondence between the compositions of

Table 8: Serpentine analyses from abyssal peridotites.

Cruise	PS86	PS86	PS86	RC2709	RC2709	RC2709	IO11/76	IO11/76
Sample	6-37	6-37	6-37	6-2	6-2	6-2	59-26	59-26
comment	vein, bladed	vein, bladed	vein, fibrous	oliv alt. net	En-Hosted	En-Hosted	vein	vein
SiO2	42.29	38.32	43.22	43.40	43.63	42.84	43.02	43.21
Al2O3	2.02	5.66	1.36	0.06	1.74	2.91	1.07	1.13
MgO	37.07	29.19	37.06	39.86	39.50	36.19	37.69	37.27
FeO*	7.04	14.42	6.73	4.79	3.00	5.95	3.66	3.58
CaO	0.00	0.00	0.00	0.02	0.00	0.14	0.02	0.00
TiO2	0.00	0.03	0.01	0.05	0.09	0.09	0.00	0.07
Cr2O3	0.03	0.05	0.04	0.00	0.00	0.00	0.00	0.00
MnO	0.08	0.32	0.11	0.06	0.09	0.11	0.16	0.21
NiO	0.00	0.00	0.00	0.27	0.07	0.07	0.00	0.05
Na2O	0.04	0.02	0.03	0.04	0.00	0.02	0.00	0.02
K2O	0.03	0.04	0.05	0.02	0.02	0.00	0.00	0.00
Total	88.60	88.05	88.61	88.57	88.14	88.32	85.62	85.54
Ions on the basis of 7 oxygens:								
Si	2.005	1.950	2.035	2.017	2.030	2.032	2.057	2.068
Al	0.056	0.170	0.038	0.002	0.048	0.081	0.030	0.032
Mg	2.620	2.213	2.601	2.760	2.739	2.558	2.686	2.658
Ca	0	0	0	0.001	0	0.007	0.001	0
Ti	0	0.001	0.000	0.002	0.003	0.003	0	0.003
Cr	0.001	0.001	0.001	0	0	0	0	0
Mn	0.003	0.014	0.004	0.002	0.004	0.004	0.006	0.009
Fe	0.279	0.614	0.265	0.186	0.117	0.236	0.146	0.143
Ni	0	0	0	0.010	0.003	0.003	0	0.002
Na	0.002	0.001	0.001	0.002	0	0.001	0	0.001
K	0.001	0.001	0.002	0.001	0.001	0	0	0
Sum A	2.06	2.12	2.07	2.02	2.08	2.11	2.09	2.10
Sum B	2.91	2.85	2.87	2.96	2.87	2.81	2.84	2.81
B/A	1.41	1.34	1.39	1.47	1.38	1.33	1.36	1.34

primary minerals and the serpentines which replace them. This is born out even in the small group of samples studied here. For example, even though the vein serpentine in sample PS86:6-37 has as much as 5.7 Wt. % Al_2O_3, olivine hosted serpentine contains almost no alumina.

The ratio of Mg (and elements which substitute for it) to (Si + Al) is somewhat low for these serpentines, compared to those listed in Deer, et al. (1966). Again, this property does not seem to be unusual for abyssal peridotite serpentines (Kimball, et al., 1985). Another important point is that petrographic

indications can be deceiving in these rocks. In Appendix I, the vein mineral analyzed twice in sample IO 11/76:59-26 (Table 8) is described as having high first order birefringence and high relief, neither of which characteristics are normally observed in serpentines. Nonetheless, these samples are all clearly serpentines and not, for example, talc (Mg/Si≈0.8), chlorite (Mg/Si = 1.5 but Al_2O_3 > 20%), or hornblende (oct/tet ≈ .6). One of the serpentines (Column 2 of Table 8) has an unusually high iron content, even for an abyssal peridotite serpentine. A concerted effort was made to locate and analyze possible high-temperature minerals (amphibole, secondary diopside, chlorite, etc.). High temperature minerals have been frequently observed in abyssal peridotites (e.g., Dick, 1979; Kimball, et al., 1985). None of the secondary minerals analyzed here were determined to be anything but serpentine.

Aragonite is occasionally found in abyssal peridotites as massive radial aggregates filling veins as large as a few centimeters across (Thompson, 1972; Bonatti, et al., 1980). In the samples studied here it occurs in a fine-grained form which is difficult to detect optically. Due to the high Sr content of aragonite found in abyssal peridotite (as much as several percent), samples with obvious aragonite were excluded from study. One sample (PS86:6-37) was found to contain aragonite during mineral separation, but was retained in the study. The effects of aragonite precipitation on isotopic and trace element systematics are discussed in a later section.

X-ray diffraction.

In order to constrain the mineralogic content of the major alteration products, X-ray diffraction patterns were run on first magnetic fractions from two abyssal peridotites, samples IO 11/76:56-58 and PS86:6-37. The first magnetic fractions were chosen so that primary phases such as olivine, orthopyroxene, clinopyroxene and spinel would not unnecessarily complicate the diffraction spectra. The first magnetic fractions were presumed to consist primarily of the alteration products of olivine: serpentine and magnetite. The samples were mounted in an ethanol slurry onto a thin aluminum holder and run in a Philips X-ray diffractometer using Cu-kα radiation. The digital data were modeled in MATLAB using a simultaneous inversion technique based on Newton's method (Menke, 1984; Shaw, 1990).

Table 9: Peaks matched by powder x-ray diffraction.

Pk	d (Å) for sample:		Chrysotile		Lizardite		Antigorite		Magnetite		Brucite	
#	56-58	6-37	d	hkl	d	hkl	d	hkl	d	hkl	d	hkl
1	7.364	7.371	7.36	002[1]	7.40	001	7.33	006				
2	7.268	7.250	7.28	002[2]								
3	4.555	4.696	4.54	020	4.60	020	4.60	020			4.77	001
4	3.668	3.661	3.66	004	3.67	002	3.66	0.0.12				
5	3.007	2.991							2.97	220		
6[3]	2.799	2.783										
7	2.536	2.534	2.53	202	2.51	201	2.50	206				
8	2.489	2.497							2.53	311		
9	2.281	2.281	2.28	203	2.31	040						
10	2.178	2.174			2.16	202						
11	2.128	2.126							2.10	400		
12	1.826	1.817	1.823	008	1.84	004						
13	1.778	1.775	1.745	206	1.80	203					1.79	102
14	1.705	1.701			1.69	311			1.72	422		
15	1.670	1.663							1.62	511		
16[3]	1.652	1.641										
17[3]	1.595	1.597										

56-58 and 6-37 denote the samples IO11/76:56-58 and PS86:6-37

[1] Orthorhombic [2] Monoclinic [3] Peak not matched.

JCPDS numbers: Chrysotile: 25-645,21-543,21-1262 Lizardite: 18-779 Antigorite: 9-444 Magnetite: 19-629 Brucite: 7-239

Figure 4 shows a typical diffraction spectrum. Using a Lorentzian spectral distribution to model the individual peaks, 16 major and minor peaks accounted for 92-93% of the total variance of the diffractograms. The residuals are also shown. Table 9 lists the peak correspondences found.

Minerals detected:

As was expected, serpentines accounted for most of the peaks in the spectrum. Many of the expected peaks for the serpentines were not found, and those that were found did not have the intensities expected (some were stronger and some weaker), probably due to preferred orientation of the minerals during preparation. The basal serpentine peak (numbers 1-2) is widened, due to the considerable variability in the basal spacing for the various serpentine polymorphs. This had the effect that two model peaks were necessary to fit the broadened peak. In the case of a pure mineral, the spacing of the basal peak could be used to distinguish the serpentines. In these heterogeneous samples,

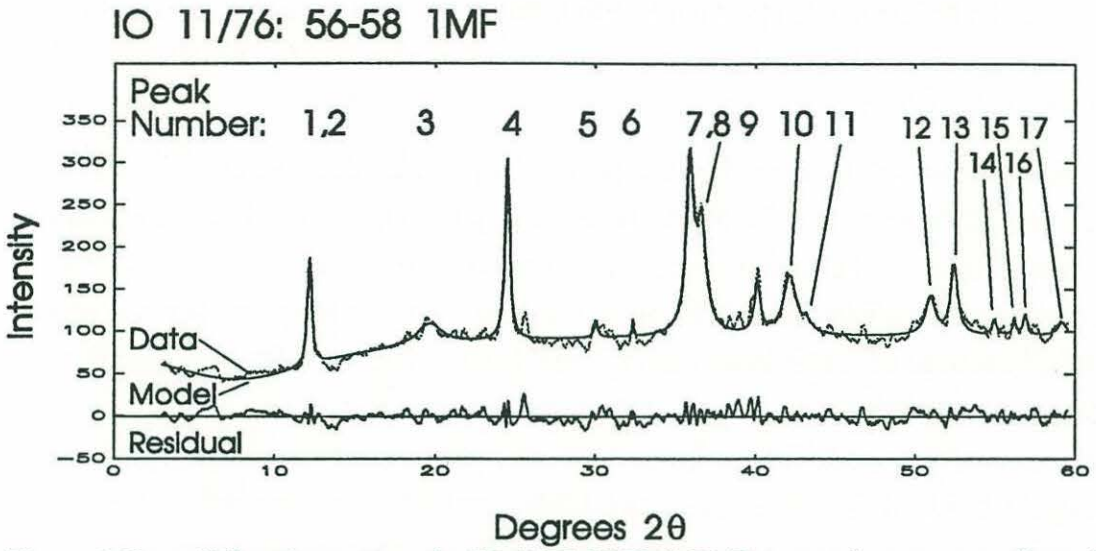

Figure 4: X-ray diffraction pattern for IO 11/76: 56-58 1MF. Data are shown as gray lines. The solid black line shows the best-fit model of 17 peaks using a lorentzian peak shape and a modified Newton's method peak optimization routine.

that was not possible. The second order serpentine reflection is well represented, and is quite sharp, reflecting the smaller variation in that spacing amongst the serpentines. The third major serpentine peak is peak 8, the lizardite (201) peak, which is very well expressed. This suggests that lizardite is the dominant serpentine in this sample. The other pseudomorphs of serpentine do not have significant peaks in this region.

Magnetite is indicated by the small peak (number 5) and the lower peak of the doublet at 37 degrees 2θ (peak 8). Nearly all magnetite peaks in the range of spacings analyzed were represented in approximately the appropriate intensities. Since magnetite has cubic crystal symmetry, its material properties are isotropic, and result in a lessened tendency to preferred orientation in the sample.

The case for brucite in the sample is debatable. It is based on peak 13, which corresponds to the (102) brucite peak, and to the lizardite (203) peak. The serpentines in this sample show the tendency for the basal peak to be suppressed relative to the higher order peaks. If this is also true for brucite, then a suppressed (001) peak (4.77 Å) could be hidden in the noise surrounding the clay region (peak 3), which also obscures the serpentine (020) peaks. Peak 13 is too strong in sample 6-37 to be only due to the relatively minor lizardite (203) peak, which under normal circumstances is 50% of the most intense peak and tied for

ninth place in the lizardite spectrum with eight other minor peaks of lizardite. The preferred orientation of the sample, however, makes it possible that peak 13 is not due to brucite at all.

Clay peaks are observed in the region from 13-22 degrees 2θ. The breadth of the peaks indicates that the clays are generally poorly crystalline. The many clays which have peaks in this region are not shown in Table 9. One important class of clay minerals (generally known under the generic name smectite) carries a variable amount of water between its basal layers, which show considerable spacing variation depending upon the extent of hydration of the clay. When samples containing smectite are heated, the smectite structure collapses to a spacing similar to that of the non-expandable clays illite and kaolinite. If smectite is present in the sample, it can be determined by exposing the samples to warm ethylene glycol vapor for a week or so; this expands the smectite structure uniformly so that a large smectite peak appears at 3-5 degrees 2θ. The samples studied here were glycolated for a week at 80 degrees C in order to expand the crystal structure of the smectites. They were then re-analyzed. The new x-ray diffraction spectrum showed no increase in the 3-5 degree 2θ region which would correspond to expandable clays.

No peaks were observed which could possibly be due to any of the primary phases, possible sample contaminants, or metamorphic minerals beyond the ones discussed. Notably absent were the expected alteration products of the magnetite present in the sample: hematite, limonite and goethite. Also missing were talc, forsterite, anthophyllite, enstatite, calcite and aragonite. Even though sample PS86:6-37 contained substantial aragonite, as evidenced by its separation during grain picking and the high Sr concentration and seawater $^{87}Sr/^{86}Sr$ of the bulk sample, no aragonite was detected in the x-ray spectrum. This is probably due to two factors. First, the amount of aragonite required to completely dominate the Sr budget of the rock is small, in the neighborhood of 1 wt. %. This would not necessarily be detectable by x-ray diffraction. Second, if the aragonite were not intimately intergrown with magnetite (as the serpentines are), it would have been less likely to be taken up in the first magnetic fraction, and would be underrepresented. In any case, x-ray diffraction is probably not useful as an indicator of the presence of aragonite; Sr concentrations in a peridotite suspected of harboring aragonite are a much more sensitive indicator.

Conclusion from XRD data

Serpentines are the major constituent of the alteration assemblage studied in the samples analyzed, in the order lizardite >> chrysotile > antigorite, which may not be present at all. Magnetite is certainly present in the samples, as are clays, though these are poorly crystalline and cannot be distinguished. The presence of brucite cannot be ruled out.

Bulk Chemistry

Bulk XRF analyses were carried out on the samples from this study. Major element and trace element compositions of the samples are reported in Table 10. The samples were analyzed in the WHOI X-ray fluorescence laboratory using the standards and methods described in Schroeder, et al. (1980). The peridotite samples were analyzed as pressed powder pellets for trace elements and as fused glasses for major elements. The major elements are thus reported on an anhydrous basis, while the trace elements are on a hydrous basis. This is only an issue if trace element concentrations are to be compared with major element concentrations (as is done when comparing Cr_2O_3 concentrations to those estimated for the primary peridotite). In this case, the volatile loss on ignition is taken into account when specifying the Cr content of the rock.

The analyses in Table 10 show considerable absolute and relative ranges in major element and trace element composition. This range in chemistry likely reflects alteration more than it does the chemistry of the unaltered rock. To a first order this can be shown by the fact that the analysis of weathered rinds and fresh cores for the samples from dredge AII107:61 nearly bracket the elemental ranges for the table as a whole.

There are a few striking aspects to the bulk chemical data set at first inspection. Sample IO11/76: 56-58 stands out as being higher in Fe, Co, Cu and Zn, but not particularly higher in manganese than other samples; it is also the lowest in MgO and next to highest in SiO_2. Sample IO 11/76: 60-61 is higher in MnO, but not in FeO or Co, than the others. Sample PS86:6-37 is higher in CaO (3.6%) than the other samples, but more than ten times higher in Sr (231 ppm.) than the others. Reasons for these first order elemental anomalies will be discussed in a later section.

Table 10: Whole rock major and trace element concentrations for abyssal peridotite.

Sample	SiO_2	Al_2O_3	MgO	Na_2O	K_2O	FeO	TiO_2	P_2O_5	MnO	CaO	SUM	LOI
IO11/76:56-58	46.51	2.91	36.35	0.30	0.05	10.04	0.05	0.04	0.15	2.74	99.15	7.58
IO11/76:59-26	45.11	1.96	43.52	0.06	0.01	7.96	0.03	0.00	0.10	0.70	99.45	11.24
IO11/76:60-61	46.18	1.30	41.21	0.18	0.03	8.78	0.05	0.03	0.21	0.93	98.90	10.55
PS86:6-37	44.41	2.29	40.15	0.15	0.01	8.39	0.06	0.01	0.13	3.59	99.18	8.85
RC2709:6-2	46.27	1.49	40.79	0.10	0.02	8.46	0.05	0.01	0.13	1.38	98.70	7.06
VULC5:41-15	45.93	3.10	38.99	0.16	0.01	8.45	0.09	0.01	0.13	2.09	98.96	10.58
VULC5:41-29	45.79	1.70	41.15	0.10	0.02	8.66	0.04	0.01	0.12	1.56	99.17	8.68
AII107:40-35	45.47	1.08	43.51	0.09	0.02	8.48	0.01	0.01	0.10	0.25	99.02	11.88
AII107:61-83C	43.17	1.86	44.06	0.07	0.01	8.28	0.02	0.01	0.13	1.48	99.08	1.6
AII107:61-83W	46.73	3.02	37.36	0.26	0.09	8.44	0.04	0.01	0.11	2.95	99.01	3.62
AII107:61-78C	44.31	2.07	42.71	0.06	0.01	8.22	0.03	0.00	0.13	1.77	99.32	1.86
AII107:61-78W	47.11	2.99	36.86	0.30	0.13	9.29	0.04	0.01	0.14	2.19	99.07	4.94
AII107:61-78M	45.17	2.47	41.85	0.14	0.04	7.30	0.03	0.01	0.14	1.80	98.94	5.86

Sample	Zr	Y	Sr	Rb	Zn	Cu	Ni	Cr	Co	Ba	V
IO11/76:56-58	6	5	9	2	95	54	1921	2760	130		133
IO11/76:59-26	7	1	4	1	38	10	2038	2894	86		60
IO11/76:60-61	17	2	12	2	89	35	2142	2182	113	22	72
PS86:6-37	37	1	231	1	44	17	2121	1867	106		54
RC2709:6-2	9	1	6	2	43	30	2101	2603	115		57
VULC5:41-15	8	3	5	2	40	21	1933	2024	95		75
VULC5:41-29	8	1	18	1	44	10	2328	1973	109		55
AII107:40-35	8	<1	5	2	30	3	2272	2067	103		51
AII107:61-83C	3	1	4	1	49	32	2346	2725	118		49
AII107:61-83W	5	3	6	3	60	24	1868	3696	106		93
AII107:61-78C	3	1	4	2	61	5	2221	2758	109		51
AII107:61-78W	5	2	7	5	69	8	1989	3435	118		89
AII107:61-78M	6	2	5	2	59	7	2210	3246	98		71
RC2709:11-7 (basalt)	72	25	213	3	54	66	181	350	50	32	217
Detection limit:	2	1	2	1		2				20	

Analyses were carried out by X-ray fluorescence. Major element concentrations are in weight percent, measured on fused glasses. They are thus anhydrous. Loss on Ignition at 1000°C. Trace element concentrations are in weight parts per million, and were measured on pressed powder pellets, dried at 110°C. The one basalt trace element analysis is provided for comparison. The capital letters appended to the sample numbers of the mylonite samples have the following meanings: W indicates a weathered rind, C indicates an unweathered core, and M indicates a serpentine vein on the margin of sample AII107:61-78.

The mylonite samples (AII107:61-78 and AII107:61-83) have particularly fresh cores and heavily weathered rims. They were analyzed primarily in order to examine the chemical effects of weathering. The implications of the mylonite data for weathering processes on the ocean floor, as distinct from hydrothermal alteration, will be discussed in a later section.

Isotopic data:

Analytical conditions.

The Nd and Sr isotopic composition and concentration analysis proceeded as follows: Samples were prepared for analysis by HF-$HClO_4$ dissolution, followed by chemical separation of alkali elements, Sr, and REE on Dowex 50 cation exchange columns. Sm and Nd were separated from the other rare earth elements using HDEHP-Teflon reverse phase ion exchange columns as described in Zindler, et al. (1979). Nd and Sr isotopes were run on the WHOI VG-354 5 collector mass spectrometer by dynamic multicollection. New algorithms and programs for the analysis of these isotopes were developed for this project and are described in detail in Appendix II.

Os isotopes and concentrations were determined by negative thermal ionization mass spectrometry (NTIMS, Creaser, et al., 1991; E. Hauri, WHOI Ph.D. Thesis, 1992). Separation of elemental Os by flux fusion and dichromate-sulfuric acid distillation, similar to Martin (1991) was followed by a bead chemistry step as described in Hauri and Hart (1993). In all, this study used very similar methods to Hauri and Hart (1993), with the exception of approximately 10x smaller sample size, with concomitant reduction in the blank, most of which is due to the Os content of the fluxing reagents (Hauri and Hart, 1993).

Bulk Nd, Sr, Os.

Table 11 shows the results of whole rock Nd, Sr and Os analysis for the samples studied. The range of Sr values extends from a nearly mantle-like isotopic composition of .7051 to a composition above the range of seawater Sr (0.70922 ± 2; Veizer, 1989). The range of Nd isotopic compositions is from the mantle field (0.5128-0.5133) all the way down to .5120. This is very close to the value for the isotopic composition of Indian Ocean seawater. The range of Os isotopic compositions is the same as that obtained by Martin (1991). The three re-analyses of rocks from that study show good agreement (within the analytical precision of that study), even though different separate pieces of the samples were used and not splits of the same powder.

Table 11: Whole rock Sr, Nd and Os isotopes.

Sample	Sr: 87/86	err	Nd: 143/144	err	Os: 187/186	Sr: ppm.	Nd: ppm.	Os: ppb.
RC2709:6-2	0.706222	23	0.512965	50	1.0418	4.13	0.197	4.483
Vulc5:41-29	0.709448	70	0.512580	174	1.0207	20.67	0.033	4.085
Vulc5:41-15	0.708204	25	0.513225	616	1.0521	3.75	0.156	3.859
AII107:40-35	0.709041	489	0.512428	61	1.0394	3.52	0.044	3.254
PS86:6-37	0.709141	27	0.513137	62	1.0149	311.48	0.091	4.984
IO11/76:60-61	0.709039	23	0.512225	10	1.0210	3.72	0.803	3.484
IO11/76:59-26	0.708875	26	0.512883	51	1.0293	2.42	0.201	4.049
IO11/76:56-58	0.709050	20	0.512195	31	1.0963	7.36	0.514	3.442
AII107:61-78C	0.705075	23	0.513158	195		5.22		
AII107:61-78M	0.707164	55				2.61		
AII107:61-83W	0.707706	28			1.0670	8.20	3.496	
AII107:61-83C	0.705448	27	0.512931	164	1.0700	1.22	0.045	

Sr isotopic compositions are reported normalized to 86/88=.1194 and relative to NBS SRM 987 = .710240. Nd isotopes normalized to 146/144=.7219. Measured value of LaJolla Nd shelf standard is .511850. Os isotopic compositions corrected for O isotopic interference and normalized to $^{192}Os/^{188}Os = 3.08271$ (Luck, et al., 1980) and $^{17}O/^{16}O = .0003708$ and $^{18}O/^{16}O = .002045$ (Nier, et al. 1950). Measured value of WHOI Os shelf is 187/186=1.045. Errors reported are relative to the last reported digit based on in-run statistics. Os isotopic composition uncertainty is approximately 0.2%. Concentrations are by isotope dilution, with a nominal precision of 0.5% for Sr and Nd and 1% for Os.

Sr in first magnetic fractions.

Excess radiogenic Sr ($^{87}Sr/^{86}Sr \geq .7092$) was first observed in serpentinites (Roe, 1965), but has not been observed in unaltered peridotites. This strongly suggests that the process of alteration itself has a role in the formation of the radiogenic Sr reservoir in abyssal peridotites. In order to study this process independently of the relatively well characterized and Sr rich mantle reservoir, a fraction was prepared which consisted only of these secondary phases.

Since the alteration assemblage typically included magnetite, the alteration phases could be separated from the bulk rock magnetically. Once the rock was ground to approximately 400-800 microns, the most magnetic portion of the sample was expected to be dominated by magnetite and serpentine. This fraction could be separated using either a hand magnet or by using a Frantz isodynamic magnetic separator on a low power setting. In either case the product consisted of strongly ferromagnetic composite grains of the olivine alteration products serpentine and magnetite. Olivine itself was probably not recovered. A low ratio of density to magnetization was necessary for a composite grain to

Table 12: First magnetic fractions and whole rocks.

First magnetic fractions

Cruise	Sample	$^{87}Sr/^{86}Sr$	K	Rb	Cs	Sr	K/Rb	Rb/Sr	$^{87}Rb/^{86}Sr$	T(s)[1]	2 pt. Age[2]
RC2709	6-2	0.72634	202.2	1.1		3.6	181.1	0.310	0.875	1366	1601
Vulc5	41-29	0.71115	154.7	0.4	2.9	5.9	410.1	0.064	0.180	759	663
PS86	6-37	0.70920	44.7	0.1	0.9	167.1	425.1	0.001	0.002	16	2308
IO11/76	56-58	0.71033	128.8	1.2		9.9	103.1	0.126	0.356	223	243
AII107	40-35	0.70919									

Whole rocks

Cruise	Sample	$^{87}Sr/^{86}Sr$	K	Rb	Cs	Sr	K/Rb	Rb/Sr	$^{87}Rb/^{86}Sr$	Crustal age[3]
RC2709	6-2	0.70622	72.6	0.121	1.1	4.1	601.8	0.029	0.082	0.6
Vulc5	41-29	0.70945	110.2	0.171	0.5	20.7	643.4	0.008	0.023	2.3
PS86	6-37	0.70914	43.3	0.044	0.2	311.5	980.4	0.000	0.000	5.0
IO11/76	56-58	0.70910	128.8	0.178	1.5	6.8	725.0	0.026	0.073	9.7
AII107	40-35	0.70904	3.5							17.0

Sr 87/86 is reported normalized to 86/88 = 0.1194 and a value for NBS SRM 987 Sr isotopic composition standard of 0.710240. Elemental concentrations are expressed in weight parts per million except for Cs which is in ppb.

[1] Model age assuming a starting $^{87}Sr/^{86}Sr$ of .7092, in Ma.

[2] Two point age calculated from whole rock and 1MF data, in Ma.

[3] Maximum age from sample locations, ridge geometries and spreading velocities.

be included in the first magnetic fraction. It is likely that the inclusion of an olivine grain in the first magnetic fraction would render it too heavy compared to its magnetization.

Table 12 shows Sr isotopic compositions and some trace element data for first magnetic fractions from selected peridotites, along with model ages and crustal ages. In 3 out of the 5 peridotites, the first magnetic fraction contained $^{87}Sr/^{86}Sr$ which was obviously in excess of the seawater value. In no case where excess $^{87}Sr/^{86}Sr$ is reported does the sample contain sufficient rubidium to produce the observed $^{87}Sr/^{86}Sr$ in any geologically reasonable period of time. In most of the cases, the absolute Sr concentration in the first magnetic fraction is quite low, so that the whole rock isotopic composition of Sr is much closer to that of seawater. There is otherwise no consistent relationship between the amount of excess ^{87}Sr, the crustal age, $^{87}Rb/^{86}Sr$ ratio, or any other measure of alteration.

In two samples (AII107:40-35 and PS86:6-37), there was no evidence of $^{87}Sr/^{86}Sr$ ratios significantly higher than seawater. In each case, however, the first magnetic fraction had a significantly higher $^{87}Sr/^{86}Sr$ than the whole rock. This

suggests that there is a component of radiogenic Sr which is more concentrated in the first magnetic fraction than in the whole rock. Alternatively, it may reflect the lack of (unradiogenic) clinopyroxene in the first magnetic fraction.

Os leaching study

In the study of the osmium isotopic system in rocks from the depleted oceanic mantle, the issue of alteration must be addressed. In particular there may be significant effects if there is incorporation of hydrogenous MnO-bearing material into the peridotite. These materials have both a high $^{187}Os/^{186}Os$ (6-8) and a high Os concentration (up to 3 ppb.), on the order of the peridotite itself (Palmer, et al., 1988). Thus, very small amounts of Mn crust contamination of the sample can produce very large isotopic effects on the host peridotite.

One consequence of the large difference in isotopic composition between the peridotite and its potential contaminant is that leaching combined with analysis of the leachate is a very sensitive tool for the detection of this type of alteration. Martin (1990, 1991) carried out a similar leaching study, but analyzed only the residue of leaching. If only a small amount of the contaminant is removed in this fashion, the residue may not change significantly in its isotopic composition. The leachate, on the other hand, is likely to record a very different mixture of contaminant to sample, and thus to be a much more sensitive tool for the detection of contamination effects. By analogy to trace elements in igneous rocks, the contaminant species is "incompatible" and the sample species is "compatible". At low degrees of dissolution the leachate contains a much higher difference in contaminant/sample than does the residue. This should make analysis of the leachate a sensitive means of detecting seawater-derived osmium in the rock.

Previous studies of hydrogenous Os bound to sediments provide chemical methods for the extraction of hydrogenous Os from a heterogeneous sample (Esser and Turekian, 1988; Ravizza and Turekian, 1989; Esser, 1991; Ravizza, et al., 1991). An *in situ* leaching technique was adopted analogous to ones used by those studies and by Pegram and Turekian (personal communication). In studies of the Os isotopic composition of sediments, a mixture comprising 5-30% H_2O_2 was found to remove only the chemically precipitated hydrogenous component of complex sediments while not attacking the meteoritic or detrital com-

Table 13: Os leaching results on lherzolite sample IO11/76:56-58.

Martin (1991):

	187/186	err	Os, ppb.	Comment
CM-1	1.081	0.015	3.077	Unleached sample
CM-2	1.068	0.014	3.01	Unleached sample
CM-3-L	1.099	0.026	3.247	Leached sample

This Study:

	187/186	err	Os, ppb.	Comment
JS-1	1.0963	0.002	3.44	Unleached sample
JS-L	1.0727	0.002	-	Leachate
JS-C[1]	1.0986	0.002	-	JS-1 corrected for cont.

[1] Calculated value of sample with labile Os fraction removed by mass balance with the other two samples.

ponents. Martin (1990, 1991) utilized HCl + H_2O_2, not wanting to oxidize the Os in the sample, as she was studying the residue of leaching only. A more aggressive approach was adopted for this study, since Martin (1990) had inconclusive results (on the same sample). It was deemed important for this study that sufficient total Os be removed from the sample + (potential) contaminant for an isotopic composition to be definitively measured.

For this study, approximately 10 grams of sample was placed directly into the distillation apparatus and leached in 0.1N H_2SO_4 and 15% H_2O_2 as an oxidizer. After the distillation apparatus was sealed, the sample + leaching solution began to evolve gas, slowly at first, then with increasing vigor. Once the frothing had subsided, heat was applied to the distillation flask, and further evolution occurred. The flask was heated to approximately the normal temperature of distillation (that of boiling 0.1N H_2SO_4) for 1 hour, then cooled. During the entire leaching procedure, the evolved gas was passed through cold HBr to trap OsO_4.

A second leach was then performed. The leaching solution was strengthened to 4N H_2SO_4 and CrO_3, the normal oxidant used in routine distillations, was added. All of the H_2O_2 in the flask had been destroyed, as evidenced by the brown color of the second solution. If the H_2O_2 had not been destroyed, it would have reduced the CrO_3 solution to blue. A second distillation (into a new beaker of HBr) was then carried out at the usual conditions of distillation (Martin, 1990; Hauri and Hart, in press; see the section on analytical methods).

Both leachates were then spiked, sealed in 30 ml. Teflon bombs and allowed to equilibrate overnight. They were then treated in exactly the same manner as all other samples with regard to bead chemistry, loading, reducing and run conditions. While the first leachate gave good results both for concentration and for isotopic composition, the second leachate did not contain significant natural Os. This suggests that the first leach mobilized all of the oxidizable Os in the sample. The bulk of the Os remains bound up in extremely resistant mineral phases which are not attacked significantly by the 4N H_2SO_4 and CrO_3 of the second leach. This is consistent with the current state of knowledge (such as it is) of the reservoirs of Os in mantle rocks. In most occurrences studied, Os resides in disseminated, very fine grains of Os-Ir alloy and platinum-group-element sulfides (Stockman and Hlava, 1984; Hattori and Hart, 1990). Such alloys and sulfides are typically difficult to dissolve with any but the most concentrated mineral acids, so it is unlikely that any of the primary Os in the sample was affected by the leaching procedure.

The fact that 0.1N H_2SO_4 and 15% H_2O_2 can mobilize a fraction of Os in peridotite suggests a new method for the leaching of Os in peridotite. The sample could be leached in a distillation flask, as was done in the first leach here, then removed from the flask, dried and analyzed with the normal flux fusion technique. In this case, analysis of the residue of leaching was made extremely inconvenient by the carcinogenic nature of the reduced CrO_3 used in the second leach. If this step is deleted, the analysis of leach and leachate in the same sample is possible. If this were applied on a wide variety of abyssal peridotites, it would be likely to shed some light on the reservoirs of Os in abyssal peridotite.

The results of the leaching of sample IO 11/76:56-58 are shown in Table 13 along with the results obtained by Martin (1990, 1991). These two leaching studies on the same rock are in generally good agreement. The details of the results of the Os leaching experiment will be discussed below in the section on alteration of abyssal peridotite where Os isotopes are discussed.

Mineral separates

Clinopyroxene separate preparation

A primary focus of this study is the evaluation of abyssal peridotites as carriers of mantle geochemical information through serpentinization and ocean floor weathering. Clinopyroxene is thought to be the mineral which carries the major fraction of the primary incompatible trace element budget of abyssal peridotites. An analysis of incompatible trace element concentrations or isotopic compositions in clinopyroxene is widely held to be representative of the peridotite composition. This assumption is inherent in almost all studies of trace elements and isotopes in peridotite clinopyroxene (e.g., Menzies and Murthy, 1976; Reisberg and Zindler, 1986; Salters and Shimizu, 1990; Johnson et al., 1990; Johnson and Dick, 1992 and many others) For this study, clinopyroxene was separated from 6 of the peridotites and leached to see whether the effects of submarine hydrous metamorphism could be removed. The removal of the seawater-derived signal would allow the direct measurement of primary Sr and Nd isotopes in mid-ocean ridge mantle-derived serpentinized peridotites.

Approximately 2-10 kg of bulk sample were crushed in a steel jaw crusher to less than about 1 cm. size. The samples were then further reduced to approximately 400-800 micron size in a rotary disk mill and washed in deionized water and ethanol. After removing the strongly ferromagnetic fractions with a hand magnet, a clinopyroxene-rich (approximately 40%) fraction was extracted from the rock using a new version of the Frantz isodynamic separator. The preparation of this fraction typically required 10-15 passes through the separator. Clinopyroxene fragments were hand-picked from this mixture to yield 100-150 mg. of nearly pure (99%) clinopyroxene. This separate was then crushed again, sieved to 200-400 micron size, washed in deionized water and acetone and picked again. Only completely clear clinopyroxene grains were used, free of inclusions of spinel, serpentine, and clay, and showing good cleavage. The amount of clinopyroxene used varied from 65 to 90 mg. of pure clinopyroxene, containing a minimum of 4 ng. total Sr (AII107:40-35) and 12 ng. Nd (IO11/76:56-58) for successful analyses.

Leaching of clinopyroxene for Nd-Sr isotopic analysis.

Leaching experiments were carried out for Nd and Sr on separated clinopyroxenes in order to try to eliminate the effects of serpentinization and weathering. Three leaches were made on each sample, using a leaching solution of 6.2N HCl + 5% HF. The first leach was at room tamperature for 5 minutes, the second was in the ultrasonic bath for five minutes and the third was in the ultrasonic bath for ten minutes followed by ten minutes in a drying oven at 125 ° C. The samples were then dried and weighed between leaches. The weight of material removed during each successive leaching step is shown cumulatively as the weight fraction dissolved in Figures 5a-e. Sr concentration and isotopic composition analyses were attempted on every leachate. Nd concentration and isotopic composition analyses were attempted in many of the leachates, but few were successful. Many of the leachates were also analyzed by isotope dilution for the abundances of the alkalis K, Rb, and Cs.

In other studies that made use of leaching of altered clinopyroxenes (e.g., Hart, 1972; Machado, Brooks and Hart, 1986) the attempt was made to find a leaching solution that would have a maximum effect on the contaminant and a minimum effect on the pyroxene. Since clinopyroxene appears to be a resistant phase during alteration, contaminants would typically be attached to the outside of grains and would not have penetrated the clinopyroxene grains. The approach was thus chosen to use a relatively strong leaching solution to try to remove grain boundaries.

In thin section, the alteration of clinopyroxene grains appears to be primarily on the grain exterior. Additionally, alteration along fractures through the clinopyroxene probably forms zones of weakness in the mineral grain. These fractures will be the planes of failure when the sample is crushed to 400 micron size for final picking. Contaminants thus end up to a large extent on the exterior of the clinopyroxene grain during leaching. Even if the contaminant dissolves at the same rate as the clinopyroxene, successive leaches will remove the contaminant preferentially, resulting in a decreasing contaminant component in each successive leaching step. If a plateau in the $^{87}Sr/^{86}Sr$ ratio is reached, then it is possible that the true $^{87}Sr/^{86}Sr$ of the clinopyroxene has been attained. In practice, there is also no reliable way of detecting whether all of the seawater Sr has been removed.

In all, 9 leaching experiments were undertaken on clinopyroxenes. The data are presented in Table 14. Sr isotopic composition was measurable on most of the leachates and the clinopyroxenes. Nd typically could only be measured on the last leachate and the pyroxene, the pyroxene only, or not at all. This probably reflects the higher Sr/Nd ratio of the components removed by leaching compared to the clinopyroxene.

Results of leaching experiments

Figures 5a-e show $^{87}Sr/^{86}Sr$ plotted against the cumulative weight fraction of clinopyroxene dissolved in each leaching experiment. Nearly all of the experiments show a monotonic decline in $^{87}Sr/^{86}Sr$ with increasing degree of dissolution. In some cases, Nd isotopic compositions could be measured on the third leachate as well as the clinopyroxene. In each case, the third leachate was lower in $^{143}Nd/^{144}Nd$ than the clinopyroxene. This agrees with the model for addition of seawater-derived Sr to the clinopyroxene which was the basis for the leaching procedure.

In Figure 5a, the two leaching attempts on sample RC 2709:6-2 are shown. The first leach of this series was a failure, in that it did not result in any isotopic analyses. The second and third leaches, numbered 6-2-2 and 6-2-3, are plotted as the lower and upper curves respectively. In both cases the first leachates have a Sr isotopic composition higher than that of the bulk sample, which has an unusually low $^{87}Sr/^{86}Sr$. The final result is $^{87}Sr/^{86}Sr$ values of .7047 and .7048. These are unlikely to be mantle values for this area (the Atlantis II Fracture Zone on the Southwest Indian Ridge), as nearby basalts do not attain values higher than 0.7029 (see Chapter 1) and the region lies far from any likely mantle "plume" sources.

There are three possible explanations for the high $^{87}Sr/^{86}Sr$ of the clinopyroxene from sample RC2709:6-2. First, there could be an unusual mantle composition beneath the Atlantis II Fracture Zone that is not reflected in the isotopic compositions of the basalts in this area. The low $^{143}Nd/^{144}Nd$ of the clinopyroxene argues against this hypothesis for the Sr isotopic composition. Though the Nd isotopic composition of this sample is unusual for this region, it is unlikely that it is coupled to the high $^{87}Sr/^{86}Sr$ by any primary mantle process. This will be discussed in detail in a later section.

Table 14: Leaching results on clinopyroxenes. The number appended to the sample name describes the analysis; the first number refers to the dissolution. The lower case letter, where present, refers to repeat analyses of aliquots of the same dissolution. An upper case I indicates concentration determination by ion microprobe (see Table 6). The following abbreviations describe the type of sample analyzed: WR (whole rock), Ln (leachate number n); CPX (leached clinopyroxene) and AR (aragonite). All trace elements are determined by isotope dilution (except for ion probe results as noted) and are reported in weight parts per million, except for Cs, which is in parts per billion. The K/Cs ratios are reported in thousands. Isotope dilution results were typically measured to a precision of better than 0.1 % and bear a nominal analytical uncertainty of 1%. Concentrations of leachates are based on the weight of dissolved clinopyroxene. In the case of repeat isotopic composition determinations on a single set of leachates (Sample Vulc5:41-29 1a and 1b), isotope dilution data on alkalis are shown twice. Sample PS86:6-37 AR (aragonite) was so under spiked that an isotope dilution calculation was not possible, indicating a Sr concentration far in excess of the expected concentration. $^{87}Sr/^{86}Sr$ is reported normalized to $^{86}Sr/^{88}Sr = .1194$ and corrected to NBS SRM 987 Sr isotopic composition standard value of 0.710240. This correction results in measured values of the secondary standard Eimer and Amend $SrCO_3$ of 0.70805. $^{143}Nd/^{144}Nd$ is reported normalized to $^{146}Nd/^{144}Nd$ of 0.7219. The average value of LaJolla Nd isotopic composition standard measured during the course of this work is 0.511848. Boldface Sr isootpic compositions are greater than that of seawater (0.7092).

Cruise	Sample		$^{87}Sr/^{86}Sr$	err	$^{143}Nd/^{144}Nd$	err	K	Rb	Cs	Sr	Nd	K/Rb	K/Cs	Rb/Sr
RC2709	6-2	WR	0.706222	23	0.512965	50	72.6	0.12	1.08	4.13	0.197	602	67	0.0292
RC2709	6-2 2	L1	0.706431	32			1054	1.93		51.5		547		0.0374
RC2709	6-2 2	L2	0.704893	23			51.6	0.12		21.25		414		0.0059
RC2709	6-2 2	L3	0.704797	24			13.1	0.02		31.11	1.976	570		0.0007
RC2709	6-2 2	CPX	0.704774	24			0.8	0.06		15.31	0.306	13		0.0003
RC 2709	6-2	WR	0.706222	23	0.512965	50	72.6	.12	1.08	4.13	0.197	602	67	0.0292
RC 2709	6-2 3	L1	0.706929	34						17.95				
RC 2709	6-2 3	L2	0.705283	574						37.05				
RC 2709	6-2 3	L3	0.705118	123						35.70				
RC 2709	6-2 3	CPX	0.704870	13	0.512994	15				24.09	1.056			
RC2709	6-2 I	CPX								30.35	1.77			
Vulc5	41-29	WR	**0.709448**	70	0.512580	174	110.2	0.17	0.53	20.7	0.033	643	208	0.0083
Vulc5	41-29 1a	L1	**0.709470**	17			368.0	1.70		7.74		216		0.2198
Vulc5	41-29 1a	L2	0.707124	254			17.9	0.48		0.62		37		0.7692
Vulc5	41-29 1a	L3	0.704043	127			10.5	0.03	0.25	0.84		321	42	0.0390
Vulc5	41-29 1a	CPX	0.702736	197			2.2	0.01	0.03	1.33		192	79	0.1332
Vulc5	41-29	WR	**0.709448**	70	0.512580	174	110.2	0.17	0.53	20.7	0.033	643	208	0.0083
Vulc5	41-29 1b	L1	0.709116	169			368.0	1.70		7.74		216		0.2198
Vulc5	41-29 1b	L2					17.9	0.48		0.62		37		0.7692
Vulc5	41-29 1b	L3	0.702776	232			10.5	0.03	0.25	0.84		321	42	0.0390
Vulc5	41-29 1b	CPX	0.702902	22	0.513147	31	2.2	0.01	0.03	1.34		192	130	0.0085
Vulc5	41-29	WR	**0.709448**	70	0.512580	174	110.2	0.17	36.9	20.7	0.033	643		
Vulc5	41-29 2	L1	**0.709245**	16						83.22				
Vulc5	41-29 2	L2	0.708416	169						4.66				
Vulc5	41-29 2	L3	0.705307	13	0.512928	30				1.89	1.382			
Vulc5	41-29 2	CPX	0.703351	158	0.513021	27				0.90	0.971			
Vulc5	41-29 I	CPX								1.29	0.83			
IO 11/76	56-58	WR	0.709100	21	0.512195	31	128.8	0.18	1.50	6.85	0.514	725	86	0.0259
IO 11/76	56-58 1	L1									5.970			
IO 11/76	56-58 1	L2	**0.710765**	27						15.09	1.684			
IO 11/76	56-58 1	L3	**0.709701**	26						16.29	16.274			
IO 11/76	56-58 1	CPX	0.708368	142						0.97	0.180			
IO 11/76	56-58	WR	0.709100	21	0.512195	31	128.8	0.18	1.50	6.85	0.514	725	86	0.0259
IO 11/76	56-58 2	L1	**0.709579**	28						6.72				
IO 11/76	56-58 2	L2	0.706716	123						4.42				
IO 11/76	56-58 2	L3	0.704374	38	0.512518	277				0.59	0.380			
IO 11/76	56-58 2	CPX	0.702644	25	0.513159	33				0.15	0.198			
PS 86	6-37	WR	0.709141	27	0.513137	62	43.3	0.04	0.22	311.5	0.091	980	197	0.0001
PS 86	6-37	L1	0.708800	85			1248	2.48	19.44	1105	0.358	504	64	0.0022
PS 86	6-37	L2	0.709094	26			66.4	0.12	0.47	168.6	3.243	541	141	0.0007
PS 86	6-37	L3	0.707994	24			6.1	0.01	0.10	29.63	1.823	413	59	0.0005
PS 86	6-37	CPX	0.703350	23	0.512960	41	31.4	0.42	12.18	6.42	1.468	75	3	0.0652
PS 86	6-37	AR	0.709169	31			42.2	0.13	1.29	Usp	0.128	317	33	
PS 86	6-37 I	CPX								5.40	2.37			
RC2709	25-139	L1	0.709003	23						9.92				
RC2709	25-139	L2	0.707700	21						2.38				
RC2709	25-139	L3	0.705657	24	0.512918	52				2.53	0.867			
RC2709	25-139	CPX	0.703173	23	0.513205	14				0.64	0.878			
AII107	40-35	WR	0.709041	489						3.52				
AII107	40-35	L1	0.709039	24						9.92				
AII107	40-35	L2	0.706703	45						2.38				
AII107	40-35	L3	0.704421	30						0.48				
AII107	40-35	CPX	0.702869	75						0.05	0.008			
AII107	40-35 I	CPX								0.87	0.06			

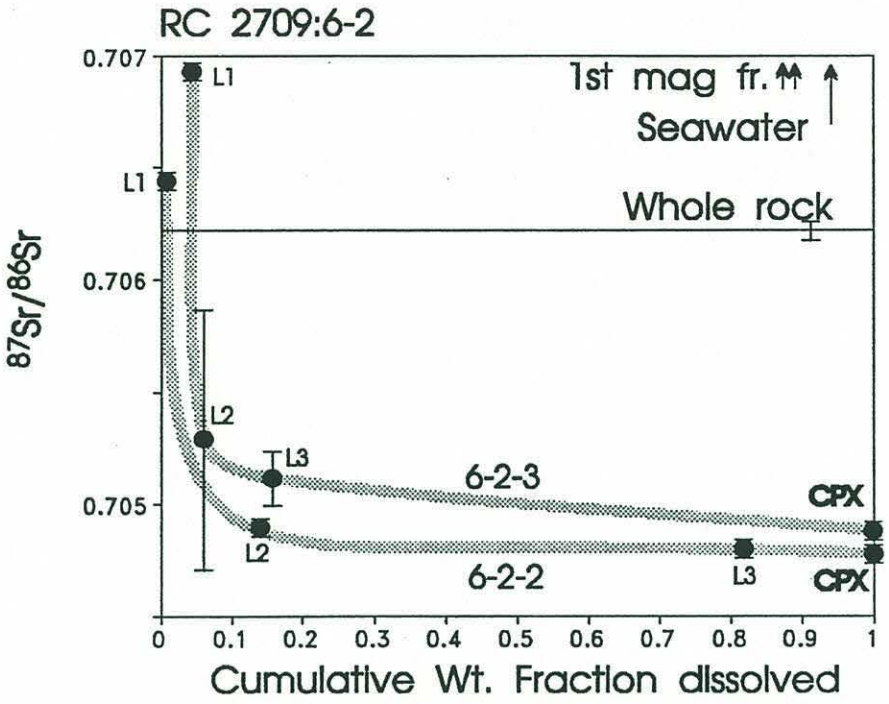

Figure 5a: Incremental leaching curve, sample RC2709:6-2. Lx denote incremental leaches; the x-axis shows the cumulative fraction of the clinopyroxene removed by the incremental leaching procedure. The residue after leaching is denoted by CPX, with a cumulative fraction dissolved of 1. The shaded line connects individual leachates of the same sample.

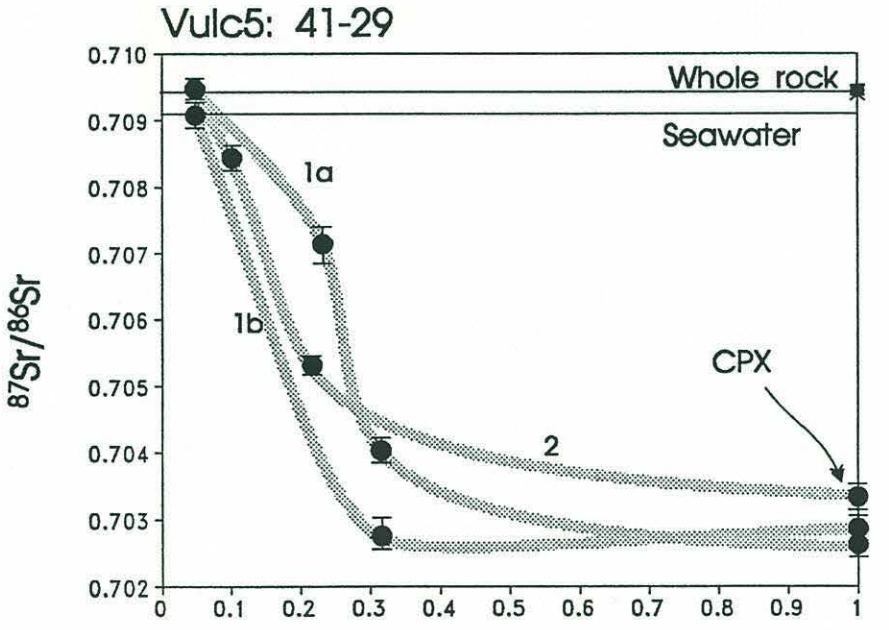

Figure 5b. Incremental leaching curve for sample Vulc5:41-29.

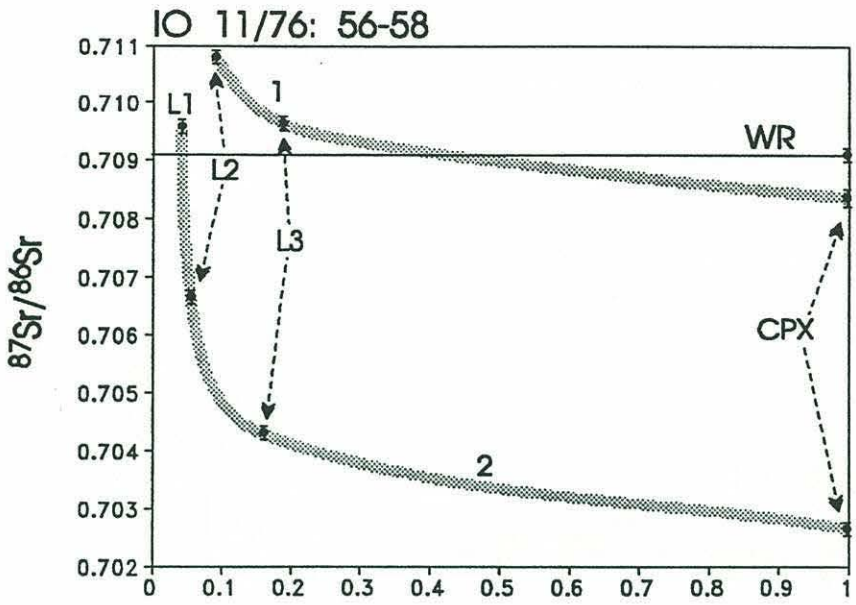

Figure 5c. Incremental leaching curve for sample IO 11/76: 56-58.

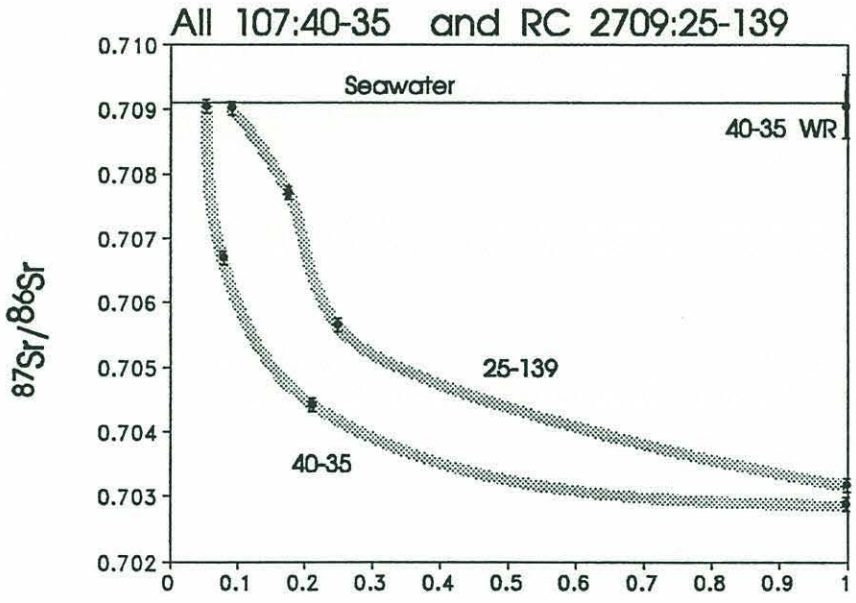

Figure 5d. Incremental leaching curves for samples AII 107:40-35 and RC2709:25-139.

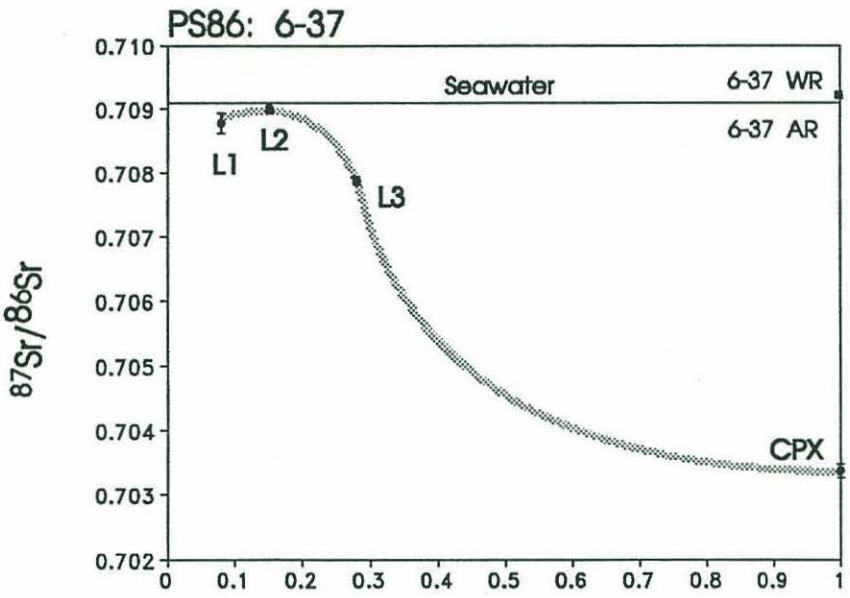

Figure 5e. Incremental leaching curve for sample PS86: 6-37. Whole rock (WR) and aragonite (AR) analyses are superimposed on each other.

A related hypothesis is that this sample represents a peridotite impregnated with an exotic enriched melt that is not reflected in the erupted basalt suite. This clinopyroxene sample was derived from a large peridotite boulder (approximately 17 Kg.) which also contained a 1 cm. thick vein of clinopyroxenite enclosed in a thin dunite selvage (Appendix I). This vein may represent cumulus crystallization of pyroxene from a late melt migrating through the peridotite, in combination with wall rock reaction (e.g., Kelemen, et al., 1992). The high $^{87}Sr/^{86}Sr$ of the sample is no evidence for or against such a hypothesis, as it is not coupled with a correspondingly low Nd isotopic composition. Though the Nd isotopic composition of this clinopyroxene is somewhat low for depleted mantle rocks, it is still too high to correspond with the Sr isotopic composition of any known enriched mantle source.

As a second alternative, seawater derived alteration products may have remained in the clinopyroxene even after grain picking and leaching. This is a more plausible hypothesis than the first. It does not explain why the two results were so similar, even though they were measured on different mineral separates and leached to different degrees. The very sharp fall-off of the leaching curve between the first and second leaches also reflects the purity of the mineral separate. The grain size of the clinopyroxene in thin section was particularly large and the clinopyroxene was relatively unaffected by alteration. For this reason, the mineral separate was of exceptional purity; it was optically the purest separate prepared for this study. This sample should be the least affected by contamination of all the samples studied in the course of this thesis. This clinopyroxene separate was the richest in Sr of all the samples, as measured both by isotope dilution and ion probe. Given also that this sample is by all measures one of the least altered peridotites in this study (as will be discussed extensively below), the reproducibly high $^{87}Sr/^{86}Sr$ of this clinopyroxene is somewhat surprising.

Third, seawater may have penetrated to depths in the mantle sufficient to allow the inclusion of seawater-derived Sr at the formation of this clinopyroxene as metamorphic diopside. This scenario is thought to be unlikely, since there is no other evidence of high-temperature hydrous phases (e.g. amphibole) in this sample. Lastly, given a sufficient reservoir of Sr and sufficient time, it is possible that the clinopyroxene may have exchanged Sr with seawater-derived minerals or with seawater itself by diffusive exchange alone, without the chemical

reactions involved in alteration. This is somewhat of an *ad hoc* explanation, but it explains the high Sr isotopic composition coupled with a Nd isotopic composition in a clinopyroxene of relatively pristine appearance.

Sample Vulc5:41-29 (Figure 5b) exhibits a more dramatic difference in isotopic composition between the first leaches and the final separate. This sample illustrates some of the difficulties of Sr analysis in the residual clinopyroxenes, where significant Ca was often present in the Sr chemical fraction (see the next section). Analysis 41-29 1b (which was 41-29 1a after a second pass through the Sr chemistry) was taken as the final composition of the clinopyroxene, due to the longer counting time that was achieved and the correspondingly better internal precision of the analysis. It is a plausible mid-ocean ridge mantle composition.

Leaching on sample IO 11/76: 56-58 failed on the initial attempt, which is to say, after three leaches, the Sr isotopic composition did not fall low enough to be a plausible mantle composition (i.e., $^{87}Sr/^{86}Sr \leq$ bulk Earth). The second attempt, by comparison, was successful, and a value of .702644$\pm$24 was measured. Figure 5c shows dissolution curves for the first and second leaching experiments carried out on this sample. The primary difference between the two leaches was the purity of the mineral separate used. The second separate was a split of the first, crushed to a finer grain size and picked again to remove impurities. This resulted in a much purer mineral separate, which managed to reach a mantle-like $^{87}Sr/^{86}Sr$. Note that in this case also, the first two leachates have a higher $^{87}Sr/^{86}Sr$ than the bulk rock and a higher $^{87}Sr/^{86}Sr$ than seawater. The isotopic composition of the first leachate is even higher than that of the first magnetic fraction separated from this rock (Table 12). This implies that some of the "orphan" ^{87}Sr discussed later in this chapter was included in the alteration material on the exterior of the grains of this sample.

Samples AII107:40-35, RC2709:25-139 and PS86:6-37 shown in Figures 5d and 5e are all successful samples. It is unfortunate that sample AII107: 40-35 did not contain enough Nd for a successful Nd isotopic analysis. That sample was recovered from the Bouvet Fracture Zone near the Bouvet Island hotspot and has one of the highest present day Sm/Nd ratios in this study (Table 6). In sample PS86:6-37, the first leachate has a lower $^{87}Sr/^{86}Sr$ than the second. Normally, the leachates are expected to decline monotonically in $^{87}Sr/^{86}Sr$. Due to the lower precision of the analysis on the first leachate, the two analyses are nearly within

analytical error of each other. The very high Sr concentration of the first leachate suggests that it contained a significant amount of aragonite, which was removed in the first few leaches.

In almost all cases, the concentration of the material removed from the clinopyroxene decreases with increasing degree of dissolution. As the more concentrated seawater alteration phases are removed from the highly depleted clinopyroxenes, the total Sr content of the mixture of alteration products and clinopyroxene removed by the leaching procedure decreases. Samples RC2709:6-2, Vulc5:41-29, PS86:6-37, and AII107:40-35 all had clinopyroxene Sr concentrations determined by ion microprobe to a relative precision of approximately 10% (Tables 6 and 13). In 3 out of the 4 cases, the concentration of Sr determined by ion probe is close to that determined by isotope dilution, within the analytical uncertainties of those two techniques. This suggests that the isotopic compositions of the clinopyroxenes in this study are also close to the primary Sr isotopic compositions. Sample AII107:40-35 has both Sr and Nd concentrations which are nearly an order of magnitude lower than those determined by ion microprobe. The fact that both concentrations are low suggests that this sample did not completely equilibrate with the isotopic spike used to measure concentration during its dissolution, or did not dissolve completely.

The analytical significance of high Ca/Sr in leachates and clinopyroxenes.

Ca contamination of the Sr fraction during chemical separation can be a significant impediment to the analysis of Sr isotopic compositions of clinopyroxenes from residual peridotite (as it was in sample Vulc5:41-29 of this study). Ca inhibits the ionization of Sr in the mass spectrometer, and results in poor runs. Sr runs contaminated by Ca typically require a higher filament temperature, the sample lasts a shorter amount of time and the internal precision is poorer than with "clean" runs. In extreme cases, the sample will not run at all, or the filament burns through before an acceptable signal strength is achieved. Ca also seems to inhibit the ionization of Rb. In some cases, residual Rb remains from the chemistry which cannot be flashed away without also flashing away the Sr. Even with these difficulties, when isotopic composition data are obtained, they are generally reliable within the internal statistics of the analysis, so long as a multicollector machine is used, as in this study.

The Ca contamination occasionally experienced in this study is the result of the extremely low Sr concentration in the clinopyroxene, which resulted in a much higher Ca/Sr ratio in the leachate solutions and leached clinopyroxenes than is the case when analyzing basalts, for example. To understand the importance of the Ca/Sr ratio of a sample in the analytical separation of these two elements, consider a typical basalt with 10% CaO and 100 ppm. Sr. The analysis of such a sample is straightforward, as it has a Ca/Sr ratio of 850, and the Ca is easily removed from the Sr during normal cation exchange procedures. Analyzing calcites precipitated from circulating solutions at mid-crustal levels (S. Hart, personal communication) is more difficult, as the CaO content is higher (56%) and the Sr content typically lower (≥50 ppm.) than in basalts. The Ca/Sr ratio of such a sample is approximately 8000. Once again, the normal cation exchange procedures are typically sufficient to separate the Ca from the Sr.

The Ca content of a residual clinopyroxene is only a factor of two lower than the calcite, but the Sr content is a factor of 50 to 100 lower. This results in Ca/Sr ratios around 164,000 for a typical abyssal peridotite clinopyroxene with 23% CaO and 1 ppm. Sr. The highest such ratio in this study is sample AII107:40-35, an extremely depleted residual peridotite from the Bouvet Fracture Zone with a Ca/Sr ratio of 3.2 million as analyzed, more than three orders of magnitude higher than the Ca/Sr ratio of a typical basalt. This clinopyroxene sample contained 4 ng. of Sr. The typical basalt Sr isotopic composition analysis (50 mg., 100 ppm.) contains 5000 ng. of Sr. The Ca/Sr ratios of the clinopyroxenes and their low levels of Sr explain the considerable analytical difficulties measuring Sr isotopic compositions in leachates and clinopyroxenes experienced in the course of this work.

Discussion

The alteration of abyssal peridotite

Abyssal peridotites have a long history of tectonism and metamorphism which begins with ductile flow in the mantle to the base of the crust. This is followed by deformation and alteration, accompanied by high and low temperature hydrous alteration during emplacement through the crust to the sea floor. Cracking and brittle faulting at late stages in this process bring seawater down into the ascending mantle, enhancing cooling and hydrating the peridotite. In the process, the mantle rocks are subjected to events of hydrous metamorphism at progressively lower pressures and temperatures until they reach the sea floor (Kimball, et al., 1985; Hébert, et al. 1990). Finally, the sample is exposed to weathering and encrustation by seawater-derived precipitates (carbonate and Mn-Fe oxides).

Most abyssal peridotites consist of a juxtaposition of mineral parageneses from a variety of pressures and temperatures, from the mantle to the sea floor. Discrete metamorphic events *probably* correspond to distinct episodes of faulting during uplift. These episodes create renewed circulation of seawater and hence renewed hydrous metamorphism. The number, timing and nature of these events is difficult to pin down precisely, due to overprinting of later events on the minerals and textures of the preceding ones. In any case, the normal progression of metamorphism in abyssal peridotites must be largely retrograde, in the absence of contact metamorphism due to dike injection.

The first section of this discussion focuses on the general equilibrium phase relationships in abyssal peridotites and on the mineral parageneses which are commonly observed and their significance. The following section on the abyssal mylonites and the section on bulk reconstruction make the case that significant mass redistribution involving the removal of Mg has occurred in the peridotites of this study. The following two sections after that develop a methodology for quantifying this mass redistribution and comparing it to the isotopic systematics of the altered peridotites. Finally, a geologic interpretation of the mass fluxes is proposed.

Equilibrium phase relationships and observed phase relationships.

Starting in earnest with the experimental work of Tuttle and Bowen (1949), the hydration-reaction of peridotite to form serpentinite has been the object of vigorous experimental (Bowen and Tuttle, 1949; Roy and Roy, 1954; Kitihara and Kennedy, 1967; Chernosky, 1973; Helmley, et al., 1977a, b; Evans, et al., 1977) and field investigation (Aumento and Loubat, 1970; Bonatti, et al., 1976; Thompson and Melson, 1972; Miyashiro, et al., 1969; Dick, 1979). The major chemical constituents of serpentinites are water, silica and magnesium. These elements account for over 80% of most abyssal peridotites. For this reason, serpentinization is often studied in the simpler synthetic system MgO-H_2O-SiO_2. The fact that the bulk of alteration phases found in altered peridotites have been predicted by experiments in the system MgO-H_2O-SiO_2 shows that this approximation is appropriate.

The five phases of greatest interest in the MgO-H_2O-SiO_2 system are forsterite, enstatite, talc, serpentine and brucite. Under conditions of metamorphism in the mantle and crust, the reactions which decompose olivine and enstatite respectively are:

$$Mg_2SiO_4 + 4H^+ <=> 2Mg^{2+} + H_4SiO_{4aq} \quad (1)$$

and

$$MgSiO_3 + 2H^+ + H_2O <=> Mg^{2+} + H_4SiO_{4aq} \quad (2).$$

The appropriate constitutive equilibria for chrysotile, talc and brucite are as follows:

$$Mg_3Si_2O_5(OH)_4 + 6H^+ <=> 3Mg^{2+} + 2H_4SiO_{4aq} + H_2O \quad (3)$$

$$Mg_3Si_4O_{10}(OH)_2 + 6H^+ + 4H_2O <=> 3Mg^{2+} + 4H_4SiO_{4aq} \quad (4)$$

$$Mg(OH)_2 + 2H^+ <=> Mg^{2+} + 2H_2O \quad (5).$$

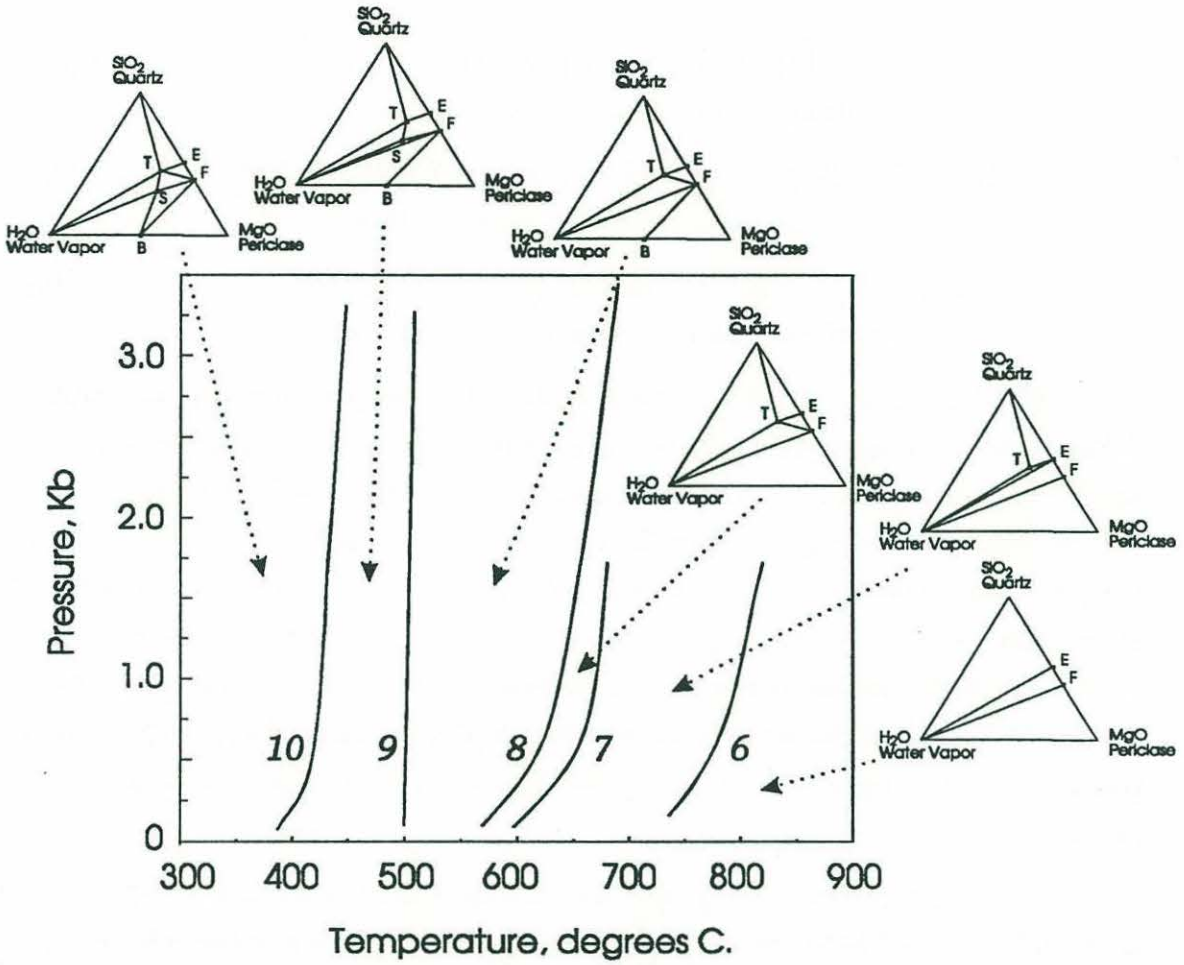

Figure 6: Equilibrium phase relationships in the system $MgO-H_2O-SiO_2$. After Bowen and Tuttle (1949) with modifications (Roy and Roy, 1954; Deer, et al., 1966). Univariate curves (keyed to reactions in the text) are shown, as are stability diagrams for the divariate regions between the numbered curves.

These reactions can be combined to form balanced equations representing phase appearances and disappearances verified experimentally by Bowen and Tuttle (1948) and many subsequent authors. The following equations are relevant to the system $MgO-H_2O-SiO_2$.

$$3MgSiO_3 + SiO_2 + H_2O <=> Mg_3Si_4O_{10}(OH)_2 \quad (6)$$

(enstatite + silica + water <=> talc)

$$3MgSiO_3 + H_2O <=> Mg_3Si_4O_{10}(OH)_2 + Mg_2SiO_4 \quad (7)$$

(enstatite + water vapor <=> talc + forsterite)

$$MgO + H_2O <=> Mg(OH)_2 \quad (8)$$
(magnesia + water <=> brucite)

$$3Mg_2SiO_4 + 2Mg_3Si_4O_{10}(OH)_2 + H_2O <=> 4Mg_3Si_2O_5(OH)_4 \quad (9)$$
(forsterite + talc + water <=> serpentine)

$$2Mg_2SiO_4 + 3H_2O <=> Mg_3Si_2O_5(OH)_4 + Mg(OH)_2 \quad (10)$$
forsterite + water <=> serpentine + brucite

The univariant curves in pressure-temperature space for reactions 6-10 listed above are shown in Figure 6, which is the classic phase diagram in the MgO-H_2O-SiO_2 system, with modifications after Bowen and Tuttle (1949). For each of the divariate regions, stability diagrams show the stable mineral assemblages in the system. With the exception of the endmember oxide compositions, all of these phases are commonly observed in abyssal peridotites, though brucite is rare. These are by no means all the possible reactions in hydrous peridotites, nor are they even all the ones in the system MgO-H_2O-SiO_2. They do provide a framework for understanding the equilibrium mineral parageneses in abyssal peridotite.

In all studies of abyssal peridotites, including this one, two distinct modes of alteration have been observed. The first is the alteration of olivine to serpentine $\pm$ magnetite and orthopyroxene to pseudomorphous serpentine (bastite). The second type of alteration is the deposition of metamorphic minerals in veins that crosscut the primary and pseudomorphic textures of the host peridotite (Shibata and Thompson, 1986; Kimball, et al., 1985; Hébert, et al., 1990). Kimball, et al., 1985 present a progression of mineral parageneses observed in abyssal peridotites from the Islas Orcadas fracture zone, in a progression from hornblende to hornblende + actinolite to chlorite + actinolite + secondary clinopyroxene to talc to serpentine.

One seeming contradiction of studies of hydrous metamorphism in abyssal peridotites (Kimball, et al., 1985; Hébert, et al., 1990) is the occurrence of high temperature vein materials (400 - 925 °C, Kimball, et al., 1985) crosscutting lower temperature (<400 °C, Helmley, et al., 1977a, b) material formed from the pseudomorphous hydration of olivine and orthopyroxene (Kimball, et al., 1985; Hébert, et al., 1990). This is an example of prograde metamorphism in a situation where none is to be expected.

There are many possible explanations for the apparent observation of prograde metamorphism. The first is that the high temperature veins formed first, originally crosscutting mantle minerals. Serpentine + magnetite and bastite then form later than the higher temperature veins. Since they are replacive in nature and locally could constitute a constant volume reaction, they do not disrupt the higher temperature veins. The high temperature veins are more resistant to alteration, being closer to equilibrium at the lower grade metamorphic conditions than are the mantle minerals. They persist metastably instead of being retrogressed to low grade.

Another explanation is that contact metamorphism has occurred. The peridotite remained relatively unaltered until a relatively low temperature, at which it was altered to serpentinite. Later the serpentinite experienced an episode of greenschist or amphibolite facies metamorphism that resulted in the later-formed vein minerals. This later metamorphism could be due to injection of melt nearby at crustal levels. All the dredge hauls studied by Kimball, et al. (1985) contained a mixture of peridotites which contained high grade metamorphic minerals and those which did not (H. Dick, personal communication). This is consistent with the high grade metamorphism being an extremely localized phenomenon.

The metamorphic history of abyssal peridotites generally may be interpreted as a complex retrogression from a high temperature anhydrous peridotite to a serpentinite. This occurs by means of progressively lower temperature and more hydrous metamorphic events, which may be disrupted by contact metamorphic events related to nearby intrusion of basaltic melts at crustal levels.

Weathering of peridotite mylonites --
evidence of metasomatism during alteration

Metasomatism, or mass flux into or out of abyssal peridotite during alteration, is a topic which has received little attention in previous studies of the metamorphic history of abyssal peridotites (Dick, 1979; Kimball, et al., 1985; Hébert et al., 1990). Metasomatism during weathering has major implications for many of the inferences drawn from abyssal peridotites studied over the past 10 years, especially their relict modal compositions and bulk compositions (Dick,

et al., 1984; Michael and Bonatti, 1985a, b; Shibata and Thompson, 1986; Johnson, et al., 1990; Johnson and Dick, 1992). Metasomatism during alteration is also likely to be an important factor in the behavior of isotopic systems during hydrous metamorphism.

One set of abyssal peridotite samples with a unique metamorphic history are abyssal peridotite mylonites and protomylonites. These rocks are represented by AII107:61-78 and AII107:61-83 and are described in detail in Appendix I. They consist of medium to extremely fine grained recrystallized peridotite. The samples have cores which consist of almost completely unweathered and unserpentinized peridotite (see discussion in Appendix I), surrounded by rims of fine-grained pseudomorphous serpentinite. There is a relatively sharp boundary between the weathering rim and the core peridotite, and the alteration appears not to have disrupted textural details such as foliation, grain size layering, and strongly deformed enstatite augen which crosscut the core/rim boundary.

Mass fluxes during weathering

Assessing the mass flux into or out of a rock involves some fairly simple considerations of mass balance (Grant, 1986). It is important to note the extent to which an altered rock can be said to conform to three possible assumptions about mass balance: constant mass, constant volume and constant immobile elements. In lightly altered (or unaltered) rocks, these may amount to the same thing. In more strongly altered rocks, they may provide clues to the process of alteration which has taken place. In the case of the abyssal peridotite mylonites, the availability of both cores and altered rims for analysis provides much more information than is usually obtainable about the protolith of an altered abyssal peridotite. Both the unaltered abyssal peridotite composition and its density can be directly determined, rather than inferred from mineral compositions and modal mineralogy, as will be the case in the next section.

The discussion in the next few sections will be based on a modified form of the isocon diagram (Grant, 1986). For a given sample in this diagram, altered vs. unaltered compositions of all elements are compared. During metasomatic alteration (which we will assume to involve hydration), the concentration of an element is determined by

$$C_i^A = \frac{M^O}{M^A}(C_i^O + \Delta C_i) \qquad (11).$$

where C_i^A and C_i^O are the altered and original concentrations of the i^{th} element, respectively, and M^O and M^A are the masses of the original and altered rock.

The formulation in Equation 11 implies some simple predictions for the concentrations of elements given different assumptions about mass behavior during alteration. These can then be represented simply in the isocon diagram (Figure 7). These predictions allow M^O and M^A to be determined and ΔC_i to be constrained in an absolute sense. Figure 7 shows the ratio C_i^A/C_i^O plotted on the Y axis versus C_i^O for the two peridotite mylonites in this study. Isocons are shown assuming constant mass and constant volume. The procedure for calculating these is outlined below.

Constant mass

If there has been no net mass flux from the system, then any change in the density of the altered rock is due to volume expansion alone. This might be the case during isochemical phase transformations such as basalt->eclogite. No change in elemental concentration takes place on a weight basis, and the line corresponding to no gain or loss of any given element is defined by:

$$C_i^A = C_i^O \qquad (12).$$

The assumption of constant mass is not a good one in the case of hydrous alteration, since water mass is added, diluting all the other elements. All the major element analyses in this study, however, are calculated to an anhydrous basis, and trace elements measured on a hydrous basis have been recalculated to an anhydrous basis for plotting on all isocon diagrams presented here. The isochemical (except for water) hydration of peridotite exemplified by equations 6-11 thus corresponds to this case in the isocon diagram. The line $C_i^A = C_i^O$ is plotted in all isocon diagrams.

Constant volume

If there has been mass removal from the rock during alteration, then the density change of the rock is due to removal of mass at constant volume, which

changes the concentrations of the elements not removed. A line of no mass removal for these elements in this case is given by

$$C_i^A = \frac{\rho^O}{\rho^A} C_i^O \qquad (13).$$

In the case of the abyssal peridotite mylonites, the densities of the alteration rind and the unaltered core were measured in the course of the sample description, so this line can be plotted on the isocon diagram. Density was not measured in the other samples.

Constant immobile elements.

It is impossible to tell *a priori* in an altered rock to what relative extent constant mass and constant volume processes have operated. For that reason, for any given element, the concentration of that element need not correspond exactly to the bounding cases described above, but will be somewhere in between them, even in the absence of gain or loss of that element. If one or more elements can be chosen which are thought to be immobile during alteration (e.g., Al_2O_3, Cr or TiO_2), then the concentrations of these elements may allow the estimation of a line of no mass loss (or isocon) for a given rock. If the element chosen is aluminum, then the equation of the isocon is

$$C_i^A = \frac{C_{Al_2O_3}^A}{C_{Al_2O_3}^O} C_i^O \qquad (14).$$

In many cases, the constant mass (metamorphic) and constant volume (metasomatic) processes affecting the rock cannot be sorted out *a priori*. An isocon fit to immobile elements is then probably the best means of establishing in an absolute sense whether there has been net mass gain or loss of a given element. The principal difficulty with this approach (as will be seen when the mylonite samples are discussed) is that the immobile elements themselves may be concentrated in phases whose abundance in the rock may vary. This is certainly the case for Al_2O_3 and Cr (spinel) as well as TiO_2 and CaO (clinopyroxene) in the mylonite samples. The primary variations of the phases that concentrate immobile elements can result in *apparent* variations in the putatively mobile elements which are not related to alteration.

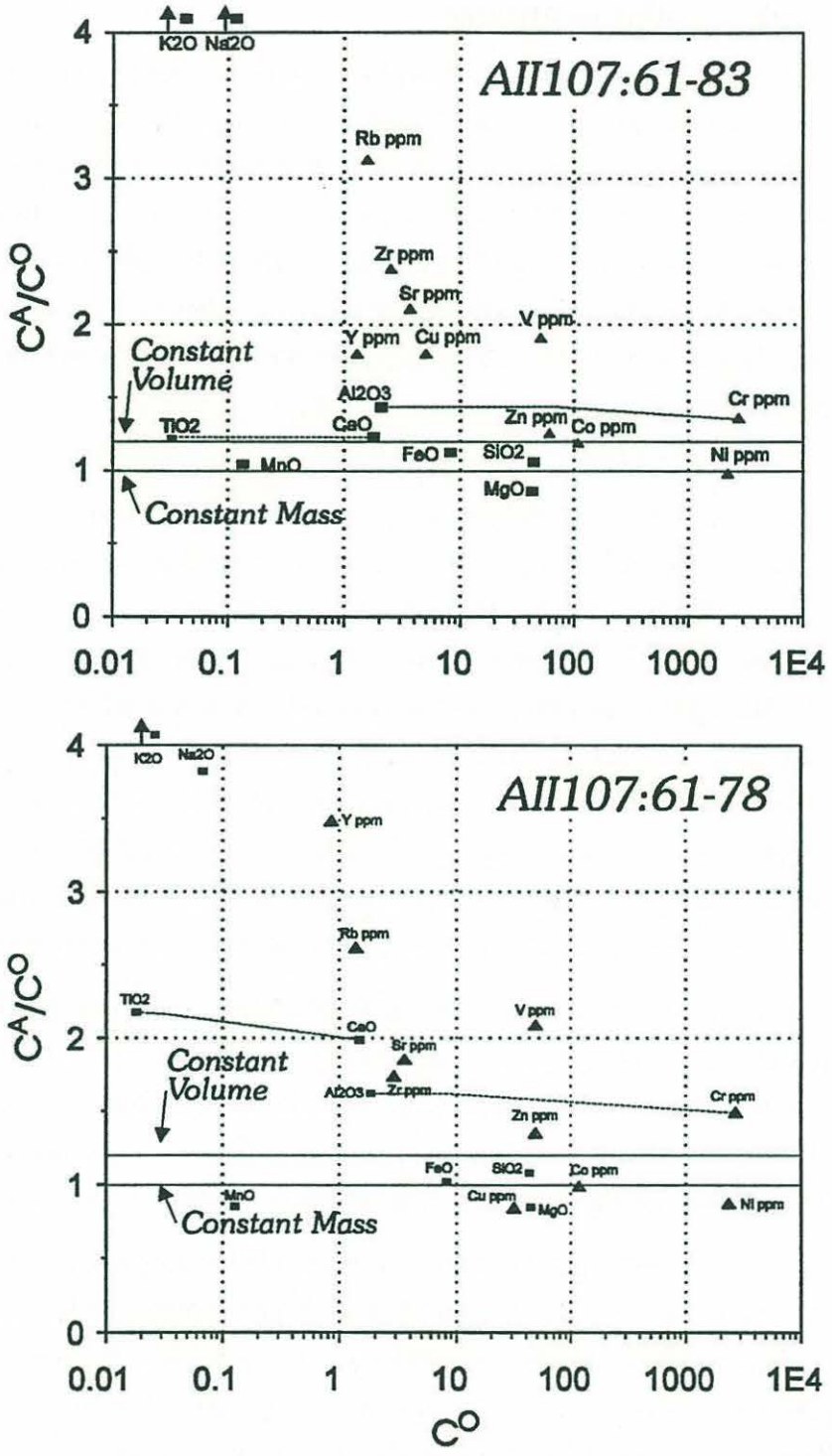

Figure 7: Isocon diagrams for abyssal peridotite mylonites. Constant mass and constant volume isocons are calculated by the method of Grant (1986). Data are from Table 10. Trace element concentrations are recalculated to an anhydrous basis. Elemental concentrations on the X-axis are shown in Wt. % for major elements and ppm. for trace elements, as marked. Some trace elements (particularly Zr, Y, Sr and Rb) are near their detection limits. Broken lines connect the element pairs Ti-Ca and Al-Cr. These elements are concentrated in clinopyroxene and chrome spinel respectively.

Application to abyssal mylonite

Grant (1986) plotted concentration in the altered sample versus concentration in the unaltered sample. For readability some of the high and low concentration elements were scaled up or down. A different approach to readability will be taken here: C^A/C^O will be plotted against C^O. The only scaling will be plotting trace elements as ppm. and major elements as Wt. %. Trace elements are all calculated to an anhydrous basis for plotting. Figure 7 shows isocon diagrams for the abyssal peridotite mylonites in this study. Since both altered and unaltered compositions are measured compositions, there is no possibility that the variations seen in Figure 7 are due to artifacts of a reconstruction calculation.

In Figure 7 it is immediately clear that many major and trace elements have clearly been redistributed in these rocks. Some elements are as much as 20% lower than unity (Cu, Ni, MgO) and some are more than 400 percent higher in the weathering rind. In between these extremes are the elements which can reasonably be thought of as being neither gained nor lost from the rock, particularly FeO and SiO_2. The concentrations of these elements could be accounted for simply by isochemical expansion of the rock, isovolumetric mass removal, or a combination of these two processes. Co, too, is well determined and is in the region where it could plausibly be considered an isocon. It is likely that the true isocon lies between that constant volume and constant mass calculated isocons.

No matter how isocons are inferred in Figure 7, it is clear that MgO and Ni have been lost from the rock. Equally unequivocal is the gain in the oxides K_2O, Na_2O, and many of the trace elements, particularly Rb and Sr. Some of these trace elements, particularly Zr, Y, Sc, Rb and Sr, are near their detection limits in these rocks. These data must therefore be viewed with some caution.

A surprise that emerges from this diagram is the apparent change in concentration of two elements, Al_2O_3 and Cr, which are thought to be wholly immobile (e.g., Grant, 1986). While aluminum as an immobile element might be enriched in some weathering residue, its extreme insolubility in water makes it highly unlikely that Al could ever be added to a rock. The fact that spinel is the major reservoir of both Al and Cr suggests that their enrichment is linked. CaO and TiO_2 are similarly linked to clinopyroxene. There are two possible explanations for the coupling of these elements: First, it is possible that the primary mineral makeup of the altered portion differed from that of the core. This would

account for the fact that Al_2O_3 and Cr content track each other in the two samples (their symbols are connected by a fine broken line in Figure 7). In both mylonite samples, Al_2O_3 and Cr are 50% higher in the altered rock than the core. This enrichment suggests that spinel is richer in the alteration rind of the samples than in the cores. Similarly, in sample AII107:61-78, CaO and TiO_2 (also connected by fine broken lines) are enriched by 100%, implying a greater clinopyroxene concentration in the altered rim than in the core of the sample. This scenario is considered unlikely, since spinel would have to be fortuitously enriched in the weathering rinds of both samples for this hypothesis to be correct.

An alternative explanation for the consistent behavior of Al_2O_3 - Cr and CaO - TiO_2 in the mylonite samples is possible. Because spinel and clinopyroxene are phases which are highly resistant to alteration, these elements themselves may define the isocon. This implies that the rock has lost both mass and volume, such that the resistant spinels and clinopyroxenes have been concentrated in the alteration rind. This hypothesis still does not account for the differing degrees of enrichment in CaO and TiO_2 relative to Al_2O_3 and Cr in the two mylonite samples. Some degree of primary compositional variation between the core and rim of the rock might still be required to explain that enrichment.

It is important to consider to what extent the mylonite alteration rims are examples of pure weathering with no serpentinization. If they represent pure weathering products of fresh peridotite, then they may be an inappropriate model for the weathering of serpentinites. If they have been serpentinized to some extent prior to their weathering, then they must be considered, like all abyssal peridotites, the products of serpentinization *and* weathering, and not the product of pure weathering. If serpentinization and weathering instead represent different stages of the same alteration process, then this point is moot.

The altered rim could be the product of both serpentinization and weathering. If the mylonite is an extremely impermeable rock due to its small grain size, cracks in the rock would provide the primary pathway for fluids during the entire formation of the rock. At moderate temperatures in the crust, serpentinization would occur primarily along these fractures and might not reach the interior. Subsequent weathering would also be concentrated along these cracks. The abyssal mylonites would thus constitute a direct analog to "normal" abyssal peridotites, with the altered and unaltered compositions in close proximity to each other. The term "weathering rind" would be a misnomer in this case, since

the alteration zone would merely represent the tendency of the peridotite to fracture along pre-existing serpentinized fissures during its emplacement to the surface.

An alternative interpretation is that the rims of the mylonites have undergone only submarine weathering of fresh peridotite since the fracturing of the rock during emplacement to the surface. This is supported by the sharpness of the boundary between weathered and unweathered material. In most other peridotites, alteration is pervasive. Only in a case such as this where the rock is relatively impermeable and the kinetics of alteration relatively slow would such a sharp alteration front be observed. This inference has serious implications for the interpretation of all abyssal peridotites. The altered rims of the mylonite samples are as completely altered (seen in thin section) as the most altered of the "normal" abyssal peridotites studied. If all of the alteration in the mylonite occurred at low temperature, then it is possible that a significant portion of the alteration of "normal" abyssal peridotites also occurs at low temperatures.

Bulk reconstruction of peridotite --
further evidence of mass fluxes

The original composition of the peridotite can be reconstructed using the measured compositions of the primary phases and the modal compositions of the rocks. Two approaches can be taken to this problem: In the first, modal compositions can be calculated using elements such as Al, which are thought to be immobile during alteration (Mottl, 1976; Bazylev, 1989). This approach requires an *a priori* knowledge of the relative mobilities of the elements during hydrous alteration of peridotite; precisely the phenomenon under investigation. It also requires a minimum of four putatively immobile components during alteration. As will be shown, four such elements are probably difficult to find, at least among the major elements.

The other approach is to count the modes directly. Dick, Fisher and Bryan (1984) use this technique to draw inferences about the primary mantle without reconstructing primary compositions. The potential drawbacks of using counted modes are the inherent uncertainties involved in point counting coarse grained rocks and the problem of differential volume change on alteration among the minerals of the rock. These problems are not intractable. Point

counting large 2"x3" thin sections (Dick, et al., 1984) yields adequate and quite reproducible counting statistics, even between analysts. The density of serpentine (2.55 g/cc) compared to typical mantle olivine (3.3 g/cc) implies an expansion of up to 30% during serpentinization. This would tend to increase the olivine mode at the expense of other minerals (e.g., Komor, et al., 1990). Other studies of peridotite alteration (Kimball, et al., 1985; Nesbitt and Bricker, 1978) seem to support the hypothesis that the hydration of peridotite generally involves mass loss at constant volume. This would explain the generally good preservation of grain boundaries, textural relationships and other primary structures in many abyssal peridotites. These features would otherwise be deformed or even destroyed by alteration that caused significant strain due to a volume expansion of up to 30%. While the weight and mole fractions of the primary minerals are changed significantly by the alteration, the volume relationships between the primary phases are retained to a first approximation.

If serpentinization in abyssal peridotites were not an isovolumetric process, the result would be a large apparent increase in olivine mode over the other phases in abyssal peridotites. When modes counted on altered abyssal peridotites (e.g. This study, Dick, et al., 1984; Michael and Bonatti, 1985a, b; Kelemen, et al., 1992) are compared with xenolith modes (as in Kelemen, et al., 1992) or recalculated modes from fine-grained, but unaltered abyssal peridotites (see Table 2), olivine is not overrepresented in the oceanic sample. This supports the hypothesis that due to a removal of mass during serpentinization, the remaining peridotite still reflects the original phase proportions to a first approximation, even though most of the rock may now consist of secondary phases. The topic of differential expansion of olivine will be covered in a later section.

Reconstruction method

The reconstruction proceeded as follows: First, the volume proportions of the minerals determined by point counting of relicts and pseudomorphs (Table 2) were converted to weight proportions by dividing through by the density of minerals of similar composition (i.e., $Mg/(Mg + Fe^{2+}) = 0.9$) found in Deer, et al. (1966). The following mineral densities were used (in g/cc): olivine: 3.3 orthopyroxene: 3.3 clinopyroxene: 3.25. In the case of spinel, there is considerable density variation depending on the composition of the spinel. The density was calculated according to the following formula: $\rho=3.52 + 1.5 * (Cr/(Cr+Al))$,

which was derived from the spinel composition and density data in Deer, et al. (1966). The densities of spinels in this study so calculated ranged from 3.73 to 4.04 g./cm.^{3}

Bulk compositions were calculated from individual mineral compositions determined by electron microprobe (Tables 3, 4, 5 and 7), weighted by the mass abundances of those phases. Where mineral composition data were lacking (for olivine or orthopyroxene), the average composition of that mineral was used. This is justified for minerals like olivine and orthopyroxene whose compositions are relatively uniform, since the compositional variation in these phases between samples is much smaller than the compositional difference between the mineral phases. Variations in composition will be dominated in any case by the modal content of the rock. Clinopyroxene and spinel were analyzed in all the samples. Despite their small abundance, these two phases can make up a substantial portion of the elemental budget of the rock for some elements. The compositions of these phases also show considerable elemental variation in abyssal peridotites (Dick and Bullen, 1984; Johnson, et al., 1990; Johnson and Dick, 1992).

The mylonites AII107 61-78 and 61-83 were treated quite differently, since their cores are unaltered and point counting was not possible. For these samples in Table 15 the composition of the unweathered core is substituted for the reconstructed composition. In order to calculate modes for these samples (Table 2) a least squares calculation of the mode based on the analyzed mineral compositions was used. The details of this calculation are given in Appendix III. The modes calculated in this way were not used to reconstruct a bulk composition; instead, the true unweathered core composition was used.

Results

Reconstructed bulk compositions calculated for the peridotites in this study are listed in Table 15. Figures 8a-j show the the reconstructed compositions plotted against the bulk compositions (Table 10). The measured bulk composition is on the Y-axis and the reconstructed composition on the X-axis. The line bulk = reconstructed is plotted as a solid line. A net gain of an element is indicated if the reconstructed and bulk compositions plot above the X=Y line, and a net loss is indicated if they plot below the line.

Table 15: Reconstructed bulk compositions.

Cruise	Number	SiO_2	TiO_2	Al_2O_3	FeO	MnO	MgO	CaO	Na_2O	K_2O	Cr_2O_3
PS86	6-37	44.15	0.059	2.38	7.92	0.14	41.93	2.64	0.12	0.0039	0.405
AII-107:	61-78	44.64	0.026	2.41	8.03	0.15	42.61	1.87	0.06	0.0005	0.395
AII-107:	61-83	43.12	0.014	1.81	8.40	0.14	44.27	1.47	0.05	0.0051	0.376
IO11/76:	60-61	43.07	0.026	0.85	8.26	0.08	45.92	0.73	0.04	0.0094	0.252
IO11/76	56-58	43.08	0.022	1.72	8.40	0.14	44.41	1.56	0.05	0.0030	0.325
IO11/76:	59-26	45.31	0.022	2.35	7.90	0.14	42.19	1.19	0.04	0.0067	0.537
AII107:	40-27	42.88	0.015	1.09	8.62	0.14	45.67	1.01	0.03	0.0031	0.228
VULC5:	41-29	43.18	0.021	1.64	8.26	0.15	43.64	1.99	0.05	0	0.354
VULC5:	41-15	44.38	0.057	2.76	8.05	0.15	41.07	2.92	0.15	0.0041	0.421
RC2709:	6-2	46.71	0.031	2.80	7.42	0.14	39.59	2.20	0.08	0.0080	0.791
AII107:	40-35	44.15	0.015	1.47	8.26	0.14	44.02	1.25	0.02	0.0046	0.386

Reconstruction algorithm is discussed in the text. Samples AII107:61-78 and AII107:61-83 are unweathered mylonite core compositions, measured by XRF (Table 10; see discussion in text).

Several patterns are apparent in the type and degree of alteration exhibited by the samples in this study. MgO and SiO_2 have significant deviations of bulk composition from reconstructed composition. The sample set as a whole shows a continuous array of Mg/Si redistribution from the Mg enriched sample IO11/76:59-26 to the extremely Mg depleted IO11/76:56-58. The degree of MgO depletion in all of the peridotites seems to correlate with the subjective degree of alteration observed petrographically (see Appendix I), but not closely with the measured alteration modes (see Figure 14 and its accompanying discussion).

The data fall neatly into two groups, between which there is surprisingly little compositional overlap in Figure 8. The first group includes the Islas Orcadas rocks IO11/76: 56-58, 60-61 and the two mylonite weathering rinds AII107:61-78 and 61-83. This group represents the most weathered samples seen in petrographic analysis (Appendix I), and have clearly lost Mg with respect to their calculated primary compositions (Figure 8b), and have spectacular additions of alkali elements (Figures 8f, 8h). These will be termed the low-Mg group in the remainder of this discussion. The second group, comprising the remaining samples, are all much closer compositionally to their calculated compositions. They have seen less redistribution of Mg and Si, and are generally lower in alkali elements than the first group. These will be termed the low-alkali group.

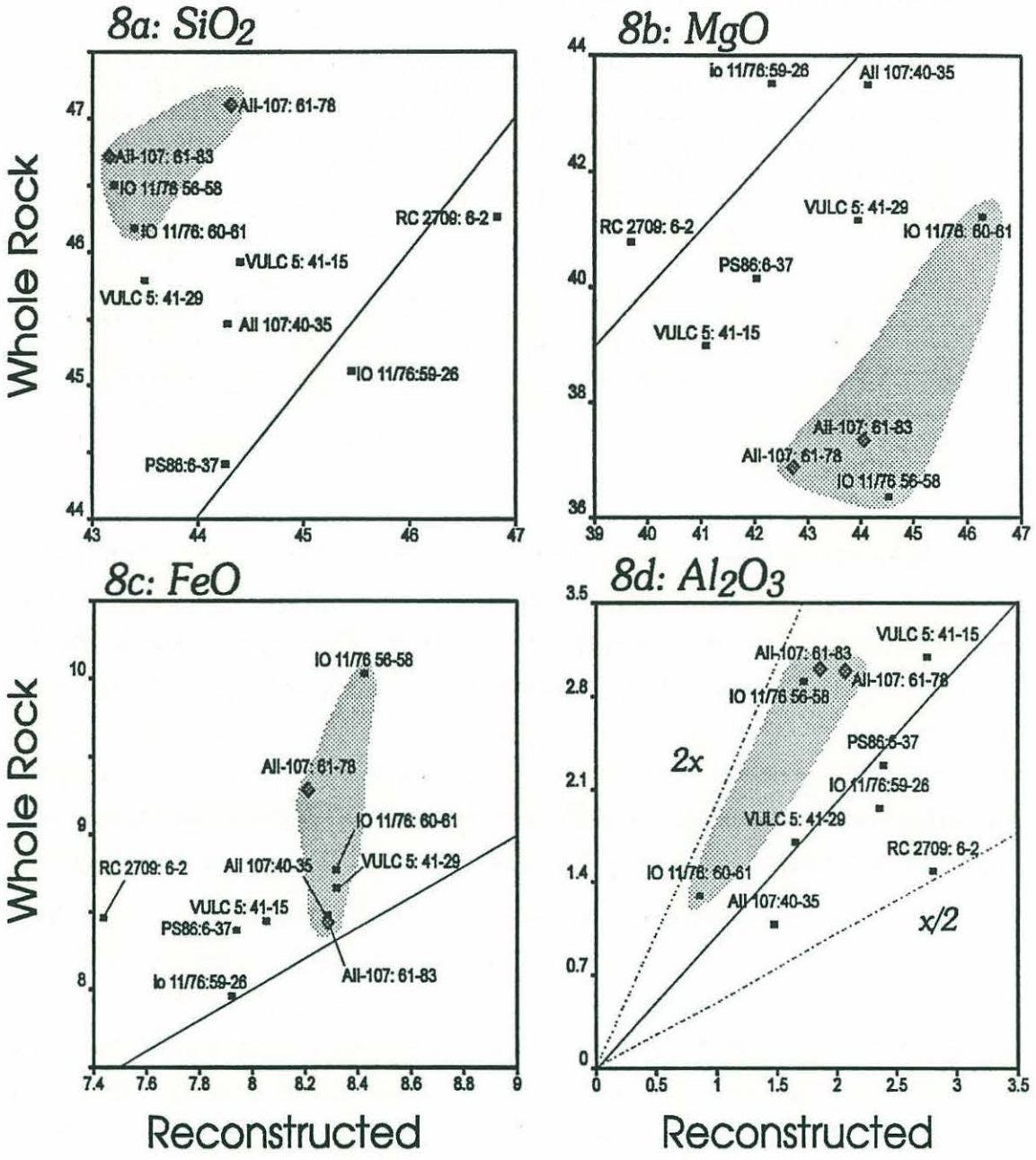

Figure 8a, b, c, d, e, f, g, h, i, j: Reconstructed and bulk compositions for abyssal peridotites. All X and Y axes are in Wt. % oxides. X axes are always the reconstructed composition, Y axes are always the measured anhydrous bulk composition. The line X=Y is shown in each graph. Samples which plot above the line indicate addition of a given element. Samples which plot below the line indicate depletion of a given element. Broken lines indicate enrichment or depletion factors as appropriate. For the mylonite samples shown as filled diamonds, the XRF analysis of the core is shown on the X axis and the XRF analysis of the weathered rim on the Y axis. The position of each sample on the graph thus has the same implication for mass flux as for the recalculated samples. The shaded areas enclose the low-Mg group of samples. These samples have compositions thought to be dominated by mass redistribution during weathering (see discussion in text).

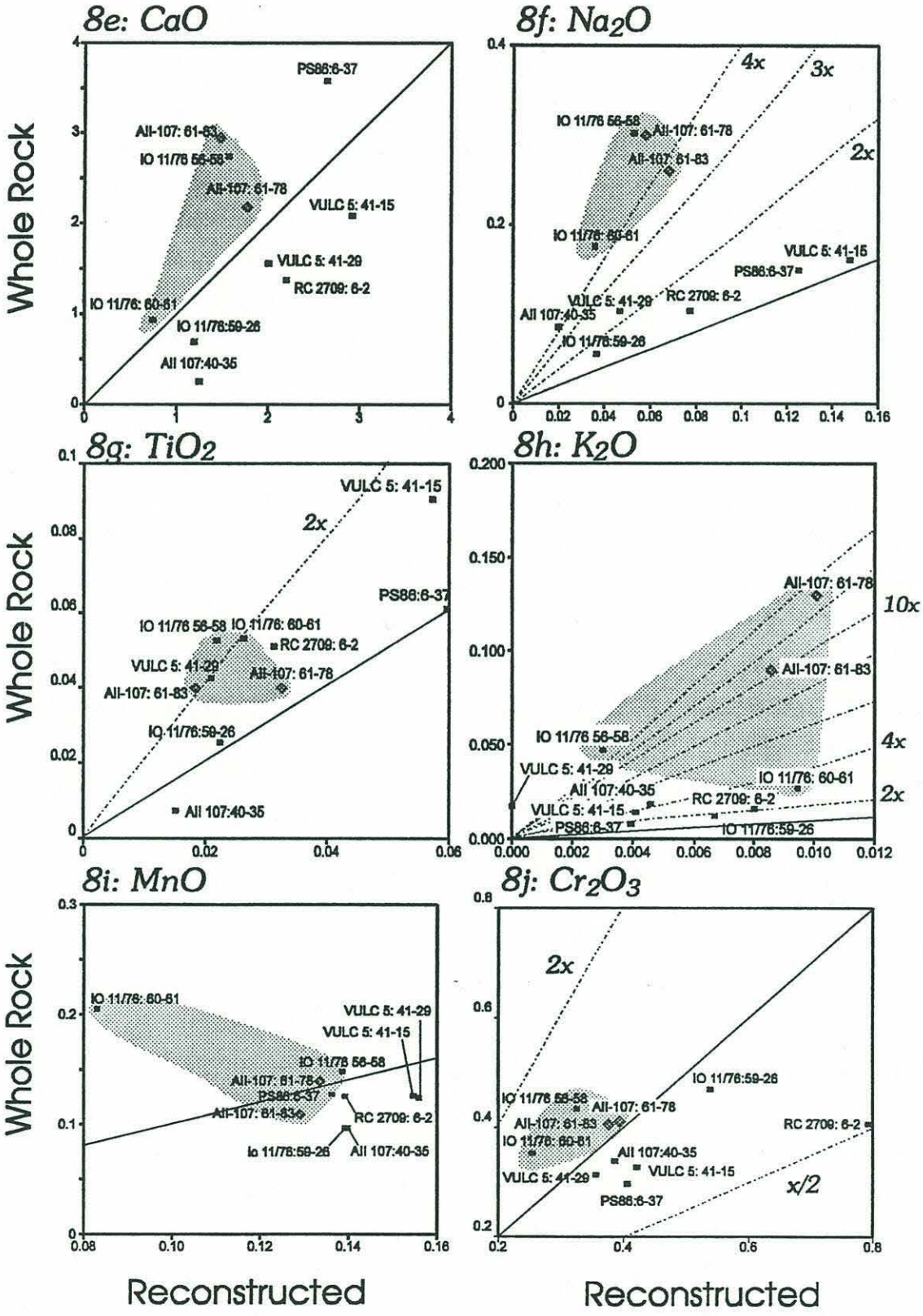
8e: CaO
8f: Na2O
8g: TiO2
8h: K2O
8i: MnO
8j: Cr2O3
Whole Rock
Reconstructed
PS86:6-37
All-107: 61-83
IO 11/76 56-58
All-107: 61-78
VULC 5: 41-15
VULC 5: 41-29
RC 2709: 6-2
IO 11/76: 60-61
IO 11/76:59-26
All 107:40-35
4x
3x
2x
10x
x/2

MgO depletion coupled with SiO_2 gain

MgO and SiO_2 together clearly reflect the separation of the samples into low-Mg and low-alkali groups. All of the low-Mg group are enriched in SiO_2 by at least 5%. It is difficult to determine the mass fluxes of MgO, SiO_2 and FeO into and out of the peridotite from one-by-one comparisons of elemental concentrations. Isocon diagrams (e.g., Figure 7) lose some of their usefulness when uncertainty in point counting and mineral analysis are incorporated into a recalculated bulk composition. Further, the densities of most of the samples were not available, so a constant volume isocon could not be shown in any case. Figure 9 shows instead the bulk and reconstructed MgO, SiO_2 and FeO concentrations plotted in a triangle diagram. In this diagram, elemental extraction or addition lines are straightforward to calculate, and mineral compositions are easily plotted. Nearly all the bulk compositions fall on roughly parallel vectors from their calculated primary composition. The direction of these vectors clearly implies either FeO and SiO_2 addition at a nearly constant ratio, or extraction of Mg. The bulk compositions of the low-Mg group plot (naturally) farthest away from the field of the calculated compositions.

As implied by their positions in Figure 8a and Figure 8b, two samples seem to show alteration vectors which do not imply MgO removal. In Figure 9, the bulk composition of sample IO11/76:59-26 lies on an MgO *addition* vector from its reconstructed composition. Sample RC2709:6-2 falls on a vector which is at a large angle to any MgO addition or extraction vector. The first sample is a relatively straightforward matter. If there are conditions which can extract MgO from peridotite during alteration, it is not unreasonable to suppose that MgO might be added to peridotite elsewhere. That would depend on the mechanism by which the extraction (or addition) takes place.

Sample RC2709:6-2 is a more difficult problem. The bulk composition itself lies within the field of bulk compositions of the other peridotites. It is the reconstructed composition which distinguishes this sample from the rest of the altered peridotite samples. Several factors may account for this deviation. The most likely explanation arises from the fact that this sample is unusual in the sample suite petrographically, due to the presence of large variations in the mineral content of the rock on the scale of the sample. This heterogeneity of the sample raises the possibility that the thin section was not representative of the bulk sample. Thus, the modes and mineral compositions used for the recon-

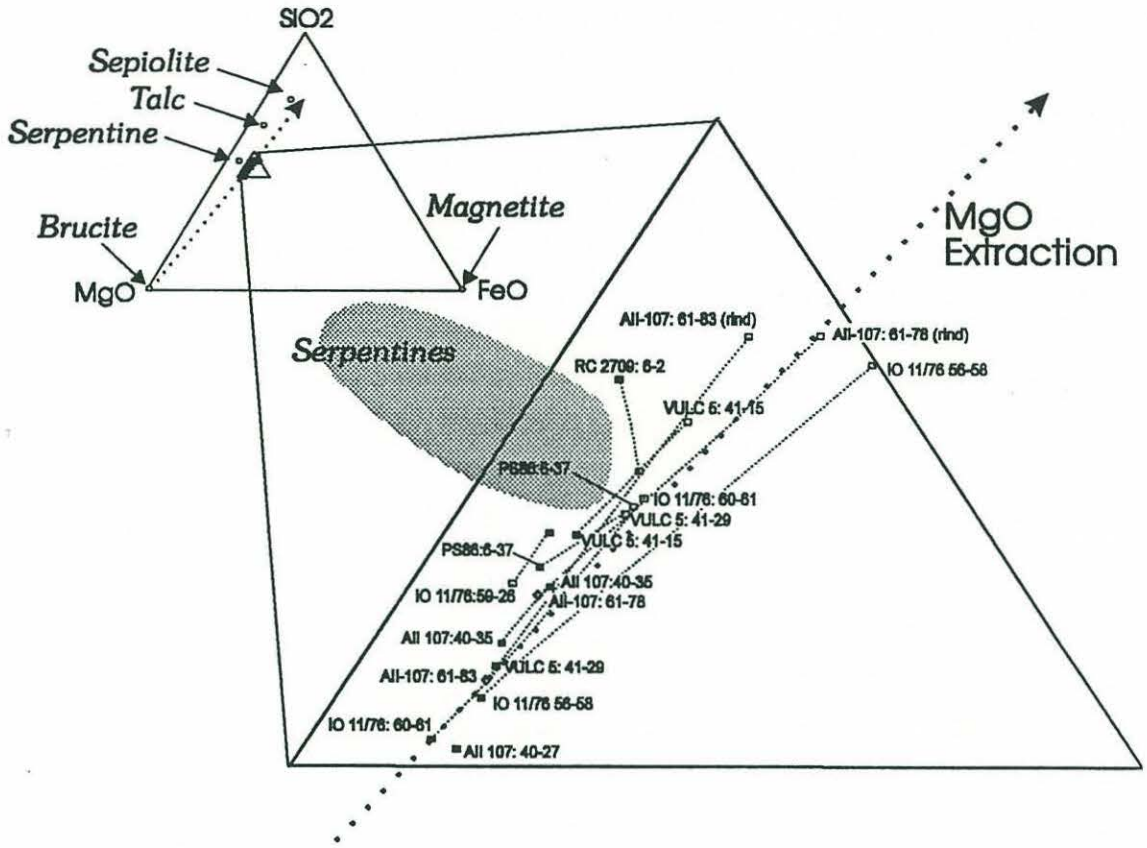

Figure 9: Abyssal peridotite bulk and reconstructed compositions in the Mg-Fe-Si ternary. Filled squares are calculated bulk compositions. Filled diamonds are unweathered core compositions for samples AII107:61-78 and 61-83. Open symbols are for whole rock abyssal peridotite compositions. Fine broken lines connect calculated (or core) compositions and bulk compositions. Large broken line indicates the effect of MgO extraction. The compositions of talc, brucite and magnetite (Deer, et al., 1966), sepiolite (Bonatti, et al., 1983) and serpentines from this study (Table 8) are shown for reference.

struction may not correspond to the analyzed bulk composition. The reconstructed composition of the rock is rich in SiO_2 compared to the other peridotites, and poor in MgO. This would be the result if orthopyroxene were richer in the thin section than in the bulk sample analyzed. In fact this section was extremely rich in orthopyroxene (44%), which is suggestive that orthopyroxene is over-represented in the mode of this sample.

With two exceptions, samples IO11/76:59-26 and RC2709:6-2, MgO depletion coupled with enrichment in SiO_2 appears to have occurred in both the low-Mg and low-alkali groups. In a later section, it is postulated that the Mg depletion seen in the low-Mg group and to a lesser extent in the low-alkali group

is due to low-temperature alteration and weathering. If this is in fact the case, then all abyssal peridotites must be considered as being affected jointly by the processes of serpentinization and weathering. Differential serpentinization of olivine can account for some of the variation in the low-alkali samples, as can serpentine veining (this will be explored in greater depth in a later section). Such processes cannot, however, be called upon to generate all the differences between bulk and reconstructed compositions seen here.

Na_2O and K_2O added

All of the samples analyzed show some evidence of gain of alkali elements. The alkali content of the samples provides a major discriminant between the two groups of samples. The low-Mg group is greatly enriched in both Na_2O and K_2O, while the other is much lower in these elements and shows a nearly linear correspondence between bulk and reconstructed compositions. In the low-alkali group, Na_2O and K_2O are surprisingly well behaved, considering their concentration in seawater and their low concentration in peridotites. These samples are generally within about a factor of two of their calculated alkali compositions. The level of enrichment of K_2O in the low-Mg samples is higher than the Na_2O enrichment in these samples. Particularly for the lower level samples, the differences between the bulk and reconstructed compositions may have a large analytical component unrelated to geology.

The precise mechanism by which the alkali elements are incorporated into abyssal peridotite is not certain. Some of the serpentines in this study (Table 8) have K_2O contents consistent with the levels of K_2O seen in the whole rock. Hébert, et al. (1990) analyzed primary and pseudomorph pairs on over 50 minerals in peridotites recovered in leg 109 of the ODP. In only one case did the K_2O content of serpentine reach the levels reported for the whole rocks in this study (Table 9). It is probable that the alkali elements are physically located in clay minerals or adsorbed onto surfaces of major minerals (e.g., serpentine) in the rock, where they may not be exposed to the electron probe. Very small amounts of low-temperature K-bearing clay minerals such as illite, smectite, kaolinite, or muscovite would easily account for the alkalis added to the rock during alteration. Their alkali contents are high enough that they might not be detectable in an x-ray diffraction spectrum, or observable in thin section.

Al_2O_3 and Cr: immobile elements

Al_2O_3 is expected to be the most immobile constituent of abyssal peridotite (Mottl, 1976; Kimball, et al., 1985; Grant, 1986). This is reasonable since it is hosted mainly by spinel, which is a resistant phase. Secondly, Al is extremely insoluble in seawater at any temperature (Janecky and Seyfried, 1986). If Al_2O_3 is truly immobile, then Figure 8d should provide a test of the errors in the reconstruction process itself. Errors in point counting or sample heterogeneity will be likely to be expressed in this way, as deviation of individual samples from equality. Systematic errors, such as disagreement between the electron microprobe and the XRF, would show up as a correlation differing in slope from the equality line. In the low-Mg group, Al_2O_3 seems to be enriched relative to the low-alkali group. This could be due to the enrichment of spinel in the weathered rock as a result of mass removal. In the low-alkali group, most of the samples fall close to the X=Y line, implying little net mass gain or loss. The exception to this is sample RC2709:6-2, an exceptional sample in many other respects as well. The low Al_2O_3 in this sample is mainly due to a low spinel mode (0.73%; Table 2). The behavior of aluminum in the rocks of this study is wholly compatible with the view of Al as an element which is highly resistant to alteration.

Cr behaves similarly to Al_2O_3, as it did in the abyssal mylonite isocon diagrams (Figure 7). In that section, model-dependent errors were not a possibility. Comparing Figures 8d and 8j, it appears that qualitatively the two elements have behaved similarly. The low-Mg group are enriched in Cr, as would be expected if mass removal had enriched the weathered rock in spinel. In the low-alkali group, sample RC2709:6-2 once again shows the greatest apparent depletion in Cr, probably due to its low spinel mode (0.73%). The remainder of the samples show a mild apparent depletion in Cr, which cannot be considered significant, given the uncertainties in the measurement of Cr concentrations of rocks and minerals and in point counting. The behavior of Cr is also consistent with its being highly resistant to moderate and low temperature alteration processes.

CaO: depleted in some cases.

CaO follows the same general pattern established in the other elements. The two groups of samples separate neatly into low-Mg (high-CaO) and low-alkali (low CaO) groups. The primary exception to this grouping is sample PS86:6-37, possibly due to the addition of aragonite, a common contaminant of abyssal peridotite (Thompson, 1970; Bonatti, et al., 1972; Shibata and Thompson, 1986). The aragonitization of peridotite and its significance for the current study is discussed below. Part of the explanation for the high CaO in the low-Mg group may lie not in aragonitization, but concentration of resistant diopside by mass removal processes (also discussed below).

If only the low-alkali peridotites are considered, there is a significant CaO depletion (except for PS86:6-37, as noted above). Miyashiro, et al. (1969) noted CaO depletion in altered peridotites, as did Shibata and Thompson (1986). The low-alkali peridotites appear to have lost about 25% of their CaO as a group. The loss of CaO in this group should not be linked to their low-alkali status; the "low-alkali" name applies to their low alkali concentrations relative to the low-Mg group only. All of the samples in the "low-alkali" group have gained Na_2O and K_2O in absolute terms. Much of the CaO depletion in these samples could be explained by the breakdown of enstatite, which accounts for about 17% of the mass budget of CaO in a typical peridotite. The remainder of the CaO loss must be explained by the breakdown of diopside, which is typically more resistant to serpentinization.

FeO, MnO and TiO_2: no consistent pattern.

FeO and MnO show few consistent patterns with respect to the low-Mg and low-alkali groups. There seems to be little correlation between measured and bulk concentration of either element. FeO shows considerable overlap between the two groups. In the low-Mg group, sample IO11/76:56-58 has a much higher FeO content than any of the other samples. Sample IO11/76:60-61 has a very high MnO content relative to its reconstructed composition. The low-Mg group seems to be higher in measured MnO as a group than the low-alkali group, which tend to have higher reconstructed MnO contents. Otherwise there is little to distinguish the two groups of samples from each other, and there is little systematic variation.

TiO_2 also shows few consistent patterns. There is considerable overlap in the compositions of the low-Mg and low-alkali groups, though there is a correlation between reconstructed and bulk compositions overall which suggests that variations in the primary composition are reflected in the final altered composition. TiO_2 is concentrated in diopside, and the low-Mg group of samples are enriched in TiO_2 as they are in CaO, which might be due to the resistance of diopside to alteration and mass removal. There are, however, three samples in the low-alkali group which are enriched in TiO_2, samples Vulc5:41-15, 41-29 and RC2709:6-2. While it is possible that these samples contain some high-Ti alteration phase (e.g. amphibole), there is little other evidence for this. RC2709:6-2 is a sample in which amphibole and other high temperature phases were sought unsuccessfully using thin sections and the electron microprobe.

Integrative measures of mass alteration.

Abyssal peridotites undergo a variety of different types of mass alteration, as will be discussed below. Many of these processes are not linked to one another in degree. For example, a rock which is relatively unweathered may be aragonitized (as in sample PS86:6-37). Nonetheless, to a first approximation, the degree of alteration is a useful abstraction, as it allows alteration processes, many of which *are* linked, to be aggregated and compared.

The alteration of abyssal peridotite is a process which is quite distinct from many other types of metamorphism in that significant mass fluxes have taken place during some part of the process. This is not usually the case during metamorphism. Consider, for example, the classic Barrovian metamorphic series, shale-slate-phyllite-amphibolite. Except for the dewatering of the minerals with increasing metamorphic grade, this series is essentially isochemical. The rocks would be difficult to differentiate on purely compositional grounds. Similarly, in the peridotite system, Equation 19 (the hydration of olivine and enstatite to serpentine; page 182) is isochemical except for the addition of water to the peridotite. The bulk composition of the system remains unchanged and nothing is gained or lost from the system besides water.

As we have seen, mass addition and removal are characteristic of the alteration of abyssal peridotites. In order to measure semi-quantitatively the degree of alteration of a sample, it is desirable to define an alteration index based

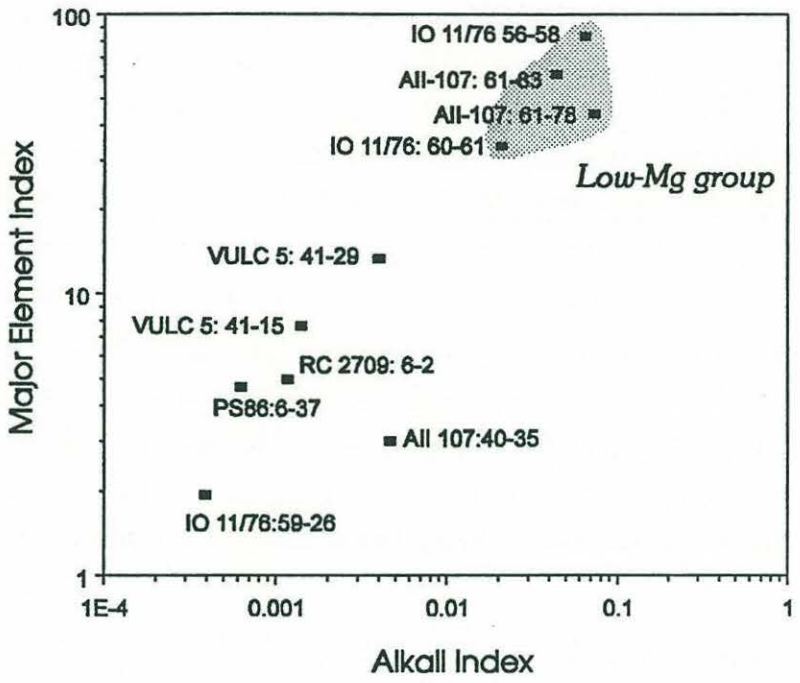

Figure 10: Alkali Index vs. Major Element Index. The major element index is the sum of squared residuals between bulk and reconstructed compositions for all major elements (Equation 15). The alkali index is the sum of squared residuals of the elements K_2O and Na_2O. For the mylonite samples (AII107 Dredge 61) the unaltered core composition is used instead of the calculated primary composition. The shaded area encloses the low-Mg group, whose compositions are thought to be dominated by weathering processes.

on major elements that describes the total difference in bulk composition between the altered and unaltered sample.

An index of alteration for major elements

We can define an alteration index as a distance between the bulk composition vector and the reconstructed composition vector in 10 component compositional space. This difference is a mismatch between a model composition and a real composition. A convenient way to describe it is the sum of squared residuals between model and data. This can be defined as follows:

$$\text{Alteration Index} = \sum (C_B - C_R)^2 \qquad (15),$$

where the summation occurs over the elements in the data set. This alteration index encapsulates the effects of all the mass fluxes which have occurred during the course of alteration of the peridotite. It will be instructive to compare this

measure of the mass flux to and from the peridotite with measures of serpentinization, hydration and isotopic exchange later in this chapter. This particular index of alteration de-emphasizes those elements which are low in concentration, so before it can be used, the degree of correlation between the depletion of MgO from the peridotites and the degree of enrichment in alkalis should be tested.

An index of alteration for incompatible minor elements.

It is not certain exactly how Mg is stripped from peridotites and alkali elements are deposited . There is thus no *a priori* reason to believe that these two processes are strongly linked. Before comparing the magnitude of mass fluxes with other processes which occur during the alteration of the rock, the assumption of a linkage between Mg loss and alkali gain should be tested. Another index of alteration can be defined using only the incompatible elements Na_2O and K_2O. This will be called the alkali index. The alkali index has the desired characteristic of providing an integrated measure of the degree of enrichment of a sample in those elements only. The alkali index is defined as in Equation 15 but uses only the elements Na_2O and K_2O. Table 16 lists the Alkali Index (AI) and the Major Element Index (MI) for each of the samples in this study. Also included is the loss on ignition (LOI) determined in the course of XRF analysis.

In Figure 10, the Alkali Index is plotted against the Major Element Index. There is excellent correlation between the two measures, though as noted above, there is no *a priori* reason to expect such a correlation. Elemental concentrations in products of a disequilibrium peridotite alteration process are dependent on the activities of the elements involved, the mineral solubilities of the reaction products and the kinetics of the individual reactions. All of these may be different for the alkalis than for silica and magnesium. The low-Mg group have very high alkali indexes and major element indexes, as expected. It is important to note that with the exception of sample AII107:40-35, the low-alkali group also has a correlation between the alkali index and the major element index. This strongly suggests that the process which produces Mg-depletion and alkali gain also have occurred in these samples, if only to a lesser degree.

Table 16: Alteration Indices. Defined as in Equation 15. Loss on ignition is in weight percent. The samples from dredge AII107:61 are represented by their weathered rinds.

Sample Number	Major element Index	Alkali Index	SiO_2/MgO	L.O.I.
PS86:6-37	4.54	0.000542	1.106	8.85
AII-107:61-78 W	44.34	0.073090	1.250	4.94
AII-107:61-83 W	61.14	0.043980	1.278	3.62
IO11/76:60-61	33.74	0.020583	1.120	10.55
IO11/7656-58	59.37	0.060759	1.279	7.58
IO11/76:59-26	2.37	0.000111	1.036	11.24
VULC5:41-29	13.16	0.003915	1.112	8.68
VULC5:41-15	7.52	0.001314	1.178	10.58
RC2709:6-2	4.91	0.001128	1.134	7.06
AII107:40-35	2.91	0.004616	1.045	11.88

The excellent overall correlation of the Alkali Index with the Major Element Index is highly suggestive that the processes that cause MgO/SiO_2 redistribution are linked to those that cause the alkali gain. In this case, seawater is a plausible source for the alkali elements. The mobility of those elements is controlled as much by the reaction chemistry of the rock with circulating solutions as by the concentrations of those elements in solution. Given the good correlation between these two independent measures of mass flux in the peridotite, they can be used interchangeably in the discussion which follows.

Nd and Sr isotopes in altered peridotites.

The alteration of abyssal peridotite by seawater may be considered, as a first approximation, to be a bulk mixing process between seawater and peridotite. The extremely low Nd/Sr of seawater relative to peridotite dictates the shape of the mixing hyperbola in $^{143}Nd/^{144}Nd$ vs. $^{87}Sr/^{86}Sr$ space to be nearly square. This is illustrated in Figure 11 where a bulk seawater-mantle mixing curve is calculated for two different mantle compositions chosen to bracket the range of depleted mantle compositions. In general, the bulk samples determined for this study fall on or near to a seawater mixing curve, calculated using reasonable values for the concentrations and isotopic compositions of seawater and peridotite. This shows that the mixing approximation is a good one to some extent. Sample PS86:6-37 is an exception to this, as is discussed below.

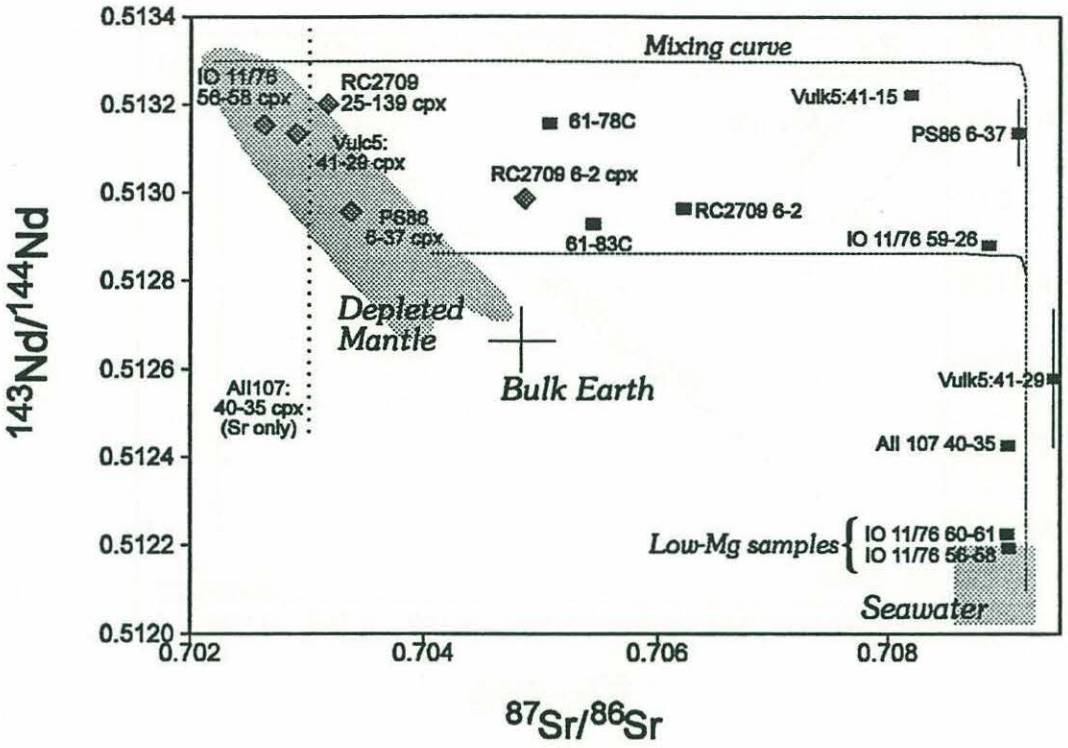

Figure 11: $^{143}Nd/^{144}Nd$ vs. $^{87}Sr/^{86}Sr$ in abyssal peridotite whole rocks and clinopyroxenes. Broken lines enclosing the data points are calculated peridotite-seawater mixing curves (described in text). Rectangles denote whole rocks, while diamonds denote clinopyroxenes. Vertical broken line shows the Sr isotopic composition of clinopyroxene sample AII107:40-35 (Bouvet F.Z.).

Mixing models

A seawater-peridotite mixing model can be used to calculate the total water/rock ratio based on the $^{143}Nd/^{144}Nd$ or $^{87}Sr/^{86}Sr$ composition of the rock. For example, in the isotopic mixing equation, the isotopic composition of the mixture is a linear combination of the isotopic compositions of the end members, weighted by the concentrations of the element of interest. If the fraction of end-member A in a binary mixture is denoted by F then the fraction of B is (1-F). The isotopic composition of the mixture, μ, can be calculated from the isotopic compositions (α and β) and concentrations (a and b) of the endmembers as follows :

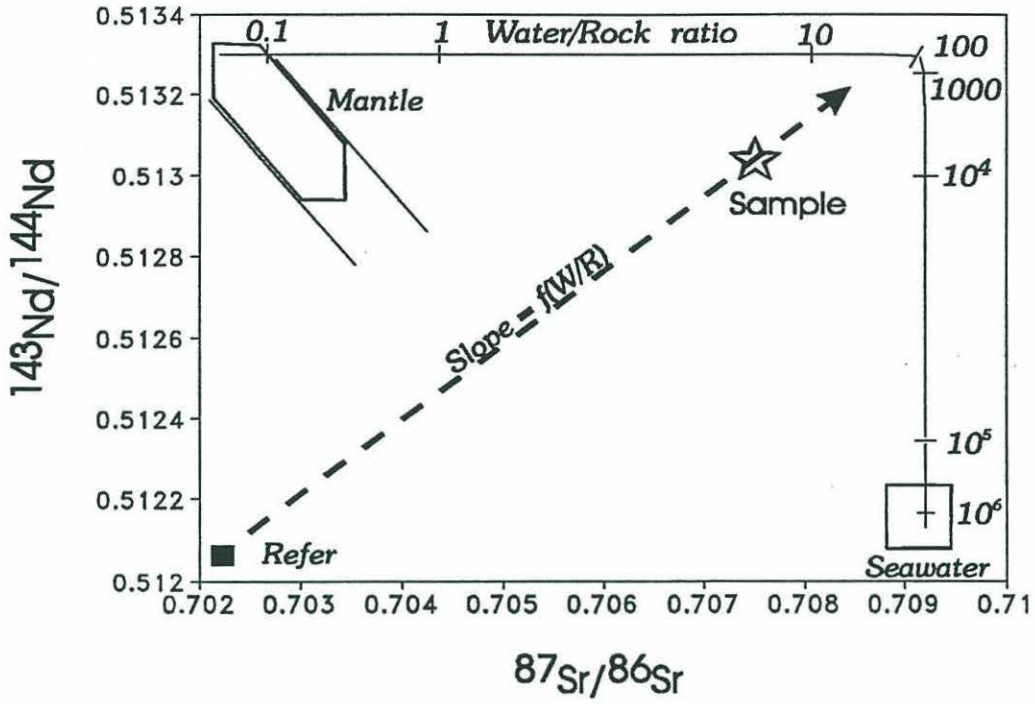

Figure 12: Cartoon illustrating the isotopic index calculation.

$$\mu = \frac{Fa\alpha + (1-F)b\beta}{Fa + (1-F)b} \qquad (16).$$

This formulation is identical to that in Langmuir, et al. (1978). Solving for F:

$$F = \frac{b(\mu - \beta)}{a(\alpha - \mu) + b(\mu - \beta)} \qquad (17).$$

This formulation shows how F can never be negative, and ranges from 0 to 1.

Taking seawater as the A component and peridotite as the B component, the water to rock ratio is simply WR = F/(1-F). There are, however, a variety of assumptions inherent in such a calculation. The first is that there are only two isotopic endmembers and that they are of known composition. This may not be a good assumption for abyssal peridotites, at the very least for Sr in abyssal peridotites. There are at least three isotopic reservoirs of Sr in abyssal peridotites, as will be discussed below. Of these, the orphan ^{87}Sr reservoir is a very small portion of the total mass budget for Sr, but its extremely radiogenic isotopic composition makes it a significant potential confounding factor in the de-

termination of water to rock ratios based on Sr isotopic mixing. An example is sample Vulc5:41-29, which has an $^{87}Sr/^{86}Sr$ of .7094 and cannot be interpreted in terms of a binary seawater-peridotite mixing model. Calculating water to rock ratios based on whole rock peridotite Sr isotopic composition determinations such as the ones in Bonatti, et al. (1970) would similarly be pointless.

Sample PS86:6-37 is another clear violation of the known endmembers assumption. The fact that the whole rock analysis has a higher $^{143}Nd/^{144}Nd$ than the clinopyroxene from the same rock is similarly incompatible with binary seawater-mantle mixing. In this case, however, an isotopic reservoir which could account for the discrepancy has never been identified in abyssal peridotites. The whole rock $^{143}Nd/^{144}Nd$ analysis has a significant analytical uncertainty attached, so the problem may be an analytical one and not a geologic one.

Second, the peridotite must act as an equal sink for Sr and Nd. If Sr and Nd are incorporated into peridotite from seawater at efficiencies that are different, then they will give systematically conflicting estimates of the total water/rock ratio. This is not typically thought of as an important factor in the study of potentially altered rocks. Sr and Nd are similar enough, chemically, that they are thought of as having practically identical solution chemistries. Almost all studies treat the alteration of Nd and Sr in terms of simple mixing equations, as is done here.

The Nd isotopic composition is more robust than Sr with respect to the assumptions implicit in calculating a water/rock ratio from the $^{143}Nd/^{144}Nd$ of the bulk sample. There is no alteration mineral commonly found contaminating abyssal peridotite which contains extremely high concentrations of Nd, as does aragonite in the case of Sr. Mn encrustations can have high Nd concentrations. These seem to be physically separated from the rock and, in the case of the present samples, do not seem to have affected the samples' compositions. There is similarly no evidence of any reservoir of Nd in peridotites that has any other isotopic composition than the mantle (clinopyroxene) and seawater. F can be calculated for Nd using Equation 16. The results are listed in Table 17. The efficiency of extraction of seawater Nd is probably not 100%, so any water/rock ratio calculated from $^{143}Nd/^{144}Nd$ must be considered a minimum. At low water/rock ratios, the Nd calculation becomes insensitive to the water/rock ratio, since the $^{143}Nd/^{144}Nd$ does not change much at water to rock ratios less than 10000.

Table 17: Isotopic Water/rock calculations.

Sample	F(Nd)	W/R	F(Sr)	W/R	slope	W/R
RC27096-2	2.68E-05	37338	0.3304	2.0	0.2151	2
Vulc5:41-29	1.49E-05	67315	0.0222	43.8	0.0662	41670
Vulc5:41-29 Cpx	3.21E-05	31108	0.8567	0.2	1.4791	0
Vulc5:41-15	3.48E-05	28725	0.0995	9.0	0.1873	157
AII10740-35	1.01E-05	98533	0.0152	64.4	0.0479	59374
PS866-37	3.21E-05	31154	0.0056	176.9	0.1493	886
PS866-37CPX	2.66E-05	37566	0.7722	0.3	0.7478	0
IO11/7660-61	3.88E-06	257819	0.0154	63.8	0.0183	170275
IO11/7659-26	2.42E-05	41252	0.0314	30.8	0.1173	5635
IO11/7656-58	2.94E-06	340702	0.0144	68.3	0.0138	231468

Method of calculation is discussed in the text. F(Nd) and F(Sr) are listed as the fractions of mantle Nd and Sr in the model mixture, respectively.

A combined Nd-Sr isotopic alteration index

For convenience in comparing the isotopic compositions of bulk peridotites with their major element chemistry, it would be useful to have a means of calculating a single, robust measure of the degree of alteration as documented by isotopes. This section will develop a method of calculating an estimated water/rock ratio from Nd and Sr isotopic compositions at the same time. The resulting combined isotopic water/rock ratio is more robust than a water/rock ratio calculated from either system alone.

Calculations of F and of the water-rock ratio using $^{87}Sr/^{86}Sr$ and $^{143}Nd/^{144}Nd$ are shown in the first four columns of Table 17 for the analyses in this study. The errors due to end-member variability are high for both Sr and Nd using this type of calculation. It is obvious that all the samples give an unreasonably low water/rock ratio of less than 200 for Sr and an unreasonably high one of more than 10^5 for Nd. A more robust calculation is made in the following way: For a given mixing model, any mixture of the two endmembers will produce a fixed $^{143}Nd/^{144}Nd$ and $^{87}Sr/^{86}Sr$ composition. The slope of a line passing through that point to an arbitrary origin has a very stable relationship to the water/rock ratio. Figure 12 depicts this technique graphically. Instead of calculating a separate water/rock ratio for each element, the point represented by that element is extrapolated to an appropriate seawater-peridotite mixing curve. Mathematically, we calculate the slope relative to a reference isotopic

composition, in this case $^{143}Nd/^{144}Nd$ = .5120 and $^{87}Sr/^{86}Sr$ = .7022. Then make the approximation:

$$\text{Water / Rock} = 10^{(c+m*\log(\text{slope}))} \qquad (18).$$

where c and m are as follows:

Range	c	m
0.0 < slope < 0.1	-.45722	-1.05992
0.1 < slope < 0.2	-3.7414	-7.65626
0.2 < slope	3.3281	-1.09556

for a case where $^{143}Nd/^{144}Nd$ in seawater =.5120, Nd concentration in seawater = 2.6e-6 ppm., $^{87}Sr/^{86}Sr$ in seawater = .7092, Sr concentration in seawater = 8 ppm., $^{143}Nd/^{144}Nd$ in peridotite = .5133, Nd concentration in peridotite = .07 ppm., $^{87}Sr/^{86}Sr$ in peridotite = .7022 and Sr concentration in peridotite = 12 ppm. Slopes for the samples of this study are shown in the fifth column in Table 17 and the water/rock ratios calculated from them in the last column. This approximation results in the much more robust water/rock approximation. While the Sr and Nd methods alone are sufficient near to the endmember compositions, the combined approach gives a more robust estimate of the total water/rock ratio over the entire range of water/rock ratios. The greatest errors in this calculation are at the extremely high and low water/rock ratios, and at the region from $W/R=10^2$-10^4. In this region, the Nd-Sr mixing curve "turns the corner". The water/rock ratio changes by almost two orders of magnitude, while the Sr and Nd isotopic compositions remain largely unaffected. In this region, the Nd retains nearly its mantle value and the Sr has already reached the seawater isotopic composition. Very small differences in the calculated slope (for example due to endmember variability or analytical uncertainty) result in large changes in the calculated water/rock ratio in this region.

Water/rock ratios calculated in this way are necessarily minimum values, since they assume perfect efficiency of Sr and Nd deposition. In a theoretical study of the alteration of basalt, Rutherford and Casey (personal communication) were only able to match the $^{87}Sr/^{86}Sr$ in basalts in ODP hole 504b using efficiencies as low as 0.25%. The efficiency of exchange is only an issue if the proc-

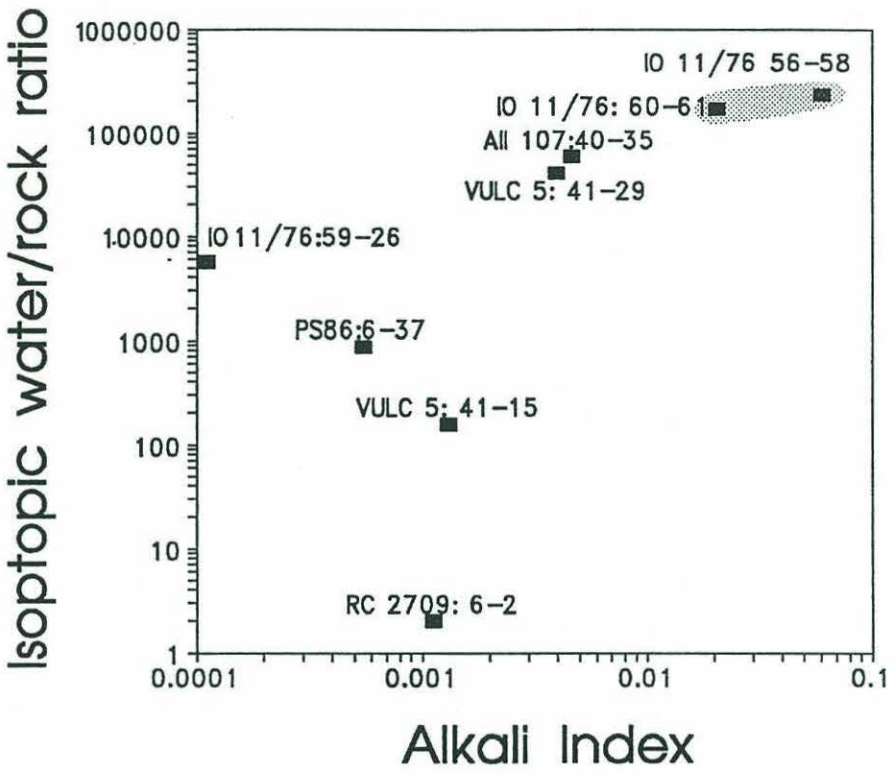

Figure 13: Alkali Index versus calculated water/rock ratio for abyssal peridotites. Shaded area indicates the low-Mg group of samples.

esses under consideration, have different efficiencies. For example, Sr isotopic exchange and Os isotopic exchange probably have different efficiencies. Sr isotopic exchange and Nd isotopic exchange probably do not. It may be of interest later if the process of Mg depletion from the peridotite has a different efficiency than that for isotopic exchange. The Mg in the rock may have "seen" more or less seawater than the isotopic ratios indicate.

Figure 13 shows the calculated water/rock ratio plotted against the alkali index from the previous section. There is a strong correlation between these two very different measures of the degree of alteration of the peridotite samples. The rocks with the greatest degree of mass alteration (samples IO11/76:56-58, and IO11/76:60-61) also have the highest calculated water/rock ratios. The samples with the lowest degree of mass alteration also have the lowest degree of alteration as calculated from Nd and Sr isotopes. This correlation implies that the causes of isotopic exchange and mass flux are similar, since they occur to a similar degree in any given rock.

The last two sections have shown strong correlations between the degree of MgO depletion in these abyssal peridotites, the degree of alkali enrichment and the degree of isotopic exchange with seawater. The next section will discuss the relationship of these linked processes to the serpentinization of the rocks, and will also discuss the conditions of temperature, water/rock ratio, and solution chemistry under which such serpentinization and metasomatism take place.

Interpretation of mass fluxes

The preceding two sections have demonstrated that the two different types of metasomatism present in abyssal peridotite are linked to each other and to the degree of isotopic exchange with seawater. This section will examine individually the alteration processes which have affected these peridotites. The relationships between these processes and serpentinization will also be discussed. The peridotites have undergone varying degrees of mass addition and removal. Some of theses, such as the aragonitization of sample PS86:6-37, are easy to account for. It is important to decide whether any of the significant mass fluxes (e.g. Mg and Si redistribution) can be caused by serpentinization alone. Differential serpentinization of olivine can result in apparent removal of Mg from peridotites when studied by the bulk reconstruction analysis used here. Veining of a rock by non-locally derived serpentine can also change the rock's composition. These possibilities will be discussed. Further, the possible conditions of temperature, water/rock ratio and solution chemistry will be discussed under which serpentinization and mass alteration occur.

Aragonite gain

Aragonite is frequently present in abyssal peridotites (Thompson, 1972; Bonatti, et al., 1980). Where it escapes detection in thin section or x-ray spectra, it can readily be detected by its extremely high Sr content (1% Sr or more). Peridotite samples exceeding the relatively low mean concentration of Sr in abyssal peridotites of 5-8 ppm. can be considered likely to contain aragonite. Some of the peridotites studied by Shibata and Thompson (1986) had as much as 1500 ppm. Sr. The bulk concentration of Sr in sample PS86:6-37 is 231 ppm. By this measure, the sample clearly includes some aragonite. No aragonite was found either in x-ray analysis of the first magnetic fraction (aragonite is nonmagnetic)

or in thin section petrography. During mineral separation, however, a white, non-magnetic mineral was separated that had pronounced cleavage. It was at first taken to be plagioclase, since it was almost completely non-magnetic. The mineral dissolved in the spike solution (weak HCl) with the evolution of gas, and the Sr content was so high that the ^{84}Sr enriched isotopic spike could not be detected in the analysis. The isotope dilution calculation was impossible for that reason (Table 14). The concentration of Sr in the aragonite mineral separate was probably in excess of 1 percent.

Samples Vulc5:41-29 and IO11/76:60-61 also show elevated Sr contents (18 and 12 ppm., Table 10). The amount of "suspicious" Sr is so low that aragonite is probably not a significant contributor to the overall mass budget of those samples. If the Sr excess is due to aragonite, the bulk Sr isotopic composition of those samples could well be dominated by seawater Sr deposited very late and at low temperatures with aragonite.

Samples IO 11/76:60-61 and PS86:6-37 also have elevated concentrations of Zr, but sample Vulc5:41-29 does not (17, 37 and 8 ppm. respectively, Table 10). If these Zr concentrations are related to the presence of aragonite in one or more of these samples, this may imply that the aragonite has a significant concentration of Zr. This sample has the highest Ti and Zr concentrations in clinopyroxene measured in this study (Table 6) so the high Zr may be primary. Assuming that the Zr concentrations are related to the aragonite, the ~8 ppm. "background" Zr may be subtracted from the 37 ppm. concentration of Zr in sample 6-37 (Table 9) to calculate a Sr/Zr ratio in aragonite at approximately 7.8. If the aragonite itself is nearly 1% Sr, this implies a very high Zr concentration of 1290 ppm. in aragonite. Previous studies of marine aragonite associated with abyssal peridotite (Thompson, 1972; Bonatti, et al., 1980) have not reported such high Zr contents in aragonite.

Aragonite is not uncommon in abyssal ultramafic rocks (Thompson, 1972; Shibata and Thompson, 1986; Bonatti, et al., 1980), and has an extremely high Sr content. Using a bulk rock (sample PS86:6-37) concentration of 311 ppm. Sr and an aragonite concentration of 1% Sr (Bonatti, et al, 1980) results in 3 weight percent aragonite in the rock, slightly more on a volume basis. This is a significant amount of aragonite, more than twice the amount, for example, of spinel in the rock. If the aragonite is extremely localized, it could still have gone unnoticed in thin section.

Bonatti, et al. (1980) argue on the basis of oxygen and carbon isotopes that aragonite forms at low temperatures (below 10 °C). Similar analysis of serpentines from the same samples resulted in temperatures of formation for those minerals in the range of 50-200 °C. This implies that aragonite precipitation is wholly unrelated to serpentinization. With the present small data set, it is impossible to speculate on a possible correlation between aragonitization and MgO loss. Bonatti, et al. (1980) and Thompson (1972) both conclude that inhibition of calcite formation by high activities of Mg^{2+} in solution is the reason for the deposition of aragonite preferentially over calcite, as shown by Bischoff and Fyfe (1968). The occurrence of aragonite in abyssal peridotites is thus evidence for high [Mg^{2+}] fluids circulating at low temperature in the ocean crust.

MnO gain

Mixing of peridotite samples with manganiferous sediments precipitated from seawater is a major issue in interpreting the Os isotopic compositions of abyssal peridotite whole rocks. The occurrence of aragonite as a water-borne precipitate implies that precipitation of manganese oxides is also possible. These commonly occur as rinds on the exteriors of boulders on the ocean floor. Some of the samples studied here had thin coatings on their exteriors. In every case, these were carefully removed during sample preparation. There is no evidence in any of these samples for Mn oxides occurring as disseminated grains or fracture fillings.

One sample (IO 11/76 60-61) has a factor of 2 enrichment in MnO over its reconstructed composition (Figure 8). The very low reconstructed MnO in this sample is primarily due to the low MnO in the olivine analysis (Table 3); none of the other phases measured in this peridotite has low MnO, so it is possible that this MnO determination is in error. Even so, the bulk MnO for this sample is the highest of any of the samples in this study and is more than 30% richer in MnO than the next highest sample. It is difficult to avoid the conclusion that some sort of Mn enrichment process has operated on this sample. Manganese crusts deposited on the surfaces of rocks exposed on the ocean floor are typically rich in Fe, Co, Cu and Os, among other refractory elements. Palmer, et al. (1988) contains analyses of a crust from IO11/76 56-58, one of the samples in this study, which is located close to IO11/76:60-61. The MnO enrichment in sample IO11/76: 60-61 without an attendant enrichment in other heavy metals (e.g., Cu,

Co) suggests either that the compositions of Mn deposits in fracture fillings may have different compositions than ones deposited in direct contact with seawater or that no Mn-bearing hydrogenous precipitate was involved and that the MnO enrichment is from some other source. The section on Os isotopes will consider in greater detail the implications of the addition of MnO-bearing minerals to sample IO11/76:60-61.

Serpentine veining

In searching for a mass alteration process which can change the bulk chemistry of a rock dramatically, serpentine veining must be considered. Typically, very small serpentine veins are though of as originating locally and are counted with the mode of the host mineral, usually olivine. Larger serpentine veins are often thought of as being exogenous to the rock and are typically not counted. The fact that serpentine veining occurs shows that significant mass redistribution can occur under conditions of serpentine formation (150-300°C; Wenner and Taylor, 1973; Bonatti, et al., 1984; Janecky and Seyfried, 1986). The serpentines from this study fall in a field which does not overlap the compositions of the abyssal peridotites, nor do they fall on any line connecting the recalculated and measured compositions. Serpentine veining can increase the Si/Mg ratio of an abyssal peridotite, but the addition vector for the serpentines in this study lie at a large angle to the observed compositional changes in the peridotites (Figure 9).

Coupled with addition of iron, perhaps in the form of a few weight percent magnetite, vein compositions might be brought in line with the alteration vectors in Figure 9. This might explain some of the mass change in some of the samples, particularly in the low-alkali group. Many of the altered compositions, even some in the low-alkali group, fall at a much higher Si/Mg ratio than any putative serpentine + magnetite vein composition. *It is not possible to produce these compositions by serpentine + magnetite addition.*

The presence of serpentine veins in the samples (as in most abyssal peridotite samples) shows that there can be mass redistribution during serpentinization. In order for this veining to have played a significant role in the mass fluxes documented here, co-precipitation of magnetite is required. The presence of significant amounts of peridotite-derived iron in hydrothermal solutions is un-

likely (Janecky and Seyfried, 1986). Additionally, iron oxide is rarely observed in serpentine veins (Appendix I). Even with the co-precipitation of iron, many of the samples in this study, particularly the low-Mg group, have compositions which could not have been produced by serpentine veining. It is therefore unlikely that serpentine veining plays a significant role in the formation of the mass effects seen in this study.

Differential olivine serpentinization

One way in which mass fluxes and serpentinization may apparently be linked is through the differential serpentinization of olivine (or orthopyroxene). If this occurs, olivine alteration products assume a greater volume proportion in the altered rock than in the protolith. When the altered and primary olivine are summed, the reconstructed primary composition of the rock has an erroneously higher olivine mode than the protolith actually had. The excess olivine component in the calculated composition causes an *apparent* loss of olivine components (i.e., MgO, and Ni) in the measured bulk composition, even in the absence of any true removal of olivine components from the system. Previous authors have commented on this phenomenon (Komor, et al., 1990), but have not attempted to verify whether it actually occurs.

To constrain the maximum effect possible due to differential serpentinization of olivine, let us assume that all the olivine in all the samples has been serpentinized, and that magnetite does not form from it. The effect of this would be that the olivine points counted would have the effective density of serpentine. Substituting the density of serpentine for that of olivine in the reconstruction calculation corrects for this effect. When this calculation is carried out, little changes in the relationship of the samples to one another in Figures 8 and 9 (as the differences between the two sets of plots are quite difficult to make out, it serves no purpose to replot Figures 8 and 9). The new reconstructed compositions are approximately 1 Wt. % poorer in MgO than the old ones and 0.5 Wt. % richer in silica than the old ones. Differential alteration of olivine moves the reconstructed composition in the same direction as the apparent mass fluxes in the data set. This is a small change indeed compared to the 3 Wt. % gain in silica and the 7 Wt. % magnesia loss seen, for example, in sample IO 11/76:56-58.

One sample from the present data set is explainable in terms of differential expansion of olivine, sample AII107:40-35. All of the other samples which showed MgO loss before still do so using the new reconstructed compositions. Samples IO11/76:59-26 and RC2709:6-2, which had shown the reverse relationships (MgO gain and SiO_2 loss) show those relationships more strongly with the new reconstructed compositions.

This simple calculation shows that differential expansion of olivine could account for a portion of the variance in the current data set. Since the percentage of alteration products pseudomorphous after each mineral is routinely collected during point counting, a volume correction could easily be made based on the degree of serpentinization of each mineral. As will be shown later, the degree of MgO depletion has a slight negative correlation with the percentage of mineral phases. This implies that the mass removal from the rock preferentially removes serpentine, decreasing the serpentine mode. This has the opposite effect to the volume expansion of olivine in point counting the rock. Considering the uncertainties already inherent in the point counting and mineral analysis, a correction for volume expansion of olivine and orthopyroxene would probably be pointless.

In any event, the bulk of the variation in the reconstructed peridotites must still be due to mass flux of Mg out of the peridotite. All of the variation in the mylonite data points with respect to their altered compositions must also be due to mass flux of Mg out of the peridotite, since point counting and olivine expansion play no role in those compositions. The preferential volume change of olivine upon serpentinization cannot be ruled out entirely in favor of isovolumetric alteration, and it must be considered as an added source of noise in the reconstruction calculation. The magnitude of the noise added to the mass flux signal is nonetheless comparatively small.

It is plausible to suppose that the mass fluxes documented in the preceding sections are linked in some other way to the serpentinization the peridotites have experienced. If this is the case there should be a positive correlation or trend apparent between the mass depletion and the degree of serpentinization. The degree of serpentinization can be expressed in several ways. The amount of volatiles in the rock (volatile loss on ignition) will be used here. Figure 14 shows loss on ignition plotted against the Alkali Index. It is clear from the figure that no positive correlation exists between the degree of serpentinization and the

degree of metasomatism. Quite the contrary, there appears to be a slight *negative* correlation between these two processes. This cannot be reconciled with any model of the mass flux on alteration whereby the mass flux occurs during serpentinization. One would then expect that greater degrees of serpentinization would generally result in greater degrees of mass flux.

The lack of any positive correlation between the degree of serpentinization and the degree of mass redistribution in peridotites suggests that these two processes are separate events which occur at different times and are not linked to one another. The weak negative trend in the data suggests that mass loss may be capable of removing serpentine preferentially to olivine. Olivine and orthopyroxene are more undersaturated in cool seawater than is serpentine, so such a hypothesis can only be based on the kinetics of dissolution of olivine. The preferential dissolution of serpentine would of course have an opposite effect on the mode of the rock than the preferential volume expansion of olivine. This may explain why the overall alteration seems to occur at constant volume.

"Dissolution mode" and Mg depletion

The preceding sections have shown that Mg depletion is a real effect and is not an artifact of the reconstruction calculation or a trivial effect of serpentinization. Another possible link between serpentinization and Mg depletion is possible if the rate of dissolution of the individual minerals varies with temperature. The reactions for the formation of serpentine from olivine and enstatite (Equations 1, 2, and 3) combine to form an isochemical reaction (no gain or loss of silica or magnesium) if the proportion of olivine to enstatite entering solution is 1:1 (Equation 19, p. 182). The entry of these phases into solution is largely controlled by their dissolution kinetics. Entry of olivine and enstatite into the solution at a 1:1 ratio is therefore likely to be fortuitous. Since olivine is much more abundant than enstatite in peridotite, there is likely to be a much larger "mode" of olivine entering the solution than enstatite. This would result in an excess of Mg in solution, which would form brucite at high temperature. Once lower temperatures are reached, the brucite would be dissolved by brucite-undersaturated seawater. If further low-temperature serpentinization occurred, the brucite would simply fail to precipitate.

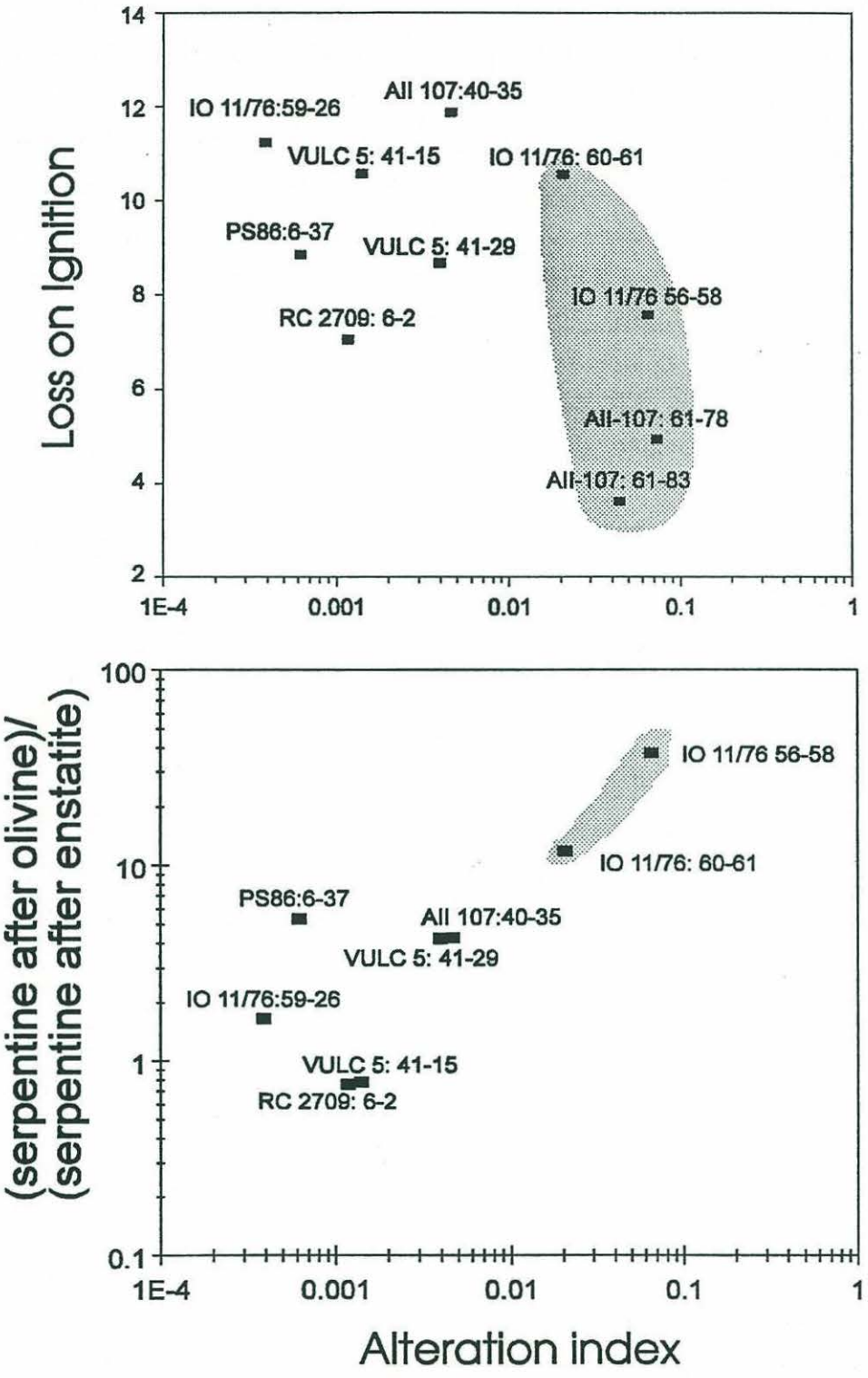

Figure 14: Alteration index vs. Loss on Ignition and dissolution mode in abyssal peridotites. Loss on Ignition is determined by measuring the weight loss after fusion of the sample at 1000° C. Serpentine replacing olivine and serpentine replacing enstatite determined by point counting of thin sections (see Appendix I). The shaded areas enclose the low-Mg group of samples.

Figure 14 illustrates the evidence for such a mechanism in the current data set. Serpentine after olivine divided by serpentine after enstatite are plotted as an indicator of the dissolution ratio of olivine to enstatite. Among the low-alkali group, there is no correlation between the olivine/enstatite dissolution mode and the degree of mass flux. It is impossible to conclude that preferential serpentinization of olivine caused the Mg-Si redistributions seen in that group of samples. If the low-Mg samples are included, a fairly strong relationship emerges. This implies that for the highly weathered samples, olivine is dissolved preferentially to enstatite. It is interesting to note that even in samples such as IO 11/76:59-26 where the enstatite appears much more altered than the olivine, the actual ratio of altered olivine to altered enstatite is still nearly 1. It is fair to state from Figure 14 that olivine is dissolved preferentially to enstatite in all but two of the peridotites and that it is essentially equal in these two rocks. This preferential serpentinization only correlates well with Mg removal from the rock in the case of the most weathered rocks, IO11/76:60-61 and IO11/76:56-58.

Water/rock ratios

The water to rock ratio required to completely serpentinize a rock at equilibrium is quite small, equal to the amount of water in serpentine. Shibata and Thompson show total water analyses for peridotite which range from 7 to 13% total water as H_2O^+. Theoretical (Silantiev, et al., 1992) and experimental (Janecky and Seyfried, 1986) studies of the alteration of peridotite commonly assume ratios of 6 to 30 times the mass of water to rock. These estimates of the water/rock ratio are based on the notion that serpentinization is the most important alteration process acting upon the peridotite and that most peridotite alteration occurs at the conditions prevailing during serpentinization.

The ability of an aqueous solution to transport Mg is dependent on the temperature of alteration and the composition of the fluid entering the peridotite. Simple mass balance requires that a fluid transporting several weight percent of magnesium from a rock have a Mg concentration of several hundred ppm., even at a water to rock ratio of 100. Such a high Mg concentration would be supersaturated in many Mg-bearing phases, even at low temperatures, and could not persist for long without precipitating those phases (Bischoff and Seyfried, 1978; Janecky and Seyfried, 1983). At higher water/rock ratios, a seawater solution might be nearly saturated with serpentine, but would have little ther-

modynamic driving force to leach Mg from the rock. Significant loss of Mg in peridotite to a solution can only occur in a case where the water/rock ratio is high enough that the fluid does not approach serpentine saturation. Thus, the mass fluxes documented in the preceding sections would imply that water/rock ratios during alteration are much higher than had been previously thought.

Isotopic exchange between peridotite and seawater provides an additional constraint on the water/rock ratio during alteration. From the discussion in the section on isotopic mixing models, it is clear that water/rock ratios during the mass redistributions documented here are higher than 100 and extend to $3x10^5$. As discussed earlier, these are minimum estimates of the amount of water which has had the opportunity to exchange isotopically with the peridotite. The qualitative estimate of water/rock ratio derived from the mass redistributions above is thus supported by the isotopic mixing calculations.

Temperatures of serpentinization and weathering.

As we have seen, the issues of temperature of alteration, water/rock ratio and concentration of leached elements in the circulating fluid are closely interrelated. So far, evidence has been presented that the mass redistribution documented in this chapter is the result of alteration at very high water rock ratios. This section will show that the temperatures at which this is possible without completely supersaturating the circulating fluid in Mg-rich minerals such as brucite are quite low. These low temperatures are distinct from the temperatures of serpentinization documented by O isotopes (Wenner and Taylor, 1971, 1973 and others) and experiments (Janecky and Seyfried, 1986).

Serpentine is a phase which is stable in peridotite at a variety of temperatures in the crust, starting as high as 500°C and extending to seafloor pressure and temperature (Bowen and Tuttle, 1949; Janecky, 1982; Janecky and Seyfried, 1986). It is possible to estimate the temperature of formation of serpentine-magnetite pairs by the fractionation of O and H isotopes between the coexisting minerals (Wenner and Taylor, 1971; 1973). Bonatti, et al. (1984) estimated serpentine-magnetite equilibration temperatures on abyssal peridotites which ranged from 233 °C down to 30 °C. Interestingly, the boron content of the rock increased dramatically as serpentine equilibration temperature decreased.

The serpentinization experiments of Janecky and Seyfried (1986) were all conducted at temperatures of 200-300 °C and 100-500 bars pressure. Serpentine was formed in all the experiments. In most of those experiments, the reacting fluid was seawater, and in all of the seawater experiments, Mg was lost from the seawater to the peridotite, and Fe and Si were lost from the peridotite. This is precisely the opposite of the Mg depletion which has been observed in this study. One may conclude from the Janecky and Seyfried (1986) experiments that Mg extraction *cannot have occurred* at the conditions of temperature, fluid composition and water/rock ratio used in those experiments. The exception to this conclusion is the one experiment in Janecky and Seyfried (1986) which was done with an Mg-free solution. This solution was intended to simulate the effect of peridotite interaction with an endmember hydrothermal solution rather than with seawater. The implications of that experiment are discussed below in the section describing the conditions under which the mass redistribution *could* have occurred.

Closed system alteration

There are many possible reaction paths which would accomplish the serpentinization and the Mg depletion of peridotites. Two of these which seem most likely will be considered here qualitatively. The first model is based on the relative kinetics of dissolution and precipitation of olivine and serpentine respectively. The second model considers much higher water/rock ratios where the fluid remains undersaturated in all the Mg-bearing phases.

Nesbitt and Bricker (1978) note the extraction of Mg from peridotites on land by circulating meteoric waters. They suggest that serpentinization and Mg extraction are linked processes which occur at low temperatures. Although the reaction path they consider applies mainly to the circulation of meteoric water through peridotite, the same rationale applies to seawater. Figure 15 illustrates the solubility relationships between the various minerals in the peridotite system at 300°C after Helmley, et al. (1977a, b) and Janecky and Seyfried (1986). At lower temperatures, the stability fields for the various minerals move to higher $\log([Mg^{++}]/[H^{+}]^2)$. This reflects the higher solubility of Mg-bearing minerals in the solution at lower temperatures. The stability relationships of the minerals involved remain qualitatively unchanged, however.

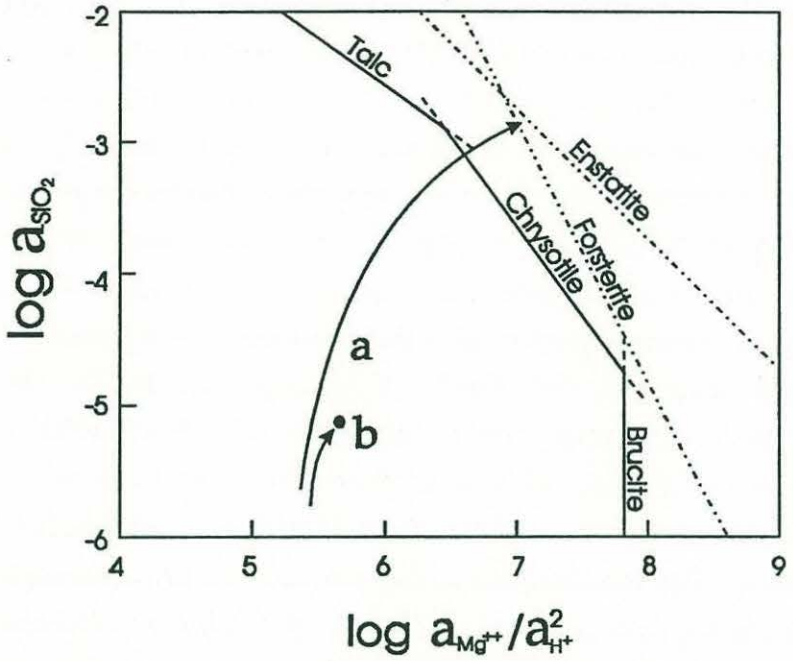

Figure 15: Solid-aqueous solution equilibria for talc, chrysotile, brucite, enstatite and forsterite. Calculated at 500 bars and 300°C after Janecky and Seyfried (1986). Path a is a hypothetical reaction path for a low water/rock closed system at relatively high temperatures. Path b shows the path of solutions in a hypothetical steady-state open system at low temperature where the solution never reaches equilibrium with the dissolving phases.

In experiments with relatively low water/rock ratios and relatively high temperatures (e.g., Seyfried and Dibble, 1980 and Janecky and Seyfried, 1986), the solution moves rapidly to saturation with enstatite and forsterite, and is supersaturated with serpentine, which precipitates. These relationships are shown by the solution reaction path labeled a in Figure 15. This reaction proceeds until one of the anhydrous phases is completely consumed. Equation 19 describes this reaction:

$$MgSiO_3 + Mg_2SiO_4 + 2H_2O <=> Mg_3Si_2O_5(OH)_4 \qquad (19)$$

To a first approximation it is not necessary to consider the reaction path beyond the point of total consumption of olivine or orthopyroxene. This point is rarely reached. The first mechanism for the extraction of Mg from the rock was proposed by Nesbitt and Bricker (1978) and considers the relative kinetics of dis-

solution of olivine and enstatite versus the kinetics of precipitation of serpentine. Specifically, they argue that Mg would be lost to the solution if the dissolution of olivine outstripped the precipitation of serpentine. The system would be driven to supersaturation in forsterite and enstatite by this mechanism, and might precipitate high-Mg phases such as brucite or Mg-Hydroxide-Sulfate-Hydrate (MHSH). Janecky and Seyfried (1986) observed several forsterite and/or enstatite supersaturated solutions (in experiments at 300°C and 200°C) which they attributed to analytical uncertainty in the determination of low levels of the concentration of Mg^{++}.

Open system alteration

A second hypothesis can be proposed, which assumes very high water/rock ratios in an open system. Such a situation would result in the seawater never reaching saturation with Mg-bearing minerals. As the solution moves through the rock, the composition of the solution may reach a steady state between the compositions of seawater and that of a solution saturated in the minerals present in the peridotite. The resulting reaction solution at low temperatures might have the approximate composition of point b in Figure 15. The lower the temperature and the higher the water/rock ratio, the farther out of equilibrium with serpentine and the mantle minerals the solution will be, and thus the more reactive.

If the reacting fluid is seawater, there is a clear limit to the temperature at which such an open system alteration process could take place. Bischoff and Seyfried (1978) and Janecky and Seyfried (1983) show that at temperatures higher than 250°C, seawater by itself precipitates the Mg-bearing phase Mg-Hydroxide-Sulfate-Hydrate (MHSH), so that at higher temperatures, the dissolution of olivine, enstatite or serpentine would at most result in the precipitation of this phase. Substantial depletion of Mg from the peridotite could only occur at much lower temperatures. It is likely that excess Mg^{++} produced at high temperatures would be precipitated as MHSH or brucite, and be dissolved again at lower temperatures during weathering.

The role of cooled hydrothermal solutions

In addition to seawater, cooling hydrothermal fluid is another Mg-undersaturated fluid which could conceivably be introduced into a peridotite body. If the fluid has reacted extensively with basalt, it would have quite distinct chemical characteristics from those of seawater. Such a solution, containing essentially no Mg in solution (Bischoff and Seyfried, 1978) would become undersaturated in Mg-rich minerals at much higher temperatures than seawater. There are two major difficulties with proposing that cooled hydrothermal fluids were responsible for the extraction of Mg from abyssal peridotites. The first is one of the pervasivenes of the Mg extraction. Almost all of the samples studied here have experienced some degree of Mg depletion. While the sample size of this study is small, it is reasonable to conclude from the data that Mg depletion is a ubiquitous characteristic of peridotite alteration on the ocean floor. Hydrothermal activity on the ocean floor is a phenomenon which is strongly localized by the availability of heat sources such as magma chambers, new intrusions of diabase dikes or newly erupted basalt flows. It would be unwarranted to call for a nearby intrusion of basalt for every peridotite occurrence on the ocean floor.

The second major difficulty with a cooled hydrothermal solution hypothesis is that such solutions are thoroughly rock dominated, both in their major element chemistry and in their isotopic composition. The isotopic compositions of such fluids would be dominated by the oceanic crust which they had circulated through, and would be very nearly similar to those of the peridotite they are reacting with. This study has demonstrated convincingly that the solutions which reacted with these peridotites during the extraction of Mg had the Nd and Sr isotopic composition of seawater.

Geologic interpretation

The large scale extraction of MgO from peridotite during hydrous alteration is a somewhat surprising result. Hydrothermal waters are generally thought to be responsible for the serpentinization of peridotite in the oceans (Seyfried and Dibble, 1980; Janecky and Seyfried, 1986). These are generally extremely poor in Mg, and Mg-mineral solubilities in water decline strongly with rising temperature (Bischoff and Seyfried, 1978; von Damm, 1990). Additionally, as discussed above, the experiments of Janecky and Seyfried (1986) show

that Mg extraction does not occur at the conditions thought to be typical of serpentinization. There are two possible scenarios under which the mass redistributions documented in this chapter can occur. First, seawater at low temperatures circulating through peridotites is sufficiently undersaturated in Mg-rich minerals that the mass flux may occur. Second, hydrothermal waters may be introduced into a body of peridotite in sufficient quantity to deplete the peridotite if those solutions have cooled substantially from their peak hydrothermal temperature.

This chapter supports the hypothesis that the mass fluxes in abyssal peridotites occur by reaction of the peridotite with seawater at low temperature, high water/rock ratio and undersaturation of the solution. Serpentinization occurs at relatively high to moderate temperatures (e.g., Wenner and Taylor, 1971, 1973; Bonatti, et al., 1980) and low water/rock ratios, where the fluid is saturated or supersaturated with Mg-bearing phases (e.g., Janecky and Seyfried, 1986). Serpentinization and mass redistribution appear to be separate events in the formation of abyssal peridotites.

As the extraction of MgO and deposition of alkalis proceeds to extremes, the rock loses tremendous amounts of mass, as in sample IO11/76:56-58, which is sufficiently friable and porous as to fit the traditional definition of a saprolite. The peridotite hydration metamorphic series (Bowen and Tuttle, 1949 and many others) runs peridotite->amphibole peridotite->talc peridotite -> talc + serpentine peridotite ->serpentinite. The metasomatic process documented here, carried to an extreme, extends this series to MgO-depleted serpentinite -> sepiolite serpentinite -> massive sepiolite. Such rocks have in fact been found associated with abyssal peridotite (Bonatti, et al., 1983). This study suggests that massive sepiolite deposits on the ocean floor are the result of Mg extraction from abyssal peridotite. The high $^{87}Sr/^{86}Sr$ compositions (higher than seawater) documented in sepiolite deposits (Bonatti, et al., 1983) also support this hypothesis.

Os isotopes

The seawater concentration of Os is unknown. It is probably less than 1 pg./l (G. Ravizza, 1992, personal communication). This estimate is lower than that used by Martin, 1990 and 1991 to evaluate seawater interaction with peri-

dotite. The $^{187}Os/^{186}Os$ composition in seawater determined by analysis of manganese nodules and manganese crusts on peridotites is nearly 10 (Palmer, et al., 1988), as opposed to about 1 in mantle peridotite. Manganese nodules typically are composed of ~30% MnO and 10% FeO, as well as enrichments in a variety of heavy metals. They are also rich in Os, having as much as 4 ppb. Os (Palmer, et al., 1988). A relatively small amount of seawater-derived osmium introduced into a sample by direct exchange or by contamination with manganese crust, then, would have a major effect on the isotopic composition of the sample. Knowledge of the behavior of Os during the alteration of peridotite by seawater or seawater-derived fluids is therefore critical for interpreting Os isotopic data in abyssal peridotites.

Seawater mixing models

Seawater-peridotite mixing models may help assess whether the isotopic compositions of peridotites are affected by the addition of Os from seawater. Using Equation 16 and a seawater Os concentration of 2 pg./l (the worst possible case), the water to rock ratio required to cause a 1% change in the Os isotopic composition of a typical peridotite (4 ppb. Os) can be calculated: The value obtained is $2x10^3$. By comparison, the sample with the highest alteration index (and lowest bulk $^{143}Nd/^{144}Nd$) required a water rock ratio of $2x10^5$ to account for its Nd isotopic composition.

Martin (1991) makes the same calculation, with the same result, and concludes that seawater Os does not affect abyssal peridotites. That study makes an implicit estimation of the water/rock ratio seen by altered peridotite based on the vein mineral analyses of Kimball and Gerlach (1985). The isotopic results of the preceding sections show that the isotopic compositions of abyssal peridotites are much more affected by seawater alteration than was implied by Kimball and Gerlach (1985). With the improved knowledge of abyssal peridotite isotopic exchange with seawater provided by this study, the task of deciding whether bulk abyssal peridotite Os isotopes are also affected by seawater becomes much more difficult.

The mixing calculation implies that no abyssal peridotite can automatically be considered free of contamination from seawater Os. Several factors mitigate against this interpretation, however. First, there is no reason to think

that the efficiency of isotopic exchange is the same for Os as it is for Nd, as the geochemistry of the two elements is quite different. This statement is supported by the isotopic data; the Nd and Sr data require a water to rock ratio of over 10^5 for sample IO11/76:56-58. The Os isotopic composition of such a mixture would be approximately 2, as compared to the measured value of 1.09. This shows that seawater-peridotite exchange for Os is much less efficient than it is for Nd and Sr.

Second, there is no reason to think that Os and Nd occupy similar phases in the fresh peridotite, that those phases would react to the same degree with seawater during disequilibrium alteration processes, or that the stable alteration phases would take up Os and Nd at the same rates. In the case of Sr and Nd these assumptions are probably somewhat better. A claim that a seawater-like Sr isotopic composition implies a contaminated Nd isotopic composition is probably more valid than a claim that a seawater-like Nd isotopic composition implies a contaminated Os isotopic composition. A crucial piece of evidence which would show such a relationship between Nd and Os would be an abyssal peridotite with a significantly elevated $^{187}Os/^{186}Os$ and a seawater-like $^{143}Nd/^{144}Nd$. Such a rock has yet to be analyzed.

Figure 16 shows bulk $^{187}Os/^{186}Os$ plotted against $^{143}Nd/^{144}Nd$, as well as a mixing curve for the 0.1 pg./l case. To a first order, the samples cannot be said to have been contaminated by seawater Os, since none of the samples falls far outside of the mantle field. That field, if shown would occupy nearly the whole diagram. If there were samples which clearly occupied the seawater leg of the mixing curve, it would be easier to state that seawater alteration is likely to have affected some peridotites. Even in the most extreme case, sample IO 11/76:56-58, the most that can be said on this basis is that seawater alteration cannot be ruled out.

The debatable point is whether there is a second-order contamination of the peridotite Os by seawater-derived Os. Such a contamination would change the $^{187}Os/^{186}Os$ by as much as one or two percent. The bulk analyses themselves shown in Figure 16 show no evidence of such contamination. IO11/75:56-58 is the most "suspicious" sample, being the most altered sample. It also has the highest water/rock ratio calculated from Nd and Sr isotopes in the preceding sections. This sample is suspicious in that its Os isotopic composition is so high. On the other hand, the next highest Os isotopic composition, sample AII107:61-

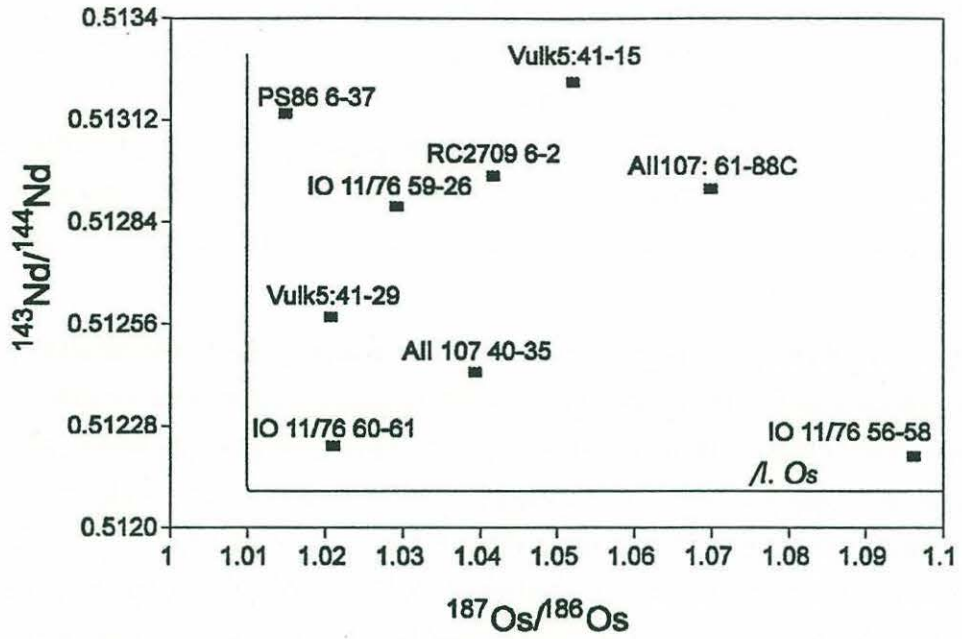

Figure 16: $^{143}Nd/^{144}Nd$ vs. $^{187}Os/^{186}Os$ in bulk abyssal peridotites.

83C is one of the freshest abyssal peridotites known, and has a mantle-like bulk Nd isotopic composition. Sample IO11/76:60-61 is almost as heavily weathered as IO11/75:56-58, and also has a high isotopic water/rock ratio, but has one of the *lowest* Os isotopic compositions measured in abyssal peridotites. If weathering and exchange with seawater dominated the isotopic composition, some correlation with the measures of that alteration developed earlier in this chapter would be expected. No such correlation exists, however. This implies that, to a first approximation, seawater exchange does not affect abyssal peridotite Os isotopic compositions, even at very high water/rock ratios.

Samples IO11/76:56-58 and 60-61 have alteration indices and water/rock ratios calculated from Nd and Sr isotopes which are broadly similar. If sample 56-58 had acquired enough Os from seawater to move it from the field of the other peridotites to its present high value, then it follows that samples 60-61 would have acquired a similar amount of seawater Os. The corrected $^{187}Os/^{186}Os$ composition of this sample would then be far lower than the lowest $^{187}Os/^{186}Os$ ever measured for abyssal peridotite, or for any unmetasomatized mantle rock.

It cannot be proven from the foregoing mixing calculations or from consideration of the Nd-Os systems together that seawater contamination plays no

role in determining the isotopic composition of abyssal peridotite. Since sample IO11/76:56-58 is only debatably affected by seawater alteration, the mixing calculations suggest that for most other, less altered peridotite samples, seawater contamination of Os isotopes is not a problem. The best way to resolve this issue is to find abyssal peridotites which have Os isotopic compositions that have clearly been affected by seawater alteration. One could then try to find compositional characteristics of rocks with seawater-derived Os and avoid those rocks. Alternatively, one could use seawater-affected peridotites to try to define leaching protocols which would remove the seawater component. At this point the one sample which seems most likely to have a seawater component (IO11/76:56-58) can not be convicted or absolved.

MnO crust contamination models

The two prime candidates for contamination with seawater Os are the samples IO11/76 60-61 and 56-58. Both of these samples are highly altered, and both show major and trace element signs that they may have incorporated a manganiferous hydrogenous component. The major element alteration indexes of the two samples are very high: 33 and 59; two of the highest alteration indexes in this study.

It is easy to make a case for the addition of a manganiferous component to sample IO11/76 60-61. The MnO content of this sample is almost double that of any other sample in this study. Such a MnO excess is to be expected when adding a component that is 30% MnO to a rock that contains, according to its reconstructed composition, 0.08 Wt.% MnO (Table 15). Assuming that all of the excess MnO in the sample comes directly from the incorporation of manganese crust, it is possible to estimate the amount of Co, Fe and Os that would be incorporated. Using the data of Palmer, et al. (1988), the weight fraction of manganese crust required to match the observed manganese excess is 0.43%.

The trace element data do not provide a definitive test at this level whether there or not there has been addition of Mn-sediment into this sample (IO11/76:60-61). Using the Co concentration of manganese crust from these same rocks measured by Palmer, et al. (1988) (2400 ppm.), the additional Co present in the sample is only 10 ppm. That amounts to only about 10 percent of

the total Co in the sample, so that test is inconclusive. A similar calculation for FeO is also inconclusive.

Using equation (16) with appropriate substitutions for Os, and the Os data of Palmer, et al. (1988), the calculated change in Os isotopic composition due to the proposed seawater-derived Os component is +4.3%. Once again, the Os isotopic data do not rule out this level of contamination. The $^{187}Os/^{186}Os$ of this sample is quite low (1.0210, Table 11). The resulting corrected $^{187}Os/^{186}Os$ would be by far the lowest $^{187}Os/^{186}Os$ yet measured in abyssal peridotites.

Sample IO 11/76:56-58 has elevated FeO and Co, and has the highest $^{187}Os/^{186}Os$ yet measured in abyssal peridotite ($^{187}Os/^{186}Os = 1.0963$). It is difficult to relate the FeO and Co enrichment of this rock to incorporation of Mn-rich material into the rock. If the FeO enrichment were due to Mn crust addition, 16% admixed MnO crust would be required. The resulting mixture would have a MnO content of 4.85%. This is clearly not the case (Table 10), as that sample is not enriched in MnO.

Using Co as a tracer of MnO crust addition as Martin (1990) does is complicated somewhat by the mass removal documented in previous sections. If Al and Cr are taken to define an isocon for the weathered rocks, and if Co is merely a resistant constituent of peridotite, then a 30-50% enrichment of Co in the rock is the result. This is greater than the degree of Co enrichment that these two samples show over the approximately 100 ppm. average of the unweathered samples. There is thus little basis for any claim that there is excess Co in either of these samples. This observation would tend to refute the hypothesis that there is significant MnO-rich crust incorporated into samples IO11/76:60-61 and 56-58.

Leaching of sample IO11/76:56-58

As described in the analytical section, a leaching experiment was performed on sample 56-58. The results from this leaching are presented in Table 13. The intent of the experiment was to leach the peridotite using a combination of acid and oxidants known to liberate hydrogenous Os in other rocks. By analyzing the hydrogenous Os as it is oxidized from the sample, this test should be a very sensitive indicator of the presence of seawater-derived Os in the sample.

In the leaching experiment, approximately 0.6 ng. of labile Os were released, accounting for about 2% of the Os in the sample. The isotopic composition of the leached Os, however, was lower than that of the unleached sample. The hydrogenous component of the sample appears to have a lower $^{187}Os/^{186}Os$ than does the unaltered peridotite. When the $^{187}Os/^{186}Os$ measured for this sample is corrected for the presence of this labile component, a 1 percent increase results. This result is difficult to reconcile with the seawater isotopic composition of Os, as it is precisely the opposite of what had been predicted from mixing. The leaching results confirm the results of Martin (1991). In that study, a similar experiment analyzed the residue of leaching only. In that study, the leached sample had a higher $^{187}Os/^{186}Os$ than the unleached sample, though the difference was within the analytical precision of the measurement technique.

It could be argued that the leaching removed a fraction of the primary (presumably lower $^{187}Os/^{186}Os$) Os from the sample, leaving refractory alteration products (with a seawater $^{187}Os/^{186}Os$ imprint). This hypothesis is consistent with the observed leaching patterns, but it is not consistent with the observed behaviors of silicate-hosted and hydrogenous Os from sediment leaching studies (Esser and Turekian, 1988; Ravizza, et al., 1991; Palmer et al., 1988). These studies used a similar leaching protocol to remove pure seawater-derived Os from their samples. It is unlikely then that this procedure would free more mantle Os than seawater Os from a sample. Given the considerable uncertainties surrounding the aqueous geochemistry of Os, such a scenario cannot be completely ruled out. With that caveat, the hypothesis that there is an addition of a seawater-derived, high $^{187}Os/^{186}Os$ component to sample IO 11/76:56-58 can tentatively be rejected.

Isotopic reservoirs in abyssal peridotite

Abyssal peridotite is widely thought to have originated in the sub-oceanic mantle (Aumento and Loubat, 1971, Miyashiro, et al., 1969; Dick, Fisher and Bryan, 1984, Michael and Bonatti, 1985; Dick, 1989; Johnson, et al., 1990). At that point the peridotite was almost certainly in trace element and isotopic equilibrium, at least on a hand sample or dredge haul scale. The presence of a melting event simplifies this assumption. Hofmann and Hart (1978) show that the presence of a partial melt significantly reduces the time necessary for equilibration of the mantle on any scale.

Since abyssal peridotites were last a part of the mantle, they have undergone a variety of processes that have resulted in the formation of isotopic disequilibrium within the sample. There are at least three distinct reservoirs of Nd, Sr, and Os isotopes commonly found in abyssal peridotites: The mantle, seawater and orphan ^{87}Sr.

The Mantle

The influence of a reservoir of essentially mantle composition is pervasive in the Sr, Nd and Os isotopic compositions of bulk peridotites. Figures 11 and 16 show mixing diagrams for Nd-Sr and Nd-Os which demonstrate this fact. Mixing curves originating at the isotopic composition of the mantle correspond to the observed Sr, Nd and Os compositions of the bulk samples at reasonable ratios of water/rock. In the case of Os, it is not clear that there is significant seawater component in any of the bulk samples. Separation of clinopyroxene and leaching allows us to determine the mantle Nd isotopic composition directly, and to come close to the mantle Sr isotopic composition. The mantle field in Figure 11 encircles the measured Nd and Sr isotopic compositions of three abyssal clinopyroxenes. Two others lie just outside the mantle field in the direction of seawater addition of Sr.

The physical repository of Os in abyssal peridotites is not known. In ore-bearing peridotites, Os and other platinum group elements reside in extremely small grains of PGE sulfide and pure PGE in minerals and grain boundaries (Stockman and Hlava, 1984). It is unclear whether this is also the case in rocks with much lower PGE contents such as abyssal peridotites, or whether at lower concentrations the Os resides as a solid solution in silicate minerals. The problem of the repository of Os in peridotites has a strong bearing on the interpretation of Os isotopic results from abyssal peridotites. The durability of that phase during alteration and weathering has a great bearing on the tendency of Os to be contaminated or exchanged with circulating fluids during alteration.

Seawater

Abyssal peridotite incorporates both Sr and Nd from seawater during its alteration. This is shown by the Nd-Sr correlation diagram in Figure 11. In this diagram, the bulk rock compositions define a mixing curve between seawater

and a variable mantle composition. The silicate reservoir of seawater Sr and Nd in altered abyssal peridotites is not well known. Of the variety of minerals which make up peridotite alteration products, most have sufficiently open structures that small quantities of incompatible elements can easily be accommodated.

The non-silicate reservoir of Sr and Nd in abyssal peridotite is certainly aragonite, which has up to 1% Sr with a seawater isotopic composition. The one aragonite measured for this study (PS86:6-37 AR; Table 14) had a Nd isotopic composition equal to that of Indian Ocean Seawater (0.51223) and a Nd concentration of .128 ppm. Aragonite thus has a lower Sr/Nd ratio (approximately 10^5) than the seawater Sr/Nd ratio (approximately $2x10^6$). This difference does not significantly affect the overall seawater/peridotite mixing relationship for Nd, however.

It is difficult to speculate on the possible repository of seawater-derived Os in abyssal peridotites, as none has ever been identified. The most likely candidate remains manganiferous sediments, as proposed by Martin (1990,1991). Two samples from this study which had major and trace element compositions suggestive of seawater contamination could not be shown to have a significant seawater $^{187}Os/^{186}Os$ contribution. A leaching study carried out on one of them showed a component of labile osmium lower in $^{187}Os/^{186}Os$ than the bulk sample. This suggests that seawater does not significantly affect the $^{187}Os/^{186}Os$ even of highly altered peridotites.

Analysis of the seawater component of abyssal peridotite can probably be accomplished by leaching out the aragonite. Leaching of aragonite may provide a method of exposure dating the peridotite. Due to the spectacular Sr content of aragonite, even very tiny amounts of aragonite should contain sufficient Sr for high-precision isotopic analysis. The oxygen and carbon isotopic compositions of aragonites studied from abyssal peridotites (Bonatti, et al., 1980) predicted very low temperatures of formation, between 0 and 30 degrees Centigrade. If this is the case, the seawater involved is quite unlikely to entrain mantle-derived strontium from either peridotites or basalts. The result is that the isotopic composition of Sr will very precisely reflect that of the seawater from which the aragonite formed. This presents the intriguing possibility that the age of formation of the aragonite may be determined by the application of high-resolution Sr isotope stratigraphy techniques. The one aragonite Sr isotopic composition

measured for this study is too similar to modern seawater in its isotopic composition to be the age of the crust that sample came from (maximum 24 Ma). That crustal age, however, is subject to significant uncertainty since the tectonics of the 12°-14°E area that the sample came from are extremely complex and have not been studied in great detail (le Roex, et al., 1992).

Orphan ^{87}Sr in abyssal peridotites

This section studies a phenomenon which has been an unsolved puzzle in isotope geochemistry for a long time. The only known reservoirs for Sr in oceanic peridotites and alpine peridotites were (and still are) assumed to be the mantle reservoir (clinopyroxene) and seawater. The isotopic composition of peridotites must lie somewhere in between. As soon as measurements were made, it became clear that some peridotites had isotopic compositions which could not be modeled as a mixture of a primary mantle composition with a seawater component because they were not between the two. These are abyssal and alpine peridotites whose $^{87}Sr/^{86}Sr$ values are *higher* than those of seawater. Once leached clinopyroxene separates were analyzed, it became clear that these high $^{87}Sr/^{86}Sr$ values were due in some way to alteration. Attention then focused on the mantle composition of clinopyroxenes (though not from abyssal peridotites) and not on the improbability of the high $^{87}Sr/^{86}Sr$ values in the first place. The high $^{87}Sr/^{86}Sr$ ratios in some abyssal peridotites are not supported by a sufficient amount of their radioactive parent Rb to be the product of *in-situ* radioactive decay, given the current concentrations of Rb and Sr and the time available for decay. For that reason, the excess radiogenic Sr will be referred to here as "orphan" ^{87}Sr.

Historical overview

The subject of the effect of alteration on the Sr isotopic system in peridotite was first taken up inadvertently by several investigators in the attempt to study the Sr isotopic composition of mantle rocks (Hurley, et al., 1964; Roe, 1965; Steuber and Murthy, 1966; Bonatti, et al., 1970). These authors noted a wide range of $^{87}Sr/^{86}Sr$ from serpentinized peridotites. Though these isotopic compositions were interpreted to be the result of mixing of seawater Sr with mantle-

derived Sr, some of the analyses had $^{87}Sr/^{86}Sr$ which was outside the range expected for the mixing of these two endmembers.

Hurley, et al. (1964) and Roe (1965) carried out the first analyses of Sr isotopes in peridotite at M.I.T. These authors analyzed Rb and Sr concentrations and Sr isotopic compositions of whole rock peridotites from a variety of tectonic settings. None of the rocks were derived from the mid-ocean ridge. These two studies immediately turned up the problem of excess ^{87}Sr in altered alpine peridotite. Though some rocks showed $^{87}Sr/^{86}Sr$ ratios low enough to be derived from a conceivable mantle source, many had isotopic compositions considerably in excess of any thinkable mantle source and also far in excess of the value (.7092) now generally accepted for recent seawater.

Hurley, et al. (1964) and Roe (1965) also noted the unsupported nature of the excess ^{87}Sr they measured. With the Rb/Sr ratios now present in the rocks, many of the samples could not possibly have evolved in a single stage from the bulk Earth, whose evolution was reasonably well constrained at that time. Steuber and Murthy (1966) concluded on the basis of a far larger, but essentially similar data set, that alpine peridotites constituted a separate class of peridotite. They concluded that alpine and abyssal peridotites are not related to basalts, either by partial melting or by crystal accumulation. This was in contrast to ultramafic nodules, which had $^{87}Sr/^{86}Sr$ ratios compatible with some genetic link between them and basalts in general.

Steuber and Murthy concurred with Roe (1965) that both alpine and abyssal peridotites show evidence of being residues of partial melting. To acquire such a high $^{87}Sr/^{86}Sr$, they must have, at one time in their history been part of a high Rb/Sr system. Partial melting was the best way to explain the low present day Rb/Sr ratios in these rocks. Nonetheless, they found that

"*If the higher $^{87}Sr/^{86}Sr$ ratios of the alpine-type intrusions were the result of an increase in the Rb/Sr ratio after the removal of basalt, the $^{87}Sr/^{86}Sr$ growth lines must intersect the basalt development region within 4.5 billion years. ... This is not the case and therefore we conclude that the alpine-type material cannot be the parental residue of basalts.*"

This conclusion was extended to abyssal peridotites by Bonatti, et al. (1970). They concluded that, based on petrographic, trace element and isotopic evidence, abyssal peridotites strongly resembled alpine-type peridotites and

thus could not be considered parental to mid-ocean ridge basalts. At that time, the lowest $^{87}Sr/^{86}Sr$ measured on an alpine or abyssal peridotite was 0.7046 (Hurley, et al., 1964), which was approximately the average (at that time) of measurements for basalts. The highest alpine peridotite $^{87}Sr/^{86}Sr$ measurement was .7864 (Steuber and Murthy, 1966) and the highest abyssal peridotite .7227 (Bonatti, et al., 1970). Bonatti, et al. (1970) went on to suggest that ancient continental crust underlying the mid-ocean ridges accounted for the high $^{87}Sr/^{86}Sr$ ratios.

The first indication that the high $^{87}Sr/^{86}Sr$ problem in abyssal and alpine peridotites might be an alteration effect came when an abyssal peridotite clinopyroxene turned out to have a significantly lower $^{87}Sr/^{86}Sr$ than its host peridotite. Metamorphic minerals plagioclase and hydrogrossular had isotopic compositions which showed significant seawater interaction, but clinopyroxene from that rock had a much lower $^{87}Sr/^{86}Sr$ of .7067 (Hart, 1972). Later re-analysis of that clinopyroxene brought this number somewhat closer to the mantle field at about .7052 (S. Hart, personal communication).

Finally, Menzies and Murthy (1976) showed conclusively that mantle-like Sr isotopic compositions were to be found by analyzing clinopyroxenes separated from alpine peridotites. This forced a re-evaluation of the earlier idea that there could be no genetic link between alpine peridotites and basalts. The same was never done for abyssal peridotites. Since that time a variety of other lines of evidence (Dick, Fisher and Bryan, 1984; Michael and Bonatti, 1985; Shibata and Thompson, 1986; Johnson, et al., 1990; Johnson and Dick, 1992) have amply demonstrated the genetic link between abyssal peridotite and mid-ocean ridge basalt. One contribution of this chapter has been to show that leached clinopyroxenes from abyssal peridotites have depleted mantle Sr and Nd isotopic compositions. The origin of the high $^{87}Sr/^{86}Sr$ reservoir sampled in abyssal peridotites remains unaddressed, and still awaits definitive resolution.

Results from this study

Four out of five samples in which the first magnetic fractions were analyzed for $^{87}Sr/^{86}Sr$ show evidence of $^{87}Sr/^{86}Sr$ higher than seawater. Three of those samples (Table 9) have measured $^{87}Sr/^{86}Sr$ which is higher than seawater. The fourth, sample PS86:6-37, probably also has a high ^{87}Sr component. This can

be demonstrated in the following way: The whole rock has a $^{87}Sr/^{86}Sr$ composition dominated by aragonite. The first magnetic fraction and bulk analyses of that sample are two different mixtures of aragonite and silicate. With the relative Sr concentration of these two samples, this implies that the first magnetic fraction has less aragonite than the whole rock, a reasonable assumption given the magnetic properties and density of aragonite. The $^{87}Sr/^{86}Sr$ can be extrapolated back to a Sr concentration of typical abyssal peridotite. The extrapolation calculation results in a $^{87}Sr/^{86}Sr$ of between .715 and .720, which certainly qualify as orphan Sr values. A simple test of this hypothesis would be to leach the PS86:6-37 1MF fraction in weak HCl to remove aragonite and analyze it.

Since the high $^{87}Sr/^{86}Sr$ of bulk peridotites turned out not to be a characteristic of the mantle (Menzies and Murthy, 1976), it has received little attention. Nonetheless, there remains a significant question as to how $^{87}Sr/^{86}Sr$ higher than seawater can form in an abyssal peridotite. There are basically two possibilities. First, the orphan ^{87}Sr may have originated outside the sample, derived either directly from ancient continental lithosphere underlying the mid-ocean ridge, or indirectly from detrital sediments. In either case, the high $^{87}Sr/^{86}Sr$ must be transported from its original high Rb/Sr reservoir to abyssal peridotites without being deposited in any other form. Orphan ^{87}Sr is unknown from any rocks from the oceans except those derived directly from abyssal peridotite (a sepiolite deposit documented by Bonatti, et al., 1983).

Mechanisms for the production of orphan ^{87}Sr

There are not many possibilities for the production of the high $^{87}Sr/^{86}Sr$ compositions in abyssal peridotites documented in this study and in the earlier studies. It must have either grown *in-situ* and had its radioactive parent rubidium removed or it must have grown in a high Rb/Sr environment and been transported to the peridotite, presumably during the course of the alteration of the peridotite.

Growth in-situ

The first hypothesis for the formation of the orphan ^{87}Sr reservoir is that it grew in place after the alteration of the abyssal peridotite introduced Rb into the peridotite. A subsequent second metamorphic event after a suitable period of time has elapsed is then required in every case to remove the Rb. There may ac-

tually be some evidence for this hypothesis. In Table 12, it is clear that, with the exception of sample RC2709:6-2 (the sample with the highest $^{87}Sr/^{86}Sr$ and youngest crustal age), the crustal age of the orphan ^{87}Sr-bearing samples correlates with the apparent age of the sample. While these are many possible causes for such a correlation, it is the one observation which seems to favor one hypothesis or the other.

For the high $^{87}Sr/^{86}Sr$ ratios to have grown *in-situ*, the following conditions must have occurred. First, the peridotite must have had sufficient Rb added during alteration to raise the Rb/Sr ratio to a very high value. Second, there must have been a significant period of closed-system isotopic growth for the high $^{87}Sr/^{86}Sr$ to form. Third, a second metasomatic event must have removed the Rb responsible for the high $^{87}Sr/^{86}Sr$. Thus far, no abyssal peridotite with $^{87}Sr/^{86}Sr$ higher than seawater has ever been found to have a sufficiently high Rb/Sr or a sufficiently old crustal age for the calculated model age and the crustal age to be even close to agreement. This requires a fourth condition, that Rb is removed from the peridotite subsequent to its addition and radioactive decay *in every case.*

Such a scenario seems unlikely. Metasomatism at high temperatures in the crust typically removes Rb from basalts (K. Gillis, personal communication), and would be likely to do so also from peridotites. Low temperature alteration adds alkalis to abyssal peridotite (as documented, for example in this study). For the orphan ^{87}Sr to be due to *in situ* growth, a low temperature metamorphic event adding Rb would have to be followed by a high temperature event removing it. There are some abyssal peridotites which might be interpreted as having such a history (see the first sub-section of the Discussion). The vast majority of abyssal peridotites, however, are believed to have undergone only monotonic decreases in pressure and temperature during their alteration history. The *in-situ* growth hypothesis would require that *all* peridotites with orphan Sr had a prograde history.

Exogenous orphan ^{87}Sr

A major possible source of orphan Sr in the oceans is the detrital fraction of oceanic sediments. These can have an unsupported $^{87}Sr/^{86}Sr$ as high as any measured in abyssal peridotites or higher. The alteration products of the breakdown of olivine have a very low concentration of Sr (less than 1 ppm.).

The detrital sediment fraction typically has a high Sr concentration (700 ppm. and higher; Boger and Faure, 1980). Extremely small amounts of a fine grained fraction of detrital sediment which is infiltrated into the peridotite would be sufficient to completely change its $^{87}Sr/^{86}Sr$. At first glance, it seems somewhat improbable that significant amounts of detrital sediment could be transported into peridotite in the absence of large amounts of nearby sediment. However, such a hypothesis is less improbable than that of *in-situ* growth.

Several results of this study lend credence to the hypothesis that the orphan ^{87}Sr is due to a detrital component. First, if the alteration of peridotite were a low water/rock, high temperature process exclusively, as previously supposed, the infiltration of significant amounts of detrital sediment to such a depth would be quite unlikely. The results of this study show, however, that a significant amount of the alteration of abyssal peridotite occurs at high water/rock ratios and low temperatures. The penetration of an extremely fine grained detrital component into the peridotite is much more likely under these circumstances. If the low-temperature Mg removal process results in increased porosity in the rock, it is quite likely that such deposition of a detrital component could occur, even deep in a massive outcrop.

Excess ^{87}Sr might or might not be correlated with the degree of alteration in the samples. This would depend on the amount of detrital component in the seawater, and on the extent to which the seawater has already been filtered by passage through other rocks. Certainly, in the small data set studied here, there is no particular correlation between degree of alteration and excess ^{87}Sr.

The hypothesis of detrital ^{87}Sr in peridotite could be tested if the circulation pattern in a particular boulder or outcrop could be inferred. A drill hole would be ideal for such a test. The detrital component would be more concentrated near the point of entry of water into the rock. Excess ^{87}Sr would be found in those rocks which had seen the most water. If a series of rocks from a single area were measured, they would be expected to show a correlation of the detrital component with the water/rock ratio. The current sample set is not appropriate for such a test, since the samples are so far apart. Both the concentration of detrital component in the seawater and the $^{87}Sr/^{86}Sr$ of that component probably varies from locality to locality, so the current sample set might not show any such correlation.

Comparison of primary peridotite isotopic compositions with abyssal basalts

Mid-ocean ridge basalts are derived from the underlying mantle by a process of decompression-induced partial melting as the mantle rises beneath the ridge axis. The current study invites the comparison between the isotopic compositions of basalts and spatially related peridotites. The nearby peridotites may have some relationship to the residual mantle that the basalts were derived from. Figure 11 shows that the comparison of Nd and Sr isotopic compositions between basalts in general (shaded area) and the leached clinopyroxene separates from this study is not inappropriate.

Considered in detail, there are many factors which complicate the comparison of spatially related basalts and peridotites. First, there is the problem of spatial relationships. The majority of peridotites are sampled at fracture zones, while the majority of basalts are sampled at spreading centers. Lateral variations in mantle composition are likely be responsible for some of the differences between measured basalt and peridotite.

While there are areas where basalt and peridotite can be sampled together (Dick, 1989), even these are probably not genetically related due to the second problem, that of secular variation. Typically, basalts sampled at mid-ocean ridges are geologically quite young. The mantle which produced recently erupted basalts is still at depth, having risen at most a few kilometers since the segregation event which produced the sampled basalts. Young basalts thus cannot be directly related to peridotites sampled nearby, since the source of those basalts remains for the most part deep in the mantle.

Last is the fact that basalts integrate melts from a variety of depths (e.g. O'Hara, 1968; Jaques and Green, 1980, McKenzie 1987; McKenzie and Bickle, 1989; Kinzler and Grove, 1992a, b). The depths of melting inferred for mid-ocean ridge basalt range as deep as 150 km. (Johnson, et al., 1990; Salters and Hart, 1990). When melts from varying depths are pooled at crustal levels, isotopic information is averaged from many regions of the mantle and lost. To the extent that mid-ocean ridge basalts are the result of pooling of melts from a variety of pressures (i.e. depths) in the mantle, it is probably impossible ever to claim that a given peridotite is the parent of a given basalt and should exhibit

similar isotopic characteristics. It is probably also impossible to claim that even an unmixed primary magma has a single peridotite parent. The only isotopic similarities which one could reasonably expect to hold between basalts and peridotites are those which persist over wide regions and great periods of time.

The caveats given above should make it clear that the following discussion does not intend to draw conclusions about the genetic link between abyssal peridotite and spatially associated basalts *per se*; other studies have already shown this connection in a far more robust fashion than is ever likely using isotopes (Dick, et al., 1984; Michael and Bonatti, 1985; Shibata and Thompson, 1986; Johnson et al., 1990; Komor, et al., 1990; Johnson and Dick, 1992). Rather, what is intended is a more general comparison of peridotite isotopic compositions with those of basalts from the same region. Because the shift of Sr and Nd isotopic compositions due to seawater interaction is so much different from that due to mantle processes, the comparison with nearby basalts will shed light on the degree of success of the leaching procedure.

12° E Area

Figure 17 shows basalts from the 12-14°E region (le Roex, et al., 1992) plotted with the one peridotite clinopyroxene analyzed from that region. The samples enclosed by the light stipple are from the entire 12-14°E region, while the ones enclosed by the dark stipple are from the same dredge haul (Dredge 6) as the peridotite sample. It is important to note that although the basalts from Dredge 6 are quite normal (for the Southwest Indian Ridge) in their isotopic compositions, their major and trace element compositions are quite unusual, being anomalously enriched in potassium, barium and other incompatible elements (le Roex, et al., 1992).

The Nd and Sr isotopic composition of sample PS86:6-37 lies within the array of basalt compositions for the western SW Indian ridge shown in le Roex, et al., 1992. The basalts from that study plot on the low-$^{143}Nd/^{144}Nd$ side of the SW Indian ridge mantle field, and they do not bracket the peridotite composition. There are two possible interpretations for these observations. First, the Dredge 6 peridotite may have an underlying Nd and Sr isotopic composition within the field for Dredge 5 and 6 basalt compositions (shown as data points labeled 5b and 6b in Figure 17). The clinopyroxene isotopic composition has

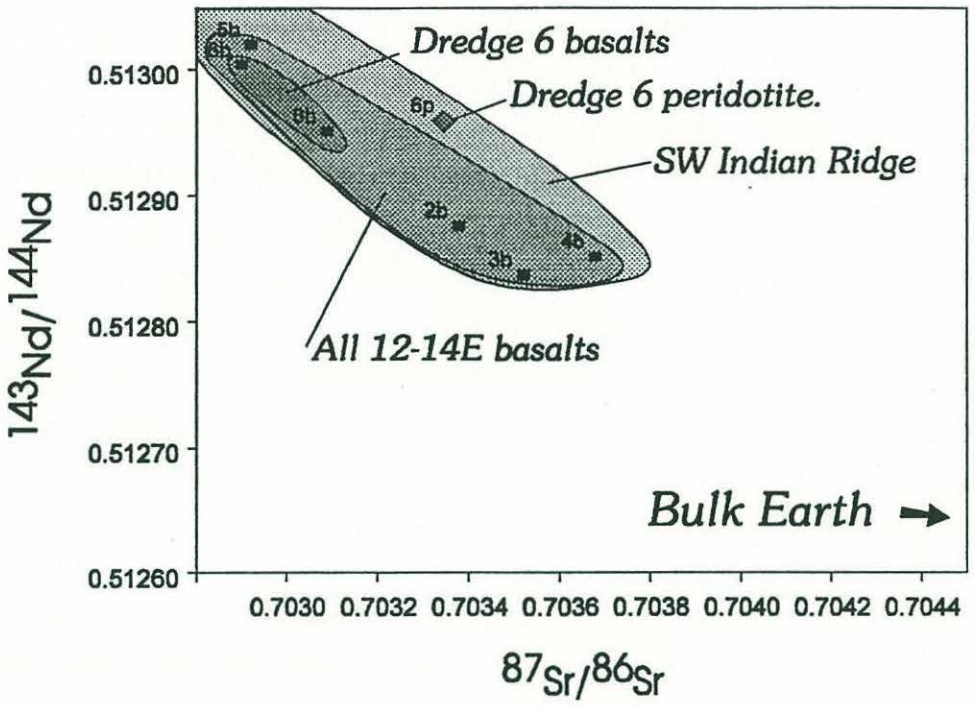

Figure 17: Peridotite and basalt compositions from the 12-14°E area. Peridotites are shown as diamonds and basalts are rectangles. Basalts from the same region as the peridotite (from le Roex, et al., 1992) are enclosed with a light shaded region, data points indicate dredge numbers; basalts from the same dredge haul with a dark region.

subsequently been changed by the addition of seawater Sr. This interpretation is plausible since the Nd isotopic composition, which would not be changed by a small seawater component, is within the range of Nd isotopic compositions for basalt dredges PS86:5 and 6.

The second possible hypothesis for the isotopic composition of the PS86:6-37 peridotite clinopyroxene relative to the nearby basalts in this area is that the underlying mantle in this region actually includes compositions like the PS86:6-37 clinopyroxene. Due to a very small sample size (7 basalts and one peridotite), compositions more similar to the peridotite clinopyroxene composition have simply not been found. The basalts that have been recovered from that ridge segment lie on the low-$^{143}Nd/^{144}Nd$ side of the SW Indian ridge mantle field, so it is possible that the difference between the peridotite clinopyroxene and the basalt field is merely a matter of small sample size.

In the following sections, the pattern of peridotite clinopyroxenes lying slightly to the high-$^{87}Sr/^{86}Sr$ side of the field of nearby basalts is repeated. The first hypothesis, that the clinopyroxene is different from the nearby basalts primarily due to seawater Sr addition is somewhat less pleasing to the analyst. It implies that leaching does not remove all seawater Sr. Nonetheless, it is difficult to call upon sampling statistics to explain clinopyroxenes which are consistently higher in $^{87}Sr/^{86}Sr$ for a given $^{143}Nd/^{144}Nd$ than nearby basalts. The seawater contamination hypothesis is therefore more likely. Even still there is a close relationship between the Nd and Sr isotopic compositions of basalts and nearby peridotites which is probably due to their being derived from the mid-ocean ridge basalt mantle. The differences can be explained by sampling statistics and recent seawater alteration.

Atlantis II Fracture Zone

Two clinopyroxenes were analyzed from the Atlantis II Fracture Zone region (Figure 18). For these two samples, the $^{87}Sr/^{86}Sr$ of the clinopyroxenes are higher at a given $^{143}Nd/^{144}Nd$ than those of the basalts. This suggests that addition of Sr from seawater has overprinted the Sr isotopic compositions of the clinopyroxenes. In terms of neodymium, one of the samples (RC2709:6-2) has a lower $^{143}Nd/^{144}Nd$ than the basalts from the transform, and one has a higher $^{143}Nd/^{144}Nd$ (RC2709:25-139). There is no reason to believe that the $^{143}Nd/^{144}Nd$ ratios are affected by the addition of seawater Nd to the samples.

The sample with the $^{143}Nd/^{144}Nd$ lower than the basalts (RC2709:6-2) is one which has a large vein of clinopyroxenite running through it. The clinopyroxene used for the mineral separate was not taken from this vein. It is possible that the vein and country rock clinopyroxenes have nonetheless exchanged Nd and Sr. The low $^{143}Nd/^{144}Nd$ in this peridotite relative to the nearby basalts would then be due to the incorporation of an isotopically enriched component from the vein in this sample.

Looking at the rare earth element pattern of this sample (Table 6 and Figure 2), it is probably justified to suspect some enrichment. The clinopyroxene is less light-rare-earth depleted than clinopyroxenes from other peridotites. The overall concentration of rare earth elements is also quite high for an abyssal peridotite clinopyroxene. Such an enriched component would be unusual in this

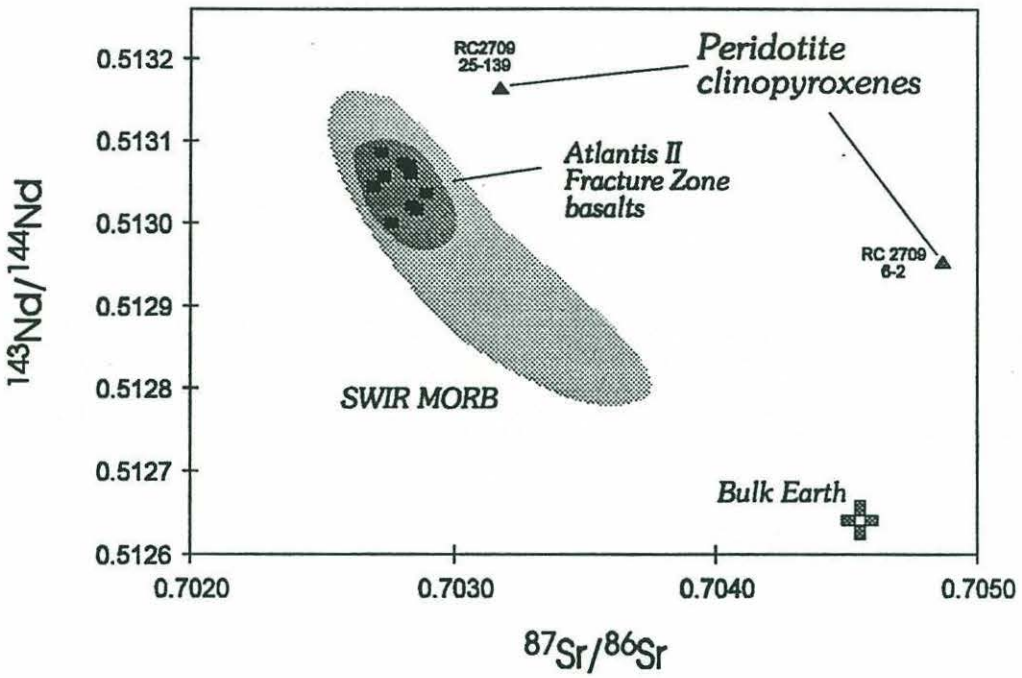

Figure 18: Peridotite clinopyroxene and basalt isotopic compositions from the Atlantis II Fracture Zone. Light shading shows the field for Southwest Indian Ridge basalts. The dark field encloses the basalt data from Chapter Two of this dissertation. Symbols as in Figure 17.

area. As discussed at length in Chapter Two, the northern ridge segment of the Atlantis II Fracture Zone otherwise exhibits little or no evidence for the presence of enriched components in the petrogenesis of the basalts.

Alternatively, the clinopyroxene may have been affected by addition of both Nd and Sr derived from seawater. This implies that the clinopyroxene has acquired a Sr and Nd isotopic composition similar to that of the whole rock ($^{143}Nd/^{144}Nd$ slightly lower, $^{87}Sr/^{86}Sr$ somewhat higher; .7062). There are some aspects to this hypothesis which are difficult to explain. First of all, if seawater is responsible for shifting the $^{143}Nd/^{144}Nd$ of the clinopyroxene by as much as .0001, the Sr isotopic composition of the sample would be identical to seawater. Neither the clinopyroxene nor the whole rock (presumably more affected by alteration) have such Sr isotopic compositions. This hypothesis would also require that Nd reside in a different alteration phase than Sr. The Sr could be leached away while the Nd remains, residing in a presumably more resistant alteration phase.

In any event, the difference between the Nd isotopic composition of the clinopyroxene in sample RC2709:6-2 and the basalts analyzed in Chapter Two is not large compared to the analytical precision of the clinopyroxene measurement and the sample standard deviation of the Atlantis II basalt population. It is entirely possible that the $^{143}Nd/^{144}Nd$ of sample RC2709 simply represents a mantle composition for this area.

The other peridotite sample from the Atlantis II Fracture Zone is sample RC2709:25-139. While the Sr isotopic composition is quite low, the Nd isotopic composition of this sample is quite high. The Nd and Sr isotopic compositions of the sample together are still to the high-$^{87}Sr/^{86}Sr$ side of the mantle field. This suggests that seawater addition has changed the Sr isotopic composition of the clinopyroxene. The Nd isotopic composition is quite interesting, being higher than that for the basalts from the same fracture zone. The fact that mid-ocean ridge basalts and peridotites have $^{143}Nd/^{144}Nd$ higher than the bulk Earth demonstrates that they must have been depleted in light rare earth elements sometime in the past. That depletion was probably caused by a partial melting process similar to the one occurring beneath the ridge axis today. One would expect a greater variety of Sm/Nd ratios in the residue than in the melt, due to the averaging effects of segregation and aggregation of melt. Over time, this would lead to a greater variability of $^{143}Nd/^{144}Nd$ in residual rocks than in basalts derived from them. Sampling statistics aside, the Nd isotopic compositions of samples RC2709:25-139 and 6-2 may be a reflection of this variability. The presence or absence of isotopic variability in abyssal peridotite due to ancient melting events will take on added importance in a later section (the section on the significance of abyssal peridotite Nd and Sr isotopic data).

59°S Fracture Zone, American-Antarctic Ridge

The clinopyroxene analyzed from the 59°S Fracture Zone has Sr and Nd isotopic compositions that once again lie to the high $^{87}Sr/^{86}Sr$ side of the trend defined by the three basalt analyses from nearby dredge hauls (le Roex, et al., 1985) shown in Figure 19. This suggests that the $^{87}Sr/^{86}Sr$ of the clinopyroxene may have been affected by the addition of seawater Sr. The Nd isotopic composition is additionally outside the group formed by the three basalt analyses, but on the high side. This is not consistent with seawater addition, but

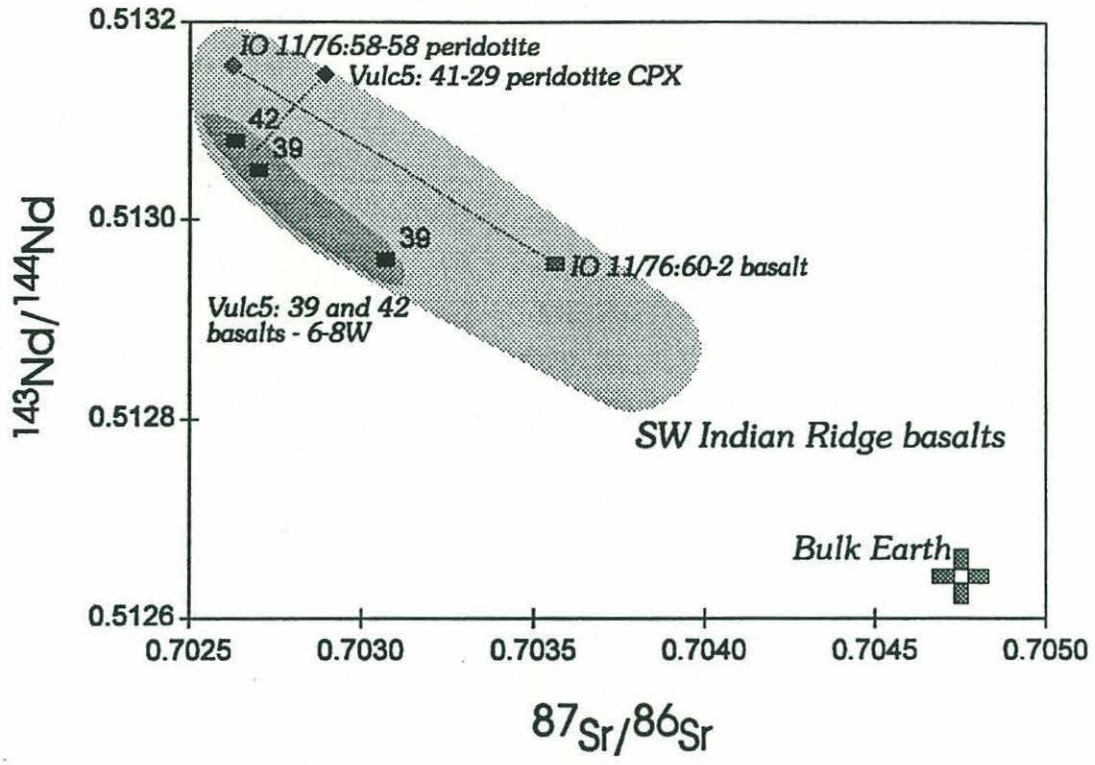

Figure 19: Peridotite and basalt compositions from the American-Antarctic Ridge and the Islas Orcadas Fracture Zone. Symbols as in Figure 17. Broken lines connect basalt and peridotite analyses.

suggests instead that the underlying Nd isotopic composition of the mantle measured by this clinopyroxene is higher than that of the surrounding basalts.

Islas Orcadas Fracture Zone

In this region there is the least basis for the comparison of basalt and peridotite isotopic compositions. Le Roex, et al. (1985) list only one analysis of basalt from this fracture zone. It would stretch the credulity somewhat to try to draw conclusions from these two isotopic analyses of rocks separated by many kilometers (they are shown in Figure 19 for comparison only). The lack of nearby basalt samples is an unfortunate circumstance; this sample had the lowest $^{87}Sr/^{86}Sr$ of the samples on which both Sr and Nd isotopic analyses were successful. The low $^{87}Sr/^{86}Sr$ is surprising considering the advanced state of alteration of this particular sample. One would have expected that this clinopyroxene would be the one most affected by seawater Sr, yet it appears to be the least.

The significance of abyssal peridotite Nd and Sr isotopic data

Mixing calculations, study of alteration and the comparison of isotopic compositions of clinopyroxenes with nearby basalts suggest that most of the clinopyroxene $^{87}Sr/^{86}Sr$ are affected by seawater alteration even after leaching. The opposite is true for Nd isotopic compositions. Mixing calculations and comparisons with nearby basalts suggest that the Nd isotopic compositions measured in the abyssal peridotite clinopyroxenes are representative of the composition of the mid-ocean ridge mantle. The following section will seek to discuss the significance of those Nd isotopic compositions. The process of melt segregation by which the residual peridotite is formed has major implications for the interpretations of the Nd isotopic compositions.

The problem can readily be illustrated with the first example. In the segregation model of Whitehead, Dick and Schouten (1984), melt and mantle rise together to discrete segregation points along the ridge, in a process which is analogous to Raleigh-Taylor instability. Segregation occurs at the highest point in the instability. The segregated melt pools and rises further, independently of the mantle which generated it. Since the segregating basalt has such a high concentration of Nd and Sr relative to the peridotite, the Nd isotopic composition of the peridotite at the point of segregation is purely a function of the composition of the last basalt segregated (Dick, 1989). This would render the measurement of abyssal peridotite clinopyroxenes merely a very difficult means of measuring a basalt isotopic composition.

Johnson, et al. (1990) provide evidence that the point of segregation is somewhat deeper in the mantle. They measured rare earth element concentrations in many clinopyroxenes which could not have been in equilibrium with any observed primitive basalt composition. This implies that the segregation process is a fractional, aggregational process. Basalts segregate at relatively deep levels in the mantle and are mixed with melts segregating at higher levels prior to eruption. The reported compositions had not been reset at the point of segregation to an aggregated basalt composition. The evidence in Johnson, et al. (1990) thus suggests that Nd isotopic compositions measured on clinopyroxenes from abyssal peridotite could be inherited from the pre-melting mantle. They might then reflect the Sm/Nd ratios which prevailed since the previous melting event, at an average age of about 2 billion years.

Elthon (1992) re-interprets the Johnson, et al. (1990) data on the basis of a refertilization model. The mantle is first strongly depleted by melting at depth beneath the ridge. As a given batch of mantle rises to the point of segregation, it is refertilized by basaltic melts ascending via porous flow from below. This scenario seems at first to be equivalent to the scenario of Whitehead et al. (1984) and Dick (1989). The primary difference is that in the latter model, mantle and melt rise together to the point of segregation, which is where porous flow begins. In both models, peridotite isotopic composition is dominated by that of a basalt coming in from outside the region of the sample itself. The data of Johnson, et al. (1990) still require that the refertilizing melts be pre-aggregational. Isotopic compositions measured on the refertilized peridotite subsequently will still reflect the isotopic composition of a small portion of mantle as before. The major difference is that the portion of mantle being sampled in the Elthon model is much larger than in the Whitehead, et al. (1984), Dick (1989) model.

When discussing the significance of these melting models for the interpretation of the Nd isotopic data in peridotites, the main issue is the size of the region of mantle sampled by the analyzed clinopyroxene. In a mantle without significant porous flow transport, the sampling scale may be as small as a hand sample. The larger the scale of porous flow of basalt, the larger a region of mantle is sampled by the basalt liquid which last set the peridodite's trace element composition. In any case, the result of the porous flow models is that a peridotite samples a basalt composition before aggregation. Sampling the trace element composition (Johnson, et al., 1990; Johnson and Dick 1992) or isotopic composition of such a liquid remains of fundamental interest for the issues of melt generation and mantle heterogeneity.

Conclusion

This study reports the results of a number of different experiments and measurements on abyssal peridotites. These were carried out with several goals. First, major element analysis of the peridotite and its primary mineral constituents examined the mass changes which occur during alteration. Second, bulk analysis of Os, Nd and Sr isotope systematics assessed the effect of alteration on those isotopic systems. Third, separation and leaching of clinopyroxene separates assessed the feasibility and validity of examining the isotopic systematics of the mantle in abyssal peridotites. Last, analysis of olivine alteration products showed that the orphan ^{87}Sr reservoir resides in those phases, and suggested a sediment infiltration mechanism for its introduction into the peridotite.

A notable characteristic of abyssal peridotite compared to most other classes of peridotite is its high degree of hydrous alteration, or the progress of the reaction olivine + enstatite + water <-> serpentine ($\pm$brucite $\pm$talc) + magnetite. One frequently overlooked aspect of this alteration is the significant mass redistribution which occurs as a result, particularly of Mg and Si. In peridotite mylonite samples, the altered and unaltered peridotite is in close juxtaposition and can be directly compared. In these samples, Mg extraction during weathering is unambiguous. In other abyssal peridotites, primary compositions can be reconstructed using the modal composition of the rock and the compositions of the primary phases. Relative to their reconstructed primary compositions, bulk compositions of abyssal peridotites generally fall on an Mg extraction line.

Two effects of alteration have opposite implications for the bulk reconstruction. Preferential serpentinization of olivine increases the apparent olivine mode at the expense of other minerals. The resulting bulk reconstruction is then more Mg rich than the protolith actually was, resulting in an apparent Mg loss where there may have been none. Preferential dissolution of serpentine would tend to decreases the apparent olivine mode of the serpentinite, with the opposite effect.

Experimental (Janecky and Seyfried, 1986) and theoretical (Nesbitt and Bricker, 1978) and empirical (Wenner and Taylor, 1971;1973; Bonatti, et al., 1980) work on peridotite alteration suggests that serpentinization reaches a peak around 150-250 °C in the crust. This chapter suggests that on further cooling, the

circulation of water in the peridotite results in extraction of Mg from the rock at relatively low temperatures, high water/rock ratios and undersaturation of the solution with magnesium.

Several possible geologic settings could produce the low temperature extraction of Mg from peridotite. One possibility is that the reacting solution is cooled hydrothermal water from lower in the crust. Such a solution would be extremely undersaturated in Mg. The problem with this scenario is the pervasivenes of peridotite alteration in areas far from igneous heat sources, such as at fracture zones. The isotopic compositions of the altered peridotites also seem to indicate that the reacting solution was seawater. Another possibility is that the Mg extraction took place near the sea floor at extremely low temperatures (0-30 ° C). At these low temperatures, even seawater is undersaturated Mg-rich phases such as brucite. The areal extent of peridotite on the ocean floor is unknown. At slowly spreading ridges where the fracture zone spacing is very close, peridotite may make up a significant fraction of the surface outcrop. Mg extraction from peridotite may thus make up a significant source of Mg to the ocean.

The Rb-Sr isotopic system is extremely sensitive to seawater exchange. Basalts have much higher concentrations of Rb and Sr than do the residual peridotites studied here, but are still quite sensitive to seawater-derived $^{87}Sr/^{86}Sr$. In peridotites, the situation is greatly aggravated by the low concentration and high degree of alteration of the rocks. Only the freshest of abyssal peridotites have whole rock $^{87}Sr/^{86}Sr$ significantly lower than that of seawater. Aggressive leaching of clinopyroxene can, in many cases, reduce the measured $^{87}Sr/^{86}Sr$ of the residue to a value reasonable for the depleted mantle. There is no way of determining the extent of residual contamination for any individual $^{87}Sr/^{86}Sr$ analysis. Comparison of leached clinopyroxene $^{87}Sr/^{86}Sr$ with those of nearby basalts suggests that residual seawater-derived $^{87}Sr/^{86}Sr$ remains in the leached clinopyroxene in most cases, even after careful separation and leaching. The leached $^{87}Sr/^{86}Sr$ compositions may not be directly useful for studying the isotopic composition Sr in the abyssal mantle. No attempt is made to relate the leached clinopyroxene $^{87}Sr/^{86}Sr$ compositions directly to mantle systematics.

The Sm-Nd isotopic system is much more robust than the Rb-Sr system to seafloor alteration. Nd is more concentrated in clinopyroxene relative to Nd in seawater than is the case for Sr. Many of the whole rock $^{143}Nd/^{144}Nd$ compositions are mantle-like, though some samples show clear evidence of seawater in-

teraction. It is appropriate to use $^{87}Sr/^{86}Sr$ ratios to monitor the degree of seawater contamination in a given sample, since $^{87}Sr/^{86}Sr$ is more sensitive to alteration and Sr and Nd can be assumed to reside in much the same physical reservoir on a mineral scale. Samples with $^{87}Sr/^{86}Sr$ lower than .7060 can generally be assumed to have a seawater contribution to $^{143}Nd/^{144}Nd$ less than $2x10^{-5}$. This is the first time that such a $^{87}Sr/^{86}Sr$ composition has been reported for abyssal peridotite. Based on this criterion, leaching of clinopyroxene samples should nearly always be successful for Nd.

The Os isotopic system in peridotite whole rocks appears resistant to submarine weathering and hydrothermal alteration. The effect of seawater on the isotopic composition of Os in peridotite was studied based on the results of bulk analysis, comparison to the other isotope and trace element systematics relevant to weathering and alteration, and leaching studies. Disturbance of Os isotopic composition could not be documented or ruled out in the abyssal peridotites. It is likely that Os either resides in a phase (such as PGE sulfide) which is resistant to alteration, or in an alteration phase which similarly does not significantly exchange Os with seawater, even at high water/rock ratios. The high concentration of Os in abyssal peridotite relative to seawater may render the isotopic composition relatively insensitive to the addition of exogenous Os.

Three important reservoirs of Nd, Sr and Os were found on a sample scale in abyssal peridotites. The mantle reservoir is well defined for Nd and Sr, but less so for Os. Nd and Sr derived from the mantle partition heavily into the clinopyroxene in a four phase peridotite. Even after significant alteration of the coexisting olivine and orthopyroxene, the clinopyroxene still retains a pristine mantle $^{143}Nd/^{144}Nd$, which can be recovered by careful mineral separation and leaching. The same is not true of $^{87}Sr/^{86}Sr$, which in nearly all cases could not be shown to be a pristine mantle composition. The physical location of Os in abyssal peridotites is still unknown, though by analogy with peridotites from other settings (Stockman and Hlava, 1984), it is more likely to exist as disseminated sulfide than as a silicate solid solution.

The seawater reservoir of Nd and Sr seems to be located in low-temperature alteration veins which crosscut the sample. Other studies of Sr alteration in peridotite (Kimball and Gerlach, 1986) have shown that the mixture of seawater/mantle derived Sr in alteration veins increases as the temperature of alteration declines. This suggests that samples which have experienced only high

temperature alteration may retain nearly unaltered Sr and Nd isotopic compositions. Samples of peridotite blastomylonite analyzed in the course of this study bear out this prediction, having pristine $^{143}Nd/^{144}Nd$ and the lowest $^{87}Sr/^{86}Sr$ ever measured on a whole rock abyssal peridotite.

Many of the samples in this study contained a fraction with very high $^{87}Sr/^{86}Sr$ ratios. These $^{87}Sr/^{86}Sr$ cannot have been produced at the current Rb/Sr ratio of the alteration fraction. The "orphan ^{87}Sr" resides in the serpentine + magnetite mesh that forms a pseudomorphous replacement of olivine. Three hypotheses are advanced for the origin of this orphan ^{87}Sr: First, that the high $^{87}Sr/^{86}Sr$ ratios grew *in situ* from Rb which was transported into the rock by high temperature alkali metasomatism, then removed later at low temperature; Second, that the high $^{87}Sr/^{86}Sr$ grew in a high Rb/Sr ancient mantle source underlying fracture zones; Third, that the high $^{87}Sr/^{86}Sr$ is derived from the detrital fraction of sediments overlying the recharge zones of water circulating through the peridotite. The first of these hypotheses can probably be ruled out, while the low temperature, high water/rock conditions of alteration documented in this chapter strongly support the last hypothesis. Infiltration of altered peridotite by detrital sediment seems the most likely explanation and awaits a definitive test.

The existence of high $^{87}Sr/^{86}Sr$ in serpentinites is one of the oldest observations of the isotopic geochemistry of Sr (Roe, 1965). At the time, it was thought to show the existence of a class of peridotites that were not a plausible source region for mid-ocean ridge basalt (Bonatti, 1970). Though it is now clear that the topic bears little direct relevance to the geochemistry of the mantle, it does represent a major unexplained fractionation of $^{87}Sr/^{86}Sr$ in oceanic crustal materials. Depending on the fraction of serpentinized peridotite incorporated into the crust, this high $^{87}Sr/^{86}Sr$ may be a significant contribution to the overall Sr mass budget of the oceanic crust, with implications for recycling crust into the mantle and for the $^{87}Sr/^{86}Sr$ ratio of the oceanic crust.

References

Aumento, F. and H. Loubat (1970) The mid-Atlantic ridge near 45°N XVI Serpentinized ultramafic intrusions. **Canadian Journal of Earth Sciences** 8:631-663.

Bazylev, B.A. (1989) Unpublished Ph.D. Thesis, University of Moscow, CIS.

Bischoff, J. and M. Fyfe (1968) Catalysis, inhibition and the calcite-aragonite problem I: The aragonite-calcite transformation. **American Journal of Science** 206:65-79.

Bischoff, J. and W.E. Seyfried (1978) Hydrothermal chemistry of seawater from 25°C to 350°C. **American Journal of Science** 278:838-860.

Boger, P.D., J.L. Boger, and G. Faure (1980) Systematic variations of $^{87}Sr/^{86}Sr$ ratios, Sr compositions, and selected major-oxide concentrations and mineral abundances in piston cores from the Red Sea **Chemical Geology** 29:13-28.

Bonatti, E., J. Honnorez and G. Ferrara (1970) Equatorial mid-Atlantic Ridge: Petrologic and Sr-isotopic evidence for an alpine-type rock assemblage. **Earth and Planetary Science Letters** 9:247-256.

Bonatti E., M-B. Honnorez-Guerstein, J. Honnorez and C. Stern (1976) Hydrothermal pyrite concretion form the Romanche trench (equatorial Atlantic): Metallogenesis in oceanic fracture zones. **Earth and Planetary Science Letters** 37:1-10.

Bonatti, E., J.R. Lawrence, P.R. Hamlyn and D. Breger (1980) Aragonite in deep sea ultramafic rocks **Geochimica et Cosmochimica Acta** 44:1207-1214.

Bonatti, E. and Hamlyn, P. (1981) Oceanic Ultramafic Rocks. I*n:* Emiliani, C. (ed.) *The Sea* John Wiley and Sons, NY.

Bonatti, E., E.C. Simmons, D. Breger, P.R. Hamlyn, and J. Lawrence (1983) Ultramafic rock/seawater interaction in the oceanic crust: Mg-silicate (sepiolite) deposit from the Indian Ocean floor. **Earth and Planetary Science Letters** 62:229-238.

Bonatti, E., J.R. Lawrence, and N. Morandi (1984) Serpentinization of oceanic peridotites: Temperature dependence of mineralogy and boron content. **Earth and Planetary Science Letters** 70:88-94.

Bowen, N.C. and Tuttle, O.F. (1949) The system MgO-SiO_2-H_2O. **Geological Society of America Bulletin** 60:439-460.

Cannat, M., D. Bideau and H. Bougault (1992) serpentinized Peridotites and gabbros in the Mid-Atlantic ridge axial valley at 15°37'N and 16°52'N. **Earth and Planetary Science Letters** 109:87-106.

Chernosky, J.V.(1973) The stability of chrysotile, $Mg_3Si_2O_5(OH)_4$, and the free energy of formation of talc, $Mg_3Si_4O_{10}(OH)_2$. **Geological Society of America Abstracts with Programs** 5:575.

Creaser, R.A., D.A. Papanastassiou and G.J. Wasserburg (1991) Negative thermal ion mass spectrometry of osmium, rhenium and iridium. **Geochimica et Cosmochimica Acta** 55:397-401.

Deer, W.A., R.A. Howie and J. Zussman (1966) *An Introduction to the Rock forming Minerals* Longman Group Limited, London. 528 pp.

Dick, H.J.B. (1979) Alteration and metamorphism of peridotite at Islas Orcadas Fracture Zone. **EOS, Transactions of the American Geophysical Union** 60-973.

Dick, H.J.B, G. Thompson, and W. Bryan (1981) Low angle faulting and steady state emplacement of plutonic rocks at ridge-transform intersections. **EOS, Transactions of the American Geophysical Union** 62:406.

Dick, H.J.B and T.B. Bullen (1984) Chromian spinel as a petrogenetic indicator in abyssal and alpine-type peridotites. *In:* Kornprobst, J. (ed.) *Kimberlites II: The mantle and crust-mantle relationships* Elsevier Science Publishers., Amsterdam p. 295-308.

Dick, H.J.B. and Fisher, R. (1984) Mineralogic studies of the residues of mantle melting: abyssal and alpine-type peridotites *in:* Kornprobst (ed.) *Kimberlites II: the Mantle-Crust Relationship* Elsevier Science Publishers B.V, Amsterdam. Pp. 295-310.

Dick, H.J.B., R. Fisher and W.B. Bryan (1984) Mineralogic variability of the uppermost mantle along mid-ocean ridges. **Earth and Planetary Science Letters** 69:88-106.

Dick, H.J.B. (1989) Abyssal Peridotites, Very-Slow Spreading Ridges and Ocean Ridge Magmatism. **The Journal of the Geological Society of London Special Volume:** *Magmatism in the Ocean basins*

Elthon, D. (1992) Chemical trends in abyssal peridotites: refertilization of depleted suboceanic mantle. **Journal of Geophysical Research** 97:9015-9025.

Esser, B.K. (1991) *Osmium Isotope geochemistry of Terrigenous and Marine Sediments.* Ph.D. Thesis, Yale University.

Esser, B.K. and K.K. Turekian (1988) Accretion Rate of extraterrestrial particles determined from osmium isotope systematics of Pacific Pelagic clay and manganese nodules. **Geochimica et Cosmochimica Acta** 52:1383-1388.

Evans, B.W. (1977), Metamorphism of Alpine peridotite and Serpentinite. **Annual Review of Earth and Planetary Science** 5:397-447.

Fujii, T. (1990) Petrology of peridotites from hole 670a, Leg 109. *In:* Detrick, R., J. Honnorez, W. Bryan, and T. Juteau, **Proceedings of the Ocean Drilling Program, Scientific Results** 106/109:19-25.

Grant, J. A. (1986) The isocon diagram - A simple solution to Gresen's Equation for Metasomatic alteration **Economic Geology** 81:1976-1982.

Hart, S.R. (1972) The geochemistry of a Lherzolite from the Mid-Indian Ridge. **Department of Terrestrial Magnetism Annual Report, 1971-1972.**

Hattori, K and Hart, S. (1991) Osmium-isotope ratios of platinum-group minerals associated with ultramafic intrusions: Os-isotopic evolution of the oceanic mantle. **Earth and Planetary Science Letters** 107:499-514.

Hauri, E. (1992) MIT/WHOI Ph.D. Dissertation.

Hauri, E. and S. Hart (1992) Re-Os systematics of HIMU and EMII Oceanic Island Basalts from the South Pacific Ocean. **Earth and Planetary Science Letters**, in press.

Hébert, R., D. Bideau and R. Hekinian (1983) Ultramafic and mafic rocks from the Garrett Transform Fault near 13° 20'S on the East Pacific Rise: Igneous petrology. **Earth and Planetary Science Letters** 65:107-125.

Hébert, R., A.C. Adamson and S. Komor (1990) Metamorphic petrology of ODP leg 109, Hole 670a serpentinized peridotites: Serpentinization processes at a slow spreading ridge environment. *In:* Detrick, R., et al. (1980) **Proceedings of the ODP, Scientific results 106/109**, Ocean Drilling Program, College Sta. TX. P. 103-115.

Helmley, J.J., J.W. Montoya, C.L. Christ, and P.B. Hostetler (1977) Mineral equilibria in the MgO-SiO_2-H_2O System I: Talc-chrysotile-forsterite-brucite stability relations. **American Journal of Science** 277:322-351.

Helmley, J.J., J.W. Montoya, D.R. Shaw, and R.W. Luce (1977) Mineral equilibria in the MgO-SiO_2-H_2O System II: Talc-antigorite-forsterite-anthophyllite-enstatite stability relations and some geologic implications in the system. **American Journal of Science** 277:353-383.

Hofmann, A and S.R. Hart (1978) An assessment of local and regional isotopic equilibrium in the mantle. **Earth and Planetary Science Letters** 38:44-62.

Hurley, P.M., H.W. Fairbairn and W.H. Pinson (1964) Rb-Sr relationships in serpentinites from Mayaguez, Puerto Rico and dunite from St. Paul's rocks: A progress report. **NAS-NRC Pub. 1188**, 149-151.

Janecky, D.R. (1982) Serpentinization of peridotite within the ocean crust: Experimental and theoretical investigation of seawater-peridotite interaction at 200°C and 300°C, 500 bars. **American Journal of Science** 283:831-860.

Janecky, D. R., and W. E. Seyfried (1983) The solubility of magnesium-hydroxide-sulfate-hydrate in seawater at elevated temperatures and pressures. **American Journal of Science** 283:831-860.

Janecky, D.R. and W.E. Seyfried (1986) Hydrothermal serpentinization of peridotite within the oceanic crust: experimental investigations of mineralogy and major element chemistry. **Geochimica et Cosmochimica Acta** 50:1357-1378.

Jaques, A.L. and D.H. Green (1980) Anhydrous melting of peridotite at 0-15 kbar. pressure and the genesis of tholeiitic basalts. **Contributions to Mineralogy and Petrology** 73:287-310.

Johannes, W. (1968) An experimental investigation of the reaction forsterite $+H_2O \Rightarrow$ serpentine + brucite. **Contributions to Mineralogy and Petrology** 19:309-315.

Johnson, K.T.M., Dick, H.J.B. and Shimizu, N. (1990) Melting in the upper oceanic mantle: an ion microprobe study of diopsides in abyssal peridotites. **Journal of Geophysical Research** 95:2661-2678.

Johnson, K.T.M. and H.J.B. Dick (1992) Open system melting and temporal and spatial variation of peridotite and basalt at the Atlantis II Fracture Zone. **Journal of Geophysical Research** 97:9219-9241.

Jenkins, D.M. (1981) Experimental phase relations of hydrous peridotites modeled in the system H_2O-CaO-MgO-Al_2O_3-SiO_2. **Contributions to Mineralogy and Petrology** 77:166-176.

Juteau, T., E. Berger and M. Cannat (1990) Serpentinized residual mantle peridotites from the MAR median Valley, ODP hole 670a: Primary mineralogy and geochemistry. *In:* Detrick, R., J. Honnorez, W. Bryan, and T. Juteau, **Proceedings of the Ocean Drilling Program, Scientific Results** 106/109:27-45.

Kelemen, P., Henry J.B. Dick and J.E. Quick (1992) Formation of harzburgite by pervasive melt/rock reaction in the upper mantle. **Nature** 358:635-641.

Kimball, K.L., F.S. Spear and H.J.B. Dick (1985) High temperature alteration of abyssal ultramafics from the Islas Orcadas Fracture Zone, South Atlantic. **Contributions to Mineralogy and Petrology** 91:307-320.

Kimball, K.L. and D. Gerlach (1986) Sr isotopic constraints on hydrothermal alteration of ultramafic rocks in two oceanic fracture zones from the South Atlantic Ocean. **Earth and Planetary Science Letters** 78:177-188.

Kinzler, R. and Grove, T. (1992) Primary Magmas of Mid-Ocean Ridge Basalts 1. Experiments and Methods. **Journal of Geophysical Research** 97 :6885-6906.

Kinzler, R. and Grove, T. (1992) Primary Magmas of Mid-Ocean Ridge Basalts, 2. Applications. **Journal of Geophysical Research** 97:6907-6926.

Kitihara, S. and Kennedy, G.C. (1967) The calculated equilibrium curves for some reactions in the system MgO-SiO_2-H_2O at pressures up to 30 kilobars. **American Journal of Science** 265:211-217.

Klein, E.M., and Langmuir, C.H. (1987) Global correlations of ocean ridge basalt chemistry with axial depth and crustal thickness. **Journal of Geophysical Research** 92:8089-8115.

Klein, E.M and Langmuir, C.H. (1989) Local versus global correlations in ocean ridge basalt composition: a reply. **Journal of Geophysical Research** 94:4241-4252.

Komor, S.C., T.L. Grove, and R. Hébert (1990) Abyssal peridotites from ODP hole 670a: residues of mantle melting exposed by non-constructive axial divergence. *In:* Detrick, R., J. Honnorez, W. Bryan, and T. Juteau, **Proceedings of the Ocean Drilling Program, scientific results** 106/109:85-101.

Langmuir, C., R.D. Vocke, G.N. Hanson, and S.R. Hart (1978) A general mixing equation with applications to Icelandic basalts. **Earth and Planetary Science Letters** 37:380-392.

le Roex, A., H.J.B. Dick, A. Erlank, A. Reid, F. Frey, and S.R. Hart (1983) Geochemistry, mineralogy, and petrogenesis of lavas erupted along the Southwest Indian Ridge between the Bouvet Triple Junction and 11 degrees East. **Journal of Petrology** 24:267-318.

le Roex, A., H.J.B. Dick, A.J. Erlank, A.M. Reid, and F. Frey (1985) Petrology and Geochemistry of basalts from the American-Antarctic Ridge, southern ocean.: implications for the westward influence of the Bouvet mantle plume. **Contributions to Mineralogy and Petrology** 90:367-380.

le Roex, A., H.J.B. Dick, and R.L. Fisher (1989) Petrology and geochemistry of MORB from 25°N to 46°N along the Southwest Indian Ridge: Evidence for contrasting styles of mantle enrichment. **Journal of Petrology** 30:947-986.

le Roex, A., H.J.B. Dick, and R.T. Watkins (1992) Petrogenesis of anomalous K-enriched MORB from the Southwest Indian Ridge: 11°53'E to 14°38'E. **Contributions to Mineralogy and Petrology** 110:253-268.

Luck, J-M., J.L. Birck and C.J. Allègre (1980) ^{187}Re-^{186}Os systematics in meteorites: Early chronology of the solar system and the age of the galaxy. **Nature** 283:256-259.

Machado, N., C. Brooks and S.R. Hart (1986) Determination of initial $^{87}Sr/^{86}Sr$ and $^{143}Nd/^{144}Nd$ in primary minerals from mafic and ultramafic rocks: Experimental procedure and implications for the isotopic characteristics

of the Archean mantle under the Abitibi greenstone belt. **Geochimica et Cosmochimica Acta** 50:2335-2348.

Martin, C.E. (1991) Os isotopic characteristics of mantle derived rocks. **Geochimica et Cosmochimica Acta** 55:1421-1434.

McKenzie, D. (1984) The generation and compaction of partially molten rock. **Journal of Petrology** 25:713-765.

McKenzie, D. and M.J. Bickle (1988) The volume and composition of melt generated by the extension of the lithosphere. **Journal of Petrology** 29:625-679.

Menke, W. (1984) *Geophysical Data Analysis: Discrete Inverse Theory* Academic Press, Orlando, Fla.

Menzies, M. and V.R. Murthy (1976) Sr-isotopic compositions from some Mediterranean alpine lherzolites. **Geochimica et Cosmochimica Acta** 40:1577-1581.

Mercier, J.-C. C., and A. Nicolas (1974) Textures and fabrics of upper mantle peridotites as illustrated by xenoliths from basalts. **Journal of Petrology** 16:454-487.

Michael, P. and E. Bonatti (1985a) Peridotite compositions from the North Atlantic: Regional and tectonic variations and implications for partial melting. **Earth and Planetary Science Letters** 73:91-104.

Michael, P. and E. Bonatti (1985b) Petrology of ultramafic rocks from sites 556, 558 and 560 in the North Atlantic. *In:* Bougault, et al. (1985) **IPOD** 82:523-528.

Miyashiro, A., F. Shido, and Ewing, M. (1969) Composition and origin of serpentinites from the Mid-Atlantic Ridge near 24° and 30° North latitude. **Contributions to Mineralogy and Petrology** 23:117-127.

Mottl, M. (1976) *Chemical exchange between seawater and basalt during hydrothermal alteration of the oceanic crust.* Ph.D. Dissertation, Harvard Univ., 188p.

Navon, O. and E. Stolper (1987) Geochemical consequences of melt percolation: the upper mantle as a chromatographic column. **Journal of Geology** 95:285-307.

Nesbitt, H.W. and O.P. Bricker (1978) Low temperature alteration processes affecting ultramafic bodies. **Geochimica et Cosmochimica Acta** 42:403-409.

Nier, A.O. (1950) A redetermination of the relative abundances of the isotopes of carbon, nitrogen, oxygen and potassium. **Physical Reviews** 77:789-793.

O'Hara, M.J. (1968) Are ocean floor basalts primary magmas? **Nature** 220:683-686.

Palmer, M.R., K.K Falkner, K Turekian and S. Calvert (1988) Sources of Osmium isotopes in manganese nodules. **Geochimica et Cosmochimica Acta** 52:1197-1202.

Quick, J. (1981) Petrology and petrogenesis of the Trinity Peridotite, an upper mantle diapir in the eastern Klamath Mountains, northern California. **Journal of Geophysical Research** 92:11837-11863.

Ravizza, G. and K. Turekian (1989) Application of the ^{187}Re-^{187}Os system to black shale geochronometry. **Geochimica et Cosmochimica Acta** 53:3257-3262.

Ravizza, G., K.K. Turekian, and B.J. Hay (1991) The geochemistry of rhenium and osmium in recent sediments from the Black Sea. **Geochimica et Cosmochimica Acta** 55:3741-3752.

Reisberg, L. and A. Zindler (1986) Extreme isotopic variations in the upper mantle: evidence from Ronda. **Earth and Planetary Science Letters** 81:29-45.

Roe, G. D. (1965) *Rubidium-Strontium analyses of ultramafic rocks and the origin of peridotite.* MIT Ph.D. Thesis. 239 p.

Roy, K. and R. Roy (1954) An experimental study of the formation and properties of synthetic serpentines and related layer silicate minerals. **American Mineralogist** 39:957-975.

Salters, V. and Shimizu, N. (1990) The widespread occurrence of HFSE-depleted mantle. **Geochimica et Cosmochimica Acta** 52:2177-2182.

Salters, V. and S.R. Hart (1989) The Hf-paradox and the role of garnet in the source of mid-ocean ridge basalts. **Nature** 342:420-422.

Schroeder, B., G. Thompson and M. Sulanowska (1980) Analysis of geologic materials using an automated x-ray fluorescence system. **X-ray Spectrometry** 9: No. 4: 198-205.

Seyfried, W.E. and W.E. Dibble, Jr. (1980) Seawater-peridotite interaction at 300° C and 500 bars: implications for the origin of oceanic serpentinites. **Geochimica et Cosmochimica Acta** 44:309-321.

Shaw, P. (1990) Class Notes for Marine Geophysics: Inverse Theory.

Shibata, T. and G. Thompson (1986) Peridotites from the Mid-Atlantic Ridge at 43°N and their petrogenetic relation to abyssal tholeiites. **Contributions to Mineralogy and Petrology** 93:144-159.

Silantiev, S.A., M.V. Mironenko, B.A. Bazylev, Y.V. Semenov (1992) Metamorphism associated with mid-ocean ridge hydrothermal metamorphism: Thermodynamic modeling experience. **Geochemical Journal International** Russian Acad. Of Sciences Vol. 7-1992:1015-1034.

Spry, A.H. (1983) *Metamorphic Textures* Pergamon Press 338p.

Steuber, A.M. and V.R. Murthy (1966) Strontium isotope and alkali element abundances in ultramafic rocks. **Geochimica et Cosmochimica Acta** 30:1243-1259.

Stockman, H.W. and D.F. Hlava (1984) Platinum group minerals in alpine chromitites from southwestern Oregon. **Economic Geology** 79:491-508.

Streckeisen, A. (1976) To each plutonic rock its proper name. **Earth Science Reviews** 12:1-33.

Thompson, G. (1970) A geochemical study of some lithified carbonate sediments from the deep sea. **Geochimica et Cosmochimica Acta** 36:1237-1253.

Thompson, G. and W. Melson (1970) Boron contents of serpentinites and metabasalts in the ocean crust: Implications for the boron cycle in the oceans. **Earth and Planetary Science Letters** 8:61-65.

Thompson, G. and Melson, W. (1972) The petrology of oceanic crust across fracture zones in the Atlantic Ocean: Evidence of a new kind of seafloor spreading. **Journal of Geology** 80:526-538.

Veizer, J. (1989) Strontium isotopes in seawater through time. **Annual Reviews of Earth and Planetary Science** 17:141-167.

von Damm, K.L. (1990) Seafloor hydrothermal activity: Black Smoker chemistry and chimneys. **Ann. Reviews of Earth and Planetary Science** 18:173-204

Wenner, D. and H. Taylor (1971) Temperatures of serpentinization of ultramafic rocks based on $^{18}O/^{16}O$ fractionation between coexisting serpentine and magnetite. **Contributions to Mineralogy and Petrology** 32:165-185.

Wenner, D.B., and H.P. Taylor (1973) Oxygen and hydrogen isotope studies of serpentinization of ultramafic rocks in oceanic environments and continental ophiolite complexes. **American Journal of Science** 273:207-239.

Whitehead, J.A., Dick, H.J.B., and Schouten H. (1984) A mechanism for accretion under spreading centers. **Nature** 312:146-148.

Wicks, F.J. and E.J.W. Whittaker (1977) Serpentine textures and serpentinization **Canadian Mineralogist** 15:459-488.

Zindler, A., S.R. Hart, F.A. Frey, and S.P. Jacobsen (1979) Nd and Sr isotope ratios and rare-earth element abundances in Reykjanes Peninsula basalts: evidence for mantle heterogeneity beneath Iceland. **Earth and Planetary Science Letters** 45:249-262.

Zindler, A. E. Jagoutz, and S. Goldstein (1982) Nd, Pb and Sr isotopic systematics in a three-component mantle: A new perspective. **Nature** 58:519-523.

Zindler, A. and S.R. Hart (1986) Chemical Geodynamics. **Annual Review of Earth and Planetary Sciences** 14:493-571.

Chapter 4: The Os and Nd Isotopic Composition of the Mid-Ocean Ridge Mantle

Chapter 4: The Os and Nd Isotopic Composition of the Mid-Ocean Ridge Mantle

Abstract

Reported here are the results of Os isotopic composition and concentration measurements in abyssal peridotite whole rocks and Nd isotopic composition and concentration in separated clinopyroxenes. The observed Os and Nd isotopic compositions cannot be reconciled with any model for the production of Re/Os heterogeneity in the mantle due only to crustal formation by partial melting, and do not overlap significantly with the compositions of continental xenoliths. Mechanisms of decoupling of the Os and Nd isotopic systems are examined in the light of the new data. Recycling of subducted crust probably cannot account for the variations seen in Nd and Os isotopic compositions. Possible mechanisms for the decoupling of the Os and Nd isotopic systems include elemental fractionation via the porous flow of basalt through the mantle, mantle metasomatism, and core formation. None of these is at present sufficiently well-characterized with respect to the two isotopic systems to be completely evaluated as a source of the observed variations.

Introduction

The depleted mantle is generally thought of as the source of mid-ocean ridge basalts (MORB). It plays a central role in the interpretation of major element, trace element and isotopic data from many other geologic settings (Gast, 1968; Schilling, 1971, 1973a,b; Hart, et al., 1973; and many others). It has a composition and a geologic history which is in some senses quite well defined, and an origin -- by extraction of the continental crust -- which is by now largely unquestioned. For these reasons, the depleted mantle serves as a benchmark in geochemistry against which all other isotopic and trace element reservoirs are measured. As such, it is important to characterize the processes which lead to the formation of the depleted mantle, particularly when new technologies provide the ability to investigate aspects of mantle evolution which were previously quite difficult to approach. This study reports the results of isotopic measurements of Nd and Os in abyssal peridotites, and explores some of the

difficulties which remain in interpreting the Nd and Os geochemistry of the mantle.

The nature of abyssal peridotites.

Abyssal peridotites represent fragments of the oceanic mantle which have undergone variable extents of partial melting (Dick, Fisher and Bryan, 1984; Michael and Bonatti, 1985) followed by tectonic uplift, hydrous metamorphism and emplacement to the ocean floor. Determining the nature of the sub-oceanic mantle in terms of isotopes and incompatible trace elements has been a primary goal of petrologists and geochemists for about the last 30 years (Gast 1968; Schilling 1971; Hart, 1971; and many since). Abyssal peridotites have received relatively little direct attention during that time, in part due to their relative rarity, their extensive hydrous alteration, and their low concentrations of incompatible elements. With careful analysis, isotopic and trace element data can be derived from abyssal peridotites reflecting their primary mantle composition (Chapter 3, Johnson, et al., 1990; Johnson and Dick, 1992).

Mid-ocean ridge basalt (MORB) is the result of melting of a peridotitic mantle and its subsequent fractionation and eruption on the ocean floor (Green and Ringwood, 1967; Ito and Kennedy, 1967; Bottinga and Allègre, 1978; McKenzie and Bickle, 1988, Kinzler and Grove, 1992a,b). This fundamental observation underlies the interpretation of rocks of peridotitic composition dredged from the ocean floor. Though some peridotites recovered from the ocean floor are regarded as igneous cumulates (Bonatti and Hamelyn, 1981, Hébert, et al., 1983), by far the majority of studied abyssal peridotites are residues of partial melting (Miyashiro, et al., 1969; Hébert, et al., 1983; Dick, et al., 1984, Michael and Bonatti, 1985, Johnson, et al., 1990; Johnson and Dick, 1992).

Correlation of peridotite chemistry, basalt chemistry and the thermal structure of the mantle (as measured by the average depth of the ridge axis or the residual geoid at the ridge axis) along slowly spreading ridges establishes the genetic link between the major element compositions of MORB and abyssal peridotite (Dick, et al., 1984). Studies of the phase equilibria relevant to melting (Jaques and Green, 1979; Kinzler and Grove, 1992a,b) have shown that abyssal peridotite is a plausible end result of the melting process. Finally, trace element contents of abyssal peridotite clinopyroxenes serve to confirm the genetic link between MORB and abyssal peridotite and to constrain possible models of the melting process (Johnson, et al., 1990; Johnson and Dick, 1992).

Three major events are thought to have influenced the composition of the mid-ocean ridge mantle over the history of the Earth. First, the formation of the Earth's core, as expressed in the concentrations of Fe, Ni and the other siderophile and chalcophile elements (and as yet not well understood; Jagoutz, et al., 1979; Jones and Drake, 1986; Morgan, 1986; Hart and Zindler, 1986). The second major event is the extraction of the crust from the mantle through Earth's history that resulted in the depletion of the crust-forming elements in the upper mantle. This depletion is recorded by the isotopic compositions of radiogenic isotope systems whose parents and daughters are lithophile elements involved in crustal formation (principally Rb-Sr and Sm-Nd, but also Lu-Hf, La-Ce and K-Ca). A mean crustal age of 2 Ga. for the continents can be calculated from these data. The last event is the partial melting process which led recently to the formation of the mid-ocean ridge basalt (Dick, et al., 1984, Michael and Bonatti, 1985; Johnson, et al., 1990). This study will examine these three events and study the role each has played, or could have played in the formation of the Nd and Os isotopic features of the current sample suite.

Particularly with abyssal peridotites, low temperature hydrous alteration and attendant serpentinization is responsible for extensively modifying the composition of the rock and for partly erasing primary textures. For this reason, inferences about the mantle beneath mid-ocean ridges can best be drawn from relict phases resistant to weathering, (e.g.: spinel, olivine, diopside and enstatite), from elements unaffected by alteration, or from characteristics which are not affected or mimicked by the serpentinization process. Chapter Three of this dissertation details how the Os, Nd and Sr isotopic systems respond to the hydrothermal alteration and weathering experienced by abyssal peridotites. Chapter Three also specifies what information about the sub-oceanic mantle can be inferred from Nd and Os isotopes measured in abyssal peridotites or mineral separates from abyssal peridotites. Chapter Three concludes that Nd isotopic compositions of clinopyroxenes and even select whole rock data can be accepted as representing mantle Nd isotopic compositions.

Os isotopes in bulk rocks used in this study are open to more interpretation in this regard. On the one hand, it has not been shown that abyssal peridotites are free of contamination by seawater. Neither has a single unambiguous case of contamination been established. Chapter Three of this dissertation discusses this issue at some length, concluding that abyssal peridotite Os isotopic compositions may be tenatively considered free of submarine alteration. As a first approximation, the samples in this study will be considered free of seawater contamination. Whether this is justified will have to await further study of Os isotopes in abyssal peridotites.

The Sm-Nd and Re-Os isotopic systems.

The Sm-Nd isotopic system is useful for the dating of mafic igneous rocks, especially those of great age, due to its resistance to disturbance during metamorphism. Additionally, Nd isotopes in mantle rocks and basalts derived from the mantle have helped to constrain the number, composition and genesis of isotopic reservoirs in the Earth's mantle (Zindler, et al., 1979; Zindler and Hart, 1986). ^{147}Sm decays to ^{143}Nd by the emission of an alpha particle, and has a half-life of 1.06×10^{10} years.

The naturally occurring element Rhenium is composed of two isotopes, ^{187}Re and ^{185}Re. The half-life of the β- decay of ^{187}Re to ^{187}Os has been measured by several methods, (Allègre and Luck, 1980, Luck and Allègre1983; Lindner, et al., 1989), but is near the value of 46 billion years. The value inferred by Luck and Allègre, 1983 is used in this study (λ=1.52±0.04x10-11 y-1, t(1/2)= 4.56± 0.11x1010 y). The naturally occurring (non-radiogenic) isotope of osmium at mass 186 is commonly used as a reference, though in practice (Creaser, et al., 1991; Hauri and Hart, in press) other isotopes are measured and the $^{187}Os/^{186}Os$ calculated from the known isotopic abundances of Os.

The Sm-Nd isotopic system is an example of a radioactive decay system in which both parent and daughter elements are incompatible during silicate melting. Nd, the radioactive daughter element, is more incompatible during partial melting than its radioactive parent Sm. Mantle residues of partial melting thus have a high Sm/Nd ratio and become more radiogenic with time than does the bulk Earth, (cf., DePaolo and Wasserburg, 1979). If the formation of the Earth's core involved its extraction from the mantle, the Sm-Nd isotopic system would be completely unaffected; neither Sm nor Nd partition into metal or

metal + sulfur liquids and thus cannot be fractionated from each other by core formation processes.

The Re-Os isotopic system behaves similarly to the Rb-Sr system during silicate melting. The radioactive parent Re is more incompatible than the daughter Os. Thus, the reservoir formed by the extraction of the Earth's crust can be expected to have lower $^{187}Os/^{186}Os$ than the bulk Earth with time. In the presence of an iron or iron sulfide liquid, however, the behavior of Re and Os are very different from that of any other commonly studied isotopic system. Nd, Sm, Rb and Sr do not partition significantly into such liquids, and thus are not fractionated from each other by core formation processes. Re, however, partitions strongly into Fe and FeS liquids and Os even more strongly (Jones and Drake, 1986, and the widely held belief that for silicate-metal partitioning DOs≈ DIr). The exact relationship between the partitioning behavior of Re and Os between silicate and Fe-rich liquids is not well known. Since both are known to partition strongly into iron-rich liquids, differences in their partitioning will result in Re-Os fractionations in the silicate residue after Fe-rich liquid is extracted. There is thus the potential for the Re-Os isotopic system to record mantle events involving silicate-metal -metal sulfide fractionation (such as core formation).

Re-Os systematics in the depleted mantle.

The mean $^{187}Os/^{186}Os$ of the Earth at present is somewhere in the range of 1.04 to 1.10, from which bulk earth $^{187}Re/^{186}Os$ ratios of 3.15 to 3.7 can be derived (cf. Luck and Allègre, 1980). This is generally consistent with a nearly chondritic bulk Earth. Re is only mildly incompatible, so that partial melting in the mantle has only a limited ability to change the Re-Os ratio in the residue. The

$^{187}Os/^{186}Os$ compositions of the residual mantle and bulk Earth are thus very close to one another. The variation in $^{187}Os/^{186}Os$ in residual mantle rocks is somewhat difficult to explain. The range of xenolith and abyssal peridotite data, for example, from .995 to 1.1 permit the formation of a depleted mantle reservoir of Os with a minimum mean age of approximately 2 Ga (Walker, et al., 1989, Martin, 1990, 1991, Hattori and Hart, 1991), in accordance with results from Sr and Nd isotopes. In order to accomplish this result using a partial melting process, some rather extreme assumptions (discussed below) must be made about the mean age of crust formation, the partitioning of Re and Os during silicate melting, and the $^{187}Os/^{186}Os$ of the bulk Earth today. While the mean age of the crust is reasonably well constrained at approximately 2 Ga from Sr and Nd isotopes, the next two sections will review independent evidence for the bulk Earth $^{187}Os/^{186}Os$ and Re and Os partitioning.

In what follows, relatively crude models for mid-ocean ridge melting will be used to model the behavior of Re, Os and other trace elements. This approach is justified, since the reservoirs and partitioning behavior of Re and Os in the mantle and their behavior during melting are still not well enough understood for more sophisticated models to be employed. It is assumed that Re and Os can be modeled using the bulk distribution between solid and melt phases, rather than the weighted contributions of the modal phases in the rock (modal melting) or those entering the melt (non-modal). This assumption is valid so long as there are no great changes in the modal composition of the solid with respect to the actual reservoirs of Re and Os.

The unknowns in the geochemical behavior of Re and Os could affect their distributions in nature in ways which are difficult at present to model. As an example, if Re and Os partitioning were controlled by the behavior of dis-

seminated sulfide grains during silicate melting, the bulk partitioning model used here would still be valid, but most modal melting models (e.g., Johnson et al., 1990 for rare earth elements) would not. The exception would be if the sulfide phase were to completely disappear during the melting process. In this case, the bulk behavior of Re and Os would be likely to change dramatically, and be controlled by their partitioning in the remaining phases only. In this hypothetical situation, Re or Os could become much more incompatible if and when the peridotite passes the sulfide-out boundary during partial melting. There is no evidence, however, from xenoliths (Morgan, 1986; Walker, et al., 1989) or from orogenic lherzolites to indicate that such a dramatic phase disappearance effect is actually taking place (Reisberg, et al., 1991).

Bulk Earth $^{187}Os/^{186}Os$

Currently, the Os isotopic composition of the mantle has been assessed in three ways: by analogy with carbonaceous chondrites (Walker and Morgan, 1989), by analysis of low-Re PGE ores associated with mantle rocks (Allègre and Luck, 1980, Hattori and Hart, 1991) and by direct analysis of mantle rocks (Walker, et al. 1989, Martin, 1991, Reisberg, et al., 1991 and this study).

The average carbonaceous chondrite Os isotopic composition reported by Walker and Morgan (1989) is $1.050\pm.02$ and the $^{187}Re/^{186}Os$ is $3.20\pm.33$, excluding the hydrothermally altered Murray (C2M) chondrite. The chondrites provide an important model for the primordial composition of the solar system and thus the Earth (cf., Anders and Ebihara, 1982), since the concentrations of non-volatile elements in the solar nebula correlate strongly with those in average chondrites.

The majority of Os isotopic compositions determined on mantle-derived rocks have been carried out on samples of native Os-Ir metal (osmiridiums) which occur naturally in some mantle rocks (Allègre and Luck, 1980; Hattori and

Hart, 1991). These samples have little Re, so that an Os isotopic determination alone is a reasonable indication of their initial Os isotopic composition. By analyzing samples from ancient continental and oceanic mantle sources it has been possible to constrain the evolution of the Re-Os system in the Earth over time. The $^{187}Os/^{186}Os$ of the Earth is thus constrained to lie approximately at 1.05, with a standard deviation of about .02 (Allègre and Luck, 1980; Hattori and Hart, 1991), which is in good agreement with the chondrite values.

The second type of analysis has been the direct study of mantle rocks themselves. This has somewhat greater validity than the osmiridium studies since rocks bearing PGE ores are almost by definition unusual rocks. Walker, et al. (1989) analyzed a number of peridotite xenoliths from South Africa, and found a range of $^{187}Os/^{186}Os$ from .995 to 1.05. Reisberg et al., (1991) studied the Ronda Ultramafic complex and measured a range from .977 to 1.053 (excluding the SW traverse and sample R85-24A for the reasons they discuss). Finally, Martin (1990, 1991) measured four abyssal peridotites which ranged from 1.02 to 1.09.

Some or all of the samples measured in the studies just mentioned may have experienced an ancient partial melting event. This ancient partial melting is required by the isotopic compositions of mid-ocean ridge basalts and it is distinct from the recent partial melting which has affected the major element and trace element compositions of the peridotites (Dick, et al., 1984; Michael and Bonatti, 1985; Johnson, et al., 1990). If the ancient partial melting affects the Re/Os ratios in the depleted mantle, the value of $^{187}Os/^{186}Os$ for the bulk Earth must be higher than the average of depleted mantle analyses. If partial melting is the only process which can affect the Re/Os ratio in the depleted mantle, then the bulk Earth $^{187}Os/^{186}Os$ must be higher than the highest depleted mantle

sample measured. This reasoning led Martin, (1991) to conclude that the bulk Earth $^{187}Os/^{186}Os$ is at least 1.1.

The meteorite model for the evolution of the Os isotopic system in the Earth after Allègre and Luck (1980) and Walker and Morgan, (1989) is somewhat at odds with the bulk Earth model required by Martin (1991). The higher bulk Earth $^{187}Os/^{186}Os$ and $^{187}Re/^{186}Os$ required by the latter model put the bulk Earth firmly outside the field of carbonaceous chondrites, without explaining how the Earth acquired a higher Re/Os ratio during its formation, or why the Earth may have formed with a non-chondritic Re/Os ratio.

Re and Os partitioning

Currently, the state of knowledge regarding the partitioning of Re and Os during silicate melting is quite poor. Partition coefficients between the major mantle phases and melt are unknown and bulk distribution coefficients (between bulk solid and liquid) can at best be guessed at. Bulk distribution coefficients estimated for Re and Os vary greatly; values for Re from 1 (Jones and Drake, 1986) to .001 (Walker, et al., 1988) have been reported, as have Os values from .08 (Watson, et al., 1987) to 140 (Walker, et al., 1988). The following discussion will attempt to narrow the reasonable ranges of these values.

Some simple considerations can provide guidance about the first order behavior of Re and Os during igneous petrogenesis. The concentration of Re does not vary by more than one or two orders of magnitude between residual peridotites, basalts, evolved basalts and granites (Morgan and Lovering, 1967a,b). This first order observation suggests that Re is not a particularly incompatible element during the major processes of crustal formation. Os, by contrast, varies by many orders of magnitude, from several ppb. in residual peridotite to less than one ppt. in granites. The Os in granite is almost entirely

^{187}Os due to the radioactive decay of ^{187}Re, so the true concentration of common osmium is even lower. The high content of Os in residues of melting relative to the spectacularly low content of Os in most natural melts is strong evidence for the compatibility of Os during silicate melting, even if the limited experimental data relevant to the question do not bear this out particularly (Jones and Drake, 1986, for the geochemically similar element Ir; Watson, et al., 1987). The Re/Os ratio of igneous rocks is primarily controlled by the compatibility of Os, which is quantitatively retained in the source during each stage of crustal evolution. The concentration of Re varies much less in concentration across a wide range of rock types.

There have been two major approaches to estimating Re and Os partition coefficients for silicate melting: inverse calculation based on the concentrations of Re and Os in average basalt and peridotite xenoliths (Walker, et al., 1988,1989) and partitioning experiments on synthetic systems (Jones and Drake, 1986; Watson, et al. 1987).

Re partitioning

What follows is an attempt to derive information about the partitioning of Re from its concentration in residual mantle rocks. This is done based on simple models involving incremental batch equilibrium. If fractional melting or incremental batch equilibrium is assumed, the very low values of D_{Re} inferred by Walker, et al. (1988; 1989) are not required to explain the concentrations of Re in basalts and residual peridotites. If the batch melting equation is defined in the normal way:

$$D \equiv \frac{C_s}{C_l}$$

$$CT = FCl + (1\text{-}F)DCl \qquad (1),$$

then F is defined as the fraction of melt and C_l, C_s and C_T are the concentration of an element in the liquid, solid and total respectively. The calculation of an incremental batch process is quite simple if the concentration of the element in the solid is to be calculated. If C_{S0} is the initial concentration in the solid before melting:

$$C_{Sn} = \frac{C_{S0}}{(F/D+(1-F))^n} \qquad (2).$$

F is the increment of melting in each batch and n is the number of increments. In the case of simple batch equilibrium, n=1. The total degree of melting is F*n.

Calculation of partition coefficients from concentrations of those elements in peridotite and basalt is essentially an inversion technique. Such a calculation is, as are all inverse methods, highly model dependent. In the case of partitioning of incompatible trace elements, the degree of model dependence increases exponentially with the inferred incompatibility of the element. For example, if a 10% batch melting model provides a consistent fit to a body of basalt and peridotite data such that the bulk D_{batch} is .001, the same data can be modeled in terms of 10 incremental batches of 1% with a D_{inc} of .04 and an *apparent* bulk D_{batch} which is still .001. This model dependent difference between bulk partition coefficients increases with the inferred incompatibility of the element, for the reason that incremental batch melting is so much more efficient at removing incompatible trace elements from the mantle.

The behavior of Re during MORB petrogenesis can be modeled in a way which reasonably explains the Re data for mantle rocks. The melting process is currently thought to be a near-fractional, near-adiabatic partial melting process, and not a batch process (Johnson, et al., 1989, Kinzler and Grove, 1992a,b). Such a process is well modeled by an incremental batch process with small increments

(Johnson, et al., 1990). Re concentrations are available for basalts (avg= 0.9 ppb.; Hertogen, et al., 1980), fertile peridotite xenoliths (avg = 0.26 ppb.; Morgan, 1986) and abyssal peridotites (avg = .162; Martin, 1990,1991). In this case the 10% batch and 10%, 10 stage incremental batch processes produce roughly the same result (D_{Re} = 0.20 and 0.23 respectively) and also result in residual concentrations which match those in abyssal peridotites.

Walker, et al. (1988) calculate a partition coefficient for Re of 0.001 based on a peridotite concentration of 0.26 ppb. Re and 30% batch melting. This produces the observed komatiite melt with $^{187}Re/^{186}Os$ from 16 to 36. Using a 10 step incremental batch process at 30% overall melting results in a D_{inc} of 0.04 and an apparent single stage batch D_{Re} of 0.001 between the starting and melt composition, which is what Walker, et al. (1988) calculate. Thus the factor of 200 difference in apparent D_{Re} calculated from basalts and komatiites reduces to a factor of 5 simply by a change in model assumptions.

Another approach to the Re partitioning problem can be found by attempting to model the peridotite Re concentration data of Morgan, et al. (1986). The spinel peridotite xenoliths studied there are assumed to lie on a melting-related silicate evolution line analogous to Jagoutz, et al. (1979) and Hart and Zindler (1986). If this is so, the strong fractionation of Re in the depleted versus the undepleted lherzolites should allow the calculation of a Re partition coefficient. Once again, the result is model dependent. Batch melting at 15 kb. to varying degrees results in a D_{Re} of 0.05. Incremental batch melting results in a D_{Re} of 0.5. It is impossible to distinguish between these models based on their fit to the data; the size of the data set does not allow this.

A linear extraction model, which is essentially a negative mixing model, extracting basalt of a fixed composition from the peridotite, conforms to the data

as well as batch or incremental batch melting, giving a $D_{Re} = C_S/C_L$ of 0.2. Extraction of a liquid of fixed composition from peridotite is a physically unreasonable model. Its converse, the re-fertilization of depleted peridotite by the addition of basalt, is not (Elthon, 1992). It is possible that refertilization of peridotite produces effects on their concentration which have until now been ascribed primarily to melting processes.

The Re concentration data given by Reisberg, et al. (1991) for the Ronda ultramafic complex can be treated in a similar fashion. It is interesting to note that the correlation of Mg/(Mg+Fe) with Re seen in that study passes through a plausible bulk Earth composition, but that extremely high degrees of partial melting (> 30%) are required to relate the most depleted to the least depleted compositions. Modeling of Re concentrations results in a linear D_{Re} of 0.31, a batch D_{Re} of 0.12 and an incremental batch D_{Re} of 0.6. Once again, the best fit to the data are by a linear basalt extraction (or refertilization) model.

An experimental study of Os and Re partitioning in diopside in a haplobasaltic system (Watson, et al., 1987) produced Re and Os partition coefficients of 0.04 and 0.08 which they claimed were good to a factor of 2. In fact, this experiment cannot easily be related to melting in the mantle for a variety of reasons. First, the crystal/liquid partition coefficient of Re for the (for Re) minor phase clinopyroxene contains little information about the bulk partitioning behavior of Re during silicate melting. Second, the experiment was carried out in a haplobasaltic system, free of iron and sulfur, both of which have a strong correlation with Re concentration in natural rocks (Morgan, et al., 1986). Thus, there is evidence that the mass budget of Re is not controlled by clinopyroxene, as it is for many incompatible elements. Third, more than half of the Re added to the experimental charges was lost to the Pt capsule the experiment was run in,

making it highly unlikely that equilibrium was attained. The authors point out some of these difficulties, stating that "...this study is of a strictly reconnaissance nature, the main idea being to test the feasibility of performing the experiments and analyzing the separated phases..."

For Re, there are only two studies in which the bulk partition coefficient for silicate melting is found to be less than 0.1. Both Walker, et al., (1988) and Watson, et al., (1987) are physical systems (one natural, one experimental) that apply in an ambiguous way to the petrogenesis of most igneous rocks. Three other instances were just discussed (MORB-peridotite mass balance; the data of Morgan (1986) and the data of Reisberg, et al. (1991) where the physics of the situation are better understood and the applicability of the data to basalt petrogenesis are more likely. In these examples, Re partition coefficients of greater than 0.1 are indicated.

Os partitioning

In the case of Os, the model dependence of the outcome is eliminated due to its compatibility, to the point that $D = C_S/C_L$ is as valid a model as any other. The difficulty instead is in estimating an average value for MORB. The one MORB sample analyzed by Martin, (1991) was blank dominated, but was certainly no more concentrated than 0.001 ppb. Of the samples studied by Hertogen, et al. (1980), most were under .002 ppb., with three exceptions of .013, .076 and .083 ppb. Abyssal peridotites average 4 ppb. This suggests a partition coefficient ranging from 76 to 2100. In fact, the absolute value of the partition coefficient for a compatible element is not tremendously important, as Os is quantitatively retained in the residue. The major control on the Re/Os ratio in the mantle is the incompatible behavior of Re, as the Os concentration of mantle rocks does not vary greatly. Just the reverse is true in crustal rocks; the concen-

tration of Re does not vary greatly and the variation in the Re/Os ratio of crustal rocks is dominated by the highly compatible nature of osmium.

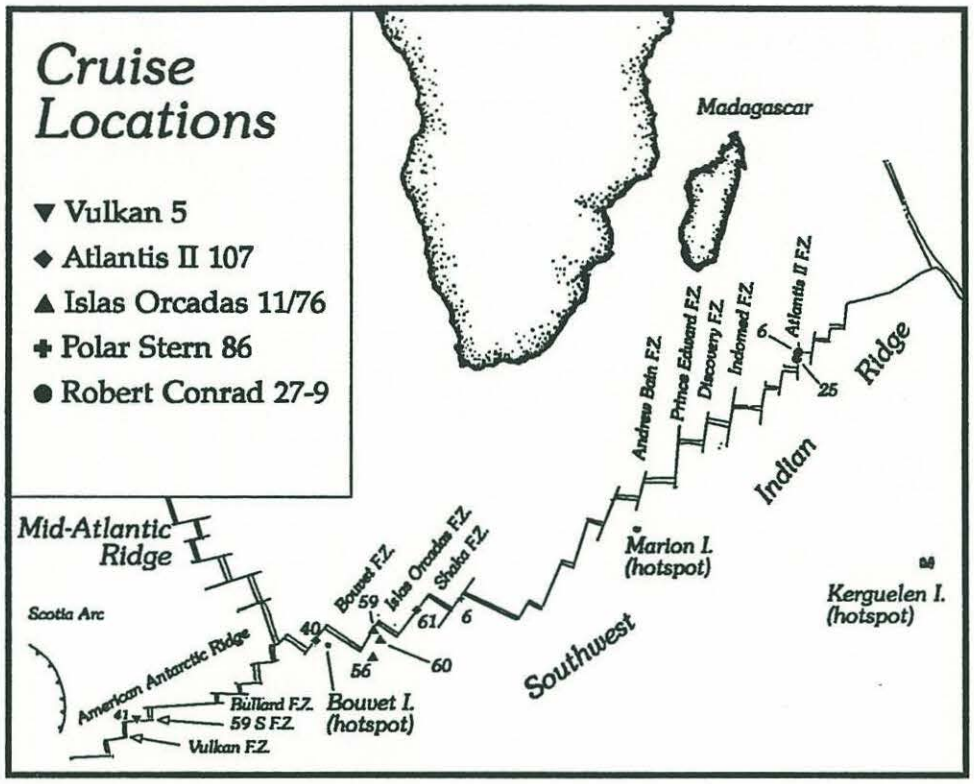

Figure 1: Location map for peridotite samples. Dredge haul numbers are listed next to the corresponding symbols.

Data

Sample Background

A total of 13 samples were studied from the SW Indian and American-Antarctic ridges. The locations, tectonic settings, and crustal ages of the samples are listed in Table 1. The samples are all lherzolites and harzburgites, having between 3 and 12 percent modal clinopyroxene, by volume. All are variably serpentinized, but do not contain abundant high temperature alteration phases or modal plagioclase. Two samples of peridotite mylonite from the Shaka fracture zone were included because of their extremely good state of preservation, being only 0-5% serpentinized in their unweathered cores.

Table 1: Sample Locations and tectonic settings.

Cruise	Sample	Latitude: Deg.	Min.		Longitude: Deg.	Min.		Tectonic Setting.
PS86	6-37	52	21.0	S	13	8.0	E	Dingaan FZ, NW wall.
AII107	61-78	53	22.5	S	9	20.3	E	Shaka FZ, SE wall.
AII107	61-83	53	22.5	S	9	20.3	E	Shaka FZ., SE wall.
AII107	40-27	54	25.4	S	1	34.2	E	Bouvet FZ., NW wall.
AII107	40-35	54	25.4	S	1	34.2	E	Bouvet FZ., NW wall.
Vulc5	41-29	59	5.2	S	16	48.5	W	59 deg. S FZ., N wall.
Vulc5	41-15	59	5.2	S	16	48.5	W	59 deg. S FZ., N wall.
RC2709	6-2	31	54.9	S	57	10.7	E	Atlantis II FZ., N RTI corner.
RC2709	25-139	32	32.2	S	57	3.8	E	Atlantis II FZ., E wall axial ridge.
IO11/76	59-26	54	3.4	S	6	30.0	E	Islas Orcadas FZ., SE wall.
IO11/76	56-58	54	5.5	S	6	17.1	E	Abyssal hills SE Islas Orcadas FZ.
IO11/76	60-61	54	27.5	S	6	29.2	E	Abyssal hills SE Islas Orcadas FZ.

Abbreviations: AII: Atlantis II; PS: Polar Stern; VULC: Vulcan; RC: Robert Conrad; IO: Islas Orcadas.

Figure 1 shows the locations of the samples. The samples were selected from fracture zones lying at variable distances from known mantle hotspots (Bouvet and Marion-Prince Edward) to show as great a range as possible in geochemistry and in geography. (Ce/Yb)n (normalized to the chondritic ratio) values in clinopyroxenes from these samples range from .0041 to 0.16 (Johnson, 1990, Johnson, et al. 1990; Chapter Three, this dissertation). This range shows that the selected samples underwent nearly the complete range of partial melting found to date in abyssal peridotites in the most recent melting event beneath the Southwest Indian and American-Antarctic ridges.

Nd analyses

Nd isotopic and isotope dilution analysis was carried out on hand-picked clinopyroxenes. Samples were crushed to approximately 400-800 micron size

and washed. The strongly ferromagnetic fractions were removed with a hand magnet. A clinopyroxene rich (approx. 40%) fraction was prepared using a Frantz isodynamic separator. Clinopyroxene fragments were hand-picked from this mixture to yield 100-150 mg. of 99% clinopyroxene. This separate was then crushed, sieved to 200-400 micron size, washed in deionized water and acetone and picked again. Only completely clear clinopyroxene grains free of inclusions of spinel, clay, and serpentine and showing good cleavage were used.

The clinopyroxene separates were leached incrementally in a mixture of 5% HF in 6.2N HCl. Typically, the first leach was cold, the second 5 minutes in an ultrasonic bath and the third 5 minutes in an ultrasonic bath, followed by 10 minutes at 125 °C. Leachates were collected and analyzed (see this dissertation, Chapter Three for details of individual leaching experiments). Nd isotopic compositions were accepted if the measured Sr isotopic composition and seawater mixing considerations were less than 0.706. This value indicates very little deviation of Nd isotopic composition of the peridotite the mixture from its primary value.

Sample dissolution and chemical separation was carried out by standard methods (Zindler, et. al., 1979). Clinopyroxene separates were split on 4 columns for separation of REE's from major elements in order to preclude overloading of the columns. Procedural blanks were measured during the course of this study of 6 and 16 pg. Nd. The quantities of Nd (12-50 ng.) analyzed were such that no blank correction was necessary. Nd concentration and $^{143}Nd/^{144}Nd$ were measured on a VG 354, 54 cm extended geometry multicollector mass spectrometer facility at Woods Hole Oceanographic Institution in multi-dynamic mode using an optimized algorithm for data collection (this thesis, Appendix II). Typical beam currents were 2x10-12 to 3x10-11 A.

Results of Nd isotopic composition and concentration measurements are listed in Table 2. See Chapter Three for details of the separation and leaching procedure and comparison of ion probe and isotope dilution results. Also listed are whole rock results from two samples which were sufficiently fresh that whole rock measurements were justified on the basis of their low $^{87}Sr/^{86}Sr$ compositions (<.706). Seawater exchange with the rock in such cases is still too low by several orders of magnitude to affect the $^{143}Nd/^{144}Nd$ isotopic composition of the whole rock sample (see Chapter Three).

Os analyses

Os isotopic composition and concentration were measured on whole rock samples. The samples were split into 2-5 cm fragments, then alteration veins along the exposed joint surfaces was removed by blasting with 200 micron sized glass beads. The samples were then washed in deionized water, blown dry, and crushed to pea-gravel size in a steel jaw crusher. Final crushing to <5 micron size was accomplished in an agate shatterbox.

Approximately two grams of sample were fused, using 4 grams of flux of the following composition: Borax: 57%, NaCO3:28%, S:5%, Ni:10%, by weight. The samples were spiked, mixed thoroughly, the flux was added, then the samples were mixed thoroughly again with the flux. The samples were then fired at 1100°C for approximately 90 minutes. NiS beads were recovered from the glass and dissolved in 6.2N HCl, leaving grains of insoluble PGE sulfide floating in the solution, which were then filtered out, dissolved in 4N H2SO4 and distilled once using the method described in Martin (1990). Single bead purification of the Os (Riesburg, et al., 1991) was then carried out.

Table 2: Abyssal peridotite isotope and trace element data.

Cruise	Sample	$^{187}Os/^{186}Os$	Os	Co	$^{143}Nd/^{144}Nd$	err
PS86	6-37	1.0148	4.98	106	.512960	41
AII107	61-78			109		
AII107	61-83	1.0677		118	+ .512931	30
AII107	40-27	1.076[1]	4.33	-		
AII107	40-35	1.0394	3.25	103		
Vulc5	41-29	1.0210	4.08	109	.513147	30
Vulc5	41-15	1.0521	3.86	95		
RC2709	6-2	1.0418	4.48	115	+ .512965	30
RC2709	6-2	"	"	"	.513016	15
RC2709	25-139	-	-	-	.513230	14
IO11/76	59-26	1.0293	4.05	86		
IO11/76	56-58	1.0963	3.44	130	.513159	32
IO11/76	60-61	1.0210	3.48	113		

$^{187}Os/^{186}Os$ ratio determined by NTIMS. In-run precision is in every case the same as or better than the between-run reproducibility of Os shelf solution of 0.003 (2s absolute). Os concentrations by isotope dilution; reported in ppb., nominal uncertainty 1%. Co concentrations by XRF, reported in ppm., nominal uncertainty 5%. Nd isotopic compositions normalized to $146Nd/^{144}Nd=.7219$, LaJolla standard value .511848 measured during the course of this study. (Ce/Yb)n determined by ion microprobe. The three IO 11/76 rocks are replicates of rocks analyzed by Martin (1991).

1 Os IC + ID data on sample AII107 40-27 from Martin, 1990; IC uncertainty is .006.
+ $^{143}Nd/^{144}Nd$ data on whole rocks with $^{87}Sr/^{86}Sr<.7060$.

Samples were loaded in HCl onto Pt filaments and reduced overnight *in vacuo*. $BaNO_3$ was loaded on top of the sample and the sample was run as OsO_3^- by the method of Creaser, et al. (1991) on the NIMA-b mass spectrometer at Woods Hole Oceanographic Institution. An operating pressure of $1x10^{-6}$ torr. was maintained using an oxygen bleed to enhance oxide emission after Hauri and Hart (1993). Repeated analysis of standard solutions results in a reproducibility of $^{187}Os/^{186}Os$ between samples of better than $\pm$.003 absolute. The results of the Os isotopic composition and concentration measurements are listed in Table 2. Also listed are concentrations of Co measured by XRF. Concentrations of other elements of interest for these samples are to be found in Chapter Three of this dissertation, Table 10.

Discussion

Coupling and decoupling of the Os and Nd isotopic systems:

Depleted mantle formation

The Re-Os isotopic system can be affected by partial melting in the mantle. Re is moderately incompatible, going preferentially into the melt rather than the solid during partial melting, while Os is almost completely retained in the solid (see the foregoing discussion on partitioning). In this way, Re/Os ratios can be lowered in the residual mantle during melting, but not raised. Given sufficient time, values of $^{187}Os/^{186}Os$ lower than the bulk earth evolution line can be explained by varying degrees of melt extraction in the past to form the Earth's crust. The crust itself acquires a very high Re/Os ratio and hence with time a very high $^{187}Os/^{186}Os$. Hattori and Hart (1991) and Martin (1991) concluded that partial melting alone was sufficient to account for the Re-Os isotopic systematics of the depleted mantle. Martin (1991) notes that there is insufficient Re in the crust to move the depleted mantle value more than a few percent from the bulk silicate Earth value.

Partial melting through time and the formation of the Earth's crust can not adequately account for the systematics of Nd and Os isotopes in the oceanic upper mantle, however. To see why this is important, we first model the behavior of the Nd and Sr isotopic systems. Figure 2a shows a melting model based on a 10 stage incremental batch process, with varying total degree of melting. It can easily be shown that any trace element ratio in the residue, or in this case, a parent/daughter ratio m, in such a process is changed in the following way:

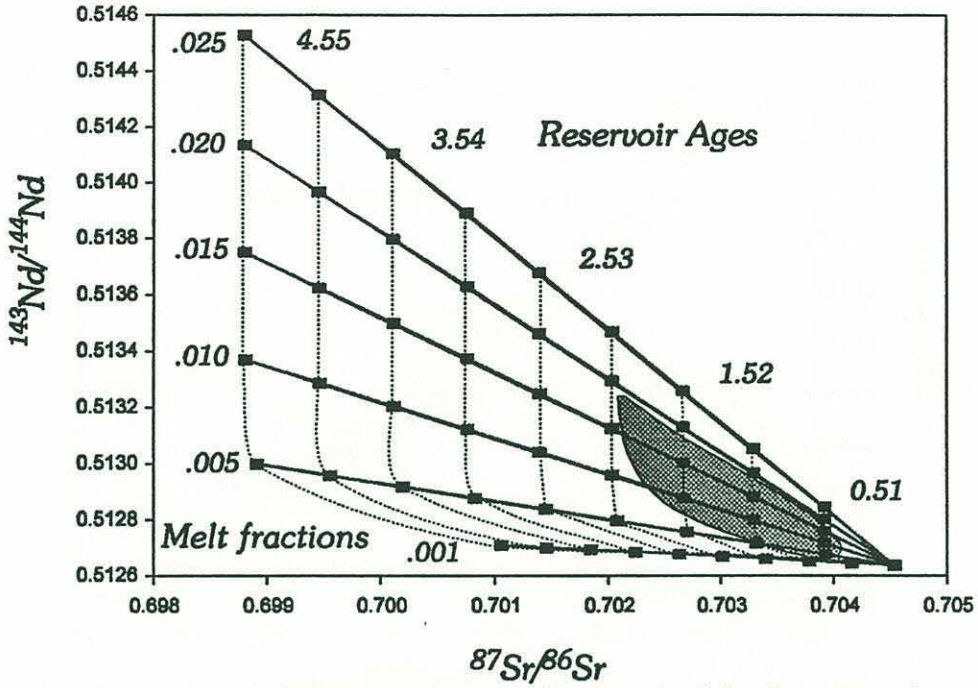

Figure 2a: Nd-Sr model depleted mantle. The purpose of this figure is to show that reasonable amounts of partial melting are sufficient to account for the Sr and Nd Isotopic composition of the sub-oceanic mantle as sampled by mid-ocean ridge basalts. Nd and Sr isotopic space is contoured for the isotopic compositions of Nd and Sr for residual mantle reservoirs of the given ages and degrees of melting. The following parameters are used:

	Sr	Nd	Os
D	.05	.022	140
D(Parent)	.001(Rb)	.03(Sm)	0.035(Re)
α	.6988	.506697	.807
μ	.086	.1967	3.36

$$\mu = \mu_0 \left[\frac{(F / D_D + (1-F))}{(F / D_P + (1-F))} \right]^n \qquad (3)$$

where F is the degree of partial melting in each increment, DD and DP are bulk distribution coefficients of daughter and parent and n is the number of increments of melting. A two-stage melting model for the secular evolution of an isotopic system in the residue can then be written:

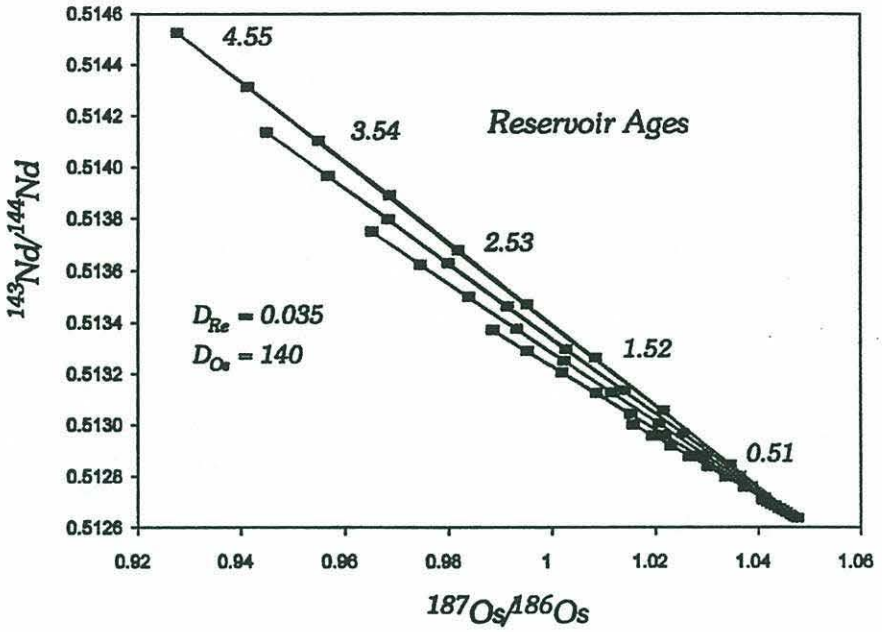

Figure 2b: Model Nd and Os in the depleted mantle. This diagram shows the isotopic compositions predicted for Nd and Os given the same model assumptions made in Figure 2a and the distribution coefficients shown for Re and Os. The distribution coefficients used are chosen to produce the greatest spread in Nd isotopic composition for a given Os isotopic composition, assuming different degrees of partial melting. More reasonable values (such as DRe=0.2 and DOs=1000, discussed in text) produce less "fanning" of the melting paths, resulting in a more linear array of possible Nd and Os isotopic compositions. This trend is compared to natural peridotite compositions in Figure 3.

$$\alpha = \alpha_0 + \mu_0\left(e^{\lambda T} - e^{\lambda t_x}\right) + \mu_1\left(e^{\lambda t_x} - 1\right) \qquad (4)$$

where a is the ratio of radiogenic daughter to a non-radiogenic isotope of the daughter element, α_0 is the initial ratio, μ_0 is the first stage parent/daughter ratio, μ_1 is the parent daughter ratio after crust extraction calculated using equation 1, tx is the age at crustal extraction and T is the age of the Earth (4.55 billion years). By varying the total degree of melting (n*F) and the time of extraction t_x of the reservoir from the bulk Earth system, the depleted mantle evolution of

any given pair of isotope systems can be modelled, if they are coupled by the crust formation process.

Figure 2a shows a model for the Nd and Sr isotopic systems constructed in this fashion. The stippled region is the range of Nd and Sr isotopic data for MORB. While the absolute values of the degree of melting and reservoir age in such a calculation are highly non-unique and model-dependent, it is plain that with reasonable values for bulk partition coefficients for the elements, such a model can easily explain the Nd and Sr isotopic variations in the depleted mantle. The spread in isotopic composition space is largely a function of the extreme incompatibility of Rb.

Using the same procedure to model the Sm-Nd and Re-Os isotopic systems (Figure 2b), it is obvious that the fanning of lines of equal melt fraction but different reservoir age observed in the previous example are not to be seen. Instead, the model predicts an extremely tight coupling of the Nd and Os isotopic systems regardless of the degree of melting. The slope of this essentially linear array can be altered by changing the model assumptions, such as the Re and Os partition coefficients, but its essential linearity cannot. Despite the incompatibility of Re, the Re/Os ratio in the residue is not sufficiently strongly affected to produce a fanning of the melt trajectories unless a bulk partition coefficient for Re less than 0.005 is used. This value for D_{Re} is almost an order of magnitude less than the lowest reasonable value (0.035, Watson, et al., 1989) and well outside of the range of conceivable partition coefficients for Re. These are shown above to be more in the range 0.1-0.5. Using a more reasonable value for D_{Re} like 0.1, the mantle array in Figure 2b becomes nearly colinear.

In Figure 3, Os and Nd data for abyssal peridotites measured in this study are plotted with the results of the model calculations. The data do not define a

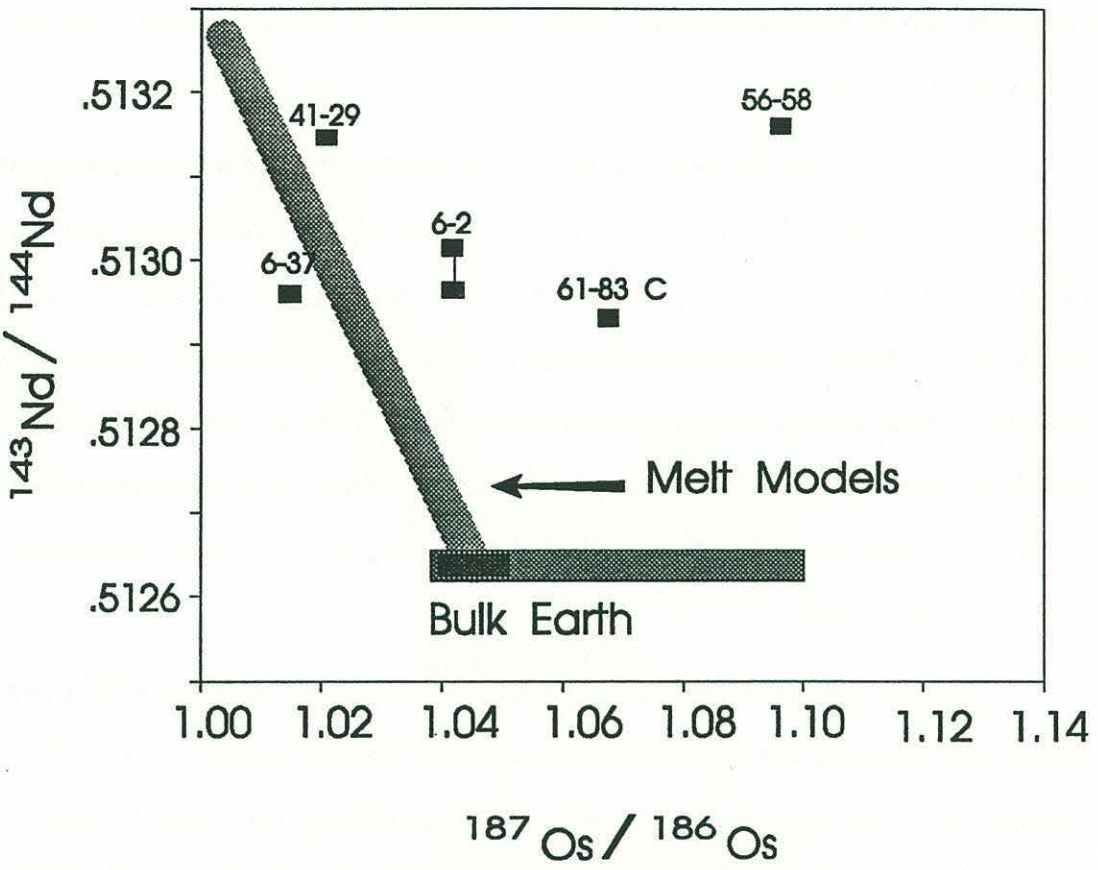

Figure 3. Os vs. Nd isotopic compositions for abyssal peridotites. Bulk Os data are plotted against clinopyroxene Nd data. Melting model shows depleted mantle compositions produced by partial melt extraction as in Figure 2a and 2b.

tightly coupled array as required by the partial melting model for the formation of the depleted mantle reservoir. Thus, partial melting cannot be the only process responsible for the variation in Re/Os and $^{187}Os/^{186}Os$ in the depleted mantle. Partial melting and crustal formation can account with difficulty for the variations of the Re-Os isotopic system alone. Coupled with the Sm-Nd system, partial melting is wholly inadequate to explain the variations seen in these abyssal peridotites.

Crustal recycling

It has long been postulated that subducted crustal material can be re-incorporated into the mantle, and could affect the compositions of mantle-derived basalts in some geologic settings. Hart and Staudigel (1982) discuss the effects which would be observed in isotope systematics if ancient crust were mixed into the mantle. Hauri and Hart (in press) extend this analysis to the specific situation of the origin of HIMU basalts (those with extremely radiogenic $^{206}Pb/^{204}Pb$, but $^{87}Sr/^{86}Sr$ and $^{143}Nd/^{144}Nd$, indicating a relatively depleted composition relative to bulk earth) from the South Pacific. The primary unknowns in such an analysis are the concentrations of Re and Os in the subducted crust. What is clear from their discussion is that Pb isotopes are a sensitive indicator of crustal recycling; an admixture of recycled crust component sufficient to change the $^{187}Os/^{186}Os$ in the depleted mantle would also change the Pb isotopic composition of the mantle to one which is too high for abyssal peridotite to be the source of mid-ocean ridge basalt. The link between abyssal peridotites and the source of mid-ocean ridge basalt is now well established (Dick, et al., 1984; Johnson, et al., 1990; Johnson and Dick, 1992). It is thus reasonable to require that any model for the formation of abyssal peridotites produce Pb isotopic ratios compatible with those of mid-ocean ridge basalts. Secondly, it is clear that the mass of subducted material recycled into the depleted mantle would have to be implausibly large for the $^{187}Os/^{186}Os$ ratios of depleted mantle rocks to be affected, unless the Re content of the subducted material is extremely high.

The Os and Re concentration of subducting oceanic crust is not well known. There are also no Pb isotopic data on abyssal peridotites (or conversely Os isotopic data on MORB). Still, it may be tentatively concluded from the data presented here that recycling of subducted oceanic crust into the upper mantle is

not a likely cause of the variations in $^{187}Os/^{186}Os$ observed in abyssal peridotites nor of their decoupling from $^{143}Nd/^{144}Nd$ ratios in these rocks.

Melt percolation

Current models of the formation of magmas at mid-ocean ridges (McKenzie and Bickle, 1988) and island arcs (Kelemen, et al., 1990, 1992) involve at least some degree of porous flow and reaction between the mantle and basaltic melts. The basaltic melt flowing through the mantle acts very much like a chromatographic column (Navon and Stolper, 1987). Trace elements move through the matrix peridotite with varying speeds, depending upon the partition coefficients of the elements between the country rock and the infiltrating basalt melt and the kinetics of elemental exchange between country rock and melt. This process may have profound implications for the comparative systematics of the Re-Os and Sm-Nd isotopic systems in the depleted mantle.

Nd, being an incompatible element will move through the matrix peridotite at a much greater rate than will Os. This may provide a mechanism for decoupling these two systems. The ratio of D_{Os} to D_{Nd} is several orders of magnitude, rather than less than one order of magnitude, as it is for other elements. Os and Nd systematics may be decoupled from each other while the systematics of Nd and the other incompatible isotope systems (Sr, Pb, Hf) may remain coupled. This hypothesis is an extension of one discussed in Chapter Three: Measurements of Nd isotopes in any residual peridotite may represent merely the last magmatic Nd composition that the peridotite saw, while the Os isotopic composition records only the *in situ* decay of the Re in the peridotite, with no exogenous component.

The degree of decoupling depends strongly on the distance which melts travel during porous flow. Once the transition is made from porous flow to

channelized flow in dikes, it becomes more difficult for the melt to dominate the incompatible element budget of the wall rock peridotite. If the length scale of porous flow is only a few meters before dike injection occurs, then there may be little disruption of Nd, Sr, Hf and Pb isotopes. If, on the other hand, melts rising from great depths are still interacting with the shallow mantle in a porous flow regime (e.g., Whitehead, et al., 1984; Dick, 1989; Elthon, 1992), then the mass budget of the incompatible isotopes in a given abyssal peridotite may be completely dominated by material which originated relatively recently in a completely different region of the mantle (Dick, 1989).

The arguments against a major role for porous flow redistribution of elements in the isotopic evolution of the depleted mantle remain largely speculative at this point. Kelemen, et al. (1992) studied mantle peridotites from a variety of tectonic settings, concluding that wall rock reaction was a pervasive characteristic of sub-continental and sub-arc mantle. Mid-ocean ridge abyssal peridotites are compatible in their major and trace element compositions with a largely residual origin. This suggests that the porous flow length scale in the sub-oceanic mantle is short, and that reaction between wall rock and basalt does not greatly affect mid-ocean ridge abyssal peridotites. The data of Johnson, et al. (1990) also lend themselves to this conclusion. It is likely that the process of transport would integrate melts to some degree, especially if that transport were from great distances. Many of the residual mantle trace element compositions that Johnson, et al. (1990) studied could not have been in equilibrium with integrated melts from elsewhere in the mantle. This suggests that significant melt-borne resetting of incompatible trace element rations did not occur.

The question of whether incompatible trace element ratios are reset in the residue during the melting process is at this point impossible to answer. Many

studies have shown (Whitehead, et al., 1984; McKenzie, 1984; Navon and Stolper, 1987; Kelemen, et al., 1990; Kelemen, et al., 1992) that porous flow in the mantle is likely to be a significant phenomenon. If porous flow does significantly affect incompatible trace element compositions, then the only elements not affected by this process would be the compatible elements. The only unaffected isotopic system would then be the Re-Os isotopic system. Further detailed field investigation of alpine and oceanic massif peridotites coupled with isotopic and trace element investigation will be required to even begin to address this problem.

Comparison with continental xenoliths

It is important to compare the results gathered here from abyssal peridotites with those from the sub-continental mantle. The subcontinental mantle is presumed to have an important component which corresponds to the depleted suboceanic source of abyssal peridotite. Second, many of the processes (melt percolation, partial melting) which abyssal peridoties may have undergone have been studied also in xenoliths. The comparison may be inappropriate to the extent that the xenoliths have undergone processes (mantle metasomatism, interaction with host kimberlite) which are not found in the sub-ocenaic mantle.

Walker, et al. (1989) studied Nd and Os isotopic systematics in mantle xenoliths from South Africa. The Nd data in that study revealed a considerable complexity in the geologic history of the samples, as many of the samples showed either unrealistically old or future Nd two point clinopyroxene and whole rock ages. Those samples cannot have recorded Nd isotopic equilibrium between the clinopyroxene and the remainder of the rock. Two other samples in that study (1033 and 5267) yielded garnet plus whole rock two point isochrons

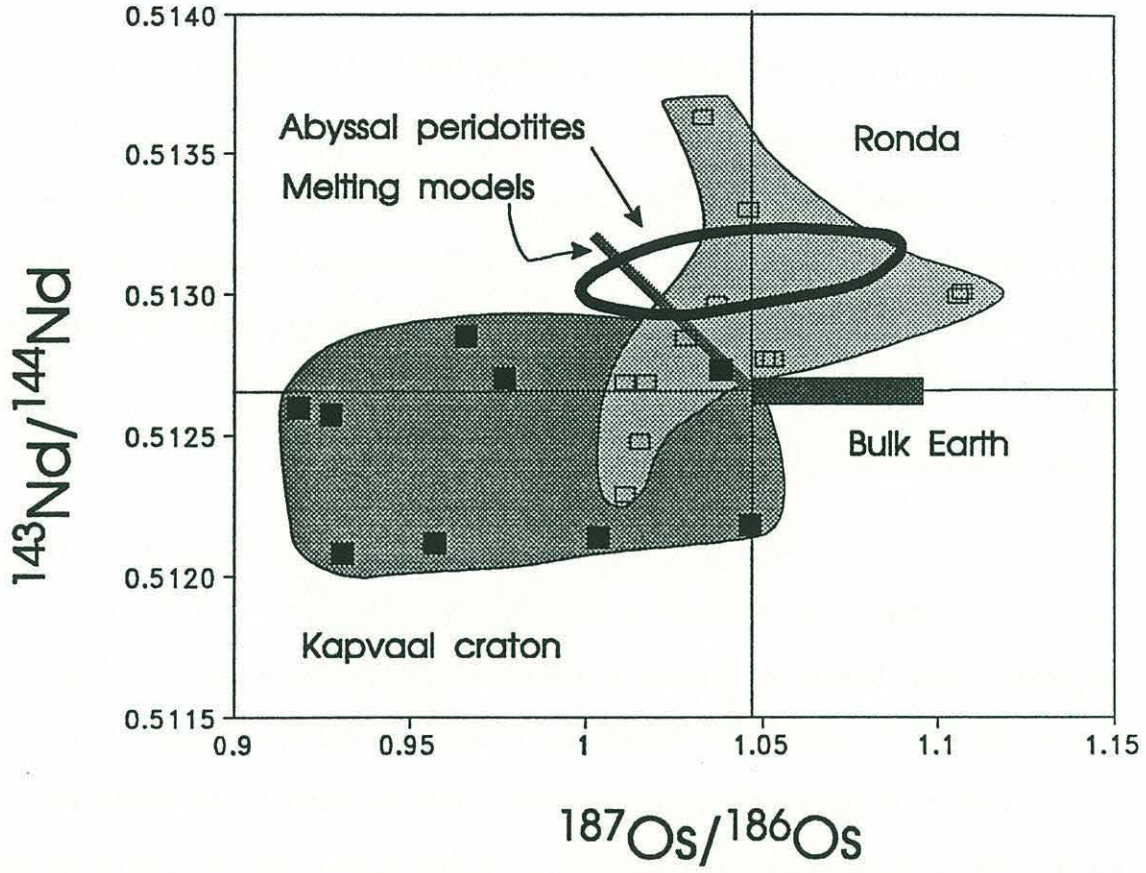

Figure 4: Os and Nd isotopic compositions in South African and Ronda peridotites. Data from Walker, et al., 1989, Reisberg, et al., 1991 and this study.

which were very close to the eruption ages of their host kimberlites, indicating that those samples were in mineral equilibrium (but may also have been in equilibrium with their host kimberlite).

Ignoring these complications for a moment, when the samples from this study are plotted with those of Walker, et al. (1989) (Figure 4), it becomes clear that there is very little overlap in either Os or Nd isotopic space between the two data sets. The locus of possible Os and Nd isotopic compositions that can be produced during varying degrees of incremental batch melting at different ages is also shown. If the abyssal peridotite data are included in the xenolith data set, as well as the orogenic lherzolite data from Ronda of Riesburg et al. (1991), a

vague elongation of the $^{187}Os/^{186}Os$ and $^{143}Nd/^{144}Nd$ data field emerges that has a positive slope. Though this is not much of a correlation, the high $^{187}Os/^{186}Os$ samples also have high $^{143}Nd/^{144}Nd$, and vice-versa. This is exactly opposite to the relationship to be expected if the values of their respective parent-daughter ratios are set by a partial melting process over time. Instead, some other process appears to dominate the continental mantle data.

The effect of mantle metasomatism

The influence of metasomatic fluids has frequently been called upon to explain trace element and isotopic patterns in mantle xenoliths (cf. Stosch and Lugmair, 1984). Many of the rocks in the Walker, et al. (1989) study had plainly been exposed to metasomatic disturbance of their Sm-Nd systematics, so that it is reasonable to speculate that metasomatic processes may be responsible for much of the variation in the Nd isotopic system in these rocks. A metasomatic fluid would be likely to have very low Sm/Nd and high Re/Os because of the general affinity of Re for incompatible elements. Such a fluid, because of its high REE concentrations would have tremendous leverage over the Sm/Nd ratio. Conversely, because of the high Re and Os concentrations in the residue, the Re/Os ratio would remain unaltered. This may be a mechanism for decoupling the Re-Os and Sm-Nd isotopic systems, but runs contrary to the observed pattern in the isotopic data from metasomatized peridotites shown in Figure 4.

$^{187}Os/^{186}Os$ ratios less than about 1.1 are only known from peridotites which have experienced metasomatism (Walker, et al., 1989; Reiberg, et al., 1991). This association is suggestive of a mechanism for the linkage of metasomatism and the Re-Os systematics of the mantle. Hartmann and Wedepohl (in press) provide an example of this phenomenon in orogenic lherzolites from northern Italy. In that study, essentially two groups of

lherzolites could be identified; unmetasomatized peridotites, none of which had greater than 30 ppm. K or less than 100 ppm. S, and metasomatized peridotites which had higher K abundances, but less than 100 ppm. S. In other words, the metasomatized peridotites were uniformly low in sulfur (in the form of sulfide).

The behavior of Re and Os with respect to metamorphic fluids is, of course, completely unknown, and so far there are few studies in which Re-Os systematics are studied along with S and other chalcophile element concentrations in mantle rocks. A mechanism for the evolution of the low $^{187}Os/^{186}Os$ peridotites of Walker, et al., 1989 and Reisberg et al., 1991 can be postulated if it is assumed that interaction with a metasomatic fluid strips the mantle of Re. If the metasomatic event is sufficiently ancient, then low $^{187}Os/^{186}Os$ ratios observed in these rocks can be frozen in. The low $^{143}Nd/^{144}Nd$ and high $^{87}Sr/^{86}Sr$ values of the metasomatized peridotites then have time to grow in. This hypothesis is worthy of further testing.

Alternatively, it has been noted that metasomatism is a process involving primarily the highly incompatible elements. Metasomatism commonly seems to affect depleted peridotites (harzburgites) more often than fertile ones. Moderately incompatible elements (including S and presumably Re) remain depleted in such rocks, while highly incompatible elements are added by the invading metasomatic fluid.

A core formation model for the Re-Os isotopic system.

The melting hypotheses illustrated in the preceding sections can be reconciled with the observations if there is some initial Re/Os heterogeneity in the mantle prior to the melt extraction events. In such a hypothesis, the melting vectors in Figures 3 and 4 originate not at a single Bulk Earth Os isotopic com-

Table 3: Partition Coefficients used in core extraction model.

Element	Silicate solid/ silicate melt	Solid Metal/ Liquid metal	Liquid silicate/ Liquid metal
Rb	.0001	-	-
Sr	.007	-	-
Sm	.038	-	-
Nd	.022	-	-
Mo	.01	2.45	.0008
W	.01	36	1
Co	3	2.3	.007
Re	.2	83	.0005
Os	1000	83	.00005
Ir	1000	83	.00005

Sources:
Rb, Sr: Cox, et al., (1979) Sm, Nd: Johnson, et al., (1990) Re, Os discussed in text. All others: Jones and Drake (1986).

position, but at a family of original Os isotopic compositions, ranging from 1.04 to 1.1, as shown by the heavily shaded bar representing the Bulk Earth in those figures. This section will attempt to demonstrate one way in which a commonly invoked model for the formation of the Earth's core could account for both the lack of correlation of Os and Nd isotopes in the depleted mantle and for the range of Os isotopes seen today in the depleted mantle.

Extraction of Os preferentially to the core has the ability to raise the Re/Os ratio of the residual mantle. It is arguable that core formation may be at least as efficient at changing the Re/Os ratio of the mantle as the extraction of a silicate melt (Jones and Drake, 1986, and the assumption that Os and Ir behave in a geochemically similar fashion). In this case, $^{187}Os/^{186}Os$ and Re/Os need not correlate with the degree of later melt extraction. $^{187}Os/^{186}Os$ would also not necessarily correlate with $^{143}Nd/^{144}Nd$, as Sm/Nd ratios are unaffected by core extraction.

Table 4: Model siderophile concentrations.

Element	CI comp.	D LS/LM	Compl. Equil. Mantle	Stage 2 Mantle	Mantle after S2 mixing	PUM: .8CM+ .19 S2+ .01 CI	"Real" Mantle
W	1	1	1	1	1	1	.11
Re	1	5x10-4	5x10-4	5x10-4	5x10-4	.01	.0075
Os	1	5x10-5	5x10-5	5x10-5	5x10-5	.01	.0075
Ir	1	5x10-5	5x10-5	5x10-5	5x10-5	.01	.0075
Mo	1	.0008	.0008	.317	.06	.073	.064
Ni	1	.0002	.0002	1	0.2	.208	.19
Co	1	.007	.007	1	0.2	.214	.21
Au	1	.0001	.0001	.0001	.0001	.010	.02
(Re/Os)n	1	-	10	10	10	1.04	1.00
(Ni/Os)n	1	-	4	20000	4003	20.71	25.33
(Co/Os)n	1	-	140	20000	4112	21.25	28.0
(Au/Os)n	1	-	2	2	2	1.00	2.67
Re/Os	.085	-	.844	.844	.844	.088	.084
$^{187}Re/^{186}Os$	3.34	-	33.4	33.4	33.4	3.49	3.34
$^{187}Os/^{186}Os$	1.046	-	3.199	3.199	3.199	1.057	1.046

All concentrations shown normalized to chondrites. Completely equilibrated mantle is assumed to be in equilibrium with a Metal + sulfur pphase which has completely segregated. The Stage 2 mantle after the extraction of a few percent of metal, leaving the bulk of the first series transition metals unaffected, but stripping siderophiles such as Re, Os and Ir efficiently. Primitive upper mantle compositon shown by mixong of 80% completely equilibrated mantle, 19% stage 2 mantle and 1% late arriving chondrites. "Real Mantle" for comparison is form Morgan (1986), Jones and Drake (1986).

In order to get around problems posed by the recent episode of crust formation, another element can be used in place of Re to evaluate the model. Of the elements measured in the course of this study, Co is a compatible siderophile (see Table 3). Even large degrees of partial melting are unlikely to affect the Co/Os ratio of the mantle to any great extent. The difference in silicate-metal partitioning between Co and Os is nearly as great as that between Re and Os. Thus, the fractionation of Co/Os and Re/Os during core formation as postulated by this model should be coupled. While the Re/Os ratio might be affected by late melting events (such as the most recent one beneath the ridge), the Co/Os ratio should remain unaffected.

With time, then, the $^{187}Os/^{186}Os$ ratio should be correlated to the Co/Os ratio, providing a test of the hypothesis. Figure 5 shows $^{187}Os/^{186}Os$ vs. Co/Os (normalized to chondrites) for the abyssal peridotites in this study compared to those from the model calculations just described. These data are at least permissive of this model given the uncertainties in their collection. Since Sm and Nd are incompatible lithophile elements, and do not partition into the liquid metal or sulfide phase, their ratios, and hence the $^{143}Nd/^{144}Nd$ ratio, would not be expected to correlate with $^{187}Os/^{186}Os$.

The model of Wänke (1981) and Morgan, et al. (1981) involving three stages of accretion and two of core formation can explain much of the variation in the $^{187}Os/^{186}Os$, $^{143}Nd/^{144}Nd$, and trace element data measured in the course of this study. Jones and Drake (1986) point out problems with this model on the basis of P and W concentrations, the amount of S in the mantle and the oxygen fugacity of the mantle during core formation (Jones and Drake, 1986). I do not intend to postulate this model as the correct one for describing the accretion history of the Earth. I do, however, wish to show how the Re/Os isotopic system can potentially be used as a sensitive and resilient marker of processes involving silicate-metallic liquid fractionation in the mantle.

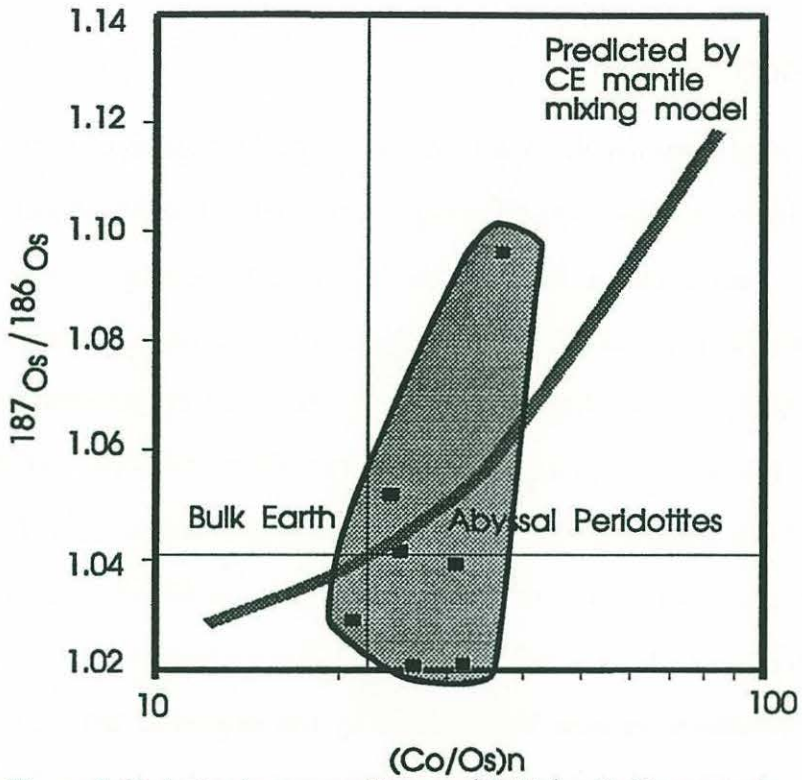

Figure 5: Os isotopic composition vs. (Co/Os)n. Co/Os normalized to Chondrites. Curve shown is the model discussed in the test which involved mixing of a late stage chondritic "veneer" with a core-extracted (CE) mantle.

Conclusions

This study reports the results of an Nd and Os isotopic investigation of abyssal peridotites. These samples represent part of the depleted mid-ocean ridge upper mantle, and as such are useful for constraining the evolution of the depleted mantle. A partial melting process alone can explain the Re-Os systematics of the mantle only with great difficulty, and requires extreme assumptions about the mean age of the Earth's crust, the partition coefficient of Re during melting and the bulk Os isotopic composition of the Earth. The Nd and Os isotopic systems taken together do not yield a tight correlation of isotopic compositions. Such a correlation would be required if the parent to daughter ratios of these two systems were both determined by the degree of partial melting during the formation of the Earth's crust. Thus, partial melting cannot be the only process which determines the Re/Os ratio in the Earth's mantle. Another process is required which is not linked to partial melting to explain the variations in the Re-Os system independently from the Sm-Nd isotopic system.

There are several processes which have the potential for decoupling the Re-Os and Sm-Nd isotopic systems and producing the variations seen in the data from this study and others. Crustal recycling is unlikely to have a strong effect on the depleted mantle, due to the enrichment of Os in the depleted mantle and the enrichment of highly radiogenic Pb in the recycled component; an amount of admixed ancient crust sufficiently large as to affect the Os isotopic composition of the depleted mantle would make it so radiogenic in Pb that it could not be the source of MORB.

Percolation of melts through the mantle and their reaction with the peridotite wall rock (Navon and Stolper, 1987; Kelemen et al., 1990, 1992) can significantly decouple the Nd and Os systematics of the host mantle, though the evi-

dence indicates that the reaction of wall rock and basaltic melt during porous flow is not a prevalent process at mid-ocean ridges (Kelemen, et al., 1992).

Planetary differentiation into mantle and core is a process which theoretically can strongly fractionate all the siderophile elements, including Re and Os (cf. Jones and Drake, 1986) from the lithophile elements such as Sm and Nd. A core formation model involving three stages of accretion and two of core segregation (Chou, 1978, Jagoutz, et al., 1979, Morgan, et al., 1981, Schmitt, et al. 1989) can explain many aspects of the siderophile and chalcophile element abundances in the mantle. The data from this study are consistent with the conclusions of that model. Combined with partial melting and crust formation, core formation provides the ability to simultaneously explain the variations of $^{187}Os/^{186}Os$ isotopic compositions, the lack of correlation of $^{187}Os/^{186}Os$ and $^{143}Nd/^{144}Nd$, and the weak correlation of $^{187}Os/^{186}Os$ with (Co/Os)n. Such a combined crust formation and core segregation model would also solve the major problems inherent in a melting-only model for the evolution of the Re-Os isotopic system by itself: It would allow the bulk Earth to have a chondritic Re/Os and $^{187}Os/^{186}Os$ ratio, would not require Re to be highly incompatible during melting, and would not require an older mean crustal age to account for the Re-Os systematics than for any other isotopic system.

Core formation models such as the one discussed here are necessarily highly non-unique and extremely difficult to test. The Re-Os isotopic systematics described here may provide a means, along with the relative abundances of the moderately siderophile and highly siderophile elements, of constraining such models.

Acknowledgments:

This work benefited from discussions with R. Teng, G. Ravizza, E. Hauri and K. Turekian. This work was funded in its early phases by an NSF Graduate Fellowship to JES, and later by a WHOI Ocean Ventures Fund grant to JES.

References

Allègre, C.J., and J.M. Luck (1980) Osmium isotopes as petrogenetic and geochemical tracers **Earth and Planetary Science Letters** 48:148-154.

Anders, E and M. Ebihara, (1982) Solar system abundances of the elements **Geochimica et Cosmochimica Acta** 46:2363-2380.

Bonatti, E., and P.R. Hamelyn, (1981) Oceanic ultramafic rocks in: C. Emiliani (ed.) **The Oceanic Lithosphere** pp. 241-283. John Wiley, New York.

Bottinga Y., and C. J. Allègre, (1978) Partial melting under spreading ridges, **Philosophical Transactions of the Royal Society of London**, Series A 288:501-525.

Chou, C.-L. (1978) Fractionation of siderophile elements in the Earth's upper mantle **Proceedings of the Ninth Lunar and Planetary Science Conference** 219-230.

Chou, C.-L., Shaw, D and Crockett, J.M. (1978) Siderophile trace elements in the Earth's oceanic crust and upper mantle. Proceedings of the Thirteenth Lunar and Planetary Science Conference, Part 2: **Journal of Geophysical Research**, Vol. 88, Supplement. pp. A507-A518.

Creaser, R.A., D.A. Papanastassiou and G.J. Wasserburg (1991) Negative thermal ion mass spectrometry of osmium, rhenium and iridium **Geochimica et Cosmochimica Acta** 55:397-401.

Depaolo, D.J and Wasserburg, G.J. (1979) Petrogenetic mixing models and Nd-Sr isotopic patterns **Geochimica et Cosmochimica Acta** 43:615-617.

Dick, H.J.B., Fisher, R. and Bryan, W.B. (1984) Mineralogic variability of the uppermost mantle along mid-ocean ridges **Earth and Planetary Science Letters** 69:88-106.

Dick, H.J.B. (1989) Abyssal Peridotites, Very-Slow Spreading Ridges and Ocean Ridge Magmatism. in: Magmatism in the Ocean Basins edited by A.D. Sanders and M.J. Norry, **Journal of the Geological Society of London Special Publication No. 42**: pp. 75-109

Elthon, D. (1992) Chemical trends in abyssal peridotites: refertilization of depleted suboceanic mantle. **Journal of Geophysical Research** 97:9015-9025.

Gast, P.W., (1968) Trace element fractionation and the origin of tholeiitic and alkaline magma types **Geochimica et Cosmochimica Acta** 32:1056-1086.

Green, D.H. and A.E. Ringwood, (1967) The genesis of basaltic magma **Contributions to Mineralogy and Petrology** 15:103-190.

Hart, S.R., J.-G. Schilling and J. Powell (1973) Basalts from Iceland and along the Reykjanes Ridge: Sr isotope geochemistry **Nature and Physical Science** 246:104-107.

Hart, S.R. and H. Staudigel, (1982) The control of alkalis and uranium in sea water by ocean crust alteration **Earth and Planetary Science Letters** 58:202-212.

Hart, S.R. and H. Staudigel, (1989) Isotopic characterization and identification of recycled components, NATO ASI series in: **Crust/mantle recycling at convergence zones** Reidel, 1989.

Hart, S.R., and A. Zindler (1986) In search of a bulk-Earth composition **Chemical Geology** 57:247-267.

Hartmann, G. and K.H. Wedepohl, (in press) the origin and composition of peridotite tectonites from the Ivrea complex (N-Italy) representing material at different stages of depletion **Geochimica et Cosmochimica Acta**

Hattori, K and Hart, S. (1991) Osmium-isotope ratios of platinum-group minerals associated with ultramafic intrusions: Os-isotopic evolution of the oceanic mantle. **Earth and Planetary Science Letters** 107:499-514.

Hauri, E.H. and S.R. Hart (in press) Re-Os isotope systematics of HIMU and EMII oceanic island basalts from the South Pacific Ocean **Earth and Planetary Science Letters**

Hébert, R., D. Bideau and R. Hekinian (1983) Ultramafic and mafic rocks from the Garrett Transform Fault near 13o 20'S on the East Pacific Rise: igneous petrology. **Earth and Planetary Science Letters** 65:107-125.

Hertogen, J., Janssens, M.-J., and Palme, H. (1980) Trace elements in ocean ridge basalt glasses: implications for fractionations during mantle evolution and petrogenesis **Geochimica et Cosmochimica Acta** 44:2125-2143.

Ito, K. and Kennedy, G.C. (1967) Melting and phase relations in natural peridotite to 40 kilobars American Journal of Science 265:519-538

Jagoutz, E., H. Palme, H. Baddenhausen, K. Blum, M. Cendales, G. Dreibus, B. Spettel, V. Lorenz and H. Wänke (1979) The abundances of major, minor and trace elements in the Earth's mantle as derived from primitive ultramafic nodules **Proceedings of the Tenth Lunar and Planetary Science Conference** pp. 2031-2050.

Jaques A.L. and Green, D.H. (1979) Determination of liquid compositions ion experimental, high pressure melting of peridotite **American Mineralogist** 64:1312-1321.

Johnson, K.T.M., Dick, H.J.B. and Shimizu, N. (1990) Melting in the oceanic upper mantle, an ion microprobe study **Journal of Geophysical Research** 95:2661-1678.

Johnson, K.T.M. (1990) Trace Element Geochemistry of Oceanic Peridotites and Silicate Melt Inclusions: Implications for Mantle Melting and Ocean ridge Magmagenesis Ph.D. Thesis. MIT/WHOI, WHOI-90-36.

Johnson, K.T.M. and H.J.B. Dick (1992) Open system melting and temporal and spatial variation of peridotite and basalt at the Atlantis II Fracture Zone. **Journal of Geophysical Research** 97:9219-9241.

Jones, J.H. and M.J. Drake (1986) Geochemical constraints on core formation in the Earth **Nature** 322:221-228.

Kelemen, P., K.T.M Johnson, A.J. Irving and R.J. Kinzler (1990) High-field-Strength element depletions in arc basalts due to mantle-magma interaction **Nature** 345:521-524.

Kelemen, P., Henry J.B. Dick and J.E. Quick (1992) Formation of harzburgite by pervasive melt/rock reaction in the upper mantle. **Nature** 358:635-641.

Kinzler, R. and Grove, T. (1992) Primary Magmas of Mid-Ocean Ridge Basalts 1. Experiments and Methods **Journal of Geophysical Research** 97 :6885-6906.

Kinzler , R. and Grove, T., (1992) Primary Magmas of Mid-Ocean Ridge Basalts, 2. Applications **Journal of Geophysical Research** 97:6907-6926.

Lindner, M., D.A. Leich, R.J. Borg, G.P. Russ, J.M. Bazan D. Simons and A.R. Date (1986) Direct laboratory determination of the ^{187}Re half-life. **Nature** 320:246-248.

Luck, J.M., and C.J. Allègre (1983) ^{187}Re-^{187}Os systematics in meteorites and cosmochemical consequences **Nature** 302:130-132.

Luck, J.M., and K.K Turekian (1983) Osmium-^{187}/Osmium-^{186} in Manganese Nodules and the Cretaceous-Tertiary Boundary **Science** v?:613-615, 11 Nov. 1983.

Martin, C.E., (1990) Rhenium-Osmium Isotope Geochemistry of the Mantle. Ph.D. Thesis, Yale University.

Martin, C.E., (1991) Osmium isotopic characteristics of mantle-derived rocks **Geochimica et Cosmochimica Acta** 55:1421-1434.

McKenzie, D., and Bickle, M., (1988) The volume and composition of melt generated by extension of the lithosphere. **Journal of Petrolgy** 29:625-629.

Michael, P. and Bonatti, E. (1985) Peridotite compositions from the North Atlantic: regional and tectonic variations and implications for partial melting. **Earth and Planetary Science Letters** 73:91-104.

Miyashiro, A., F. Shido, and Ewing, M. (1969) Composition and origin of serpentinites from the Mid-Atlantic ridge near 24° and 30° North latitude. **Contributions to Mineralogy and Petrology** 23:117-127.

Morgan, J.W., and J.F. Lovering (1967a) Rhenium and Osmium abundances in chondrite meteorites **Geochimica et Cosmochimica Acta** 31:1893-1909.

Morgan, J.W., and J.F. Lovering (1967b) Rhenium and osmium abundances in some igneous and metamorphic rocks **Earth and Planetary Science Letters** 3:219-224.

Morgan, J.W., G. Wandless, R. Petrie, and A. Irvine (1981) Composition of the Earth's upper mantle - I. Siderophile trace elements in ultramafic nodules. **Tectonophysics** 75:47-67.

Morgan, J.W. (1986) Ultramafic Xenoliths: Clues to the Earth's Accretionary History **Journal of Geophysical Research** 91,B12:12375-12387.

Navon, O. and E. Stolper (1987) Geochemical consequences of melt percolation: the upper mantle as a chromatographic column. **Journal of Geology** 95:285-307.

Newsom H.F., and H. Palme (1984) the depletion of siderophile in the Earth's mantle: new evidence from molybdenum and tungsten **Earth and Planetary Science Letters** 68:354-364.

Reisberg, L., Allègre, C. and Luck, J-M. (1991) the Re-Os systematics of the Ronda Ultramafic Complex of southern Spain. **Earth and Planetary Science Letters** 105:196-213.

Schilling, J.-G. (1971) Sea-floor evolution- rare earth evidence: **Philosophical Transactions of the Royal Society of London** A268:663-706.

Schilling, J.-G. (1973) Iceland mantle plume: geochemical evidence along Reykjanes Ridge **Nature** 242:565-571.

Schilling, J.-G. (1973) Afar mantle plume: geochemical evidence. **Nature and Physical Science** 242:2-5.

Schmitt, W., H. Palme, and H. Wänke (1989) Experimental determination of metal/silicate partition coefficients for P, Co, Ni, Cu, Ga, Ge, Mo, and W and some implications for the early evolution of the Earth. **Geochimica et Cosmochimica Acta** 53:173-185.

Stosch H.G. and G.W. Lugmair (1984) Evolution of the lower continental crust; granulite facies xenoliths from the Eifel, West Germany **Nature** 311:368-370.

Sun, S.S., (1982) Chemical composition and origin of the Earth's primitive mantle **Geochimica et Cosmochimica Acta** 46:179-192.

Sun, S.S. (1985) Multistage accretion and core formation of the Earth **Nature** 313:628-629.

Walker, R.J., Carlson, R.W., Shirey, S.B., and Boyd, F.R. (1989) Os, Sr, Nd and Pb isotope systematics of southern Africa peridotite xenoliths: Implications

for the chemical evolution of subcontinental mantle **Geochimica et Cosmochimica Acta** 53:1583-1595.

Walker, R.J., Shirey, S.B., and Stecher, O. (1988) Comparative Re-Os, Sm-Nd and Rb-Sr isotope and trace element systematics for Archean komatiite flows from Munro township, Abitibi belt, Ontario **Earth and Planetary Science Letters** 87:1-12.

Walker, R.J. and Morgan, J.W. (1989) Rhenium-Osmium Isotope Systematics of Carbonaceous Chondrites **Science** 243:519-522.

Wänke, H., (1981) Constitution of the terrestrial planets. **Philosophical transaction of the Royal Society of London.** A303:287-302.

Watson, E.B., Othman, D.B., Luck, J-M. and Hofmann, A. W. (1987) Partitioning of U, Pb, Cs, Yb, Hf, Re, and Os between Chromian diopsidic pyroxene and haplobasaltic liquid. **Chemical Geology** 62:191-206.

Whitehead, J.A., Dick, H.J.B., and Schouten H. (1984) A mechanism for accretion under spreading centers. **Nature** 312:146-148.

Zindler, A., S.R. Hart, F.A. Frey, and S.P. Jacobsen (1979) Nd and Sr isotope ratios and rare-earth element abundances in Reykjanes Peninsula basalts: evidence for mantle heterogeneity beneath Iceland **Earth and Planetary Science Letters** 45:249-262.

Zindler, A. and S.R. Hart (1986) Chemical Geodynamics **Annual Review of Earth and Planetary Sciences** 14:493-571

Chapter 5: Conclusions

Chapter 5: Conclusions

This thesis has been a study of the composition of the mid-ocean ridge upper mantle with respect to isotopes, major elements, and trace elements. The first section includes a study of the effects of fracture zones on the petrogenesis of mid-ocean ridge basalt (Chapter Two). This subject is intimately intertwined with that of mantle composition as studied through the compositions of mantle-derived basalts. In Chapter Three studies the submarine alteration of abyssal peridotite along with its effects on major elements and isotope systems. the various isotope reservoirs are studied in order to yield useful information about their number, origin and techniques for their analytical separation. Particular attention is paid to the separation, identification and analysis of the mantle reservoir, on which Chapter Four is based. The final chapter examines the Os and Nd isotopic characteristics of the sub-oceanic upper mantle and their implications for crustal formation, core extraction and the isotopic evolution of the mantle over the history of the Earth.

Genesis of ocean ridge basalts and major tectonic features.

The transform fault effect (Fox, et al., 1980; Natland and Melson, 1980; Stroup and Fox, 1981; Bender, et al., 1983; Langmuir and Bender, 1983) is a paradigm for understanding the genesis of magmas erupted close to transform faults on the mid-ocean ridge system. Juxtaposition of relatively old lithosphere with the young rift system at a ridge transform intersection has a thermal effect on the melting regime beneath the rift immediately adjacent to the transform (Natland and Melson, 1980; Stroup and Fox, 1981; Fox and Gallo, 1984). The purpose of Chapter Two is to examine critically the evidence for a

transform fault effect at the Atlantis II Fracture Zone and at other documented fracture zones.

Three important issues must be addressed with regard to any basalt data set from a fracture zone before the evidence for a transform fault effect can be evaluated. First, the geologic setting of the samples must be carefully documented, in the context of an overall understanding of the geology of the area. Second, calculated liquid lines of descent for the rift near and far from the transform must be permissive of a generally similar crustal-level fractionation history. Steps must be taken in the interpretation of the data to shut out the effects of low and moderate pressure fractionation from affecting the analysis. Third, isotopic study of the basalts in question must be permissive of their derivation from similar mantle sources.

No previous study purporting to demonstrate a transform fault effect (Natland and Melson, 1980, Bender, et al., 1984, Perfit, et al., 1983, Langmuir and Bender, 1984) has adequately addressed more than two of the above criteria. All of these are necessary, but not in themselves sufficient to rule out effects on the liquid line of descent related to mantle compositional heterogeneity. The Atlantis II Fracture Zone provides a limiting case for the study of mantle thermal effects. Its age offset is very great, its geology has been studied in detail (Dick, et al., 1991), and combined elemental and isotopic analysis provide the best yet understanding of all of the issues of source heterogeneity, tectonic setting, and high level crustal fractionation identified here. For these reasons, the transform fault effect observed at the Atlantis II Fracture Zone should be the maximum observable transform fault effect.

When combined with isotopic and morphologic information, the major element data indicate that the Atlantis II Fracture Zone transform volcano is

the product of a lower degree of partial melting than the adjacent ridge segment. The lowered degree of partial melting is interpreted as the result of a transform fault effect. The calculated magnitude of that thermal effect, however, is small relative to that calculated for other fracture zones, given the great age offset of the Atlantis II Fracture Zone.

When temperature offsets at fracture zones are compared to the expected thermal effect, no clear trend emerges. At the very least, the thermal offset should increase steadily with age offset, which it does not. We conclude from this that the variations in liquid lines of descent produced by random fluctuations in mantle sources, mantle upwelling, and polybaric fractionation are significant compared to those expected from transform fault thermal effects. Greater care in sampling, study of the geologic setting, documentation of polybaric fractionation effects and mantle source heterogeneity in each area are necessary before transform fault-related thermal effects on the genesis of magmas can be separated from purely compositional effects.

Seafloor alteration and the isotopic compositions of altered mantle rocks.

Seafloor alteration and crustal level alteration of abyssal peridotites have a dramatic effect on the mineralogy and the compositions of these rocks. The isotopic compositions of Sr, Nd and Os in abyssal peridotite are a combination of the various reservoirs of those elements within the peridotite. In order to understand the genesis of those reservoirs, isotopic analyses of bulk rocks, mineral separates and leachates were carried out. Major element, trace element and mineralogical analyses of the rocks and their alteration products were also conducted.

Chapter Three reports the results of a number of interrelated experiments and measurements on altered abyssal peridotites which were carried out with one overriding aim: to assess the effect of alteration on the major element composition of the rocks and on the isotopic systems, Os, Nd and Sr in abyssal peridotites. In addition, this information will help to assess the feasibility and validity of examining the isotopic systematics of the individual isotopic reservoirs, particularly the mantle reservoir. Also reported and discussed are several other observations made which are relevant to the alteration of abyssal peridotite.

The most notable aspect of abyssal peridotite compared to other classes of peridotite is its high degree of hydrous alteration, or the progress of the reaction olivine + enstatite + water <-> serpentine + magnetite ($\pm$ brucite $\pm$ talc). One frequently overlooked aspect of this alteration is the significant mass redistribution which occurs as a result, particularly of Mg. Bulk compositions of abyssal peridotites generally fall on an Mg extraction line relative to their reconstructed unaltered compositions. Given the general insolubility of Mg-bearing phases in seawater, this result is somewhat at odds with what is known about the chemistry of seawater and hydrothermal solutions and with the temperature of alteration assumed for abyssal peridotites. Mg bearing minerals are particularly insoluble in seawater at moderate and high temperatures. One is drawn inescapably to the conclusion that the alteration of abyssal peridotite includes both serpentinization and weathering, which occurs at lower temperatures and higher water/rock ratios than are typically assumed for serpentinization.

The Rb-Sr isotopic system is extremely sensitive to seawater alteration. This is so even in basalts, which have much higher concentrations of Rb and Sr

than the residual peridotites studied here. In peridotites, the situation is greatly aggravated by the low concentration and high degree of alteration of the rocks; only the freshest of abyssal peridotites had whole rock $^{87}Sr/^{86}Sr$ significantly lower than that of seawater. Aggressive leaching of clinopyroxene can, in many cases reduce the measured $^{87}Sr/^{86}Sr$ to a value reasonable for the depleted mantle, but there is no way of determining the extent of residual contamination for any individual analysis. The leached $^{87}Sr/^{86}Sr$ compositions are nearly meaningless as regards the isotopic composition of the mantle. No attempt is made to relate the leached clinopyroxene $^{87}Sr/^{86}Sr$ compositions directly to mantle systematics.

The Sm-Nd isotopic system is much more robust during seafloor alteration than the Rb-Sr system. This is due in part to the greater fraction of the mass budget of Nd contributed by mantle clinopyroxene than is the case for Sr in altered peridotite. Many of the whole rock $^{143}Nd/^{144}Nd$ compositions are mantle-like, though some of the data show clear evidence of seawater interaction. It is appropriate to use $^{87}Sr/^{86}Sr$ ratios to monitor the degree of seawater contamination in a given sample, since $^{87}Sr/^{86}Sr$ is more sensitive to alteration and Sr and Nd can be assumed to reside in the same physical reservoir on a mineral scale. Samples with $^{87}Sr/^{86}Sr$ lower than .7060 can generally be assumed to have a seawater contribution to $^{143}Nd/^{144}Nd$ less than $2x10^{-5}$. Based on this criterion, leaching of clinopyroxene samples is nearly always successful for Nd.

The Os isotopic system in peridotite whole rocks is extremely resistant to submarine weathering and hydrothermal alteration. No instance of disturbance of Os isotopic composition could be documented in the abyssal peridotites. This result is based on the results of bulk analysis, comparison to the

other isotope and trace element systematics relevant to weathering and alteration, and leaching studies. It is likely that Os either resides in a phase (such as PGE sulfide) which is resistant to alteration, or that upon alteration, an insoluble phase is immediately formed which similarly does not significantly exchange Os with seawater, even at high water/rock ratios. The high concentration of Os in abyssal peridotite also renders the isotopic composition insensitive to the addition of exogenous Os.

Three important reservoirs of Nd, Sr and Os were found on a sample scale in abyssal peridotites. The mantle reservoir is well defined for Nd and Sr, but less so for Os. Nd and Sr derived from the mantle partition heavily into the clinopyroxene in a four phase peridotite. Even after significant alteration of the coexisting olivine and orthopyroxene, the clinopyroxene still retains a pristine mantle $^{143}Nd/^{144}Nd$ and often also $^{87}Sr/^{86}Sr$ which can be recovered by careful mineral separation and leaching. The physical location of Os in abyssal peridotites is still unknown, though by analogy with peridotites from other settings, it is more likely to exist as disseminated sulfide than as a silicate solid solution.

The seawater reservoir of Nd and Sr is physically located in low-temperature alteration veins which crosscut the sample. Other studies of Sr alteration in peridotite (Kimball and Gerlach, 1986) have shown that the mixture of seawater/mantle derived Sr in alteration veins increases as the temperature of alteration declines. This suggests that samples which have experienced only high temperature alteration would retain nearly pristine Sr and Nd isotopic compositions. Samples of peridotite blastomylonite analyzed in the course of this study bear out this prediction, having pristine $^{143}Nd/^{144}Nd$ and the lowest $^{87}Sr/^{86}Sr$ measured in this study on a whole rock peridotite.

Many of the samples of this study contained a fraction which contains very high $^{87}Sr/^{86}Sr$ ratios. These $^{87}Sr/^{86}Sr$ cannot have been produced at the current Rb/Sr ratio of the mineral fraction. The existence of high $^{87}Sr/^{86}Sr$ in serpentinites is one of the oldest observations of the isotopic geochemistry of Sr (Roe, 1965). The "orphan ^{87}Sr" resides in the complex serpentine + magnetite mesh that forms a pseudomorphous replacement of olivine. Three hypotheses are advanced for the origin of this orphan ^{87}Sr: First, that the high $^{87}Sr/^{86}Sr$ ratios grew in situ from Rb which was transported into the rock by high temperature alkali metasomatism, then removed later at low temperature; Second, that the high $^{87}Sr/^{86}Sr$ grew in a high Rb/Sr ancient mantle source underlying fracture zones; Third, that the high $^{87}Sr/^{86}Sr$ is derived from the detrital fraction of sediments overlying the recharge zones of hydrothermal fluids invading the system. In the absence of evidence for high water/rock ratios during alteration, none of these hypotheses is a satisfying explanation of the data. That high water/rock ratios are commonly documented in abyssal peridotite makes it likely that the source of the orphan ^{87}Sr is a detrital fraction of suspended sediment borne by the invading seawater. Such a sedimentary component would contain abundant apparently unsupported ^{87}Sr.

Nd and Os isotopic composition of the mid-ocean ridge mantle.

Chapter Four reports the results of an Nd and Os isotopic investigation of abyssal peridotites. These samples represent part of the depleted mid-ocean ridge upper mantle, and as such are useful for constraining the evolution of the depleted mantle. A partial melting process alone can explain the Re-Os systematics of the mantle only with great difficulty, and requires extreme assumptions about the mean age of the Earth's crust, the partition coefficient of Re during melting and the bulk Os isotopic composition of the Earth. The Nd

and Os isotopic systems taken together do not yield the tight correlation of isotopic compositions which would be required if the parent daughter ratios of these two systems were both determined by the degree of partial melting during the formation of the Earth's crust. Thus, partial melting cannot be the only process which determines the Re/Os ratio in the Earth's mantle. Another process is required which is not linked to partial melting to explain the variations in the Re-Os system independently from the Sm-Nd isotopic system.

Planetary differentiation into mantle and core is a process which theoretically can strongly fractionate the siderophile elements, including Re and Os (Chou, 1978; Jagoutz, et al., 1979). A core formation model involving three stages of accretion and two of core segregation (Chou, 1978, Jagoutz, et al., 1979, Morgan, et al., 1981, Schmitt, et al. 1989) can explain many aspects of the siderophile and chalcophile element abundances in the mantle. The data from this study are consistent with the conclusions of that model, which, combined with partial melting and crust formation provides the ability to simultaneously explain the variations of $^{187}Os/^{186}Os$ isotopic compositions, the lack of correlation of $^{187}Os/^{186}Os$ and $^{143}Nd/^{144}Nd$, and the weak correlation of $^{187}Os/^{186}Os$ with (Co/Os)n. Such a combined crust formation and core segregation model would also solve the major problems inherent in a melting-only model for the evolution of the Re-Os isotopic system by itself: It would allow the bulk Earth to have a chondritic Re/Os and $^{187}Os/^{186}Os$ ratio, would not require Re to be highly incompatible during melting, and would not require an older mean crustal age to account for the Re-Os systematics than for any other isotopic system.

Core formation models such as the one discussed here are necessarily highly non-unique and extremely difficult to test. The Re-Os isotopic sys-

tematics described here may provide a means, along with the relative abundances of the moderately siderophile and highly siderophile elements, of constraining such models.

References

Bender, J.F., Langmuir, C.H. and Hanson, G.N. (1984) Petrogenesis of glasses from the Tamayo region, East Pacific Rise. **Journal of Petrology** 25:213-254.

Chou, C.-L. (1978) Fractionation of siderophile elements in the Earth's upper mantle **Proceedings of the Ninth Lunar and Planetary Science Conference** 219-230.

Dick, H.J.B. (1989) Abyssal Peridotites, Very-Slow Spreading Ridges and Ocean Ridge Magmatism. in: **Magmatism in the Ocean Basins** edited by A.D. Sanders and M.J. Norry, Journal of the Geological Society of London Special Publication No. 42: pp. 75-109.

Dick, H.J.B., Schouten, H., Meyer, P., Gallo, D., Bergh, H., Tyce, R., Patriat, P., Johnson, K.T.M., Snow, J. and Fisher, A. (1991) Tectonic evolution of the Atlantis II Fracture Zone, **Proc. Ocean Drilling Program** v. 118 part B.

Fox, P.J., R.S. Detrick and G.M. Purdy (1980) Evidence for crustal thinning near fracture zones; implications for ophiolites *in:* Panayioutou, A. (*ed.*) **Ophiolites; Proceedings, International Ophiolite Symposium** p. 161-168.

Fox, P.J., and Gallo, D.G. (1984) A tectonic model for Ridge-Transform-Ridge plate boundaries: implications for the structure of oceanic lithosphere. **Tectonophysics** 104:205-242.

Jagoutz, E., H. Palme, H. Baddenhausen, K. Blum, M. Cendales, G. Dreibus, B. Spettel, V. Lorenz and H. Wänke (1979) The abundances of major, minor and trace elements in the Earth's mantle as derived from primitive ultramafic nodules **Proceedings of the Tenth Lunar and Planetary Science Conference** pp. 2031-2050.

Kimball, K.L. and D. Gerlach, (1986) Sr isotopic constraints on hydrothermal alteration of ultramafic rocks in two oceanic fracture zones from the South Atlantic Ocean **Earth and Planetary Science Letters** 78:177-188.

Langmuir, C.H., and Bender, J.F., (1984) The Geochemistry of oceanic basalts in the vicinity of transform faults: observations and implications. **Earth and Planetary Science Letters** 69:107-127.

Morgan, J.W., G. Wandless, R. Petrie, and A. Irvine (1981) Composition of the Earth's upper mantle - I. Siderophile trace elements in ultramafic nodules. **Tectonophysics** 75:47-67.

Natland, J.H. and Melson, W.G. (1980) Compositions of basaltic glasses from the East Pacific Rise and Siqueiros Fracture Zone, near 9N, *in:* **Initial reports of the Deep Sea Drilling Project** 54:705-723. U.S. Government Printing Office.

Nesbitt, H.W. and O.P. Bricker, (1978) Low temperature alteration processes affecting ultramafic bodies **Geochimica et Cosmochimica Acta** 42:403-409.

Perfit, M.R., Fornari, D.J. Malahoff, A., and Embley, R.W. (1983) Geochemical Studies of Abyssal Lavas Recovered by DSRV Alvin from Eastern Galapagos Rift, Inca Transform, and Ecuador Rift 3. Trace element Abundances and Petrogenesis. **Journal of Geophysical Research** 88, B12:10551-10572.

Roe, G. D., (1965) Rubidium-Strontium Analyses of ultramafic rocks and the origin of peridotite. MIT Ph.D. thesis. 239 p.

Schmitt, W., H. Palme, and H. Wänke (1989) Experimental determination of metal/silicate partition coefficients for P, Co, Ni, Cu, Ga, Ge, Mo, and W and some implications for the early evolution of the Earth. **Geochimica et Cosmochimica Acta** 53:173-185.

Stroup, J.B. and Fox, P.J. (1981) Geologic investigations in the Cayman Trough: evidence for thin crust along the mid-Cayman Rise **Journal of Geology** 89:395-420.

Zindler, A. and Hart, S.R., (1986) Chemical Geodynamics. **Annual Reviews of Earth and Planetary Sciences** 14:493-571.

Appendix I: Sample Descriptions

Introduction

For the purposes of studying the compositions of abyssal peridotites and behavior of the various isotopic systems during alteration, it was necessary to select a suite of peridotite samples which would be appropriate to the task. Sample selection was based on a number of positive factors:

- Range of melt depletion.
- Range of tectonic settings, near to and far from regional hot spots.
- Geographical coverage
- Previous analysis (trace element or isotopic) available.

In addition, there were two negative factors which were used to avoid samples whose geochemical histories would be likely to be complicated by poorly understood processes. First, samples were selected to be completely free of plagioclase feldspar. The interpretation of plagioclase in abyssal peridotites is different from that in ultramafic nodules, where it is considered a commonly occurring mantle phase. In abyssal peridotites, plagioclase is thought to represent the addition of basaltic melt to the peridotite at very shallow levels in the mantle or crust (Dick, 1989). In this case, the trace element budget of the peridotite would be very likely dominated by the contribution of the incoming basaltic melt, which itself has an independent and long history of melting, fractionation and aggregation. For this reason, the confounding influence of basalt melt admixtures was avoided by selecting samples which were wholly free of plagioclase.

Second, samples were chosen to be free of high grade metamorphic minerals. Extensive conversion of primary phases to high grade metamorphic minerals may indicate a long residence time at middle crustal levels. Whereas the likely origin of water involved in low-temperature hydration of peridotite may be constrained to some extent (e.g., von Damm, 1990), the origin and evolution of high temperature metamorphic fluids in the ocean crust are almost entirely unconstrained. Secondly, in many abyssal peridotites, crosscutting relationships of metamorphic minerals have shown that the first metamorphism that an abyssal peridotite is exposed to is at low grade (Juteau, et al., 1990), while high grade minerals form later by the hydrous prograde or contact re-metamorphism of low temperature minerals at conditions ranging from the zeolite facies up through the greenschist facies to the amphibolite facies (Evans, 1977). Although prograde metamorphism of serpentinites is an interesting topic in itself, and deserving of extensive study, it was decided that the first serious study of isotope systematics in the oceanic mantle should not include these rocks. Hydrous high temperature metamorphism would likely mobilize incompatible trace elements, has an unknown effect on Os, and could lead to the growth of phases (such as phlogopite) with very high Rb/Sr ratios, which would complicate the Sr isotopic system. For the reasons enumerated above, samples showing extensive high temperature hydrous metamorphism (e.g., the samples studied by Dick, et al., 1979 and Kimball, et al., 1985) were not included in this study.

Chapter 3, Figure 1 shows the locations of samples analyzed in this study. Most of the samples are from the Southwest Indian Ridge and the American-Antarctic Ridge. Each sample is listed with its location, tectonic setting relative to the fracture zone it is from, crustal age, nearest hot spot and the distance.

Sample descriptions

Descriptions of Peridotite Samples

Because of the tremendous textural differences between the abyssal peridotite mylonites and "normal" abyssal peridotites, they are described in separate sections here. In the tables in this section, the lizardite column refers to serpentine pseudomorphous after olivine.

PS 86: 6-37

Olivine	Lizardite	Enstatite	Bastite	Diopside	Spinel	Alt. 1	Σprimary.
13.9	51.3	15.7	9.6	6.9	1.4	0.4	37.9

This is an atypically fresh abyssal peridotite, rich in clinopyroxene. The overall appearance is that of a greenish, non-foliated rock, with dark (altered) olivines (65.2 % primary modal olivine) surrounded by orthopyroxene (25.3%) clinopyroxene (6.9%) and spinel (1.4%). The texture is protogranular in the Mercier and Nicolas (1974) classification of upper mantle peridotite textures.

Olivine

Relict Islands of olivine commonly 200-400 microns in diameter enclosed in a mesh of serpentines and magnetite. Original grains were 4-5 mm. across as determined by simultaneous extinction and the continuity of textures from relict olivine to relict olivine. The shapes of the original grains, insofar as they can be determined are equant, not embayed and there are few inclusions or intergrowths with other minerals. Ribbon textures or elongation of mineral grains are not observed, although there is undulose extinction.

Enstatite

Large grains >10 mm. across, generally equant, although sometimes intergrown with spinel or clinopyroxene. There are inclusions of clinopyroxene and spinel in the orthopyroxene as well. Undulose extinction is common.

Clinopyroxene

High birefringent grains 2-3 mm. in diameter, with ubiquitous fine exsolution lamellae. Frequently kinked and bent, but not dramatically so. Undulose extinction, but no visible formation of subgrains or polygonalization.

Spinel

Brown blobs of spinel intergrown with orthopyroxene, clinopyroxene, and olivine in typical fashion. About 1 mm. diameter grains, perhaps 10 of them in the whole section

Alteration Products:

Ol. -> Serpentine + Magnetite

The dominant secondary mineral in this rock is lizardite after olivine, followed by magnetite after olivine. In counting modes, it is frequently impossible to distinguish directly between lizardite and magnetite. It is impossible to estimate the abundance of magnetite in any given sample with any accuracy, and the attempt will not be made.

Enstatite -> Bastite

Enstatite is most commonly altered to a fibrous serpentine, most likely lizardite or chrysotile. This is sufficiently common that bastite after enstatite can be counted as a separate phase.

Clinopyroxene and spinel

These minerals are sufficiently well preserved that alteration outside of vein-filling material is quite rare. Thus no separate tabulation is necessary for alteration products pseudomorphous after clinopyroxene and spinel.

Vein minerals

The vein minerals in this sample consist primarily of lizardite, antigorite and chrysotile, though these are difficult to unambiguously distinguish from one another under the microscope. In the descriptions that follow I refer to amorphous serpentine as lizardite, fibrous serpentine as chrysotile and bladed serpentine as antigorite, although it is clear that such a textural distinction is in many cases pure fiction. Other potential vein filling phases include talc, amphibole and phlogopite.

Vulc5: 41-15

Olivine	Lizardite	Enstatite	Bastite	Diopside	Spinel	Alt. 2	Σ primary.
13.9	51.3	15.7	9.6	6.9	1.4	0.4	37.9

This is a highly altered peridotite, green in color, with no particular foliation or mineral preferred orientation. This is an extremely poor thin section, with abundant plucking of minerals with cleavage and incorporation of grinding paste underneath the section makes some mineral identification difficult. The sample contained large pockets of grinding compound that fooled several experienced observers into thinking it was garnet.

Olivine

Olivine has disintegrated completely into an interlocking mat of serpentine + magnetite in this rock. The magnetite proportion seems to be lower than is commonly the case, I will estimate magnetite at 10% of the total former olivine. This estimate is probably higher than the actual volume representation of magnetite, since the magnetite is quite fine-grained. Some areas of the sample exhibit relatively fresh neoblastic olivine which is strain free and contrasts strongly with the poorly preserved olivine in the rest of the sample, which are typically missing their relict cores due to plucking. Undulose extinction is ubiquitous in these grains, and the combination makes it difficult to determine whether grains are elongated or what the original grains size was.

Enstatite

Practically no enstatite is preserved, and thus it is difficult to distinguish from olivine, except for the absence of magnetite, the association with diopside and spinel and the texture of the alteration material. In serpentine after enstatite, the fibrous minerals are typically aligned in a nearly parallel fashion, in contrast to the olivine, which has alteration products following former olivine parting surfaces in a nearly perpendicular mesh-like configuration. Where enstatite is preserved, it is fibrous in appearance (due to bastite formation), has straight extinction, low birefringence, and frequently cut by dilatent veins of serpentine. Altered enstatite will almost certainly be under-counted in this rock.

Clinopyroxene

The clinopyroxene is strongly exsolved into clinopyroxene and orthopyroxene-rich bands. The exsolution lamellae are commonly bent, showing some spectacular kink bands. There is also a partial breakdown of the clinopyroxene grains to secondary phases, but not sufficiently to warrant a separate tabulation. Still far better preserved than enstatite or olivine. The grains are also polygonalized, locally with the formation of subgrains. Neoblasts are strain-free and unaltered.

Spinel

These are typically intergrown with enstatite or diopside. For the most part they are pale brown (very pale for spinel) to opaque (oxidized). Extinction is visible with crossed nichols.

Alteration Products

Isotropic mineral 1:

This "mineral" has high relief, is non pleochroic, isotropic, elongated, and looks pseudomorphous after spinel. Its greasy texture and isotropic character make it likely to be garnet. In fact, this "mineral" on closer examination turns out to be alumina polishing compound filling plucked out holes left by olivine or spinel grains. The track of the plucked out mineral grain is still clearly visible in the surface of the section. This mineral will be ignored and the point counting results recalculated excluding this mineral.

Isotropic mineral 2:

This mineral has low relief, iron staining, and dendritic fingers of opaque material protruding into it (these are not spinels). At high magnification it becomes a mass of extremely fine-grained material. Probably a fine grained chlorite (coarser grained chlorite is abundant in this sample) or serpentine.

Vein mineral 1

Tiny high birefringent veins crossing through heavily altered enstatite. Vein ends at grain boundary unlike serpentine veins, which tend to cross into the altered olivine on either side.

Chlorite

Felt-like masses, sometimes very fine grained. No relict textures (e.g. after olivine or orthopyroxene.) are visible. It will be classed separately from ex-orthopyroxene.

RC 2709 6-2A

Olivine	Lizardite	Enstatite	Bastite	Diopside	Spinel	Σ primary.
19.6	28.5	37.3	7.1	6.1	1.2	64.4

This is a coarse grained, greenish, unfoliated rock, it is generally one of the freshest abyssal peridotites in the collection. This particular section is far from the large clinopyroxene-rich vein which cuts through the sample, as was the part of the sample taken for bulk studies of isotopes, major element composition and mineral separates. A point count may be misleading as to the total clinopyroxene content. The clinopyroxene-rich vein is defined by somewhat isolated large (~1 cm.) grains or clots of grains of clinopyroxene. These are distributed in a tabular arrangement which cuts across the entire sample. The vein is enclosed in a several cm. thick area which seems to contain no other pyroxene, being composed almost exclusively of olivine alteration products. This sample clearly exhibits classic protogranular peridotite texture, where large olivine grains form a continuous network, while the other phases, spinel, diopside, and enstatite, are closely associated with one another.

Olivine

Olivine comprises 48.1 percent of this rock. This sample contains extremely coarse (>20 mm. max.) grains which do not appear elongated. The preservation state of the olivine varies remarkably from one end of the thin section to the other, suggesting that the alteration in this case may not be a pervasive feature. Olivine is altered to a typical mesh-like latticework of serpentine and magnetite with large relict cores in which many primary features are preserved: Undulose extinction, bubble trains, (fluid inclusions?) , and subgrains.

Enstatite

The enstatie in this sample consists of arge clear grains 2-5 mm. in diameter. It is partially bastitized, and seems to be underrepresented in this sample, which is dominated by the presence of a diopside vein. Undulose extinction in these enstatites is crosscut by serpentine veins. Orthopyroxene and clinopyroxene are difficult to distinguish in this sample, since many of the clinopyroxenes do not have well developed exsolution lamellae.

Clinopyroxene

There are two populations of clinopyroxene in this sample. Some of the clinopyroxenes in this rock do not appear to contain exsolution lamellae, others do. The exsolved pyroxenes have curved exsolution lamellae but have clearly inclined extinction. Exsolution lamellae are also kinked and crosscut by serpentine veins in places.

Spinel

Spinel seems underrepresented in this sample, even though the counted mode show a normal amount of spinel. It appears as wormy intergrowths of the usual variety with fine veins of serpentine crosscutting them. Very dark, possibly oxidized, so it is sometimes difficult to distinguish small spinel grains from magnetite.

Alteration Products

The enstatite-hosted veins have an unique appearance. On analysis, they turn out to be serpentine of the most common variety (Chapter 3, Table 8).

Vulc5: 41-29

This is a dun colored, slightly foliated rock, in a relatively poor state of preservation, with the exception of diopside, which appears particularly well preserved. Dun coloration is due to the oxidation/hydration of magnetite to various hydroxides of iron, including hematite, limonite, and goethite in association with clays after the primary minerals. It is not associated with an overall difference in mineral assemblage, primary or secondary, and is not apparently a function of the degree of alteration of the sample either. The process which forms dun-colored peridotite is independent of the main alteration event which produced the serpentine in the rock, and is related to weathering on the sea floor. This rock, however, does not turn out to belong to the group of highly weathered rocks (the low-Mg group of Chapter 3), but nevertheless shows some petrographic signs of weathering.

Olivine

The primary mineral is only preserved in tiny <1 mm. relicts, floating in a sea of iron oxides, hydroxides and serpentine. The resultant almost opaque mass makes it impossible to estimate the grain size of the original olivines, the grain shape extent of development of deformation textures, etc. Similarly, the proportion of magnetite present in the alteration product is impossible to assess. Some undulose extinction is visible in olivine relicts.

Enstatite

Enstatite is poorly preserved, and is largely altered to bastite. The bastite has a subtly different appearance near to small fractures in the grain, so there may be multiple generations of bastite in these enstatites. The typical grain size is 5-7 mm. Enstatite and diopside surrounding spinel are thoroughly reduced to masses of serpentine. There seems to be a variety of exsolved orthopyroxene, since the proportion of what texturally looks like clinopyroxene but has straight extinction is very high. It is difficult to tell orthopyroxene. from clinopyroxene at times in this rock.

Clinopyroxene

This rock contains diopsides which are heavily exsolved and have high relief. The grain size is typically 5-7 mm. Exsolution lamellae are typically bent and extinction is undulose. The state of preservation is otherwise quite good, however. The grains are clear and pale green in plane polarized light, and not cloudy or filled with tiny bits of serpentine. this is an excellent candidate for mineral separation. Only in the vicinity of spinels is the diopside visibly strongly altered.

Spinel

In this sample, spinel forms wormy symplectic intergrowth with altered diopside and orthopyroxene. It is oxidized on fracture surfaces and is frequently opaque. Spinel generally occurs where grains of orthopyroxene., clinopyroxene and olivine are in close proximity, but typically is enclosed by an area of unidentifiable alteration products.

Alteration Products

Enstatite is converted to bastite and olivine to serpentine + magnetite in this sample. There is one small vein of chlorite, which is counted separately.

IO 11/76 60-61

Olivine	Lizardite	Enstatite	Bastite	Diopside	Spinel	Σ primary.
3.3	75.7	6.7	6.4	7.3	0.3	17.6

In addition to being poorly preserved, this section is poorly made. It is wedged on one side, thick on the other, and plucked all over, thus complicating the description. This is a dun-colored, foliated sample, however, the iron staining is not so bad that the serpentine + magnetite is opaque as in other sections. The staining is patchy, and in many places, serpentine + magnetite are visible. This sample is quite friable, and cuts easily in the rock saw. The density of this sample is so low that it is noticeably lighter than other abyssal serpentinites.

Olivine

Olivine is poorly preserved, and its grain size indeterminate. Relicts of primary olivine showing deformation banding, subgrain formation, and undulose extinction float in a mass of mesh-textured serpentine + magnetite. Estimated magnetite is 5% of the total of primary olivine.

Orthopyroxene

In one half of the thin section, enstatite is elongate, while it is equant in the other half. Elongate porphyroclasts are about 10 mm. by 2 mm., while equant porphyroclasts are about 10 mm. in diameter. Many are severely bastitized. Undulose extinction and kink banding of exsolution lamellae are common. The porphyroblasts are intergrown with spinel in some places.

Clinopyroxene

Diopside is not well represented in this sample, though it is reasonably well preserved. The grain size of diopside is approximately 800 microns. Undulose extinction, kink banding and exsolution are common.

Spinel

Wormy symplectic intergrowths with serpentine pseudomorphs of diopside and enstatite. The spinel is oxidized on fracture surfaces and opaque. Spinel generally occurs where grains of orthopyroxene, clinopyroxene and olivine are in close proximity, but typically the other phases in proximity to spinel are heavily serpentinized, to the point of being unrecognizable.

Alteration

Other than hydration products of olivine and enstatite, I am unable to identify any interesting alteration products. Neither can Henry.

IO 11/76 56-58

Olivine	Lizardite	Enstatite	Bastite	Diopside	Spinel	Σ primary.
1.1	74.9	14.7	2.0	6.0	1.0	22.8

This is a dun-colored abyssal peridotite, which is extensively altered. Nonetheless, porphyroblastic primary textures can be observed. This thin section was only available for study as a small format thin section, and for that reason only 2521 points were counted, at a finer point spacing than was the case for the other samples in this study. This sample is extremely friable and extremely porous, and thus was very difficult to section. Several attempts at multiply impregnating this sample with epoxy were necessary before the sectioning could proceed. The sample cuts very easily in a rock saw, and shows a rough, soft, cut surface which implies the presence of weak clay minerals. The rock is noticeably light, even compared to other abyssal serpentinites.

Olivine

Few to no relict olivines are visible, though there are obvious holes where olivine relicts have been plucked out in the thin sectioning process. For the most part pluck holes have sharp borders where the margin of the impregnating epoxy can be seen, implying that the formation of the hole postdated the impregnation of the sample. There are a few olivine cores which are not plucked. The only olivine grains which are well preserved are a few small olivine neoblasts ringing enstatite. The grain size of the olivines is not determinable, nor are textures and undulosity. Neoblastic olivines are unstrained and clear, without kink bands or undulose extinction.

Orthopyroxene

Enstatite is better preserved in this rock than is the olivine. Cleavage is pronounced, and is decorated or highlighted by clinopyroxene exsolution lamellae. The cleavage is cut by veins which pinch out at the grain boundaries and are bordered by altered material. The enstatite typically occurs in clots with clinopyroxene and spinel which are ringed by olivine and enstatite neoblasts. The largest enstatites were as large as 7 mm., but typical enstatites are 3-4 mm.

Diopside

Considering the advanced state of alteration of the olivine, diopside is surprisingly well preserved. Through-going cracks in the diopside are filled with alteration material, but otherwise the crystal itself looks good. The diopside is a clear pale-green in plane polarized light, and are is cloudy at the margins of through-going cracks. The diopside is strongly exsolved into ortho- and clinopyroxene and is somewhat kinked.

Spinel

The spinel is typical in appearance. It has a characteristic wormy habit, with thorough-going cracks filled with serpentine. Spinel is mostly opaque in this sample, implying that it has been oxidized.

Alteration

This is a strongly altered samples, though it is remarkable how well preserved the clinopyroxenes are. Olivine is almost completely converted to serpentine + magnetite, even though enstatite is reasonably well preserved. This may have some connection to the MgO depletion of this rock.

IO 11/76 59-26

Olivine	Lizardite	Enstatite	Bastite	Diopside	Spinel	Alt. 1	Alt. 2	Σ primary.
6.1	51.9	5.0	31.1	2.1	1.1	1.5	0.8	15.3

This is a greenish thin section cut from a massive slab of serpentinite which is green-black in color, with distinctly visible pale gray enstatites. It does not generally look as thoroughly altered as IO 11/76:56-58, though there are some unusual-looking alteration minerals in this sample.

Olivine

Olivine is extensively altered to serpentine + magnetite in a typical mesh texture, though relicts of olivine are abundantly visible. Grain size cannot be determined, although kink bands and undulose extinction are observable in many of the relict grains. There are fewer neoblastic olivines in this sample (a characteristic of porphyroblastic textures) than in sample IO11/76:56-58.

Orthopyroxene

Enstatite is in very poor condition in this sample, replaced by bastite and possibly talc. there is also a second replacement mineral which is deep green and fibrous. Almost no primary enstatite is visible.

Diopside

Diopside is also poorly preserved, but seems to be in better condition than the enstatite. It is strongly exsolved, with bent exsolution lamellae. Most of the pyroxene in this sample which looks like pyroxene is clinopyroxene. Enstatite is nearly unrecognizable as such.

Spinel

The spinel has a typical appearance. It has a wormy texture, with small thorough-going cracks. Most of the spinel is opaque in this sample, implying that it has been oxidized.

Alteration products:

Replacing mineral

A deep green, fibrous mineral replacing clinopyroxene. Possibly epidote, secondary clinopyroxene or amphibole. this would be a good candidate for being electron probed.

Vein mineral (serpentine)

This thin section contains a high birefringent, non-micaceous vein material. It has good crystallinity, and occurs in veins which crosscut all primary and secondary textures. Amphibole? This vein material later turned out to be serpentine (Chapter 3, Table 8).

AII 107: 40-35

Olivine	Lizardite	Enstatite	Bastite	Diopside	Spinel	Alt. 1	Σ primary.
1.2	69.4	9.1	16.2	3.2	0.5	0.1	14.0

This is a dun colored rock with almost no primary olivine remaining. The sample may be classified as being porphyroclastic (Mercier and Nicolas, 1974) primarily from the arrangement of the pyroxene and spinel grains. This sample is listed in the dredging catalog at 170g. That weight applied only to a small chip removed from the boulder and sectioned. The sample weighs in excess of 20 kilograms. The larger piece of this sample was discovered in the dredging collection in the course of sample selection for this study. The exterior of this rock is more dun colored than the interior for some centimeters into the rock. The interior of the boulder is more greenish in appearance, and is apparently unweathered, but still has a dun-colored cast, as

opposed to many other rocks which are greenish-black through and through. This rock has several important features: First, it is the only peridotite from the Bouvet Fracture Zone with recoverable clinopyroxene, albeit only very little. This makes it an extremely important rock for any study utilizing mineral separates. Second, it is one of the few abyssal peridotite boulders of sufficient size that noticeable differences in weathering exist between the margins and the core. Third, even the core of the boulder still has a dun coloration, implying either that weathering has penetrated into the core of a boulder nearly 0.5 meters in diameter, or that the dun coloration can be caused by some other process than weathering. This sample would make a good test of the sediment infiltration hypothesis advanced in Chapter 3 to explain orphan ^{87}Sr in abyssal peridotite. The weathered margins of this sample would be expected to contain a high ^{87}Sr component, while the core has already been shown to be largely free of such a component (Chapter 3, Table 12). There is some indication of high ^{87}Sr in this rock, as shown by the fact that the first magnetic fraction $^{87}Sr/^{86}Sr$ analysis is higher than the one for the whole rock.

Olivine

The grain size of olivine in this sample is indeterminate, due to its advanced state of weathering. What olivine remains seems to be primarily associated with pressure shadows of small (.5-1 mm.) relatively strain-free grains surrounding enstatite porphyroclasts. It is possible that neoblastic olivine is less permeable than porphyroclasts of olivine. This would account for the good state of preservation of most peridotite mylonites. Also, the neoblastic olivine is in equilibrium at a lower pressure than olivine porphyroclasts, and thus may have less residual strain energy in its lattice waiting to express itself as cracking. Otherwise, the olivine is a mesh-textured mat of interconnected serpentine and magnetite. The magnetite mode appears to be approximately 15% of the ex-olivine mode.

Orthopyroxene

This is a thick section, so orthopyroxene porphyroblasts all have birefringent interference colors which are somewhat too high, making it somewhat harder to distinguish from other minerals. Enstatites are mantled by relatively fine grained orthopyroxene-clinopyroxene-olivine assemblages that look like pressure shadows composed of neoblastic minerals. Alternatively, the orthopyroxene might have acted to prevent the alteration of the nearby minerals in some way. Some grains which were clearly once orthopyroxene are now felt-like masses of serpentine (without magnetite). The enstatites are not elongated and are approximately 10 mm. in diameter.

Clinopyroxene

Diopside occurs as small isolated grains with exsolution lamellae which are bent and kinked and show undulose extinction. They only occur in proximity to enstatite and spinel grains, and don not seem to occur a disseminated grains of clinopyroxene. They are typically 2-3 mm. in diameter.

Spinel

The spinel has a typical appearance. It has a wormy texture, with small thorough-going cracks. Most of the spinel is opaque in this sample, implying that it has been oxidized.

Description of Peridotite Mylonite Samples

AII 107: 61-78

Olivine	Lizardite	Enstatite	Bastite	Diopside	Spinel	Σ primary.
64.7	0.0	26.9	0.0	6.7	1.2	99.5

This is a dun-colored peridotite mylonite consisting of highly deformed recrystallized olivine orthopyroxene clinopyroxene and spinel. The mode above is calculated from the compositions of primary minerals and the bulk composition of the rock. The calculation is carried out in Appendix III. In hand specimen it has a strongly foliated appearance, with easily visible porphyroblasts of enstatite and crosscutting veins. In fact, there is no mineral preferred orientation in the sample. The apparent layering is defined entirely by grain size variations in olivine. It is dun colored only on the outside, where there is a 0.5-1 cm thick weathering rind. the interior of the rock is pale green in color.

Olivine

Has highly variable grain size, from about 1 mm. to sub-micron size. The larger clusters of olivine crystals are in elongate masses suggesting the original grain boundary outlines, which appear to be stretched to about a 10:1 ratio. Where larger olivine aggregates occur, the closest approach to a porphyroblastic texture visible for its mineral lies in dramatic ribbon olivines, where stretching and subgrain formation has led to the complete disaggregation of the original crystal. Flow structures, folding and relict pressure shadows are evident on many of these olivine ribbons. A pronounced foliation is developed primarily due to the stretching of olivine crystals, ribbon structures and variations of olivine grain size.

Orthopyroxene

Enstatite is only visible as porphyroblasts 1 mm.-0.1 mm. in size, but it is probably present in the recrystallized groundmass as well. In the groundmass, the characteristic cleavage is difficult to make out. Porphyroblastic enstatite is present as pale first-order birefringent enstatite or bronzite porphyroblasts whose edges are rounded, but not embayed or noticeably absorbed. All the porphyroblastic enstatites have straight extinction and pronounced cleavage. In many cases cleavage planes are deformed and/or extinction is undulose. In some grains, the formation of deformation bands and sub-grains is evident. Head sections of orthopyroxene (those showing both sets of cleavage at nearly 90 degree angles; optical axis figures are sometimes obtainable on them) are thoroughly plucked in this section, so optical axis figures are not obtainable.

Clinopyroxene

Diopsides are apparently present as porphyroblasts only, though as in the case of enstatite, there is probably groundmass diopside as well. They are rounded, somewhat polygonalized, ubiquitously undulose, with deformed cleavage and pronounced exsolution. The diopside ranges in size from 1 to 0.1 mm., though it does not appear to be present at the smallest grain sizes. Pressure shadows occur which are filled with strain-free recrystallized clinopyroxene.

Spinel

Chrome spinel appears very much as in "normal", "undeformed" abyssal peridotites. It is dark brown almost isotropic spinel with inclusions of unstrained enstatite and diopside. No visible deformation banding formation of subgrains or reduction in grain size of any kind is present.

Alteration:

Pervasive alteration of olivine to serpentine + magnetite or olivine to clays is not seen in this sample, in marked contrast to non-mylonitized abyssal peridotites. The only evidence for high or low grade metamorphism is in fine sets of veins which crosscut the mylonitic foliation.

The earliest vein generation is a set of 0.01 mm. thick veins filled with felt-like masses of chlorite and/or laths of amphibole. These branch and anastamose and crosscut each other in several successive generations, but are mostly very small and very few. The veins tend to have a halo consisting of darkened fine grained olivine which extends for as much as 0.5 mm. on either side.

A later vein set is made up of very fine veins of opaque material with no halo of any kind. These tiny veins seem to emanate from the Mn rind on one side of the specimen. Their total volume is very small. In all the total alteration products do not exceed 1% of the volume of the rock (in it's unweathered interior).

Alteration of olivine to what appear to be clays occurs in an approximately 0.5 cm thick band at one edge of the sample. On the other edge of the sample, much thinner "clay" alteration is overgrown by a 1-2 mm. thick crust of what appears to be Mn oxide with small inclusions. On analysis, this "Mn oxide rind" turned out to be a vein of black serpentine, similar in composition to other serpentines analyzed in the course of this study (see Chapter 3, Table 10 for the "crust" composition and Table 8 for the other serpentines).

AII107: 61-83

Olivine	Lizardite	Enstatite	Bastite	Diopside	Spinel	Σ primary.
72.4	0.0	19.8	0.0	5.78	1.4	99.4

This is a peridotite blastomylonite marked by extreme grain size variations, a variety of deformation textures in its constituent minerals (except spinel). It appears strongly foliated in hand sample and has the approximate mineralogy olivine (85%) orthopyroxene (10%) clinopyroxene (5%) and spinel (1%). It also has a weathering rind which is bright dun in color, with a pale green interior.

Olivine

The olivine grain size is highly variable, from about 1 mm. to sub-micron size. The larger clusters of olivine crystals are in elongate masses suggesting the original grain boundary outlines. The primary grains appear to be stretched to about a 10:1 ratio. Where larger olivine aggregates occur, the closest approach to a porphyroblastic texture visible for its mineral lies in dramatic ribbon olivines, where stretching and subgrain formation has led to the complete disaggregation of the original crystal. Flow structures, folding and relict pressure shadows are evident on many of these olivine ribbons. A pronounced foliation is developed primarily due to the stretching of olivine crystals, ribbon structures and variations of olivine grain size.

Orthopyroxene:

Pale first-order birefringent enstatite porphyroblasts occur whose edges are rounded but not embayed or noticeably absorbed. All have straight extinction, and pronounced cleavage. In many cases the cleavage planes are deformed and/or the extinction is undulose. In some grains, the formation of deformation bands and sub-grains is evident. Head sections are thoroughly plucked in this section, so optical axis figures are not obtainable.

Clinopyroxene:

Diopside is rounded, somewhat polygonalized, and ubiquitously undulose, with deformed cleavage and pronounced exsolution. The grain size of diopside ranges from 1 to 0.01 mm.,

though diopside does not appear to be present at the smallest grain sizes. Pressure shadows occur which are filled with strain-free recrystallized clinopyroxene.

Spinel

This mineral has very much the same appearance as in "normal" peridotites. It is dark brown, almost isotropic chromian spinel with minute inclusions of unstrained enstatite and diopside. No visible deformation banding, formation of subgrains or reduction in grain size of any kind are observed.

Alteration:

Pervasive alteration of olivine to serpentine + magnetite or olivine to clays is not seen in this sample, in marked contrast to non-mylonitized abyssal peridotites. The only evidence for high or low grade metamorphism is in fine sets of veins which crosscut the mylonitic foliation.

The earliest vein generation is a set of 0.01 mm. thick veins filled with felt-like masses of chlorite and/or laths of amphibole. Similar serpentine rich veins are also present. These branch and anastamose, crosscutting each other in several successive generations. They are mostly very small and very few. They tend to have a halo consisting of darkened fine grained olivine which extends for as much as 0.5 mm. on either side of the vein. A later generation of veins has a mica mineral with or without opaques. Pyroxenes cut by these veins become fogged and "rotten", suggesting that they are being broken down to fine-grained alteration products by the circulation of fluid through these small veins. A network of tiny veins containing opaque material alone as seen in sample AII107:61-78 is not observed in this sample. There is a 0.1 to 5 mm. thick zone of clay rich alteration on the outside of this rock, with a thin veneer of MnO coating still sticking to it in places; never more than 0.1 mm. in thickness. This thin veneer is more likely to be *bona fide* MnO rind, but it was not analyzed.

Discussion of mylonites:

The high temperature history of both of these rocks is virtually identical; the main differences between the two samples lie in their low temperature histories. The protolith for both rocks is an anhydrous spinel lherzolite, about which little more can be said due to the pervasive e shear textures developed in the constituent minerals. The appearance is similar to that of peridotite mylonites from ophiolites and from some peridotite xenoliths.

A full range of high grade ductile deformation textures is developed in these rocks, including, in order from the lowest to highest strain phenomena:

* Bending of pyroxene cleavage planes.
* Undulose extinction of olivine, orthopyroxene and clinopyroxene.
* Subgrain formation in olivine, orthopyroxene. and clinopyroxene.
* Deformation banding in olivine.
* Ribbon textures in olivine.
* Extreme grain size reduction in olivine.

These textures point unambiguously to ductile deformation at high metamorphic grade as their cause. Since large scale hydration of the primary minerals has not occurred, the deformation occurred during anhydrous metamorphism, unlike the later metamorphism which deposited veins of amphibolite facies hydrous minerals throughout both rocks.

The fact that the various minerals show the extreme deformation to different extents suggests a progression of textural development. Early deformation is penetrative and affects all minerals

more or less equally. As olivine develops smaller grain sizes due to its more efficient formation of deformation structures, it concentrates the strain, effectively strain softening the rock. Thus the remaining minerals do not experience the grain size reductive effects of the extreme strain to the degree that the olivine does.

Amphibolite facies alteration is evident in the formation of veins containing chlorite and amphibole or serpentine + opaque in both samples. Amphibole occurs mostly when either of these types of veins cross a pyroxene grain. Halos of darkened fine grained olivine are probably due to the production of magnetite in the partial breakdown of olivine.

A late generation of veins containing possible muscovite + opaque crosscut the two former types of veins. Occasional veins of unidentified opaque material occur in 61-78, and appear to emanate from the MnO rind in some cases. Crosscutting relationships for this vein set are not clear.

Conclusions from mylonites:

The unrecrystallized cores of these rocks contain abundant evidence that they were derived from spinel peridotites substantially like those found elsewhere on the mid-ocean ridge system, in ophiolites and in certain alpine peridotites. The deformation textures associated with the formation of ductile mylonites in peridotite have been observed in many of these settings, although not commonly before in the oceans.

Abyssal peridotite mylonite is the freshest form of abyssal peridotite, showing practically no alteration of primary minerals to hydrous ones. Amphibolite facies metamorphism is limited to occasional veins of chlorite-amphibole + opaque and serpentine + opaque. Lower temperature alteration is shown by mica rich veins crosscutting the earlier veins. Conservatively, the total metamorphic alteration of these rocks does not exceed, , 1%.

Clay rich orange weathering rinds affect both rocks to a depth of 0.1 to 5 mm. In addition, sample 61-78 has a 1-3 mm. thick rind of MnO rich material on one side.

Sample handling and preparation.

Samples were cut, sectioned, and photographed. Slabs were cut for the weathering study. Weathering rinds were cut off of the slabs to expose the unaltered core of the sample. Core pieces were further cut to minimize the amount of vein material included.

Cruise	Sample number	Weight	Density	Description
AII 107	61-78 M	21.06	3.01 g/cm^3	Black serpentine rind coating approx. 3 mm. thick; 1/3 of the sample by volume.
AII 107	61-78 C	9.37	2.93	Fresh core with minimal veins
AII 107	61-78 W	25.66	2.44	Weathering rind, 5-7 mm. thick, no MnO.
AII 107	61-83 C	32.87	3.28	Fresh core, no visible veins.
AII 107	61-83 W	24.52	2.69	Weathering surface, 7-11 mm. thick.
Vulc5	41-29 WR	15.74	2.50	Typical abyssal peridotite.

The densities recorded for these rocks bear out the remarkable freshness. A typical abyssal peridotite is included for reference

Modal analysis

Modes were counted on all samples, except the mylonites. 2500 to 3000 points were counted per large format (2"x3") thin section at a spacing of approximately 0.5 mm. The only exception among the normal peridotites was ample IO 11/76:56-58, which was only available in small format (1.5"x2"). The mylonites were not countable, however it was possible to calculate modes for the samples based on a least squares inversion of phase compositions and bulk compositions. This calculation is described in Appendix II.

It was typically possible to count both primary phases and the secondary phases pseudomorphous after them with some confidence. Separate tallies were kept for serpentine + magnetite and olivine, bastite and enstatite. Clinopyroxene is typically small enough and well enough pre-

served that keeping a separate total for clinopyroxene would have no purpose. Where there is sufficient vein material, separate tallies are kept for them.

Sample	Olivine	Lizardite	Enstatite	Bastite	Diopside	Spinel	Alt. 1	Alt. 2	Σ primary.
PS 86:6-37	13.9	51.3	15.7	9.6	6.9	1.4	0.4[1]		37.9
Vulc5:41-15	1.4	37.8	6.8	34.6	10.6	1.1	5.4[2]		18.8
RC 2709:6-2	19.6	28.5	37.3	7.1	6.1	1.2			64.4
Vulc5:41-29	4.3	62.9	7.1	14.9	9	0.8	0.4[2]		21.2
IO 11/76:60-61	3.3	75.7	6.7	6.4	7.3	0.3			17.6
AII 107:40-35	1.2	69.4	9.1	16.2	3.2	0.5	0.1[3]		14.0
IO 11/76:56-58	1.1	74.9	14.7	2.0	6.0	1.0			22.8
IO 11/76:59-26	6.1	51.9	5.0	31.1	2.1	1.1	1.5[1]	0.8[3]	15.3
AII 107:61-78	64.7	0.0	26.9	0.0	6.7	1.2			99[4]
AII 107:61-83	72.4	0.0	19.8	0.0	5.78	1.4			99[4]

[1]Serpentine after (poss.) amphibole. [2]Chlorite. [3]Unidentified. [4]Estimated.

Discussion and conclusion

The samples from this study are petrographically, mineralogically and texturally representative of abyssal peridotites as a group. The two exceptions are the abyssal peridotite mylonites, samples AII107:61-78 and 61-83, which are members of a relatively rare class of abyssal peridotites which has undergone extreme high-temperature and pressure deformation, but little, if any, serpentinization. The mineral constituents of abyssal peridotites are altered to differing degrees. By far the most resistant phase to serpentinization is spinel, which appears in almost identical form in every sample studied, including the mylonites. Some of the more extremely weathered samples (e.g., IO11/76:56-58) show at most an increased opacity of the spinel, which may be related to its oxidation. Diopside is also a resistant phase. Most samples of abyssal peridotite, including the ones in this study, contain diopside which is much fresher and better preserved than the orthopyroxene in the sample.

Olivine and enstatite break down to differing degrees during alteration. Olivine is so much more prevalent in abyssal peridotites than enstatite that equal weathering on an absolute basis will *appear* as if more enstatite had broken down than olivine. If, for example, 50 percent of the rock has broken down at 1:1 olivine : enstatite, all the enstatite of a typical abyssal peridotite would be consumed, but less than half of the olivine. As a simple calculation on the table above shows, none of the rocks in this study has a "dissolution mode" with a dissolved olivine to dissolved enstatite ratio of less than one, even though many of the rocks *appear* to have preferentially lost enstatite. Many of the rocks have a ratio of dissolved olivine to dissolved enstatite of much greater than one. This implies that some process that has operated on the rocks preferentially breaks down olivine to enstatite. A major finding of Chapter 3 is a Mg depletion of the rocks, and the depletion is correlated with the dissolution mode of the samples (Chapter 3, Figure 14, and its accompanying discussion). Thus, it is fair to infer that low-temperature processes and weathering have a dramatic effect on the petrographic appearance of the rock, as well as its chemical composition.

Sample	Lizardite / Bastite[1]	Alteration Index[2]	Alteration type
IO 11/76:59-26	1.66	2.37	Greenish black, serpentine dominated.
PS 86:6-37	5.34	4.55	Green, serpentine dominated.
RC 2709:6-2	0.76	4.92	Green, serpentine dominated.
Vulc5:41-15	0.78	7.53	Green.
AII 107:40-35	4.28	2.91	Dun colored.
Vulc5:41-29	4.22	13.17	Dun-colored.
IO 11/76:60-61	11.8	33.74	Dun colored, clay
IO 11/76:56-58	37.4	59.37	Dun colored, clay.
AII 107:61-78		44.34	Dun-colored, clay.
AII 107:61-83		61.14	Dun colored, clay.

[1] (Serpentine after olivine)/(Serpentine after enstatite).

[2] Chapter 3, Table 16.

The table above shows the dissolution modes of the samples, their alteration index and the style of their alteration. It is fairly clear from this table that there is a progression from greenish-black serpentinite to dun-colored clay serpentinite which correlates roughly with the degree of alteration and with the dissolution mode. More weathered samples are more likely to be dun-colored, and contain clay. These are the low-Mg group of samples whose bulk composition has been dramatically and pervasively changed by the weathering process they have undergone.

References

Dick, H.J.B. (1979) Alteration and metamorphism of peridotite at Islas Orcadas Fracture Zone. **EOS, Transactions of the American Geophysical Union** 60-973.

Dick, H.J.B., R. Fisher and W.B. Bryan (1984) Mineralogic variability of the uppermost mantle along mid-ocean ridges. **Earth and Planetary Science Letters** 69:88-106.

Evans, B.W. (1977), Metamorphism of Alpine peridotite and Serpentinite. **Annual Review of Earth and Planetary Science** 5:397-447.

Juteau, T, E. Berger, and M. Cannat (1990) Serpentinized residual mantle peridotites from the M.A.R. Median valley, ODP Hole 670A: Primary Mineralogy and geothermometry. in: Detrick, R. J. Honnorez, W.B. Bryan, T. Juteau et. al., (1990) **Proceedings of the Ocean Drilling Program, Scientific Results** Vol. 106/109.

Kimball, K.L., F.S. Spear and H.J.B. Dick (1985) High temperature alteration of abyssal ultramafics from the Islas Orcadas Fracture Zone, South Atlantic. **Contributions to Mineralogy and Petrology** 91:307-320.

Mercier, J.-C. and A. Nicolas (1974) Textures and Fabrics of Upper Mantle Peridotites as Illustrated by Xenoliths from Basalts. **Journal of Petrology** 16:454-487.

von Damm, K.L. (1990) Seafloor hydrothermal activity: Black Smoker chemistry and chimneys. **Annual Reviews of Earth and Planetary Science** 18:173-204.

Wicks, F. J. and E. J. W. Whittaker (1977) Serpentine Textures and Serpentinization **Canadian Mineralogist** 15:459-488.

Appendix II: Analytical Techniques

Appendix II: Analytical Techniques

Appendix II: Analytical techniques.

Introduction:

In the course of this study, most of the new techniques which were developed were in the realm of mass spectrometry and mass spectrometer control. The goals of this work were fourfold. First, it was necessary to use mass collection schemes not provided for in the basic control software. Second, it was necessary to improve the performance of the software for working with small sample sizes. Third, it was necessary to monitor machine conditions (such as the peak shape and resolution) not provided for in the existing software. These were deemed crucial to the correct interpretation of the data. Fourth, where new programming was involved, the attempt was made to remove the overlay writer from the details of low level operation of the machine in order to simplify overlay writing and to encapsulate and re-use standard code. This chapter will describe in detail the new arrangements for running Nd, Sr and various isotope dilution measurements, the changes I have made to the existing control software and the new software I have developed.

This appendix will be broken up into four parts. They are in reverse order of importance to this thesis, but in a logical order proceeding from the hardware to the finished product. The first chapter will describe the changes I made to the low level control toolbox ("MEASURE") provided by VG. The second will describe a new medium level analysis toolbox ("SNOLIB") I wrote to automate many common mass spectrometric tasks and to eliminate code duplication. The third will describe new overlays I wrote to measure Sr and Nd. The fourth will describe the setup I used with the existing VG software for the analysis of static Sr and Nd, and isotope dilution measurements on Sm.

Low level control

Introduction

The changes I made to MEASURE were by and large for the purposes of improving the amount of information available to the operator during the run and for improving the time performance of the routines. The overriding concern was that the new MEASURE should be completely compatible with overlays designed for the old version. Where this was not completely possible, the reason for the incompatibility was an important one and the changes needed to the old overlays very small. In reading this section it is important to refer also to the VG software manual, as all of the routines I modified are described in some detail there.

MEASURE: Main control program

The program itself only comprises about 120 lines of code. The remainder (about 5000 lines) consists of subprograms which provide the interface to the machine. One area that needed changing was the `Problems:` subroutine, which was programmed to immediately reload MEASURE and start it on encountering a software error. This behavior was a nuisance to development since it became impossible in many cases to determine the cause of the problem that had caused the ON ERROR condition in the first place. The solution was to insert a wait loop so that the machine could be stopped and the contents of memory examined when an error occurred, hence the following code:

```
1341    FOR I=1 TO 240
1342       DISP "Awaiting Operator Intervention  ",240-I
1343       BEEP
1345       WAIT 1
1346    NEXT I
```

The program waits for 4 minutes beeping furiously in order to attract an operator before continuing as it did before to reload MEASURE and try again.

The other major change is a small one but significant, as it causes an incompatibility with overlays designed to run under the original MEASURE. The change is in the COM declaration block, where

```
310     COM /Collectors/ Acol,Ncol,Ocol,Vacol,V(8)
```

is now

```
310     COM /Collectors/ Acol,Ncol,Ocol,Vacol,V(8),Noise(8)
```

The purpose of this change is to provide a storage location for the noise reading accompanying the DVM readings stored in V(*). this has the unfortunate result that subprograms containing the statement

```
310     COM /Collectors/ Acol,Ncol,Ocol,Vacol,V(*)
```

will now generate an "Invalid COM Declaration" error when loaded. The simple way to correct this is to add the Noise(*) array to the COM declaration as follows :

```
310     COM /Collectors/ Acol,Ncol,Ocol,Vacol,V(*),Noise(*)
```

F_optm: Optimizing the focus.

An output line was added which tells the operator what the change in focus is for each plate. The wait (line 2410) could profitably be halved or quartered to improve focussing speed, but I did not do it.

Init: Initializing the machine

When I began work on the software project, there were two versions of the subprogram **Init** actively in use at the same time. One was in the main body of MEASURE code and one was in a separate program file called MEAS1 which is loaded and executed each time MEASURE is run. As a consequence, when MEASURE is run, the second copy of **Init is** loaded on top of the first in memory. Since they were both very similar (if not identical), it became impossible for me to determine which copy was executed when **Init** was called from the body of MEASURE. This situation probably came about when someone in the past stopped MEASURE during the execution of **Init** and re-stored MEASURE to disk. The solution was to delete the copy of **Init** in MEASURE but leave a stub so that the situation would be immediately noticeable if it ever happened again.

Init determines offsets for the Faraday cups and the Daly detector when it is run. These offsets are then subtracted from the DVM readings so that the zero measurements will read something near zero. The 5-second noise on the measurement is now printed out (see the section on **Read_di** for a discussion of this feature) for the DVM offset, the Faraday offset and the Daly offset. This will help to identify noisy channels quickly and to help identify the source of the noise.

The calibration of the magnet is subject to a certain amount of drift with time and with power outages (a common occurrence at WHOI). The process of calibrating the magnet requires two days, to load filaments load the machine, pump it down, measure beams of different elements and enter the results into the MS file. It is possible to continue running if the high voltage is set to bring the calibration close for the element of interest. **Init** will refuse to continue, however, if the voltage is not within the range 8.000$\pm$0.01 kV. A bypass was installed to allow the operator to circumvent this check. In the event of a software induced restart of MEASURE (as will happen with certain software errors and

machine faults) the program waits approximately three minutes beeping furiously to attract an operator, then proceeds. In any case, the high voltage value is printed out.

Power outages affect the measurement system in another way; The HP 9816 has no internal battery-backed clock, so when the power goes out or it is turned off, the system time must be reset. If the operator forgets to do this, the analysis time and date (see the section on **Timetaken**) will be incorrect. A loop was added to force the operator to set the system date to a reasonable time before it will continue.

Mascan: Scanning for a beam.

Two changes were made to the behavior of **Mascan**: First, the center of the scan is flagged in the printout sent to the screen, in order to help the operator judge better the quality of the mass calibration. Second, the criterion for declaring a beam found was changed. `Thrsh` is the variable used to store the threshold over which the machine would declare the beam found. Previously, that would be whenever a signal larger than `Thrsh` was detected. This limited the lower limit of a detectable beam to about twice the amplitude of occasional voltage spikes seen in the Daly detector; 200 DVM units or about 2mV. These spikes were never seen on successive readings of the Daly cup. Thus the criterion was changed so that `Thrsh` has to be exceeded on two consecutive Daly readings to be accepted as evidence that a beam is present. The lowers the smallest detectable beam from about 2 mV to about 0.5 mV (about 5×10^{-17} A). This is a useful modification, as much smaller beams may now be detected than before, without fear of a false alarm.

Peakcenter

The wait between peak and off-peak readings was shortened from 0.5 to 0.2 seconds to improve the speed of the routine. The wait could probably be shortened still further, since the value of the peak and off-peak measurements only needs to be known to about $\pm 10\%$ for the routine to function properly. An output line was added to show the field value at the peak and the difference between the initial value and the old value.

Read_di: Taking a reading from the DVMs.

When taking a five-second integration using the current hardware setup, five one second readings are taken and averaged. This provides the opportunity to calculate the standard deviation of the readings in order to know such interesting quantities as peaktop noise and noise on the baseline which are critical to believing in the basic health of the machine. In fact, as soon as this routine was installed, one of the DVMs was determined to be on the edge, and failed soon thereafter.

In the first loop where the five readings are taken, The sum (V(I11)) and sum of squares (Ex2(I11)) are accumulated (I11 is the loop variable):

```
7810        FOR I0=1 TO Nreads
7820          FOR I11=1 TO Ncol
7830            ENTER Axial_addr+(I11-Acol);Dvm
7831            Temp=Dvm*1.E+5
7840            V(I11)=V(I11)+Temp
7841            Ex2(I11)=Ex2(I11)+Temp*Temp    ! Sum of squares. JES
7850          NEXT I11
```

Next, when the accumulated sum is divided by the number of readings to produce the average, the small sample standard deviation is calculated using:

$$\sigma = \sqrt{\frac{\sum(x^2) - N\bar{x}^2}{(N-1)}} \qquad (1).$$

In the following fashion:

```
7890        FOR I0=1 TO Ncol
7891          V(I0)=V(I0)/Nreads
7892          IF (Nreads>1) THEN
7893            Noise(I0)=SQR((Ex2(I0)-Nreads*V(I0)*V(I0))/(Nreads-1))
7894          ELSE
7895            Noise(I0)=0
7896          END IF
7897          !
7900          V(I0)=INT(V(I0)-Offset(I0)+.5)
7910          V(I0)=V(I0)+1.E-4*(NOT V(I0))
7920        NEXT I0
```

The result is stored in the array Noise(*) which was added to the COM declarations of every subprogram in the general partition which used the /Collectors/ variable block.

Pressure: Read the Ion Gauge

This routine is taken entirely from a program written by Mark Kurz of the same name. The only modification is to place it in the MEASURE toolbox and have it output to the device specified for the line printer by **Init** (@Lpt). The DVM and ion gauge are accessed through absolute assignments, so if the hardware setup is changed, this routine must be modified.

Print_focus: Print out focus parameters

This routine is provided so that eventually an overlay will not have to concern itself with the values of focus parameters, merely calling this routine and another (as yet unwritten) called, e.g. **Focus** to accomplish everything.

Print_fil: Print out filament currents.

This routine similarly serves as a means of abstracting the actual filament operation from the overlay. The currents of the side and center filaments are printed out in an appropriate way:

```
11649 Print_fil: SUB Print_fil
11650    !
11651    !  Prints out filament currents in a nice fashion.
11652    !  JES 7/9/91
11653    !
11654    COM /Filaments/ Fil,Pampc,Pamps,Pratec,Prates,Pstate,Ra1,Ra2,
Trp1,M(*),Mt(*),Mxc(*),P(*)
11656    COM /Select/ @Vdu,@Lpt,@Ms,Ms_hpib,Pr1,Pr2,Bu$
11657    !
11658    IMAGE K,2D.3D
11659    OUTPUT @Lpt USING 11658;"Filaments:   Center ",M(1)
11660    IF Trp1 THEN
11661       IMAGE #,K,2D.3D
11662       OUTPUT @Lpt USING 11661;" Side: ",M(2)
11663    END IF
11664    SUBEND
```

Print_bdinfo: Print out bead information.

This is a very simple data abstraction routine which prints out the information on the bead currently in position. The overlay then does not need access to this information.

Process automation

Introduction

The low level toolbox provided by VG in the form of MEASURE provides a two tiered model for control program development. Most machine functions are controlled by subprograms in MEASURE, though at a fairly low level, so that to operate the machine one must directly modify the variable that MEASURE itself uses. This is good in that the machine is controlled very directly, but bad in that it is not always easy to predict the side effects of changing one of MEASURE's global variables, and the usage of the functions that MEASURE provides is not well documented. For example, to focus a beam one has acquired, one must use the following construct:

```
422     COM /Focii/ Fno,Foc(*),Fstep(*),Fms(*),Fml(*),Foc$(*)
.
.
.
.
461             FOR Fno=3 TO 9
462               CALL F_optm
463               IF Abrt THEN SUBEXIT
464               CALL Refresh
465             NEXT Fno
```

This requires a fair amount of code for an operation which is done exactly the same way every time. Ideally, this code would be encapsulated into one routine which could be called without even having access to the arrays containing the focus parameters. Then focussing the machine would simply be a matter of calling an **Opt_focus** subprogram once. Declaring the COM block /Focii/ would not be necessary, and the code would be at once clearer and easier to maintain.

At a higher level of abstraction, the fundamental set activities needed to do a successful mass spectrometric analysis can be identified and provided for. Then the operator need only write the code which is specific to the type of analysis being performed. This was the attempt when writing the SNOLIB library. The fundamental set includes:

- Warming up the filaments before analysis.
- Getting an initial beam.
- Setting up the mass positions needed for data collection.
- Collecting data
- Reducing data and calculating the quantities of interest
- Data output and reporting.

Of these only the fifth item is sufficiently unique that new code must be written for each situation. Certain well defined types of data collection such as single collector peak jumping and static multicollection do not require even this coding.

The routines contained in SNOLIB were written with the specific purpose in mind of making overlay creation an easier process. The primary idea is that the overlay writer can call routines which carry out the most common operations of mass spectrometry in an automated fashion, without having to worry about the details of how they work. Thus an overlay for a new type of isotopic analysis can be written with just a few lines of code, most of which is devoted to the new aspects of the analysis, rather than the mechanics of getting a beam, setting up for peak jumping or collecting data at successive mass positions.

An added benefit of the toolbox approach is that improvements to the toolbox routines apply to all the overlays that use the toolbox, so that if, say peaktop noise calculation is deemed to be necessary, it can be added in one place, rather than in half a dozen separate overlays. This is also one of the principal drawbacks, as it becomes difficult to customize a toolbox routine for a particular situation. The routines are designed to be as widely applicable as possible and none of them requires the use or modification of global variables.

Ramp_fil: Filament warmup control

This is essentially a replacement for one use of the MEASURE subprogram **Raisfil**. It is intended for the situation where the current is being ramped from zero to some initial current for beam acquisition. Instead of ramping the filament current in a linear fashion, the current switches immediately to 1/2 the target current, it ramps in one minute to 3/4 of the target current and uses the remaining time to get to 100% of the target current. If the beneficial effects of warming up the filament obey an Arrhenius law, as does the emission of thermal ions, this will result in a more efficient use of the warmup time, since the beneficial effects of a slow warmup occur in the last few percent of the ramping process. A shorter warmup time can then be specified for the same effect. While for an individual analysis the difference might be small, say twenty minutes, the cumulative effect of a few barrels run with fast ramping is a fair piece of machine time (at $300/day).

The usage of this subprogram is as follows:

```
CALL Ramp_fil(Tc(*),Ma,Ai,Tm)
```

where Tc(*) is an array containing the two target currents, Ma is the mass to be monitored during warmup Ai is the aiming current (**Ramp_fil** will return early

if 75% of the aiming current is reached) and Tm is the time for the warmup in centiseconds (I did not choose these units).

Get_beam: Finding an initial beam

Get_beam has the straightforward task of increasing the current gradually while scanning for a beam at a given mass. If no beam is found by a filament current 20% higher than the initial current, an attempt is made to cycle throughout the focus to find the beam. Thus, if the mass calibration is a little off, or if the initial focus is a little off, a beam will still be found. If both are off, the impact on the sample will be minimized and the routine will set the Abrt variable. The usage is as follows:

```
362 Get_beam:SUB Get_beam(Fi,Ma,Ai)
```

where Fi is the filament to turn up (1 for center, 2 for side), Ma is the mass to scan for, and Ai is the aiming current for the beam to be acquired. For example, to migrate an existing VG triple filament overlay to use this code the fragment

```
Fi=1                        ! Single filament
Ai=Aimr                     ! Aiming intensity for Re
Ma=186.91                   ! Mass to look for Re at.
CALL Get_beam(Fi,Ma,Ai)     ! Off we go.
```

would replace the first approximately 50 lines of code.

Peakshape: Measuring peak shape and resolution.

The shapes of the peaks of masses of interest is of critical importance to the functioning of the VG 354 mass spectrometer. **Peakshape** provides a convenient method to test this quantity. It scans across the mass of interest, interpolating the 10% and 90% peak height levels and calculates the industry standard 10% height resolution. This and the other quantities calculated are described in the comments in the code:

```
4520    !
4530    !   Dispersion    is the peak separation in mass units between
4540    !                 adjacent peaks.
4550    !
4560    !   Resolution    is ( Dispersion / 10% peak width ) x m
4570    !                 Specification for this machine is 430 or
higher.
4580    !
4590    !   Side slope    is ( 90% width / 10% width ) x 100.
4600    !                 Data are questionable below 58%.
4610    !
4620    !   Symmetry      is (Right (10% - 90%) / Left (10% - 90%) ) x
100
4630    !                 or its inverse (always < 100%).
```

```
4640    !                    Should be 90% or better.
4650    !
4660    !    JES   4/30/90
4670    !
```

Usage is as follows:

```
CALL Peakshape(Ma,Cn)
```

where Ma is the mass of interest and Cn is the Field value of the center of the peak. The peak must have been acquired and focussed first for this routine to work. The results may be less reliable if the beam is very unstable.

Set_peaks: Finding and setting peaks for peak jumping

Set_peaks and **Dynam** are a matched pair of routines to set up for and complete a multi-dynamic data collection program. **Set_peaks** has the following usage:

```
503 CALL Set_peaks(Nm,Np,Massb(*),Maxpe,Icore)
504   !
505   !   Nm    = Number of masses (including zeros)
510   !   Np    = Number of peaks
520   !   Massb(*) = Mass positions to be calculated (Nm of these)
530   !   Maxpe    = Expected Maximum peak (0= doesn't matter)
540   !   Icore    = Expected abundance of maximum peak
550   !
```

The parameters Maxpe and Icore allow a certain amount of verification that the spectrum being measured is the correct one. Odd values can come about by bad overspiking, mass interference due to bad chemistry, and very bad miscalibration of the magnet. All of these have been observed at one time or another, and do not necessarily preclude getting good data, but are a condition that the operator will probably want to know about.

Set_peaks will center up on as many peaks in the peak jumping sequence as it can (in some imaginable peak jumping sequences, there may be no peak in the center cup at one or more mass positions, and obviously never for the zero), and calculated field positions using the VG provided routines. It then tests the beam growth rate and returns.

Set_peaks communicates with **Dynam** the field positions to be used through the global array Chan(*), declared in the general common block. If one wishes to set up another peak switching regimen than the one set up in

Set_peaks, one must declare the entire general COM block to get access to Chan(*) and reset the field values that way.

Dynamic: Taking multi-cup, multi-channel data

Dynamic takes as input a series of field values and a storage location and proceeds to take data at those positions, subtract the baseline, calculate statistics on the baseline, print them out and return. **Dynamic** has a private storage area where it keeps previously taken zeros. If the number of zeros matches the number called for in the current measurement and they are less than five minutes old, they are averaged with the set that **Dynamic** takes in the current run. The usage is as follows:

```
5010 CALL Dynamic(Nm,Ch(*),Nc,Nz,Sn,Data(*))
5020!
5030!   Where:
5040!         Nm    = Number of mass positions (not including zero)
5050!         Ch(*)= Field values for all Nm+1 mass positions.
5060!         Nc    = Number of cycles.
5070!         Nz    = Number of zeros.  (Max 15/Block)
5080!         Sn    = Single collector mode: affects printout only.
5090!         Data(Cycle,Channel,Collector) Must be at least Nm by Nc by
Ncol.
5091!         This is the array for raw data.
```

It is then up to the user to calculate the ratios of interest, including any necessary interpolation, etc. If interpolation is necessary, the time each channel was taken can be found in the common block

```
5420    COM /Data/ Dtime(*)
```

If some aspect of the zero measurement becomes of interest, the zero information can be found in the following common block:

```
5430    COM /Zeros/
Zeros(*),Noldz,Ztime,Avg_zero(*),Zero_noise(*),Ser_zero(*)
```

Dynamic printout is quite easy to decipher; uncorrected, non-zero-subtracted raw data are printed out along with the mass in the axial cup. Zeros are easy to spot as they are at the beginning and end of each run and are usually at a half-mass position. A typical printout looks like this:

Ax. Mass	L2	L1	Ax	H1	H2
151.3	-2	-8	7	0	0
144	1776	944	167002	668	459
145	879	1859	58436	1388	-1
146	1925	680	121773	0	458
151.3	-2	-8	9	-2	-2
Zero:	-2.00	-8.00	8.00	-1.00	-1.00
Error:	0.00	0.00	1.41	1.41	1.41
Noise:	5.50	4.42	2.07	3.16	2.61

This printout is from 21 July, 1991 and is the first run of a La Jolla Nd standard. The axial detector in this case is the Daly detector, so the axial readings are a factor of 100 or so higher than the other cups. The uses to which the data are put are explained in greater detail in the section on the Nd multidynamic overlay, Ndt5.

Dynam prints out statistics on the zero which are important for keeping track of the health of the machine. The average zero is printed out; this is the value which is subtracted from the data taken by each cup prior to exit. It is nearly always close to 0, though the faraday offset is known to drift slightly with time, so over the course of a full barrel, the absolute value of the zero can vary as much as $\pm$ 50. There is another bug which afflicts every version of MEASURE on the machine in which the faraday offsets for the high three cups (stored in Offsets(*) in the COM block /Offsets/) are somehow overwritten with bogus values, usually around 1100. This results in an unusual looking printout, but the data are still good.

The error quoted is the small sample standard error of the mean of the zero measurements. This is intended to characterize the degree to which the value of the zero measurement is known. The noise quoted is the average of the 5-second noise readings for each cup over all the zeros. The peaktop cannot be any quieter than the baseline, so if the **Error** reading is less than the **Noise** reading, the noise on the zero is not contributing significantly to the overall uncertainty of any of the calculated ratios. If the **Error** reading is much less than the **Noise** reading (as it is in the example printout above), then the length of time spent reading the zero could be reduced without affecting the analysis.

By itself, the **Noise** value is a measure of the health of the amplifying electronics for the cups. When this routine was installed, it was immediately discovered that one of the DVM's was marginal. While the noise was visible to the trained eye watching the DVM during data collection, it was not obvious in

the way that it was when the Noise reading on the zero for the axial cup suddenly became 60.00 rather than 4.00.

Taking static data is quite easy using **Dynamic**, since static multicollection is just a special case of dynamic multicollection (at least as far as **Dynamic** is concerned). In that case, Nm is 1 since there is one mass position for peaktop integration, and Ch(*) contains two values; one for the peaktop and one for the zero.

Report: Printing out results

(n.b.: This subprogram is still experimental and has not been added to the library yet)

This subprogram will take an array of isotope ratios, calculate statistics on them and print them out in a legible format. It will additionally format a one line string containing averages and errors in preparation for saving it to disk. This is stored in the variable Out$ in the common block /Report/. At the end of the overlay, when the best data have been taken, this line can be saved to disk by **Disk_out**. The usage is:

```
CALL Report(First,Last,R(*),Ydim,Nr,err_opt)
```

where First is the number of the first ratio to be used and Last is the number of the last ratio to be used. R(cycle,ratio) is a two dimensional array containing Cycle by Ratio ratios. Nr is the number of ratios to be printed out and err_opt specifies whether errors will be given in percent (=1) or permil (=2).

Disk_out: Storing results to disk.

(N.B. this subprogram has not yet been added to the library.)

The subprogram **Disk_out** stores the lastest Out$ manufactured by **Report** and writes it to the file specified. If this is the first bead of a given MEASURE run, a header with ratio names is written to disk first. If the file does not exist, it is created.

Nd dynamic multicollection

Introduction

At the beginnig of this work there was an existing program for the analysis of Nd provided by VG. There were three fundamental difficulties with actually using this code in practice. The first was the lack of certain diagnostic measurements to assure the quality of the data. The second, and more important, was the necessity of measuring ^{150}Nd for purposes of isotope dilution. The third was one of performance: the existing dynamic multicollection software was not much faster than single cup peak jumping. In order to run small samples, optimum performance from the multi-cup hardware was required.

In order to work at low concentrations it was decided that it was necessary to write an overlay which addresses these specific issues with regard to data collection.

Previous setup

The peak setup for the old overlay was as follows:

Magnet Position:	L2	L1	Ax	H1	H2
I	140	142	143	144	145
II	141	143	144	145	146
III	142	144	145	146	147
Mass offset:	-3	-1	0	+1	+2

These major calculations were performed:

- Correction of 142/144 for the presence of Ce by measurement at 140 in position 1,
- Correction of 143/144 for mass interference caused by ^{144}Sm by measurement at 147 in H2, position III.
- Calculation of "magic" ratios of 143/144, 142/144 and 145/144
- Measurement for display of interpolated 146/144.

Current peak setup

The peak setup which was chosen to enable the measurement of 150/144 was as follows:

Magnet Position:	L2	L1	Ax	H1	H2
I	142	143	144	145	148
II	143	144	145	146	149
III	144	145	146	147	150
Mass offset:	-2	-1	0	+1	+4

Data are now collected using the subprogram **Dynamic**. Major changes to the operation of the code are as follows:

- The 146/144 ratio is now measured by direct multicollection and explicit gain correction in positions II and III.
- Cups 1-4 are used for the "magic" calculation instead of 2-5.
- ^{144}Sm is not corrected for, though it is measured in a separate operation before data collection begins.
- 142/144 is measured uncorrected for Ce interference. This allows a semi-quantitative measurement of the Ce/Nd ratio which can be used to re-check the quality of column chemistry. Interference of the tail of 142 at mass 143 is unlikely until the 142/144 ratio is quite large, perhaps 5 or 10.
- "Magic" 150/144 is calculated (derivations of all "magic" ratios can be found in the next section).

Derivation of "Magic" ratios

When collecting static multicup data, the limit of attainable accuracy in the results is controlled in most cases by the degree to which the relative gains of the various detectors and their attendant amplifying circuitry is known. In the absence of mass fractionation in the ion source, the cup gains could be easily determined by placing an invariant isotope pair into a given cup pair to calibrate it, then measuring the isotope pair of interest. In actual practice, the cup gains and mass fractionation are inseparably bound together, such that a complete description of each is necessary to even begin to calculate the other. It is, however,

possible to calculate both at the same time. If X and Y are isotope ratios of interest, and X=m1/m2 and Y=m3/m4, the classic power law for mass discrimination on the ion source is written as follows (Hart and Zindler, 1989):

$$\frac{Y_M}{Y_T} = b\left(\frac{X_M}{X_T}\right)^a \tag{2}$$

where b=1 in this case and a=(m3-m4)/(m1-m2). If we define f such that

$$f = \left(\frac{Y_M}{Y_T}\right)^{1/(m3-m4)} - 1 \tag{3}$$

a complete description of any isotope pair can be arrived at:

$$X_M = X_T(1+f)^{(m1-m2)}\left(\frac{G1}{G3}\right) \tag{4}$$

where (G1/G3) is ratio of the absolute gains of the cups used to collect ratio Xm. The "magic" occurs when mass positions and isotope pairs are chosen such that a second isotope pair can be multiplied by the first to make the second two terms cancel. The equation isl then left with only measured ratios, known normalizing ratios and the true ratio of interest, which can easily be solved for. $^{143}Nd/^{144}Nd$ serves as an example.

<u>143/144</u>

Referring to the table of peak positions above, we can see that two measurements of 143/144 are carried out; their total description is as follows:

$$\left(\frac{143}{144}\right)_M^I = \left(\frac{143}{144}\right)_T^I (1+f)^{-1}\left(\frac{G2}{G3}\right) \tag{5}$$

$$\left(\frac{143}{144}\right)_M^{II} = \left(\frac{143}{144}\right)_T^{II} (1+f)^{-1}\left(\frac{G1}{G2}\right) \tag{6}$$

choosing to divide through by 146/144 will cause everything to cancel. The equation for 146/144 taking mass fractionation and cup gains into account is as follows:

$$\left(\frac{146}{144}\right)_M^{III} = \left(\frac{146}{144}\right)_T^{III}(1+f)^2\left(\frac{G3}{G1}\right) \tag{7}$$

Multiplying (5) and (6) and dividing by (7) produces the following result:

$$\left(\frac{143}{144}\right)_M^{I}\left(\frac{143}{144}\right)_M^{II}\left(\frac{146}{144}\right)_M^{III} = \left(\frac{143}{144}\right)_T^{I}\left(\frac{143}{144}\right)_T^{II}\left(\frac{146}{144}\right)_T^{III} \tag{8}$$

Using 146/144 is intentional, since that ratio is used for normalizing for mass fractionation already, the value of $(146/144)_T$ is fixed by international convention (except for Caltech) as .7219. $(143/144)_T$ is then easily solved for.

$$\left(\frac{143}{144}\right)_T = \sqrt{\left(\frac{143}{144}\right)_T^{I}\left(\frac{143}{144}\right)_T^{II}} = \sqrt{\left(\frac{143}{144}\right)_M^{I}\left(\frac{143}{144}\right)_M^{II}\left(\frac{146}{144}\right)_M^{III}\Big/\left(\frac{146}{144}\right)_T^{III}} \tag{9}$$

Equation 9 is used in the Ndt5 overlay to calculate the $^{143}Nd/^{144}Nd$ ratio.

<u>145/144</u>

For 145/144, the equivalents of equations (4) through (6) can be written

$$\left(\frac{145}{144}\right)_M^{I} = \left(\frac{145}{144}\right)_T^{I}(1+f)\left(\frac{G4}{G3}\right) \tag{10}$$

$$\left(\frac{145}{144}\right)_M^{I} = \left(\frac{145}{144}\right)_T^{I}(1+f)\left(\frac{G3}{G2}\right) \tag{11}$$

$$\left(\frac{146}{144}\right)_M^{II} = \left(\frac{146}{144}\right)_T^{II}(1+f)^2\left(\frac{G4}{G2}\right) \tag{12}$$

and $(145/144)_T$ solved for:

$$\frac{\left(\frac{145}{144}\right)_M^I \left(\frac{145}{144}\right)_M^{II}}{\left(\frac{146}{144}\right)_M^{II}} = \frac{\left(\frac{145}{144}\right)_T^I \left(\frac{145}{144}\right)_T^{II}}{\left(\frac{146}{144}\right)_T^{II}} \tag{13}$$

150/144

The case of 150/144 is a little more difficult, as the mass range is so great that another isotope ratio is needed to help make the $(1+f)^6$ term drop out. In this case :

$$\left(\frac{150}{144}\right)_M^{III} = \left(\frac{150}{144}\right)_T (1+f)^6 \left(\frac{G5}{G1}\right) \tag{14}$$

$$\left(\frac{146}{144}\right)_M^{III} = \left(\frac{146}{144}\right)_T (1+f)^2 \left(\frac{G3}{G4}\right) \tag{15}$$

$$\left(\frac{148}{144}\right)_M^{I} = \left(\frac{148}{144}\right)_T (1+f)^4 \left(\frac{G5}{G3}\right) \tag{16}$$

results in:

$$\frac{\left(\frac{150}{144}\right)_M^{III}}{\left(\frac{146}{144}\right)_M^{III} \left(\frac{148}{144}\right)_M^{I}} = \frac{\left(\frac{150}{144}\right)_T}{\left(\frac{146}{144}\right)_T \left(\frac{148}{144}\right)_T} \tag{17}$$

and

$$\left(\frac{150}{144}\right)_T = \left(\frac{150}{146}\right)_M^{III} \left(\frac{146}{144}\right)_T \left(\frac{148}{144}\right)_T \Big/ \left(\frac{148}{144}\right)_M^{I} \tag{17a}$$

The added difficulty here is knowing the natural 148/144 ratio, which I arbitrarily set at 0.24087 from the VG table of the isotopes.

146/144

The measured 146/144 ratio is of interest to the operator primarily to monitor the progress of the run and the quality of the data being generated. It is not used in any way for calculation of other isotope ratios. The previous overlay, NdtQ, used interpolation on the axial collector to determine this ratio, with an unfortunate performance penalty of two additional magnet cycles per block. This was changed to static measurement of 146/144 in mass positions II and III with explicit gain correction based on recent Constant Current Source gain measurements. This approach saves the interpolation code and the extra magnet cycles, and is adequate for the purpose.

Checking for Sm interference

The degree of Sm interference in the Nd signal is assessed by integrating at an axial mass position of 147 on the Daly detector. This is divided through by the Daly gain (calculated elsewhere) and the most recent 146/144 ratio to get the $^{144}Nd/^{144}Sm$ ratio:

$$\frac{^{144}Sm}{^{144}Nd} = \left(\frac{147}{146}\right)_M \left(\frac{^{144}Sm}{^{147}Nd}\right)\left(\frac{^{146}Nd}{^{144}Nd}\right) \tag{18}$$

The correction to be applied to $^{143}Nd/^{144}Nd$ is also calculated.

$$\Delta_{\left(\frac{143}{144}\right)} = \left(\frac{^{143}Nd}{^{144}Nd}\right) \Big/ \left(\frac{^{144}Sm}{^{144}Nd}\right) \tag{19}$$

Note that the value chosen for 146/144 and 143/144 is unimportant, as the entire range of observed values of these ratios in natural rocks and in reasonable mass spectrometer runs does not exceed the target 5 % precision for this measurement. No correction is carried out or action taken directly from this measurement. Experience has shown that Sm-contaminated Nd runs have very stable Sm/Nd ratios , and that a post hoc correction can be applied as necessary. This measurement is provided to allow the operator to rule out the possibility of Sm interference at mass 144 causing some anomaly in the data.

Sr dynamic multicollection

Introduction

The deficiencies of the VG code with respect to low-level multi dynamic Sr analysis were threefold. First, the performance was worse than comparable single collector machines. Second, although there was an algorithm in place for the correction of Rb interference, the extent of that interference was never reported to the operator. Third, as with the Nd program, certain possible diagnostic measurements were not being made.

The overlay I developed grew out of the Nd overlay I wrote at a point some time in January, 1991. As a result, when I modularized the Nd code, the Sr code was already written, debugged, and producing data. At this time, the Sr overlay (Srs5) does not use the modular library, and its development is frozen while data are actively being collected. At some time in the future, the Sr overlay should be migrated to use the modular code so that it can take advantage of performance and diagnostic advantages built into that code. Migrating the code all at once will be easier than incorporating those changes one by one. The use of the modular code will result in an additional 20% increase in time efficiency of the data collection.

Previous setup

The old overlay made use of only the center three cups. It used eight magnet positions with two zero positions, and required two dead cycles at the beginning of each run for its extensive use of interpolation. The peak setup was as follows:

Magnet position	L1	Ax	H1	Comment
1=9	86	87	88	Magic 87/86
2=10	87	88	89	Magic 87/86
3=11	82	83	84	not used
4	83	84	85	84 & 85 (H1)
5	90.4	91.4	92.4	Bkg for Ax & H1 only
6	84	85	86	Rb for Ax
7	85	86	87	Magic 87/86, Rb on L1
8	90.4	91.4	92.4	Bkg for L1 only
9	86	87	88	* Magic 87/86
10	87	88	89	* 86/88 interp.
11	82	83	84	*

This peak setup is complex and it logic is difficult to penetrate. There are a number of interesting details, such as the completely unused magnet position (numbers 3 and 11) or the fact that the main loop of magnet positions begins at one, cycles through to 11 on the first pass, and thereafter cycles back to position 4, copying the data from positions 9 through 11 to positions 1 through 3 and re-using them. The re-use of data between cycles additionally has a smoothing effect which results in artificially low internal precisions for analyses using this overlay.

The major features of the program are that 87/86 is calculated by magic on mass positions 1 +2 and 7+9, using the identical formulation as used by the new overlay. 86/88 and 84/88 are calculated by interpolation on the axial cup. Rb correction is done for each cup independently, presumably to avoid cup gain corrections. Additional details of the calculations perfomed by this code (including example raw data reduced by hand reproducing the values arrived at by SrsT) are contained in the handout "Decrypting SrsT Printout" which I distributed in February, 1991 to the VG 354 group.

Peak setup

The new code was designed to be as simple as possible. Interpolation was dispensed with entirely. Rb detection and correction were moved to a position between runs where a much more sensitive method could be employed (this is described in a later section). The peak setup is as follows:

Magnet position	L2	L1	Ax	H1	H2	Comment
IV	89.5	90.5	91.5	92.5	93.5	Prev. Bkg
I	84	85	86	87	88	
II	85	86	87	88	89	
III	86	87	88	89	90	
IV	89.5	90.5	91.5	92.5	93.5	Bkg.

Derivation of "Magic" ratios

The "magic" ratios are derived in a manner similar to the derivation for Nd, so the preliminary steps need not be repeated here.

87/86

For the 87/86 ratio, a complete description is as follows:

$$\left(\frac{87}{86}\right)^{I}_{M} = \left(\frac{87}{86}\right)_{T}(1+f)\left(\frac{G4}{G3}\right) \tag{20}$$

$$\left(\frac{87}{86}\right)^{II}_{M} = \left(\frac{87}{86}\right)_{T}(1+f)\left(\frac{G3}{G2}\right) \tag{21}$$

and

$$\left(\frac{86}{88}\right)^{II}_{M} = \left(\frac{86}{88}\right)_{T}(1+f)^{2}\left(\frac{G2}{G4}\right) \tag{22}$$

result in

$$\left(\frac{87}{86}\right)^{I}_{M}\left(\frac{87}{88}\right)^{II}_{M} = \left(\frac{87}{86}\right)_{T}\left(\frac{87}{86}\right)_{T}\left(\frac{86}{88}\right)_{T} \tag{23}$$

and finally

$$\left(\frac{87}{86}\right)_{T} = \sqrt{\left(\frac{87}{86}\right)^{I}_{M}\left(\frac{87}{86}\right)^{II}_{M}\Big/\left(\frac{86}{88}\right)_{T}} \tag{24}$$

Note that the measurement at mass 86 taken in magnet position II is not needed in the final calculation. This allows another 87/86 to be calculated using the last two magnet positions:

$$\left(\frac{87}{86}\right)_{T} = \sqrt{\left(\frac{87}{86}\right)^{II}_{M}\left(\frac{87}{86}\right)^{III}_{M}\Big/\left(\frac{86}{88}\right)_{T}} \tag{25}$$

The geometric mean of these two values is taken as the final 87/86 ratio.

84/88

The 84/88 ratio is a little more complicated because of the four a.m.u. between them, but the principle is familiar:

$$\left(\frac{84}{88}\right)^{I}_{M} = \left(\frac{84}{88}\right)_{T}(1+f)^{-4}\left(\frac{G1}{G5}\right) \tag{26}$$

$$\left(\frac{86}{88}\right)_{M}^{III} = \left(\frac{86}{88}\right)_{T} (1+f)^{2} \left(\frac{G1}{G3}\right) \tag{27}$$

$$\left(\frac{86}{88}\right)_{M}^{I} = \left(\frac{86}{88}\right)_{T} (1+f)^{2} \left(\frac{G3}{G5}\right) \tag{28}$$

leading to

$$\frac{\left(\frac{84}{88}\right)_{M}^{I}}{\left(\frac{86}{88}\right)_{M}^{III}\left(\frac{86}{88}\right)_{M}^{I}} = \frac{\left(\frac{84}{88}\right)_{T}}{\left(\frac{86}{88}\right)_{T}^{2}} \tag{29}$$

and

$$\left(\frac{84}{88}\right)_{T} = \frac{\left(\frac{84}{86}\right)_{M}^{I}\left(\frac{86}{88}\right)_{T}^{2}}{\left(\frac{86}{88}\right)_{M}^{III}} \tag{30}$$

which is used in the overlay. Note the arabic superscript "2" on the $(86/88)_T$ term in equations 29 and 30 denoting that the "true" (86/88) term is squared. One complication which has nothing to do with the mathematics of the magic calculation is the dispersion between the 84 and 86 peaks differs significantly from that between 86 and 88. This results in poor 86/88 data in situations where the peak shape is marginal. A partial solutiion to the problem is to set the L2, Ax cups to 86+88, mark the position of the L2 cup, then do the same for 84+86, then move the cup to the position which splits the difference. This results still in measurements on the L2 cup which are on the side of both the peaks measured, but the data seem to be acceptable at the cost ofsome operator inconvenience at cup-setting time.

The total solution to the question of 84/88 measurements is to do away with the magic calculation entirely and to set the low cup centered on 84 when 86 is in the axial cup. 84/88 can then be calculated using an explicit gain correction. The errors inherent in explicitly gain-corrected isotope ratios are on the order of 0.01% and thus are irrelevant to the isotope dilution calculation which has inherent errors on the order of 0.1%.

86/88

The 86/88 ratio is calculated with explicit gain correction from multicollected ratios taken in magnet positions 1, 2 and 3, which are then averaged.

Checking for Rb

Rubidium contamination is an unfortunate occurrence which can strike anytime, any sample, including shelf Sr solutions (via filament contamination). By far the best solution is to make sure that the chemistry is clean, that the filament is clean, that the source is clean, and that the sample is well conditioned in the outgasser. Even still, it is possible now and again for there to be some Rb in with the Sr on the filament. In this case, it is important to try to measure the amount of Rb, flash it away if possible and correct for it if necessary. This entire operation adds some complexity to the Srs5 overlay, but it is worth it in terms of the quality of analysis generated.

There is a crude Rb measurement carried out in the initial stages of setting the peaks. In the `Peakhop` section of the code, the heights of all the peaks that have been found are determined, the maximum peak is divided by the sum of the other peaks to yield Icor, the aiming current correction factor. In the case where there is a large amount of Rb, (like for example ^{87}(Rb+Sr) > ^{86}Sr) this ratio can be affected. In normal Sr this ratio is 0.83. If the ratio is significantly different from 0.83 (the range is 0.73 to 0.87), some problem is indicated, such as Rb or hydrocarbon interference. The overlay waits for a few minutes, then rescans the peaks to see if the problem has solved itself. In cases of severe Rb contamination, this has occurred.

Once the beam is found, peaks centered and the first few sequences of preliminary data are measured, Rb is measured with the axial detector set to the Daly at mass 85. The 85/87 ratio is then measured directly on the axial and H2 cups. If the Daly gain has been measured previously, that value is used; otherwise avalue of 80 is assumed for the Daly gain correction. The ^{87}Sr/^{87}Rb ratio is calculated and printed out. This ratio should typically be greater than 75,000 for the analysis to proceed. Otherwise some action must be taken.

Flashing Rb

Flashing a sample to remove Rb is by no means the optimum situation. It causes a pressure burst in the source which could cause problems. The greatest danger is that the pressure burst could cause an arc from the high voltage source to the case. The computer has no means of switching the high voltage to standby during the flash. Flashing additionally plates the Rb, as well as volatile impurities in the sample into the source and focussing plates. It is also not without risk for the sample, as filaments have been known to burn out during flashing (filaments are more susceptible to burning out when there is a sample

loaded). Flashing is considered a last resort in order to get data which would otherwise be unobtainable.

The 86/88 is first measured by multicollection on L1 and H1 in the subroutine Check_68. If it is too low, no flashing is aborted. Otherwise, the current for the flash is calculated and the magnet is set so that no beam is in the cups. The current is turned up for 4 seconds. Following that, there is a waiting period at the original filament current for the sample to cool down. The Sr peaks are then set up again, the 86/88 and $^{87}Sr/^{87}Rb$ ratios are measured again and the go/no-go decision for the next flash is made. The program will keep flashing unless the 6/8 and 87/87 ratios have not improved twice in a row, the 6/8 ratio drops below the minimum, or the 87/87 ratio goes above 75,000.

In most cases, the 6/8 ratio improves tremendously, the filament current required to reach the specified beam current decreases dramatically and Rb is gone after one or two flashes. On the other hand, the peak shape, resolution and abundance sensitivity of the machine seem to experience sharp deterioration after flashing of just a few samples, so it is advisable to avoid the Rb instead.

There is a parameter added to the PROC file for Srs5 for the flashing aggressiveness. This sets parameters such as the strength of the flash, the minimum 86/88, and so forth. The values for all of these are set out in this table:

Parameter:	**Prm(2) :**			
	0	**1**	**2**	**3**
Initial intensity	0	0	15%	20%
Increment	0	0	1.5%	2%
Max. # of flashes	0	6	2	7
Minimum 86/88	-na-	.1196	.1198	.1198
Cooldown (sec)	-na-	600	60	60
Comment:	No flash.	Has the effect of waiting 10 minutes.	Moderate flashing.	Aggressive flashing.

Correcting for Rb

In the event that flashing is unsuccessful or ill-advised (for example if the 86/88 ratio is too low) the attempt is made to correct for the presence of the Rb. The subroutine Check_rb is called which measures the level of ^{87}Rb present and calculates the correction. First a zero is taken at the normal zero position. The magnet is then set to put 85 into the axial cup:

Mag. pos.	L2	L1	Ax	H1	H2
Zero	89.5	90.5	91.5	92.5	93.5
85 peak	83	84	85	86	87

The $^{87}Sr/^{87}Rb$ ratio is calculated as follows:

$$\left(\frac{^{87}Sr}{^{87}Rb}\right)=\left(\frac{^{87}Sr}{^{85}Rb}\right)\left(\frac{^{85}Rb}{^{87}Sr}\right) \tag{31}$$

This is the value used for assessing the degree of Rb contamination of the Sr beam. In general, runs with $^{87}Sr/^{87}Rb$ of greater than 75,000 can be thought of as free of Rb. This corresponds to a correction of $^{87}Sr/^{86}Sr$ of less than $1x10^{-5}$. The correction itself can be calculated in this fashion:

$$\Delta_{\left(\frac{87}{86}\right)}=\frac{\left(\frac{^{87}Sr}{^{86}Sr}\right)}{\left(\frac{^{87}Sr}{^{87}Rb}\right)} \tag{32}.$$

When Rb correction is in effect, the two measurements at either end of the run are time interpolated back to the time of the measurements on the peaktops and the correction is made to the raw ratios. The correction of Sr data for the presence of Rb is tricky in that the presence of Rb spike can totally invalidate the correction. If the value of $^{87}Sr/^{87}Rb$ rises above 75,000 during the course of the analysis, Rb correction is suspended.

Other analyses

Static Nd Runs

Peak setup for ID and IC

In contrast to the situation with regard to the dynamic software, the static software was versatile, adaptable and functioning correctly, if somewhat slow. It was decided to attempt to get Nd data in static mode to about .01% or better (±0.00005 in the 143/144 ratio) in order to get the most out of small samples. The cup placement should be chosen so that static and dynamic runs could be completed on the same barrel, and so that ^{150}Nd is collected. The following cup strategy was devised:

Cup:	L2	L1	Ax	H1	H2
Offset:	-2	-1	0	+1	+4
Type 11:	143	144	145	146	(149)
Type 12:	144	145	146	147	150

In this way, Type 11 allows Nd IC runs can be done with the Daly detector on ^{145}Nd for centering and focussing at low beam currents. Almost any sample should give some data at that level. The next step is to take ID data at a slightly higher beam current, perhaps about 50 mV of ^{144}Nd, this is accomplished by specifying type 12 for sequence number 2 . Then back to type 11 for IC measurements at that beam strength. Finally, 144 measurements are taken at 100 mV (this takes about 12 minutes). If the sample is still showing signs of life after that, then it probably has enough strength to be run in dynamic mode.

Data reduction and uncertainties

Once the raw data are obtained, they are reduced in the industry-standard manner within the unmodified VG multicollection program. from there the data handling is identical to the dynamic multicollection case: the isotope dilution calculation is carried out, the concentration calculated, and the 143/144 ratio is corrected for the influence of the spike in both the 143/144 and 146/144 ratios.

The biggest potential source of error in the static Nd measurement is in the calibration of the cup gains. The specified cup gain drift (50 ppm in 5 hours) makes the calibration of the cups for every few samples necessary. Even then, the drift limits the reproducibility of each sample probably to about 80-100ppm (or about ±0.00005 in the 143/144 ratio). This is why the dynamic multicollection method is preferred in almost any situation where sufficient sample is available for the beam time required for dynamic multicollection.

Sm Isotope dilution analysis

Chemical procedure

Sm is collected from the HDEHP columns in 0.6 NHCl, and is subsequently dried down with alternating $HClO_4$ and HNO_3 in order to form Sm-NO_3. The Sm is then loaded directly onto Ta single filaments in 1:1 HCl:H_3PO_4, dried down at about 2A in air, then conditioned at 1.3A for 1 hour in the outgassing bench at a pressure of better than $1x10^{-6}$ Torr.

Data collection

Sm is run as Sm^+ metal in general multicollection mode. The optimum peak setup is as follows:

Cup:	L2	L1	Axial	H1	H2
Offset:	-2	-1	0	+1	+4
Mass:	146	147	148	149	152

This data collection scheme has several advantages over the 149-150-152 peak jumping scheme used at MIT. First, there is no possibility of isobaric interference from ^{150}Nd, as the 150/152 ratio is collected, but not used. Further, as ^{150}Nd is used as the spike in this lab, the interference could not be corrected for using the natural 146/150 ratio. While there is the possibility of isobaric interference at mass 152 by ^{152}Gd, the natural abundance of that isotope is 0.2% of total Gd, and any error would be introduced into the fractionation correction, which is already an approximately 1% effect. There is also an interference at mass 148 by ^{148}Nd, but once again, measurements made at mass 148 are discarded.

An additional advantage of this data collection scheme is that it requires the same cup placements as the dynamic multicollection routine for Nd isotopic composition and Isotope dilution measurement. Although the Nd cup setting is for different masses whereby the dispersion between the Nd masses and the Sm masses is not identical, it is close enough to allow meaningful analyses if the peak top is sufficiently flat. Nd and Sm samples from a single batch of chemistry can be loaded together in one barrel and run unattended.

Sm samples generally run at a filament current between 1.4 and 1.8, with a beam intensity of 1E-11 A Sm (about 100 mV 152 Sm). In-run precisions of better than 0.01 % were produced routinely.

Data reduction

The General Multicollection program provides an automated method of collecting static isotopic data. The ratios 149/147 and 152/147 are collected in static mode with no correction for gain differences between the faraday cups. $^{149}Sm/^{147}Sm$ is then corrected for mass fractionation using a power law relationship. The Sm concentration is then calculated using the standard isotope dilution equation.

A variety of errors are introduced into the data by simplification of the data reduction in accounting for several effects. These errors are well below the level of the weighout error (about 0.5% for most , which dominates the error budget of the Sm isotope dilution calculation. they are also well below the level of the error in spike calibration (about 0.1%), which is the irreducible source of error in the calculation of the Sm/Nd ratio.

The most important error unaccounted for is the lack of gain correction between the faraday cups. This is an error on the order of 0.1 % in itself and affects the raw 149/147 ratio as well as the 152/147 ratio used for the fractionation correction. The magnitude can be observed by comparing runs of shelf (unspiked) Sm by static multicollection and by single cup peak switching (dynamic multicollection is possible, but not worth the effort). The primary difference between the two results should be due to the error in the gain correction (or lack thereof). The following results were obtained for a single bead of Sm standard.

Shelf Sm:	**149/147**	**2*sigma**	**2*sigma**
		err. abs.	**err. %**
Calculated:	0.918381	0.00119	.13
Peak jumping:	0.918520	0.00036	.04
Static:	0.918193	0.00009	.01
Difference:	0.000327	0.00045	

The difference between the peak jumping and static mode collection is nearly within the in-run precision of the two measurements. The effect on the 147/149 ratio of a similar order of magnitude error in the 152/147 measurement is de-magnified by the fractionation calculation, and can be neglected. The primary place where this difference enters into the Sm concentration calculation is in the calculation of $(149/147)_N - (149/147)_M$, so the effect can be nullified by using measured natural $^{149}Sm/^{147}Sm$ for this purpose.

Another effect which would be seen in the comparison of peak jumping and static modes is the cup mismatch/peak flat problem. When the cups are set for Nd, the cup separations are not quite correct for measuring the Sm masses. the effect is sufficiently small that the critical cups are well on the flats of the peaks they are measuring for Sm, but small variations in peak flatness could produce a corresponding error in the measured 149/147 ratio. As evidenced by the data in the table, this effect is not sufficiently great to cause a problem at the level of analysis here.

Appendix III: Reconstruction of rock modes by linear least squares.

Introduction

In cases where a rock is too fine grained for traditional point counting, it may become necessary to reconstruct the mode of a rock using electron microprobe analyses of the major element composition of constituent phases and the bulk chemistry of the sample. This was necessary in this study due to the extremely fine-grained nature of the peridotite mylonites under examination, but the problem also crops up in experimental petrology, where the composition of run products is known, and the bulk composition of the charge is known, but the proportions of the mineral phases in the charge are difficult to determine. The approach in such a case is to try to determine which linear combination of the compositions of the constituent phases will result in the observed bulk composition of the sample.

This approach requires the assumption that all of the phases in the sample are identified and known. This may not be the case, for example, if phases are present in the unmeasureable portion of the sample which are not accounted for (extremely fine grained alteration phases, for example). Second, there must be chemical differences between all of the phases: Lizardite could not be distinguished from chrysotile in this fashion.

Approach

The problem can be expressed algebraically as

$$\mathbf{A} * x = b \qquad (1)$$

Where **A** is a matrix consisting of column vectors containing the major elements compositions of the minerals which comprise the rock, x is a column vector (as yet undetermined) containing the modal proportions of those minerals, and b is a column vector containing the bulk composition of the rock. The effect of matrix multiplication of **A** and x is to combine the columns of **A** in the proportions given in the vector x to produce b. If **A** is a square matrix, having equal numbers of rows and columns, that is if the number of elements analyzed is equal to the number of phases, then x is perfectly determined and can be found directly:

$$x = \mathbf{A}^{-1} * b \qquad (2).$$

where $\mathbf{A}^{-1}$ is the inverse of **A**. This approach works perfectly in the sense that a vector x can always be found which produces a right side b with no residuals. This is the equivalent, for example, of connecting two points in a data set with a straight line. When the number of elements determined exceeds the number of phases involved, an exact solution is usually no longer possible, and a solution must be found which will have errors, in that the model solution **A**x can not perfectly reproduce the right side vector b. One approach to the problem is to eliminate elements (rows of **A** and b) until the number of elements matches the number of mineral phases. If this is done in a sensible fashion, elements are chosen which have large differences from mineral to mineral, so that the leverage on the modal proportion determined is large. This is the conceptual equivalent of drawing a line between the extreme points in a trend to represent a 2-dimensional data set.

A more satisfying approach is presented in Strang (1986) which uses all the data at hand and allows a check of the validity of the solution as well. This approach can be formulated as follows:

$$(\mathbf{A}^T\mathbf{A})\ x = \mathbf{A}^T b \qquad (3).$$

By multiplying both sides of equation 1 by A^T (the transpose of A), the matrix A becomes square without any loss of information. Solving for the vector x, the solution becomes:

$$x = (A^TA)^{-1}A^T b \qquad (4).$$

This solution minimizes the sum of squared residuals in the outcome $(Ax-b)^2$ and as such is a least squares solution to the overdetermined system of equations (Strang ,1986, p.37). It is the conceptual equivalent of using a linear regression to determine the best line trhough a 2-dimensional data set. In fact, if the matrix A consists of a single vector of values for the independent variable and a unit vector, and the vector b contains the dependent variables, the x vector determined by this method is mathematically identical to the intercept and slope determined by linear regression (Strang, 1986, p. 39).

An Example

In this study it was necessary to determine the modal composition of two mylonite samples which were to be analyzed for Os isotopes. Although every sample has a unique set of mineral compositions, the data set was too sparse to allow completely independent determination of either sample; one sample was missing an olivine analysis and the other was missing a spinel analysis. For the other two major minerals, the major element compositions were very similar, so it was decided to use the data available to assemble A for both samples:

	Olivine	Enstatite	Diopside	Spinel		
SiO2	40.81	53.88	51.33	0		
TiO2	0	0.035	0.14	0.035		
Al2O3	0	4.25	5.21	50.80		
FeO	9.41	6.11	2.89	13.63		
MnO	0.16	0.14	0.08	0.08	=	A
MgO	49.77	33.88	17.89	19.81		
CaO	0	1.56	20.27	0		
Na2O	0	0.06	0.70	0		
Cr2O3	0	0.43	0.82	15.02		

By reducing the number of elements used in the analysis, a square matrix could obviously be achieved. TiO2, Na2O and MnO do not contribute to the mass budget of either the minerals or the bulk rock. This leaves six major constituents of the minerals in the rock, and only four mineral phases. Of the remaining two, FeO and Cr2O3 seem to have the smallest dynamic range and could be eliminated, however the outcome would then be almost guaranteed not to minimize the errors in all the elements in the final outcome. In the least squares approach, (A^TA) is calculated:

4231.083	3942.5679	3012.37	1114.464
3942.568	4108.9463	3443.60	977.0045
3011.962	3443.0671	3401.86	670.9032
91.04875	312.70598	706.988	2933.529

and inverted:

0.003546	-0.005154	0.0021	-0.00011
-0.00506	0.0088507	-0.00448	-1.6E-06
0.001989	-0.004452	0.003032	3.36E-05
-5E-05	0.0002894	-0.00032	0.000336

giving the matrix $(A^TA)^{-1}A^T$:

```
-0.0252  0.00011 -0.0166 0.00693 -0.0005 0.0394 0.03232 0.00116 -0.0022
0.04054 -0.00032 0.01419 -0.0065 6.4E-05 -0.032  -0.077 -0.0026 0.00011
-0.0031  0.00027 -0.0014 0.00059 8.8E-05 0.0024 0.05518 0.00186 0.00108
-0.0028 -2.3E-05 0.01666 0.00345 0.00151 0.0016 0.00067 -0.0002 0.00492
```

Which is a matrix of 9 columns and 4 rows, corresponding to the 9 elements and 4 mineral phases analyzed. The two b vectors, which are the bulk analyses of the peridotites, are as follows:

	6178c	**6183c**
SiO2	44.31	43.17
TiO2	0.03	0.02
Al2O3	2.07	1.86
FeO	8.22	8.28
MnO	0.13	0.13
MgO	42.71	44.06
CaO	1.77	1.48
Na2O	0.06	0.07
Cr2O3	0.36	0.36

And so, multiplying through, we get two solutions for modal composition:

Calculated modes:

	6178c	**6183c**
Olivine	0.6472	0.7237
Enstatite	0.2685	0.1980
Diopside	0.0667	0.0578
Spinel	0.0119	0.0138

We can back multiply A*x to get a model b vector to compare to the bulk compositions we have measured:

Calculated whole rock compositions:

	6178c	**6183c**
SiO2	44.30	43.17
TiO2	0.02	0.02
Al2O3	2.10	1.85
FeO	8.09	8.38
MnO	0.15	0.15
MgO	42.74	44.04
CaO	1.77	1.48
Na2O	0.06	0.05
Cr2O3	0.35	0.34

Calculating residuals,

	6178c	**6183c**
SiO2	-0.01	0.00
TiO2	-0.01	-0.00
Al2O3	0.03	-0.01
FeO	-0.13	0.10
MnO	0.02	0.02
MgO	0.03	-0.02
CaO	0.00	0.00
Na2O	0.00	-0.02
Cr2O3	-0.01	-0.02

we find that the least squares approach has accounted for every element to the precision of the XRF analysis with the single exception of iron, which has residuals of 1.1 and 1.6 percent.

Conclusions

A least squares approach can be used to calculate the modal composition of fine grained rocks given only mineral analyses of all phases and a bulk composition for each rock. The algebraic least squares technique is useful in a large variety of inverse problems in geology, and can be done using almost any spreadsheet program (for example Lotus 1-2-3, Excel, Quattro Pro, or Wingz) which allows matrix multiplication and inversion. Using this technique is a simple and easy way of applying linear least squares to the overdetermined problem in a more general way than the widely used linear and multiple linear regression techniques.

References

Strang, G.S., (1986) **An Introduction to Applied Mathematics**, Wellesly-Cambridge Press, 758 pp.

Appendix IV: An analysis of errors in the normative pl-px-ol ternary

Abstract

This study investigates the propagation of analytical error into the CIPW normative ternary diagram pl-px-ol. The projection scheme tends to generate a certain degree of correlation which is not due to any geologic process, but is instead due to the error propagation. The magnitude of the non-geologic correlation (ρ=0.78) is sufficient to produce a false trend in the diagram. When discussing the degree of correlation of a basalt magma series in this projection, this additional correlation due only to the propagation of analytical error must be taken into account.

Samples from the Atlantis II Fracture Zone Transform Volcano have a range of values and a degree of correlation which preclude their being related only by the analytical imprecision of the instrument. At least some of the variance in that data set is geologic in origin.

Introduction

The CIPW norm calculation (Cross, et al., 1903) is a useful means of representing the major element compositions of basalts. It has distinct advantages over examining individual elements in pairs, as it provides a method for sensibly combining all 10 major elements in a group of analyses at the same time. Since the normative components represent the stoichiometry of phases occurring naturally in igneous rocks, the reduction in total information should also be minimized by such a calculation. In studying mid-ocean ridge basalts (MORB) the normative minerals plagioclase, pyroxene and olivine are customarily plotted in a ternary diagram (e.g., Bryan and Dick, 1982). Since these phases comprise the bulk of the normative mineralogy of basalts, this diagram succeeds in presenting 10-dimensional information in a two dimensional plot.

This dissertation makes prominent use of the CIPW pl-px-ol ternary, particularly in Chapter 2. In that chapter, details of the aggregate melting process were visible in the CIPW normative pl-px-ol ternary which were not obvious in individual oxide plots, or even multiple oxide plots (Chapter 2, Figure 3). The three geologically distinct groups of basalts studied in Chapter 2 formed more distinct groupings in normative space than they did in any other representation studied.

This appendix will discuss the extent to which analytical errors propagated through the normative calculation can affect the interpretation of basalt compositions determined by electron microprobe. The two topics to be addressed are to what extent correlation is added to liquid lines of descent by the error magnification inherent in the calculation and, secondly, what significance can be attached to variations in the major element compositions of basalts from the Transform Volcano at the Atlantis II Fracture Zone.

Approach

Analytical uncertainties in the electron microprobe.

Kinzler (1991) and Sisson, (1990) give similar estimates of the underlying population standard deviations of the elemental concentrations in individual electron microprobe analyses. The two estimates are very close to one another. This analysis adopts the values in Kinzler (1991) as being typical of the uncertainties in state of the art electron microanalysis of basalts. The uncertainties, in percent relative to the values in the analysis, which are in percent by weight, are given in Table 1. These errors are assumed to be uncorrelated and normally distributed.

Oxide	1σ error, %
SiO_2	0.2
TiO_2	1.7
Al_2O_3	1.3
FeO	1.8
MgO	0.7
MnO	17.6
CaO	0.8
K_2O	10.0
Na_2O	2.2
P_2O_5	33.3

Table 1: Analytical uncertainties for 10 major elements based on repeat secondary basalt standard analysis, (Kinzler, 1991).

Errors: correlated and uncorrelated.

This section will review the statistical analysis underlying the study of correlated and uncorrelated normally distributed populations, which includes the study of analytical errors. This

material is presented more completely in Taylor (1982), Chapters, 4, 5 and 9 and Devore (1987) Chapters 4 and 12. If a random, continuously variable population is sampled repeatedly (N times), the sampled values will be the result of

$$x = x_0 + \delta \qquad (1)$$

where x_0 is the underlying real value of the sampled quantity and δ is an analytical error. If these errors are normally distributed, as the errors inherent in many physical measurements seem to be, then the best estimate of the underlying value x_0 is the mean ($X = (\Sigma x)/N$), and the probability of a given value of x occurring is given by:

$$f_{x,\sigma}(x) = \frac{1}{\sigma\sqrt{2\pi}} e^{-(x-X)^2/2\sigma^2} \qquad (2).$$

Equation 2 is the univariate normal probability distribution function and has a characteristic bell shape. Equation 2 also introduces σ, a width parameter for the bell-shaped distribution that is one of the most commonly calculated statistics for sampled data, as it provides an estimate of the uncertainty inherent in each measurement of x. σ is defined as

$$\sigma = \sqrt{\frac{\sum (x-X)^2}{(N-1)}} \qquad (3).$$

If measurements of two physical quantities are taken, they may be said to be correlated if the value of x depends in some way on the value of y. The concept of correlation is one of the fundamental concepts in statistics, and was invented for the purpose of interpreting the patterns in intelligence test scores in the late 19th century. This application was also the first instance of the abuse of correlation as well (see the excellent discussion in Gould, 1981). The application of correlation to error analysis in physical measurement is as follows. If two quantities x and y are measured which are correlated they may be defined as

$$x = x_0 + \delta_{xy,x} + \delta_x$$
$$y = y_0 + \delta_{xy,y} + \delta_y \qquad (4).$$

where $\delta_{xy,x}$ and $\delta_{xy,y}$ are the components of x and y errors respectively which are dependent on each other. The probability of particular values of x and y is given by

$$f_{X,Y,\sigma_x,\sigma_y,\rho}(x,y)=\frac{1}{2\pi\sigma_x\sigma_y\sqrt{1-\rho^2}}e^{-\left[\left(\frac{x-X}{\sigma_x}\right)^2+\left(\frac{y-Y}{\sigma_y}\right)^2-2\rho\left(\frac{x-X}{\sigma_x}\right)\left(\frac{y-Y}{\sigma_y}\right)\right]\Big/2(1-\rho^2)} \quad (5).$$

Equation 5 is known as the Bivariate Normal Distribution Function. It introduces the parameter ρ which is a measure of the degree of correlation of x and y errors. ρ is also commonly referred to as Pearson's R, and is defined as follows:

$$\rho=\frac{\sum(x-X)\sum(y-Y)}{\sigma x\cdot\sigma y} \quad (6).$$

ρ has possible values between 1 and -1. Absolute values of ρ near 1 indicate a strong correlation and the sign of ρ is equal to the sigh of the slope of the correlation. as ρ goes to 0, Equation 5 reduces to Equation 2 for x multiplied by Equation 2 for y.

Monte Carlo propagation of errors through the norm calculation.

Most programming languages contain a facility for the generation of random numbers. Typically, however, these random numbers are not normally distributed, but are uniformly distributed, each value in the defined range of the function having equal probability. In order to make the conversion from uniform deviations to normally distributed deviations, the algorithm of Press, et al. (1988) is used. Figure 1 shows a histogram of 3200 model normally distributed random numbers with a mean of 0 and standard deviation of 1. This particular instance of the univariate normal distribution is known as the Standard Normal Distribution.

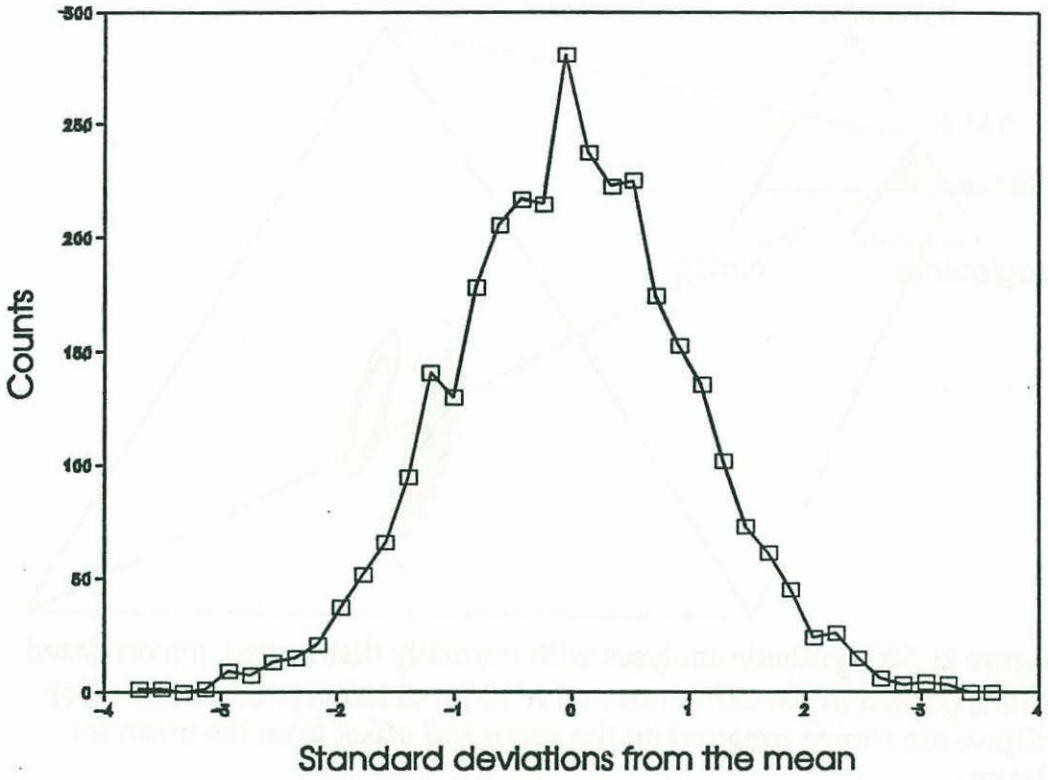

Figure 1: Histogram of 3200 normal deviates. Calculated using the algorithm of Press, et al. 1988). Mean is 0.0 and Standard deviation is 1.0.

A synthetic major element data set was calculated using the same algorithm as in Figure 1, the starting composition of basalt glass RC2709:12-6 (Johnson and Dick, 1992) and the analytical uncertainties listed above in Table 1. Model input parameters are listed in Table 2. The plagioclase, pyroxene and olivine contents of the resulting 500 data points were summed, normalized to 100%, and then plotted in a ternary diagram. Mapping the ternary components into the Cartesian space of

Oxide	Mean	1σ error, %
SiO_2	50.74	0.2
TiO_2	1.82	1.7
Al_2O_3	15.57	1.3
FeO	9.85	1.8
MgO	6.78	0.7
MnO	10.15	17.6
CaO	0.23	0.8
K_2O	3.47	10.0
Na_2O	0.25	2.2
P_2O_5	0.25	33.3

Table 2: Monte Carlo model input parameters. Glass composition is that of sample RC2709:12-6 and analytical uncertainties are from Kinzler, (1991).

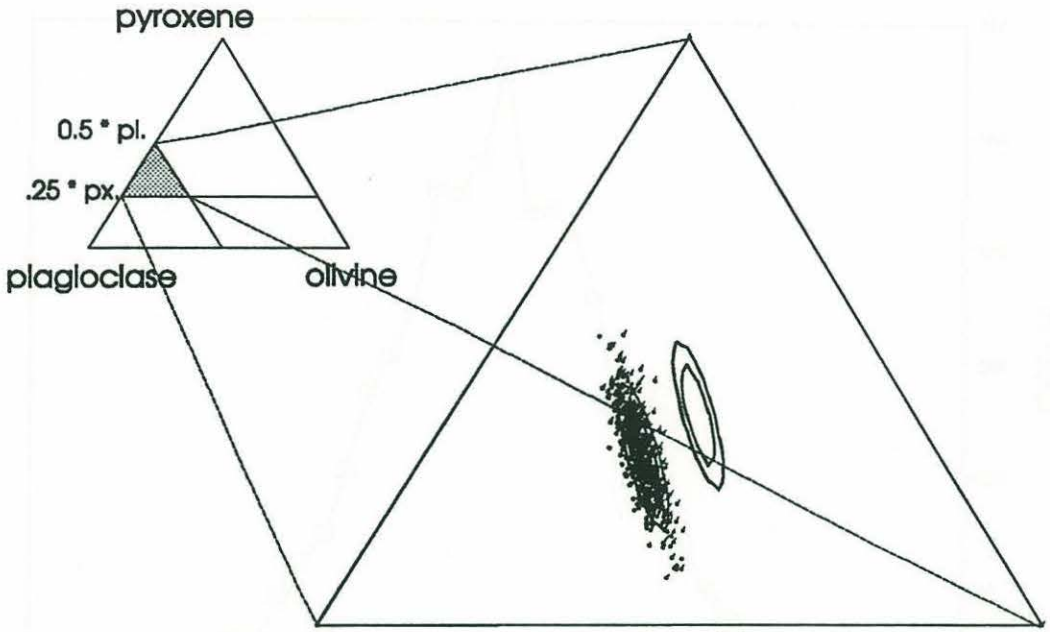

Figure 2: 500 synthetic analyses with normally distributed, uncorrelated errors, plotted in the CIPW normative pl-px-ol ternary. 1σ and 2σ error ellipses are shown centered on the mean and offset from the mean for clarity.

the ternary diagram is quite simple; if a+b+c=1, then:

$$y = c \cdot \sqrt{3}/2 \qquad x = \frac{c}{2} + \frac{b}{(1-c)} \qquad (7).$$

The synthetic data are plotted in CIPW normative pl-px-ol ternary space in Figure 2. Error ellipses corresponding to 1σ and 2σ are also plotted. These are calculated using the bivariate uniform probability distribution function for the given values of σ_x, σ_y, and ρ. The error ellipses are repeated next to the cloud of data points for clarity. There is a high degree of correlation for random analytical errors propagated through to pl-px-ol normative space. The random uncorrelated errors end up with a value of ρ (= Pearson's R) equal to 0.7846. This is likely to artificially inflate the correlation coefficient of any geologic variation which results in a trend parallel to the error ellipse.

The semimajor axis of the error ellipse in this diagram is nearly perpendicular to the plagioclase-pyroxene edge of the diagram. Analytical

errors thus do not have as great a leverage on the normative plagioclase-pyroxene ratio as on the olivine/(plagioclase + pyroxene) ratio. The implication of this observation is that differences in the normative plagioclase/pyroxene ratio are between rock suites are highly significant, and are relatively unaffected by analytical error magnification caused by the CIPW normative calculation.

Discussion

Interpreting data from the Atlantis II Fracture Zone.

The electron microprobe data from the Atlantis II Fracture Zone transform volcano (Johnson and Dick, 1992; this thesis, Chapter 2) are plotted in Figure 3 in the CIPW normative pl-px-ol ternary. Error ellipses are as in Figure 2. Three features of this data set are noteworthy. First, the error ellipses trend at a slight angle to the trend of the data. Second, the data span a greater than 2σ range in the ternary diagram, in a direction which indicates olivine + plagioclase fractionation. Third, the data are more highly correlated than would be the case if the variance were entirely due to analytical error.

It would seem difficult to accept a null hypothesis that the transform volcano basalt glasses lie in a cluster dominated by analytical error. The range of the variations (greater than 2σ in a geologically reasonable direction) alone is sufficient to suggest this. It is true that the analyses in question were carried out at the University of Cape Town, and thus the errors attached to the MIT electron probe may not be strictly applicable to the present problem. The fact that the two instruments are the same make and model and that similar procedures and standards are used in the two laboratories suggests, however, that this is not the source of the excess variance.

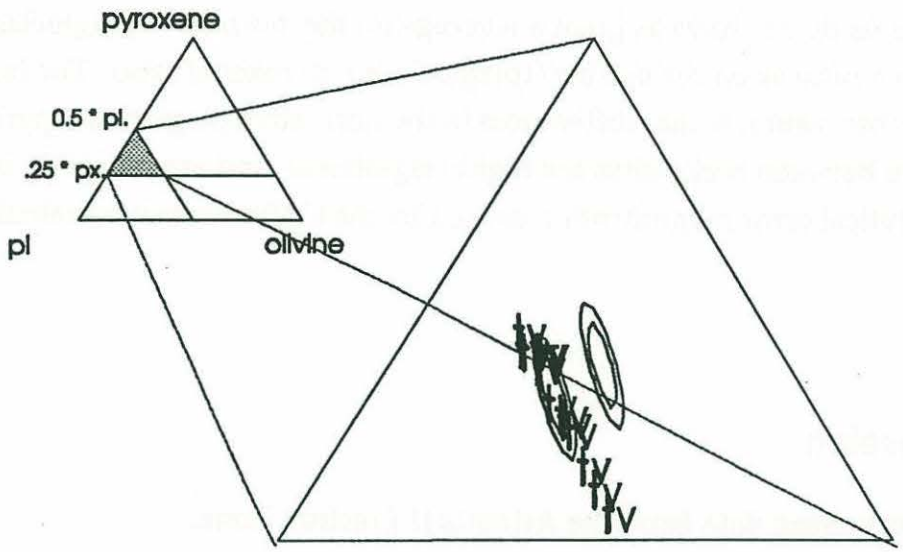

Figure 3: Atlantis II Fracture Zone Transform Volcano basalts plotted as in Figure 2, along with 1σ and 2σ error ellipses. The coefficient of linear correlation (ρ or Pearson's R) for the basalt suite is 0.984

The Transform Volcano data are highly correlated, with a ρ value (coefficient of linear correlation) of 0.984. This value is well above the threshold value of 0.95 set by Bryan and Dick, (1982) to demonstrate the colinearity of the basalt liquidus trends they measured. In the synthetic data, the correlation in is produced entirely in the CIPW calculation and ternary calculation. An increase in the uncorrelated input errors does not result in an increase in the degree of correlation of the errors. Rather, all the errors would increase, resulting in a larger error ellipse, but not a more strongly correlated one. For this reason, the correlation in excess of 0.78 (the correlation in the synthetic data set) is attributable to geologic causes.

The latter two arguments seem strong enough to reject the null hypothesis that the variations in the Transform Volcano basalt data are due only to the propagation of analytical errors through the CIPW norm calculation and projection onto ternary pl-px-ol space.

Some correlations may be artifacts.

The fact that uncorrelated analytical errors propagate into the CIPW normative ternary with a correlation has implications for the interpretation of

basalt glass data in general which are potentially serious. In this study, the basalt glasses in question defined a liquid line of descent with a linear correlation coefficient of .984. Some of this correlation is due only to the magnification of correlation due to the CIPW calculation and projection into the ol-px-pl ternary.

It is beyond the scope of this paper to propose a statistically rigorous means of determining the magnitude of the correlation due only to geologic variations in the data set. Common sense would dictate that correlation coefficients in this diagram be scaled taking into account the fact that when the geologic correlation is 0, the correlation in the diagram due only to the propagation of analytical error is 0.78. That approach would lead to a correction formula of this nature:

$$R_{corr} = (R_{meas} - R_{anal})/(1- R_{anal}) \qquad (8).$$

Applying this correction to the Atlantis II Fracture Zone data, a "geologic" R of 0.927 can be calculated. In Bryan and Dick (1982), for example, liquid lines of descent are calculated based on data sets having a coefficient of linear correlation of 0.95 or better. By the above logic, those data sets having a correlation of 0.95 would have a corrected correlation of no better than 0.77. This is nonetheless a strong degree of correlation, and does not alter any of the conclusions of that paper, however the result points out the potential dangers of using this particular diagram to calculate a liquid line of descent for a given magma series.

Conclusions

This short study has investigated the propagation of analytical error into the CIPW normative ternary diagram pl-px-ol. The projection scheme tends to generate a certain degree of correlation which is not due to any geologic process, but is instead due to the error propagation. When discussing the degree of correlation of a basalt magma series in this projection, the additional correlation due only to the propagation of analytical error must be taken into account.

Samples from the Atlantis II Fracture Zone Transform Volcano have a range of values and a degree of correlation which precludes their being related only by the analytical imprecision of the instrument. At least some of the variance in that data set is geologic in origin.

References.

Bryan, W.B., and H.J.B. Dick, (1982) Contrasted abyssal basalt liquidus trends: evidence for mantle major element heterogeneity. **Earth and Planetary Science Letters** 58:15-26.

Cox, K.G., J.D. Bell, and R.J. Pankhurst (1979) *The Interpretation of the Igneous Rocks* George Allen and Unwin.

Cross, W., J.P. Iddings, L.V. Pirsson and H.S. Washington (1903) *Quantitative Classification of Igneous Rocks* University of Chicago Press.

Devore, J.L. (1987) *Probability and Statistics for Engineering and Science* 2nd. ed. Brooks/Cole Publishing Co.

Gould, S.J., (1981) *The Mismeasure of Man* W.W. Norton and Co., NY.

Johnson, K.T.M. and H.J.B. Dick, (1992) Open system melting and temporal and spatial variation of peridotite and basalt at the Atlantis II Fracture Zone **Journal of Geophysical Research** 97:9219-9241.

Kinzler, R. (1991) MIT, Ph.D. Thesis.

Miyashiro, A., Shido, F. and Ewing. M. (1970) Crystallization and differentiation of abyssal tholeiite and gabbros from mid-ocean ridges **Earth and Planetary Science Letters** 7:361

Press, W.H., B.P. Flannery, S.A. Teukosky and W.T. Vetterling (1988) *Numerical Recipes in C: The Art of Scientific Computing* Cambridge University Press.

Sisson, T. (1991) MIT Ph.D. Thesis.

Taylor, J.R. (1982) *An introduction to Error Analysis: The Study of Uncertainties in Physical Measurements* University Science Books.